PERFORMANCE, EMISSION AND COMBUSTION STUDIES OF A MODIFIED VEGETABLE OIL IN A COMPRESSION IGNITION ENGINE

A thesis submitted to the Delhi Technological University, Delhi in the fulfillment of the requirements for the award of the degree of

Doctor of Philosophy

in

Mechanical Engineering

by

ANKIT SONTHALIA
(2K16/PhD/ME/26)

Under the supervision of

Dr. NAVEEN KUMAR
(Professor)

Department of Mechanical Engineering
Delhi Technological University
Shahbad, Daulatpur, Bawana Road
Delhi – 110042, India
September, 2020

DECLARATION

I hereby declare that the thesis titled **"Performance, Emission and Combustion Studies of a Modified Vegetable Oil in a Compression Ignition Engine"** is an original work carried out by me under the supervision of Dr. Naveen Kumar, Professor, Department of Mechanical Engineering, Delhi Technological University, Delhi. This thesis has been prepared in conformity with the rules and regulations of Delhi Technological University, Delhi. The research work reported and results presented in the thesis have not been submitted either in part or full to any other University or institute for the award of any other diploma or degree.

Ankit Sonthalia

2K16/PhD/ME/26

Research Scholar

Mechanical Engineering

Department

Delhi Technological University,

Delhi

Date: 21/08/2020

Place: Delhi

CERTIFICATE

This is to certify that the work embodied in the thesis titled **"Performance, Emission and Combustion Studies of a Modified Vegetable Oil in a Compression Ignition Engine"** by **Ankit Sonthalia**, (Roll No.: **2K16/PHD/ME/26**) in partial fulfillment of requirements for the award of Degree of **Doctor of Philosophy in Mechanical Engineering**, is an authentic record of student's own work carried by him under my supervision.

This is also certified that this work has not been submitted to any other University or institute for the award of any other diploma or degree.

Dr. Naveen Kumar
Professor
Mechanical Engineering Department
Delhi Technological University,
Delhi

Dedicated to my Family & Friends whose constant support helped me in completing this Research

ACKNOWLEDGEMENT

Vaagdevi College of Engineering, and Dr. B.P. Kiran from Synthesis with Catalysts Pvt. Ltd.

I shall ever cherish the affection and blessings showered on me by my parents. Whatever I have achieved in my professional life; it is all because of them. I cannot express in words their efforts put by them to nurture me. I am also indebted to my younger brother Mr. Sanchit who always extended help whenever required. I place my sincere respect and a deep sense of gratitude to other family members.

Finally, I am unable to express my sincere gratitude in words for the affection, encouragement and moral support by my wife during the research work. I am ever beholden to my wife Dr. Shilpi for not giving due attention and time during the present work.

There are many more persons who have helped me directly or indirectly to complete this research work. I take this opportunity to thank all of them and apologize for their names not being here.

Last but not the least, I thank the Almighty for giving me the strength and patience to complete this work in all respects, leading to the path of success.

Ankit Sonthalia

Delhi

ABSTRACT

The Indian transportation sector relies heavily on the diesel operated compression ignition engines. However, the combustion of diesel produces greenhouses gases which are a major threat to the environment as well as the humans. Alternatives to diesel are gaining importance for operating the engine as they can curb the greenhouse gases and are a key for addressing the energy security. One such alternative is used cooking oil, which the world, India in particular is generating in large quantities. The government of India is now emphasizing on the conversion of the used cooking oil into biodiesel. However, many studies show that the biodiesel cannot completely replace diesel due to its inherent issues. The biodiesel is produced from the used cooking oil by the transesterification method. Another method, namely hydroprocessing can also convert the used cooking oil into a fuel with properties closer to diesel.

In the present research, the used cooking oil was converted to diesel like fuel by using the hydrotreating method and experiments were carried out on an engine to study the effect of the fuel on its performance and emission. The research was carried out in four phases.

In the first phase, the hydrotreated oil was produced from the used cooking oil in the presence of a ruthenium based catalyst in a batch reactor. The reaction parameters namely reaction temperature, hydrogen pressure and reaction time were varied. Design of experiments were used for optimizing the process parameters. The Taguchi method was selected as it reduces the number of experiments which saves time and money. The aim was to increase the conversion percentage and diesel like fuel selectivity and reduce the naphtha selectivity. Since multi-objective optimization was required, Fuzzy logic was incorporated. The optimized parameters were 360°C reaction temperature, 40bar initial reaction pressure and 200min reaction time. Confirmation experiment was

carried out using these parameters and the conversion efficiency and diesel like fuel selectivity was 89.7% and 88.2%, respectively.

The physico-chemical properties, evaporation temperature, ignition probability and Sauter mean diameter of the blends of the hydrotreated oil and diesel were studied in the second phase. The GC-MS profile of the pure hydrotreated oil shows that the fuel has straight carbon atoms in the range of C_{11} to C_{20} and heptadecane is the predominant hydrocarbon. Properties like viscosity, density, calorific value, flash point, etc. were measured and found to be within the limits of ASTM standards. The fuels were also stored for a period of one year to study their stability in terms of density, viscosity and calorific value. The properties of the stored fuel changed slightly with time and their rate of change was also low.

The hydrotreated fuel was mixed with diesel in various proportions and engine tests were carried out in the third phase. The results show that the brake thermal efficiency decreases with increase in the hydrotreated fuel share in the blend. The heat release for the blends starts earlier than diesel due to higher cetane number and the peak heat release is also lower than diesel. The HC, CO and smoke emissions for the test blends decreases up to 30% blend, further increase in the blending of hydrotreated oil resulted in increase in the emissions. The NO emissions were lower than diesel for all the test samples. The maximum reduction in NO (neat), HC (30% blend), CO (30% blend) and smoke emissions (30% blend) is 23.2%, 14.4%, 13.83%, and 13.3%, respectively.

It the third phase of testing, it was observed that 30% blend of hydrotreated oil resulted in lowest emissions but the thermal efficiency was low. The thermal efficiency with 20% blend of hydrotreated oil was higher than 30% blend but the emissions with 20% blend were higher. To improve the shortcomings of the two samples addition of

waste cooking oil biodiesel to the two samples was explored. Therefore, in the last phase, experiments were carried out by blending waste cooking oil biodiesel (5%, 10% and 15% on volume basis) in 20% and 30% blend of the hydrotreated oil. The results show that the heat released increases with the biodiesel addition on account of higher ignition delay but its starts earlier than diesel and its maximum value is still lower than diesel. The brake thermal efficiency of the biodiesel blended fuels increases and as the percentage of biodiesel increases the thermal efficiency increases. Among the blended fuels, the maximum thermal efficiency was observed to be 30.96% with 15% biodiesel mixed in 20% hydrotreated oil and 65% diesel. The lowest HC, CO and smoke emissions at full load were observed to be 1.73g/kWh, 24.02g/kWh and 49.2% respectively with 15% of biodiesel mixed in 30% hydrotreated oil. Among the biodiesel blends, the lowest NO emission is observed to be 3.61g/kWh with 5% of biodiesel mixed in 30% hydrotreated oil, whereas highest NO emission (3.98g/kWh) is observed with 15% of biodiesel mixed in 20% hydrotreated oil.

LIST OF CONTENTS

LIST OF PLATES

LIST OF FIGURES

LIST OF TABLES

NOMENCLATURE

A/F	Air to Fuel Ratio
ANN	Artificial Neural Network
ANOVA	Analysis of Variance
ASTM	American Society for Testing and Materials
ATDC	After Top Dead Center
AVL-437	AVL-437 Smoke Meter
BSEC	Brake Specific Energy Consumption
BSFC	Brake Specific Fuel Consumption
BTE	Brake Thermal Efficiency
BTDC	Before Top Dead Center
°C	Degree Celsius
°CA	Degree Crank Angle
CA50	Crank Angle At Which 50% of Heat is Released
CH_4	Methane
CFPP	Cold Filter Plug Point
CI	Compression Ignition
CN	Cetane Number
CO	Carbon Monoxide Emission
CO_2	Carbon Dioxide
CoMo	Cobalt Molybdenum catalyst
CoV	Coefficient of Variance
CP	Cloud Point
cSt	Centi Stoke
CV	Calorific Value
DMDS	Dimethyl Disulphide
DPF	Diesel Particulate Filter
EEV	Enhanced Environmentally Friendly Vehicles
EGR	Exhaust Gas Recirculation
EGT	Exhaust Gas Temperature
FAME	Fatty Acid Methyl Ester

Performance, Emission and Combustion Studies of a Modified Vegetable Oil in a Compression Ignition Engine

FFA	Free Fatty Acids
FTIR	Fourier Transform Infrared
GCMS	Gas Chromatography Mass Spectrometry
HDC	Hydrocracking
HDCX	Hydrodecarboxylation
HDCN	Hydrodecarbonylation
HDM	Hydrodemetallation
HDN	Hydrodenitrogenation
HDO	Hydrodeoxygnation
HDS	Hydrodesulfurization
H100	100% HVO
H10D90	10% HVO and 90% Diesel
H20D80	20% HVO and 80% Diesel
H30D70	30% HVO and 70% Diesel
H40D60	40% HVO and 60% Diesel
H50D50	50% HVO and 50% Diesel
H20B5	20% HVO, 5% Biodiesel and 75% Diesel
H20B10	20% HVO, 10% Biodiesel and 70% Diesel
H20B15	20% HVO, 15% Biodiesel and 65% Diesel
H30B5	30% HVO, 5% Biodiesel and 65% Diesel
H30B10	30% HVO, 10% Biodiesel and 60% Diesel
H30B15	30% HVO, 15% Biodiesel and 55% Diesel
H100	100% HVO
HC	Unburned Hydrocarbon
HFRR	High Frequency Reciprocating Rig
HVO	Hydrotreated Vegetable Oil
IMEP	Indicated Mean Effective Pressure
IR	Infrared
JME	Jatropha Methyl Ester
LM	Levenberg – Marquardt
LTB	Larger The Better
MAPE	Mean Absolute Percentage Error
MMT	Million Metric Tons

MPCI	Multi Performance Characteristics Index
Mtoe	Million Tons of Oil Equivalent
NiMo	Nickel Molybdenum catalyst
NOx	Oxides of Nitrogen Emission
NO	Nitric Oxide
NTB	Nominal The Better
PAH	Polynuclear Aromatic Hydrocarbons
Pd	Palladium
Pd/C	Palldium/Carbon catalyst
PDPA	Phase Doppler Particle Analyzer
PM	Particulate Matter
Pt	Platinum
rpm	Revolutions per Minute
Rh	Rhodium
RMSE	Root Mean Square Error
Ru	Ruthenium
SCG	Scaled Conjugate Gradient
SMD	Sauter Mean Diameter
SOx	Oxides of Sulphur
S/N	Signal to Noise Ratio
STB	Smaller The Better
TDC	Top Dead Center
TPES	Total Primary Energy Supply
ULSD	Ultra Low Sulphur Diesel
UDDS	Urban Dynamometer Driving Schedule
WCO	Waste Cooking Oil
WHSV	Weight Hourly Space Velocity

CHAPTER 1

INTRODUCTION

1.1 Current Energy Scenario

The economic and social growth of any country is dependent upon energy. The consumption of fossil fuels has increased exponentially by both developed and developing countries. Fig. 1.1 compares the total primary energy supply (TPES) of the world in 1973 and 2018. The world's energy consumption in 1973 was 6101 Mtoe (Million tons of oil equivalent) which increased to 13864 Mtoe in 2018 [1,2], an increase of 127%. The major energy sources for 85.18% of the total energy consumption comprises of oil, coal, and natural gas.
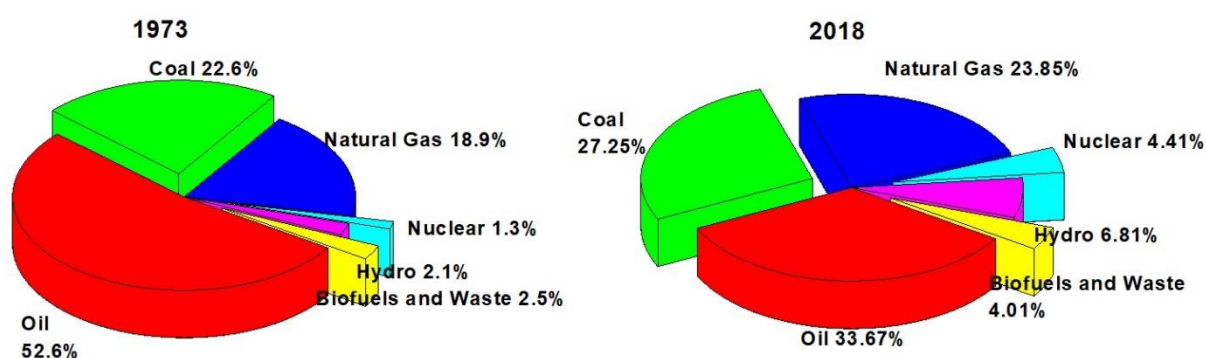
Fig. 1.1. Comparison of total primary energy supply in 1973 and 2018 [1,2].

1.1.1 Energy scenario in India

India is among the fastest growing economies of the world and energy is the wheel to its growth. However, the oil reserves in India are miniscule in comparison to its requirements. In 1947, the oil available was 0.25 million tons which increased to about 38.09 million metric ton (MMT) in 2011-12. India is highly dependent upon imports of crude oil to cater to its need for agriculture, automobiles and industrial applications. For the year 2017-18, India produced nearly 35.68 MMT, whereas India imported nearly 220.43 MMT at the average cost of US$56.43 per barrel. The cost to the exchequer for importing the oil was INR 5,65,951 crores. 95% of energy requirement of the transportation and agricultural sector is fulfilled by the imported oil. The diesel

requirement in India was about 53 MMT in 2007-08 which has grown over to 79.7 MMT in 2017-18 [3]. Thus, India needs to take steps to reduce its dependence on oil with the growing needs of energy.

1.2 Need for Alternatives

Fossil fuels still provide more than half of the world energy demands. The gap between the demand and supply of the energy is increasing due to rapid urbanization and industrialization. It is estimated that oil, coal, and natural gas would be available for the next 33, 105 and 35 years, respectively. Therefore, it is expected that till 2112 coal will be available and after 2042 it will be the only fossil fuel available [4].

1.2.1 Environmental Issues

The technologies used for extraction, transportation and processing of fossil fuels are harmful for the environment. During extraction, transportation and storage, spills or leaks can cause both water and air pollution. The refining process also has harmful effect on the environment. Moreover, the combustion of the fossil fuel in the engines are the major cause of the environmental pollution. The major constituents of fossil fuels are carbon and hydrogen and traces of sulfur which when combusted produces various gases along with soot, ash and other organic compounds which degrades the air quality. The most harmful emissions include carbon monoxide (CO), hydrocarbons (HC), oxides of nitrogen (NOx), oxides of sulfur (SOx), benzene, poly aromatic hydrocarbons (PAH), aldehydes and particulate matter (PM). In the past efforts have been made to improve the fuel quality and vehicle technology. Carbon dioxide (CO_2) from fossil fuel combustion and other greenhouse gases such as methane (CH_4) are responsible for warming of earth resulting in melting of polar ice caps, rise in the level of sea and change in climate like heat waves, drought, floods, stronger storms, increase in number of wild fires etc. Studies also show that these pollutants when mixed with

moisture or other atmospheric compounds or triggered by sunlight can change their form and become hazardous aerosols or acids that can damage the aquatic and terrestrial ecosystem [5–7].

Therefore, a paradigm shift towards alternate energy consumption can be seen throughout the globe. In 2018, 4% of the world energy consumption comprised of renewable sources such as geothermal, wind, solar, biomass and waste [2]. As compared to 2015, the energy consumption from renewable sources increased by 53% [8]. The Indian government also emphasized the need of cleaner environment and technologies for energy generation. Therefore, the government accepted the outcomes of the Paris climate summit and is investing heavily in solar and wind energy power plants along with a new Biofuel Policy 2018.

1.3 Compression Ignition Engines and Alternative Fuels

Compression Ignition (CI) engines are the backbone of the transportation and the agricultural sector. They are also used in off-road vehicles and for power generation. The main attractions to its use are ruggedness in construction, usage simplicity and ease of maintenance. Other features are high thermal efficiency, high torque and low fuel consumption. Low pumping losses, lean air fuel mixtures and high compression ratio results in high thermal efficiency of these engines. However, these engines emit gases that not only pollute the environment but are harmful for the humans as well.

The diesel engines emits particulate matter in the small particle form at concentration above 10 million particulates per cm^3. The diameter of the primary carbon particles lies in the range of 0.01 to 0.08 micron, whereas the diameter of the agglomerated particles is in the range of 0.08 to 0.25 microns with nearly 90% of the particles having diameter less than 1 micron. Several government agencies have classified the particulate matter as "human carcinogen" or "probable human

carcinogen". They increase the risk to the heart and respiratory diseases such as asthma and bronchitis. Presence of two or more benzene ring hydrocarbons in the particulate matter also called polynuclear aromatic hydrocarbons (PAHs) are known human carcinogens. The soluble organic fraction of the particulate matter containing four and five rings are the most harmful compounds [9].

A long lasting solution to the above mentioned problems can be use of renewable alternative fuels which can either partially or completely replace the conventional fossil fuels in the CI engines. However, if the alternate fuels have to be regularly used on long-term basis then large resource base is required so that the resource is available throughout the year and the investment is also justified. Such alternative fuels should be compatible with the associated systems of the engine such as hoses, fuel tank and pump. The alternative should also be compatible with the existing transportation, fuel storage, and retail infrastructure.

1.3.1 Vegetable oil as an alternate fuel

To operate the diesel engine with an alternate fuel, the fuel should have properties close to diesel. Vegetable oils derived from the plant seeds are among the few alternatives that match the conventional diesel. Its energy density, cetane number and heat of vaporization are comparable with diesel. However, its viscosity is many folds higher than diesel. High viscosity affects the spray atomization, vaporization and fuel-air mixing.

The use of vegetable oil offers significant cost-effective and perpetual opportunities for rural employment particularly for growing, harvesting and processing of plants that provides the oil. The energy security of any country can be attained by multifaceted actions such as a purposeful policy on production of oil and natural gas, use of hybrid and electric vehicles and search for low cost alternative fuels which can

reduce dependence on oil imports. India having 17% of the world population requires to use both renewable and exhaustible energy resources. The decentralized agro-based form of energy production can provide a sound base for village centred economy and also attain a high level of energy security.

The vegetable oils are carbon neutral i.e. the plants take in carbon dioxide from the atmosphere for photosynthesis and produce the oil. When the oil is combusted in engines, the carbon is released back into the atmosphere thus balancing the carbon dioxide. However, conventional diesel fuel are produced from fossil fuels and the carbon present in them was stored for millions of years which is being released after their use in engines. This causes the carbon dioxide levels to increase in the atmosphere thereby causing global warming. With vegetable oil use in diesel engines, the sulfur dioxide emissions are eliminated as the oil is free of sulfur resulting in reduction of acid rain. Also, the accumulation of sulfuric acid in the crankcase is reduced over time. Their combustion in diesel engines also reduce polycyclic aromatic hydrocarbons, nitrated polycyclic aromatic hydrocarbons emissions. The lack of carcinogenic and toxic aromatics (benzene, toluene and xylene) in the oil shows that the gases formed after combustion will have less impact on the environment and human health. It also result in less offensive exhaust odour which is a real benefit when machinery or vehicles are used in confined environment or underground mines. A wide variety of feedstock are available, some of them are listed in Table 1.1.

An ideal diesel fuel is a saturated hydrocarbon with no branch chains, containing 12 to 18 carbon atoms. Whereas, the vegetable oil is a triglyceride having different lengths of non-branched chain molecules and with different degrees of saturation. They have high amount of oxygen present in them and the molecules are typically four times that of diesel molecules.

In comparison to diesel, the heating value of vegetable oils is nearly 10% less as they have oxygen present in their molecules. The kinematic viscosity of vegetable oil is nearly 30mm^2/s which is much higher than diesel (3.01mm^2/s) resulting in pumping and atomization problems. The vegetable oil has higher density than diesel whereas its volatility is lower resulting in lower evaporation rates. Hence they cannot be used in spark ignition engines. Vegetable oil has higher carbon residues resulting in higher smoke emissions during combustion. As compared to diesel, the flash and fire point of the vegetable oil is higher making it safe to store. However, its cloud point is also high in comparison to diesel thus it tends to thicken or freeze at low atmospheric temperatures. Their cetane number (32-40) is also lower than diesel. They are miscible in diesel and can form stable blends for long periods. These properties show that vegetable oils are suitable to be used only in CI engines. However, there are short-term and long-term problems when vegetable oils are used in the diesel engines (Table 1.2).

Table 1.1. Feedstock for alternate fuel

| Feedstock | Distribution | Plant Type | Oil Content (%) | | Reference |
			Seed	Kernel	
Vegetable oils					
Sleichera triguga (Kusum)	Northern India, the western Deccan, Sri-Lanka, Malaysia, Indonesia, Java, etc.	Tree	-	55-70	[10,11]
Sapium sebifeum L. Roxb (Stillingia)	Native to Japan, China, India and also grows in southern coastal United States	Tree	13-32	53-64	[10,11]
Guizotia abyssinica L. (Niger)	Ethiopia and India	Herbaceous Annual	50-60	-	[12]
Hevea brasiliensis (Rubber seed oil)	South East Asia, India, Nigeria, Brazil, West Africa	Tree	40-60	40-50	[13]
Jatropha curcas L. (Jatropha)	India, Thailand, Pakistan, Indonesia, Nepal, Malaysia, Philippines,	Tree	20-60	40-60	[11,14]

Simmondsia chinesis (Jojoba)	Sonoran and Mojave deserts	Shrub	45-55	-	[11,15]
Madhuca indica (Mahua)	India	Tree	35-50	50	[11,14]
Sapindus mukorosso (Soap nut)	America, Asia, Europe	Tree	51.8	-	[16]
Ricinus communis (Castor)	Brazil, Cuba, China, France, Italy, India, and countries of the former Soviet Union	Tree/Shrub	45-50	-	[10,11]
Pongamia pinnata (Karanja)	native of Western Ghats in India, Northern Australia, some regions in Eastern Asia, Fiji	Tree	25-50	30-50	[14,15]
Calophyllum Inophyllum (Beauty leaf tree)	Australia, East Africa, Southern coastal India to Malaysia	Tree	50	-	[17,18]
Michela chaampaca	China, Burma, eastern Himalayas, Assam, and Western Ghats in India	Tree	45	-	[10,14]
Azadirachta indica (Neem)	Native to India, Australia, Bangladesh, Burma, Cuba, Malaysia, Pakistan and Sri Lanka	Tree	20-30	25-45	[10,11,14,15]
Linum usitatissimum (Linseed)	Asia, Argentina, Canada, and Europe	Herbaceous annual	35-35	-	[11,19]
Milletia pinnata (Pongam oil tree)	Malaysia, Australia, China, India, Pacific Islands, and Japan	Legume Tree	27-39	-	[20]
Moringa oleifera (Drumstick tree)	Africa, Asia, Latin America, Oceania	Tree	35	-	[21,22]
Aphanamixis piolystachya (Pithraj)	Growing in India, China	Tree	-	35	[10]
Asclepias syriaca (Milkweed)	Distributed to the northeast and north-central United States	Herbaceous perennial	20-25	0.019	[10,11,23]
Ricinus communis (Castor oil plant)	Australia, Native to Africa and Eurasia	Tree	45-50	-	[24]

Waste cooking oil	All countries	-	97.02	-	[25]
Lingo cellulosic biomass					
Bagasse	Almost every country in the world	-	-	-	[26]
Wheat straw	Almost every country in the world	-	-	-	[27]
Rich Straw	Almost every country in the world	-	-	-	[28]
Barley straw	Almost every country in the world	-	-	-	[29]
Animal Fats					
Tallow	Almost every country in the world	-	-	-	[30]
Lard	Almost every country in the world	-	-	-	[30]

Table 1.2 Problems with using vegetable oils as engine fuels [31]

Problem	Problem Cause
Short – term	
1. Cold weather starting	High viscosity, low cetane number, low flash point of vegetable oil
2. Plugging and gumming of filters, lines, and injectors	Natural gums (phosphatides) in vegetable oil. Ash
3. Engine knocking	Very low cetane of some oils. Improper injection timing
Long – term	
4. Coking of injectors, carbon deposits on piston and head of the engine	High viscosity, incomplete combustion of fuel. Poor combustion at part load
5. Excessive engine wear	High viscosity, incomplete combustion of fuel. Poor combustion at part load Possibly free fatty acids in the vegetable oil. Dilution of engine lubricating oil due to blow-by of vegetable oil.
6. Failure of engine lubricating oil due to polymerization	Collection of poly-unsaturated vegetable oil blow-by in crank-case to the point where polymerization occurs

1.4 Used cooking oil as a potential CI engine fuel

Enormous amount of waste cooking oil (WCO) is generated all over the world from fast food centres, restaurants, households and food processing industry. It is estimated that nearly 1,000,000 to 3,000,000 tons/year of waste cooking oil is generated in the European Union. In the US, the generated amount is 5.2 billion to 7 billion gallons

a year whereas in Japan alone nearly 600,000-1,000,000 tons of WCO is generated annually [32]. In India, nearly 6.5 billion gallons of used cooking oil was generated in the year 2018 [33]. The disposal and storage of WCO is both costly and troublesome. Most of the used cooking oil is poured into the sewer system resulting in pollution of lakes, rivers, seas and underground water which leads to human health and environmental problems. If the used oil is reused, then the money spent of waste treatment can be minimized and the environmental pollution also will reduce. WCO can be used as a fuel as it is readily available and it is cheaper than diesel. Also its physical and chemical properties are close to diesel. Table 1.3 shows a comparison of the properties of diesel and waste cooking oil. Waste cooking oil use as a fuel can provide considerable economic benefits as the energy requirements of industries and automobile sectors can be met. Many researchers have converted used cooking oil into biodiesel using the transesterification process and tested on different types of diesel engines [34].

Table 1.3 comparison of properties of waste cooking oil and diesel [35]

Properties	Diesel	Waste Cooking Oil
Density at 20°C (kg/m^3)	840	880
Lower Heating Value (kJ/kg)	42490	39600
Viscosity (cSt) @ 30°C	4.59	45
Flash Point (°C)	52-96	218
Cetane Number	45-55	40-45
Auto ignition Temp. (°C)	260	320
Flame Velocity (cm/s)	30	3-6
Flammability Limits (vol.% in air)	0.7-5	0.1-0.3
Boiling Point (K)	436-672	657
Molecular weight (g mol)	170	875.75
Carbon residue (%)	0.1	0.54
Sulfur content (% wt)	0.149	0

1.5 Hydroprocessing of oils

The vegetable oil can be upgraded (biodiesel) by the transesterification process wherein the triglycerides are converted into mono alkyl esters using either methanol or ethanol. The catalyst amount used in the process is changed in accordance to the free

fatty acid (FFA) content of the vegetable oil. However, the process is applicable when the FFA content is less than 2.5 wt%. Oils having higher than 2.5 wt% FFA content, a pre-treatment is required for reducing its FFA content so that the transesterification can be carried out. The biodiesel produced from transesterification has low oxidation stability and cetane number because of high degree of unsaturation and presence of long chains [36]. Long-term biodiesel use in diesel engines causes corrosion and deposit problems in fuel injection systems [37].

Other technologies for upgrading the vegetable oil are high pressure-temperature treatment, fluid catalytic cracking (FCC) and gasification by the Fischer-Tropsch process. In high pressure-temperature treatment no catalyst is used and temperature and pressure greater than 250°C and 250bars, respectively, is utilized for upgrading the vegetable oils. Any kind of heavy and complex hydrocarbon can be upgraded to diesel and gasoline using the FCC method. The syn-gas is converted into hydrocarbons in the presence of transition metals in the Fischer-Tropsch process. However, significant amount of gaseous component is formed in the Fischer-Tropsch process, whereas the other methods suffer from coke formation [38].

Hydroprocessing is a general term used to describe the reactions, such as hydrogenation, hydro-deoxygnation (HDO), hydro-denitrogenation (HDN), hydro-desulfurization (HDS), hydro-cracking (HCR) and hydro-demetallation (HDM). To remove heteroatoms (sulfur, nitrogen, oxygen, metals) and for cracking and saturation of olefins and aromatics, the petroleum refining industry uses the well-known cracking and hydroprocessing technique [39]. The process can also be used for converting bio-based feedstock into straight chain alkanes having C_{12} to C_{18} carbon atoms. The fuel has high cetane number (55-65) and its properties are better than diesel produced via transesterfication process [40]. As the fuel is similar to diesel, existing infrastructure of

diesel for storage, transportation and retail can be utilized, the existing engines can be used without any modifications and the process is flexible with the use of feedstock [41]. These bio-based alkanes/olefin mixtures having chemical structure C_nH_{2n+2} are called by different names such "Hydrotreated vegetable oil (HVO)" [42], "hydrogenated vegetable oil" [40], "renewable diesel fuel" [36,43], "second generation biodiesel" [44], "paraffinic renewable diesel" [45,46], "hydroprocessed vegetable oil" [41], "bio-hydrogenerated diesel (BHD)" [47], and "super cetane" [41].

1.6 Thesis Organization

The thesis entitled "**Performance, emission and combustion studies of a modified vegetable oil in a compression ignition engine**" is divided into six chapters and its outline are as follows.

Chapter 1 introduces the reader to the energy scenario of the world and India in particular. It shows that India's energy consumption is increasing every year and there is an urgent need to look for the alternatives to fossil fuel due to their serious effect on the environment. For the Indian economy compression ignition engines are the prime movers, therefore, it is imperative to search for alternatives to diesel. The significance of vegetable oil as replacement to diesel is then discussed in the chapter. However, the straight oils are not preferable for operating the diesel engine. Hence these oils are suitable for conversion into fuels with diesel-like properties. Hydroprocessing is one such process, which converts the vegetable oil into diesel like fuel.

In the second chapter, the existing literature is reviewed critically. The chapter is divided into two broad sections. First the conversion of straight vegetable into diesel like fuel using hydrotreating process is discussed. The effect of reaction parameters like the hydrogen pressure, reaction time and temperature on the conversion efficiency of the process is discussed. In the second section, the engine performance by using the

hydroprocessed fuel is discussed. The chapter also consists of the research gap and objectives of the present research.

In the third chapter, the procedure for the production of the hydrotreated oil is discussed in detail, along with the optimization of the fuel production. The methods and instruments for finding the physico-chemical properties of the fuel is also discussed. The chapter also discusses the hot plate test setup and the Spraytec setup for finding ignition probability and Sauter mean diameter, respectively. The development of engine test setup and the test procedure is described. Lastly, the accuracy and uncertainty in measurement is reported in the chapter.

In the fourth chapter, results of the experiments carried out to produce the hydrotreated oil is discussed in detail and the findings are compared with the existing literature. The production of the oil is optimized using Taguchi and Fuzzy logic approach. Using the optimized process, the fuel is produced and its properties is discussed in detail.

In the fifth chapter, the results of the tests performed on the developed engine setup is discussed. The experiments were first carried out with the hydrotreated oil and diesel blends and then biodiesel was added into the two best blends to study its effect on the engine performance. The chapter discusses these results in detail and compares the same with the literature. Lastly, in chapter six, the major findings of the research is summarized and the future recommendations are provided.

CHAPTER 2

LITERATURE REVIEW

2.1. Introduction

Vegetable oil use in diesel engines dates back to several decades. Rudolf Diesel, predicted that the plant derived oils will be used to operate his engine, but due to the high cost of the oil as compared to diesel, their use became unacceptable. After the oil crisis, research again began on using vegetable oil as a substitute to diesel. The research further gathered pace when it was known that the combustion of fossil fuels was deteriorating the environment quality due to increased emissions and increase in prices of the crude petroleum oil. Vegetable oils was considered as a suitable alternative to diesel since many of its properties were close to petroleum diesel. However, direct use of vegetable oil resulted in major engine problems as their viscosity and carbon residue is high. By modifying the fuel or the engine this can be overcome.

Vegetable oils can be either blended with diesel or they can be transesterified or preheated to lower their viscosity so that they can be used in a diesel engine with considerable success. Hydrotreating is another process for converting vegetable oil into diesel-like fuel or gasoline-like fuel. The process can be extended to convert waste cooking oil, raw vegetable oil, algal oil and animal fat into fuels with very high yield in the presence of a catalyst. The oils can be converted into iso-paraffin and n-paraffin in the range of gasoline, jet fuel and diesel. The calorific value, cetane number of the obtained products is high, their saturation level is also higher as compared to biofuel produced from conventional methods [48]. Fig. 2.1 shows the oil obtained from different processes such as oil produced from liquefaction of wet biomass, pyrolysis oil, and wax obtained from Fischer-Tropsch synthesis can be converted into fuels. This study is an attempt to convert the vegetable oil into hydrotreated vegetable oil using catalysts and the use of the produced oil in a diesel engine. A detailed literature review

on the process, reaction mechanism, and effect of various parameters on the reaction and the use of the fuel in the diesel engine is carried out.
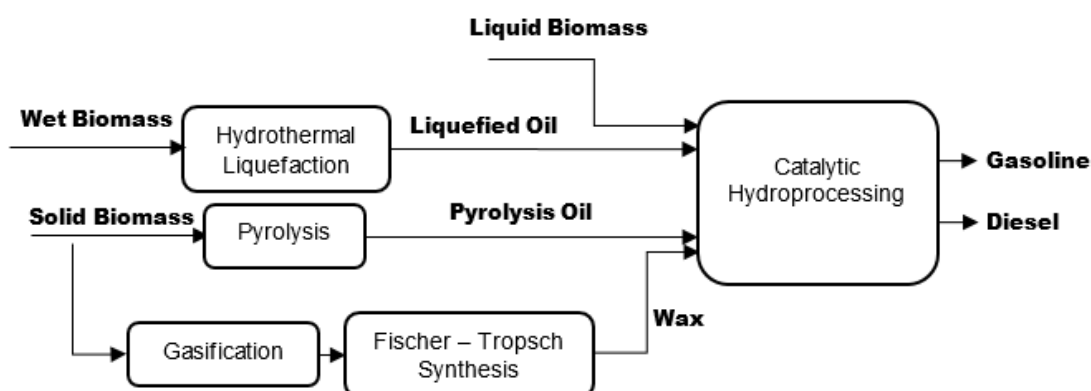
Fig. 2.1. Catalytic hydroprocessing for biomass conversion and upgrading towards fuels production.

2.2. Processes Involved

The oil is hydrotreated at high temperature and pressure in the presence of a catalyst using excess hydrogen. The treatment unit consist of three primary sections: (i) preparation of the feed, (ii) feed reaction, and (iii) product separation.

Initially the oil and high pressure hydrogen is mixed at a higher temperature and later the feed enters the reactor. The reactor is fixed bed type which contains the catalytic beds at a set temperature. In the next section, the reactions occurring in the reactor are described in detail. The products formed in the reactor are separated in the separator section wherein they are cooled using a condenser. Then the products enter a gas-liquid separator where gas and liquid molecules are separated. Excess hydrogen along with by-products such as CO, CO_2, H_2S, NH_3, and H_2O are present in the gas. The gas can be treated to improve the overall efficiency of the system by removing the by-products and feeding the gas back to the system. The separated liquid product flows to a container placed on a weighing balance, to know the conversion percentage. The obtained liquid can then be fractionated and separated into products like naphtha, kerosene, and diesel [48].

2.3. Reaction Mechanism

For the hydrotreating process, the temperature is varied between 300-400°C and the pressure ranges from 6-20MPa [49–52]. Initially the double bond present in the triglyceride is broken so that it becomes saturated, then cracking is carried out [53]. Excess hydrogen is introduced in the process so that the double bond is broken. The vegetable oil chain length is large and complicated, by cracking the oil, the chain length reduces and the boiling point of the resulting oil is within the range of gasoline, diesel or jet fuel. Fig. 2.2 shows the reaction mechanism wherein cracking converts the triglyceride into its fatty acids and propane. Almost all vegetable oil contains oxygen but no sulfur and nitrogen. The major problem with transesterification process is its incapability to remove oxygen which reduces its oxidation stability and heating value and it also increases its corrosivity and acidity. Thus removing the oxygen in necessary. Three different reaction pathways namely hydro-decarboxylation (HDCX), hydro-decarbonylation (HDCN) and hydro-deoxygenation (HDO) are possible for the removal of oxygen [49]. Fig. 2.2 shows that HDCX and HDCN reaction pathway result in odd number of carbon atoms. HDCX reaction yields CO_2 as by-product and HDCN reaction yields water and CO as by-product. Carbon monoxide, carbon dioxide and water can then react on the catalyst surface to form methane (methanation reaction Eq. 2.1-2.3) and CO (water gas shift reaction, Eq. 2.4). Whereas, HDO reaction pathway yields alkanes with even number of carbon atoms and oxygen which combines with hydrogen to form water [54–59]. HDO, HDCX, and HDCN relative activities is the main feature, as they affect the hydrogen consumption, yield of the product and inhibition of the catalyst [60]. Kochetkova [59] observed that 16 moles of hydrogen are required for converting Rapeseed oil to 6 moles of water, one mole of propane and rest hydrocarbon by the HDO route. With only seven moles of hydrogen, the oil is converted

into one mole of propane and 3 moles of CO_2 by the HDCX route. However, if by water gas shift reaction all the CO_2 is converted to CO, which is subsequently converted to methane, then 19 moles of hydrogen is consumed through the HDCX reaction pathway. Moreover, with HDCX reaction route the hydrocarbon yield is 94% of the HDO reaction route.

$$CO + 3H_2 \rightleftharpoons CH_4 + H_2O \qquad (2.1)$$

$$2CO + 2H_2 \rightleftharpoons CH_4 + CO_2 \qquad (2.2)$$

$$CO_2 + 4H_2 \rightleftharpoons CH_4 + 2H_2O \qquad (2.3)$$

$$CO_2 + H_2 \rightleftharpoons CO + H_2O \qquad (2.4)$$
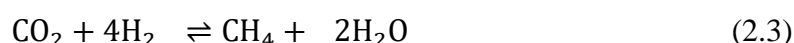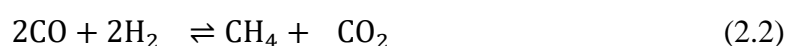
To control the reaction pathway, the operating parameters such as catalyst [61], reaction temperature and operating temperature [62,63] play a major role. Soybean oil was hydrotreated by Veriansyah et al. [53]. The authors found HDO reaction route is favoured by NiMo (Nickel Molybdenum), CoMo (Cobalt Molybdenum), and Pt (Platinum) catalysts, whereas HDCX reaction pathway is favoured by Ru (Ruthenium), Ni, and Pd (Palladium) catalysts. The order of the n-C_{17}/n-C_{18} ratio was Ru/Al_2O_3 (39.6), Ni/SiO_2-Al_2O_3 (29.3), Pd/γ-Al_2O_3 (11.9), NiMo /γ-Al_2O_3 (2.49), CoMo/γ-Al_2O_3 (2.16), Pt/γ-Al_2O_3 (0.92). The Palm oil was hydrotreated using Nickel-Molybdenum and Pd/C bimetallic catalyst [64]. Higher decarboxylation/decarbonylation rate is observed with NiMo catalyst as the C_{15}-C_{16} ratio is in the range of 4.8 to 5.8. With Pd/C catalyst, decarboxylation/decarbonylation reaction is prominent as the temperature increases. With monometallic catalysts (like nickel with aluminium oxide as base catalyst) decarboxylation hydrocarbon products are only produced [65,66], whereas the reaction takes place through HDO route when molybdenum with aluminium oxide as base catalyst is used [67].

The effect of hydrogen pressure, reaction temperature, liquid hourly space velocity (LHSV), hydrogen to oil ratio on reaction pathway was studied by Srifa et al. [60] using

sulfided NiMo catalyst. HDO, HDCN and HDCX reaction pathway were observed with the catalyst, with HDO pathway being the dominant one. However, at high temperature or lower pressure, HDCN/HDCX reaction pathway is promoted over HDO pathway. During the hydroprocessing of Sunflower oil, Kikhtyanin et al. [68] found that as the temperature increases, the C_{17}/C_{18} ratio also increases which indicates that the HDCN/HDCX reaction rates are higher than HDO reactions. Moreover, Guzman et al. [62] while hydroprocessing Palm oil found that at high operating pressure the HDCN and HDCX reactions rate are lower since the ratio of C_{17}/C_{18} and C_{15}/C_{16} decreased in the obtained oil. Similar results were observed by Krar et al. [69] and Mikulec et al.[44]. The LHSV has no significant effect on the reaction pathway as observed by Yang et al. [70] and Sankarnarayanan et al. [71]. The authors argued that deoxygenation of (H_2) C-O bond in triglyceride is slower than the breaking of –C (=O)-C_{17} bond. Therefore, the deoxygenation rate of free fatty acids is similar to decarboxylation/decarbonylation reaction. Moreover, Krar et al. [69] observed that hydrogen to oil ratio promotes decarboxylation/decarbonylation reactions.
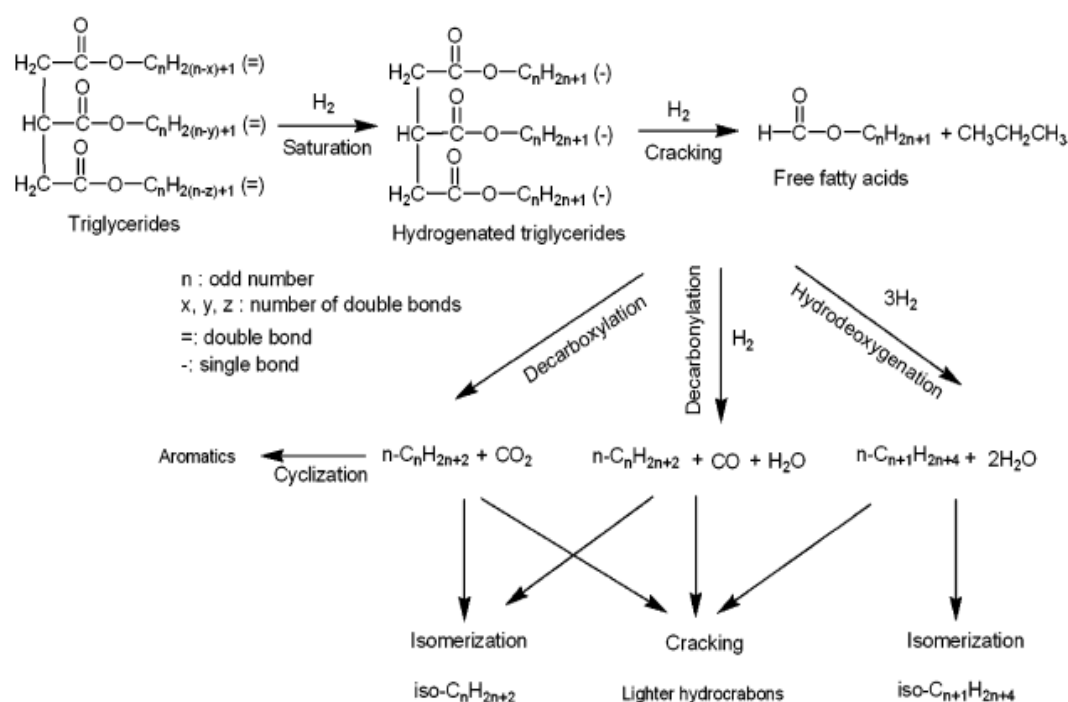
Fig. 2.2. Reaction pathways for conversion of triglycerides by hydroprocessing [53]

The hydrocarbons formed are straight chains having high cetane number, cloud and pour point, melting point and cold filter plug point (CFPP) [72]. Isomerization, i.e. transforming the straight chains into branched chains can lower the cloud point, pour point and CFPP [73]. A NiMo hydrotreating catalyst was used by Bezergianni et al. [42] and the effect of temperature on isomerization was studied. As the temperature increases, the percentage of iso-paraffins increases. At 398°C (36 wt. %) the highest paraffin is observed, and at 330°C (5.6 wt. %) the lowest paraffin is observed, resulting in improvement in cold flow properties but at the expense of decrease in cetane number. The iso/n-paraffin ratio was also varied by Yang et al. [70] by varying the operating parameters. With rise in temperature the iso/n-C_{16} ratio and iso/n-C_{17} ratio increases whereas the iso/n-C_{15} ratio and iso/n-C_{18} ratio decreases. The C_{18} ratio decreases mainly due to cracking of the hydrocarbons at higher reaction temperature. Similar results were obtained by Gong et al. [54].

Weight hourly space velocity (WHSV) also affects the isomerization of C_{16}-C_{18}, but it is constant for C_{15} due to its lower content in the organic liquid product (OLP). The isomerization rate decreases with increase in hydrogen pressure, as the hydrogen is absorbed on the active sites of the catalyst thus reducing the reaction. Hydrogen to oil ratio has little impact on iso/n-paraffin ratio. Simacek et al. [43] with a hydrocracking catalyst achieved a cloud point of -11°C and CFPP of -14°C, which further reduced to -20°C with flow improver. The cold flow properties can also be improved by blending of HVO with diesel [74]. Co-processing the oil with a heavy gas oil is another method [75]. Heavy gas oil and waste cooking oil was co-processed at 310, 330 and 350°C. The lowest pour point was observed when the waste content was maximum and the highest temperature. Kikhtyanin et al. [68] used Pd/SAPO-31 catalyst with Sunflower oil for producing fuel with cloud and pour point

less than -50°C. Similarly, Hancsock et al. [76] used Pt/HZSM-22/Al$_2$O$_3$ for isomerization of pre-deoxygenated Sunflower oil, resulting in a fuel with good low temperature properties and high cetane number. In another work [77], the effect of different percentages of nickel in NiP/SAPO-11 catalyst was studied by deoxygenating fatty acid methyl ester (FAME). With no nickel content, less amount of iso-alkanes is formed which is due to special acid sites on SAPO-11. These acid sites are responsible for the generation of the carbon cations which are consequently isomerized. However, due to stearic hindrance of FAME, the isomerization rate is low. The isomerization rate reaches a maximum at 3% weight of nickel content since the active metal sites for HDO reaction increases and acid sites for isomerization also increases. Moreover, further increase in content of nickel results in decrease in isomerization rate since support may be occupied by the metal oxides or phosphides which cannot be reduced to active sites.

Bezergianni et al. [78] compared a single-step with two-step process for the waste cooking oil hydroprocessing. In the single-step process only hydroprocessing is carried out whereas in two-step process first hydroprocessing and later isomerization is carried out. For hydrotreating NiMo/γ-Al$_2$O$_3$ catalyst is used whereas for isomerization a light amount of zeolite and high amount of NiW catalyst is used. With only hydroprocessing, the fuel produced has higher cold flow properties, whereas the fuel produced using two-step process has lower CFPP. However, two-step process tends to increase the production of lighter products such as kerosene and naptha. The cetane index and heating value of the fuel produced was high with two-step process. The authors also found that the energy requirement, operating cost and hydrogen consumption of two-step process is high. Therefore the authors suggested that the fuel produced from one-step process can be blended with diesel (<10% v/v) and the blend properties satisfy the required legislation for winter diesel (EN590 diesel standard).

2.4. Effect of various operating parameters on fuel production

Many studies on the effect of catalyst type, reaction temperature, and hydrogen pressure on fuel production from various vegetable oil exists. In the subsequent sections, the work carried by various researchers on different parameter is studied. Table 2.1 summarizes the studies conducted by various researchers.

Table 2.1 Studies on the Hydroprocessing of Pure Vegetable Oils

Feedstock	Catalyst	Conditions T (°C), P (MPa) & LHSV (h^{-1})	Reference
Jatropha Oil	Mesoporous α- alumina used as a supports sulfide TMN/ α- Al$_2$O$_3$	T: 300-400, P: 6-8, H$_2$/oil ratio: 1000-2000 lit/hr. and LHSV: 1- 10.	[79]
Palm Oil	Commercial 5 wt.% Pd/C & synthesized NiMo/γ-Al$_2$O$_3$	T: 350-450, P: 2-6, Reaction time: 0.25-5 hr	[64]
Palm Oil	NiMoS$_2$/γ-Al$_2$O$_3$	T: 270–420, P: 1.5-8, LHSV: 0.25-5; H/C:250–2000 Nm^3/m^3;	[60]
Palm Oil	NiMo/γ-Al2O3	T: 350, P: 4–9, WHSV: 2, H$_2$/oil:20 mol/mol	[62]
Sunflower Oil	commercial CoMo/Al$_2$O$_3$	T: 300–380, P: 2–8, LHSV: 1.0–3.0 h^{-1} and H$_2$/Sunflower oil volume ratio: 200–800 Nm^3/m^3.	[69]
Sunflower Oil	commercial hydrocracking catalyst consisting of supported metal sulfides	T: 360-420, P: 18, Liquid feed flow (Sunflower oil) and hydrogen flow was 49 g h^{-1} and 0.049 N m^3 h^{-1}	[43]
Sunflower Oil	NiMo/Al$_2$O$_3$/F	T: 280−380, P: 2−8, LHSV = 0.75−3, H$_2$/oil :400−600 Nm^3/m^3	[80]
Sunflower Oil	Pt/HZSM-22/Al$_2$O$_3$ Pt/SAPO-11	T: 280−380, P: 3−8, WHSV: 1−4, H$_2$/oil = 250−400 N m^3/m^3	[76]
Sunflower Oil	Pd/SAPO-31	T: 310−360, P: 2, WHSV: 0.9−1.6, H$_2$/oil = 1000 N m^3/m^3	[68]
Karanja Oil	Commercially sulfide CoMo and NiMo catalyst supported on Al$_2$O$_3$	T: 300−380, P: 1.5−3.5, weight hourly space velocity 1.1−5 h^{-1}; H$_2$/oil ratio: 400−600 v/v	[81]
Rapeseed Oil	Three catalyst with varying composition of NiO and MoO$_3$	T: 260-340, P: 7, LHSV: 1 h^{-1}, H$_2$/oil: 22 g h^{-1}	[82]
Rapeseed Oil	Co-Mo / Al$_2$O$_3$ +SiO$_2$	T: 320-380, P: 4, WHSV: 1h^{-1}, H$_2$/oil: 240m^3/ m^3	[59]
Rapeseed Oil	NiMo/Al$_2$O$_3$	T: 310−360, P: 7−15, WHSV: 1.0, H$_2$/oil: 920 N m^3/m^3	[83]
Rapeseed Oil	NiMo/Al$_2$O$_3$, Mo/Al$_2$O$_3$, Ni/Al$_2$O$_3$	T: 260−280, P: 3.5, WHSV: 0.25−4.0	[84]
Rapeseed Oil	sulfided NiMo/γ-Al$_2$O$_3$	T: 260, P: 3.5, WHSV: 1−4, H$_2$/feed: 50 mol/mol	[67]
Rapeseed Oil	(multiple grades) sulfided CoMo/γ-Al$_2$O$_3$	T: 310, P: 3.5, WHSV: 2, H$_2$/feed :100 mol/mol	[85]
Soybean Oil	NiMo/γ-Al$_2$O$_3$	T: 350−400, P: 1−20, batch	[50]
Soybean Oil	NiMo/γ-Al$_2$O$_3$	T: 360, P: 14, batch	[86]
Soybean Oil	NiMo/γ- Al$_2$O$_3$, Pd/γ-Al$_2$O$_3$CoMoS/γ- Al$_2$O$_3$, Ni/SiO$_2$−Al$_2$O$_3$/γ- Al$_2$O$_3$, Ru/ Al$_2$O$_3$	T: 400, P: 9.2, batch	[53]
Waste Cooking oil	commercial hydrotreating catalyst	T: 330−398, P: 8.3, WHSV: 1.0, H$_2$/oil: 4000 scfb	[42,87]

Waste Cooking oil	NiMo/B$_2$O$_3$− Al$_2$O$_3$	T: 300−350, P: 7, batch	[88]
Waste Cooking oil	commercial hydrocracking catalyst	T: 350−390, P: 13.8, WHSV: 1.5, H$_2$/oil: 6000 scfb	[89]
Waste Cooking oil	commercial hydrocracking catalyst	P: 8.27-9.65, H$_2$/Oil ratio: 543- 890 nm^3/m^3, LHSV: 0.5-1.5 h^{-1}, T: 370	[90]

2.4.1. Effect of catalyst on production

Two types of catalysts can be used for hydrotreating the triglycerides, first noble metals such as Platinum (Pt), Palladium (Pd), Ruthenium (Ru), Rhodium (Rh), etc. [53,62,64,68,76], second transition metals such as Nickel (Ni), Cobalt (Co), Molybdenum (Mo), and Tungsten (W) [50,67,70,82,84]. Different supports such as alumina, zeolites and carbon can be used as supports. The cost of noble metals is high and their lifetime is short as compared to transition metals. Co, Ni and Mo are the most employed catalysts both in monometallic and bimetallic form [59–62,82,84]. The possibility of compounds containing oxygen is higher with monometallic catalysts as compared to bimetallic catalysts, since the bimetallic catalysts can easily deoxygenate the intermediates before they are desorbed from the active sites of the catalysts [84].

Kiatkittipong et al. [64] hydroprocessed crude Palm oil using Pd/C catalyst resulting in 51% diesel yield. With degummed Palm oil, the yield increased to 70% with a reaction duration of one hour, whereas with Palm distillate the maximum diesel yield is 81%. NiMo/γ-Al$_2$O$_3$ catalyst was also used by the authors for hydroprocessing degummed Palm oil and fatty acid Palm oil. The NiMo catalyst resulted in higher yield with degummed Palm oil, whereas Pd/C catalyst resulted in higher diesel yield with fatty acid Palm oil. Sotelo-Boyas et al. [91] used Pt/H-ZSM-5, Pt/H-Y, and sulfided NiMo/γ-Al$_2$O$_3$ catalyst for hydroprocessing Rapeseed oil. The cracking activity of the zeolite supported platinum is high due to the presence of stronger acid sites thereby increasing the production of green gasoline. However, the platinum supported on H-Y, resulted in higher production of green diesel. Moreover, the production of iso-paraffin

is higher with zeolites. Pd, Ru, Ni, Pt, NiMo, and CoMo catalyst were compared on the basis of their conversion efficiency and product composition [53]. For CoMo catalyst the n-alkane content is less than 55% whereas with Pd or Ni catalyst it was more than 80%. The authors from their study concluded that transition metals are more suited for triglycerides hydroprocessing due to their higher oxygen removal and conversion efficiencies at low cost.

Bezergianni et al. [92] employed three commercial catalyst for studying the effect of catalyst on waste cooking oil. Catalyst A was hydrotreating catalyst, catalyst B was mild hydrocracking catalyst and catalyst C was severe hydrocracking catalyst. The authors observed highest conversion efficiency and diesel selectivity with catalyst A, whereas catalyst B use resulted in steep reduction in heteroatoms and nearly 99% saturation of double bonds. However, catalyst C due to its hydrocracking nature resulted into lower hydrocarbons and more of gaseous components resulting in lower efficiency. The waste cooking oil was completely converted into hydrocarbons by Toba et al. [88] the authors found that nickel based catalyst is more suitable for hydrodeoxygenation as compared to CoMo since the latter prevents production of olefins. The composition of NiO and MoO_3 were varied in the catalyst by Simacek et al. [82]. There was no effect of the catalyst on n-heptadecane content but the n-octadecane content varied. The authors also observed that the increase in reaction temperature, increases the n-heptadecane content and the n-octadecane content decreased. Zhao et al. [93] hydroprocessed carinata oil and studied the effect of different molar ratios of Zn/Mo on the produced fuel content. Lower acid content was observed in the biofuel loaded with Zn and Mo with Al_2O_3 as compared to only Al_2O_3. The metal loading on Al_2O_3 promotes the acidity of the catalyst which is responsible for promoting the HDO reaction and increasing the hydrocarbon content. The

hydrocarbon content increased till a Zn/Mo molar ratio of 2, further increase in the molar ratio resulted in decrease in hydrocarbon content. The aggregation of zinc oxide particles in higher Zn/Mo ratios leads to accelerated deactivation of the catalyst. By using different catalyst the fuel yield with Rapeseed oil also varied [84]. After 1 hour reaction time, the hydrocarbon yield with Ni or Mo varied from 30% (260°C) to 80% (270°C), whereas with NiMo, after one hour reaction time the hydrocarbon yield varied from 90% (260°C) to 100% (270°C). Monnier et al. [94] evaluated the performance of nitrides of vanadium, tungsten and molybdenum with oleic acid. With molybdenum nitride eight times more octadecane was produced as compared to vanadium and tungsten nitride. The molybdenum nitride is a good water gas shift reaction catalyst resulting in the shift of thermodynamic equilibrium of CO, CO_2, H_2O, and H_2. The hydro-deoxygenation activity of the catalyst was more since the hydrogen consumption was higher and water formation was more. Karanja oil was hydrotreated by Nimkarde et al. [81] using sulfided NiMo and CoMo catalyst in a fixed bed reactor. Nickel based catalyst resulted in maximum fuel conversion (90%) at 653K. HZSM-5, fluid catalytic cracking (FCC) and CoMo were used for pomace oil hydrotreating [95]. FCC and HZSM-5 catalyst promotes cracking hence large quantity of lighter hydrocarbons were produced by their use. The aromatic compounds content was also higher. With CoMo catalyst, diesel like fuel was produced with lower aromatic content.

Co-processing of vacuum gas oil and Sunflower oil in the ratio of 70/30 v/v was hydrocracked using three catalysts [96]. Three catalyst: catalyst A is a mild hydrotreating catalyst, catalyst B is a severe hydrocracking catalyst, whereas, catalyst C use increased diesel production were used by the authors. Catalyst A works well with low pressure; hydrocracking was performed with catalyst A and catalyst B at 1000Tpsig. On the other hand, catalyst B and catalyst C were compared at 2000 psig

pressure. Catalyst B use resulted in the highest conversion of the liquid along with highest naphthalene selectivity. The liquid product contained both gasoline and diesel, but the diesel selectivity is more. Catalyst B worked well in reducing oxygen whereas catalyst C is more efficient in reducing sulfur and nitrogen. Heavy gas oil and waste cooking oil were also co-hydroprocessed by Bezergianni et al. [97] using NiMo and CoMo catalyst. The authors used 10 and 30% of waste cooking oil on volume basis for the process using three reaction temperatures (330°C, 350°C and 370°C). For CoMo catalyst, presence of WCO has an adverse effect on desulfurization and denitration, while is has positive effect on NiMo catalyst. Moreover, WCO addition favours conversion, selectivity, and saturation for both the catalysts. The maximum conversion efficiency of 55% is obtained using CoMo at 330°C with 30% WCO. The selectivity of diesel is highest with NiMo at 330°C. At low temperatures the diesel selectivity is higher since the cracking of fuel is lower. The authors concluded that NiMo is suitable for co-processing of WCO and heavy gas oil mixtures whereas CoMo is more suited for heavy gas oil. Kumar et al. [98] co-processed refinery gas oil and Jatropha oil using sulfided $CoMo/Al_2O_3$, $Ni-W/SiO_2- Al_2O_3$, and $NiMo/Al_2O_3$. 97.9% yield of $C_{15}-C_{18}$ is seen with NiMo, with Ni-W the yield is 80.8%, and with CoMo the yield is 49.2% with pure Jatropha oil. Fresh NiMo and CoMo catalyst use HDO reaction pathway for oxygen removal from Jatropha whereas NiW favors HDCN/HDCX reaction pathway. Resulfidation of NiMo tends to slightly favour the HDCN/HDCX route. The diesel range with NiMo varied between 88-92% during co-processing. Also the gas oil desulfurization is better during co-processing.

The catalyst support plays a major role in its activity. The industry widely uses alumina for removing sulfur content of the fuel. Therefore, many studies are present that have used alumina support for hydroprocessing of biomass oil. The problem with

alumina is its deactivation by nitrogen and coke formation after prolonged use. The pore size of alumina is also small which makes vegetable oil processing difficult since their molecule size is big. Other supports have also been used for hydrotreating such as carbon [99], clays [100], oxides like MgO, SiO_2, TiO_2, ZrO_2 [59,101,102], zeolites like UsY, NaY [103,104], and mesoporous materials like HMS [105], MCM-41[106], and SBA-15 [107] etc.

Mo_2C catalyst supported on multi-walled carbon nanotubes was used by Han et al. [99]. The authors found the conversion efficiency to be 90% and diesel like fuel selectivity to be 91%. The cost of activated carbon is low, its BET surface area is high, wide pore size, low acidity and metals can be smoothly recovered from the spent catalyst [99]. CoMo catalyst was supported on activated carbon for co-processing Jatropha and gas oil [108]. In comparison to mesoporous alumina support, the C_{15}-C_{18} content was higher for activated carbon. Pure Jatropha oil was hydroprocessed using mesoporous titanosilicate supports [109]. A large quantity of kerosene range hydrocarbons is observed with five times more isomerized fuel and slight improvement in activity as compared to alumina supports. Higher acidity, favourable metal support interactions, and better metal dispersion are the probable reason for the increase in yield. Three different hierarchical structure of titanium oxide support with nickel and cerium as catalyst were used to hydroprocess Jatropha oil [110]. The structures include TiO_2 nanopowder, titanium nanotubes (TNT) and titanium nanosheets (TNS). The catalyst preferred decarboxylation/decarbonylation reaction route as the concentration of n-C_{17} is the highest. The lowest triglyceride efficiency is observed with TNS support (54%), which increased to 71% with TiO_2 and the highest efficiency is observed with TNT support (85%). USY, ZSM-5, Zeolite β, γ-Al_2O_3, and AL-SBA-15 were used as supports for NiMoC catalyst. Use of zeolites result in more cracking activity as they

have a specific pore structure which result in more gasoline and gaseous products. High amount of hydrocarbons in the range of diesel was produced with mesoporous γ-Al_2O_3 and AL-SBA-15. 100% conversion and 97% diesel selectivity is observed with AL-SBA-15 supported catalyst, which can be attributed to high surface area, significant porosity and regular channel structure.

The catalyst deactivation is the loss of activity and product selectivity with reaction time. The regeneration or replacing cost of catalyst can be high. The catalyst deactivation can take place due to: (1) active sites poisoning caused by chemisorption of heteroatoms, (2) deposition of coke on catalyst surface resulting in coking, (3) sintering/thermal deposition due to breakdown of catalyst and support surface area because of crystalline growth, (4) internal pores loss during crushing [38]. Guzman et al. [62] hydroprocessed Palm oil using NiMo catalyst and found that the acidic sites of the alumina support favoured the esterification reactions resulting in the formation of high molecular weight esters in the fuel thereby deactivating the catalyst. Continuous change in Pd/SAPO-31 catalyst with increase in on-stream time was observed by Kikhtyanin et al. [68]. The concentration of Pd was same both before and after use but the dispersion decreased from 50 to 11% for used catalyst. The metal particles are sintered during the reaction which reduces the catalyst's function, resulting in lower deoxygenation of fatty acids and lower conversion of n-alkanes to iso-alkanes. The presence of oxygenates resulted in faster deactivation of the catalyst. WCO was hydrocracked at three different temperatures to assess the effect of days on stream (DOS) on the catalyst conversion efficiency [89]. The experiments were conducted in duplicate; in the first run (Run-A) the data was sampled at an earlier stage and in the second run (Run-B) the data was collected at a later stage of the experiment. For Run-A, with increase in temperature the conversion increased. Whereas for Run-B, the

conversion at 370°C is 70.8% at 34 DOS and at 350°C it is 72.72% at 26 DOS. Therefore, the catalyst activity decreases after at least 34 DOS and the increase in temperature cannot compensate for the activity decrease, this is due to the blockage of catalyst pores by large molecules of the oil.

Presence of sulfur compounds in the feedstock is beneficial for increasing the catalytic activity. The deoxygenation performance is improved by addition of di-methyl-di-sulfide (DMDS) to the catalyst [85]. Since the acidity of the catalyst improves as metal sulfide is formed through decomposition of DMDS. A small percentage of DMDS and tetra-butyl–amine (TBA) were added to the catalyst to maintain its constant activity [89].

2.4.2. Effect of temperature on production

The reaction temperature is the most important parameter for controlling the products formed during the hydroprocessing. Bezergianni et al. [87] hydrotreated waste cooking oil, and studied the effect of temperature on conversion, selectivity, product yield, saturation of double bonds and heteroatom removal, rest of the parameters were kept constant. At high temperatures the oil is cracked resulting in formation of gasoline molecules as the yield of gasoline increased from 0% at 330°C to 10.2% at 398°C. Sulfur and nitrogen were removed from the liquid product, however, oxygen removal rate at lower temperature was low which increased with increase in temperature. Bromine index is a measure of amount of unsaturation present in the liquid. The authors observed that the bromine index decreases with increase in temperature. Sulfided TMN/mesoporous α-alumina was used by Jha et al. [79] to hydroprocess Jatropha oil. They found an increase in converted triglycerides with the increase in temperature. Also, the C_{15}-C_{18} hydrocarbon molecules increased at 340°C and the oligomerized ($>C_{18}$) hydrocarbons decreased. While hydrocracking triglycerides using CoMo

catalyst, Anand et al. [111] found similar results. At lower temperatures, oligomerized hydrocarbons were formed, whereas at higher temperature C_{15}-C_{18} hydrocarbon molecules were formed.

Kubicka et al. [84] hydroprocessed Rapeseed oil and found the conversion to be in the range of 80 to 90 wt.%, and at 270°C, complete conversion of triglycerides was observed. Similarly Simacek et al. [83] observed complete conversion at 360°C. Kikhtyanin et al. [68] found that the complete conversion of Sunflower oil is possible in the temperature range of 320-350°C with Pd/SAPO–31 catalyst, whereas Hancsok et al. [76] with Pt/HZSM-22/Al_2O_3 catalyst completely converted Sunflower oil at 350°C. While hydrotreating the pomace oil, Pinto et al. [95] found an increase in methane and other gaseous hydrocarbon products as the reaction temperature and time increases. The authors attributed it to higher cracking reactions as observed by increase in hydrogen consumption and 30 to 40% increase in CO and CO_2 which shows that HDCN/HDCX reactions are favoured. At 300°C, only 3% fatty acid content was found while 96% of the light fractions were converted into hydrocarbons. Moreover, at 430°C, the hydrocarbon content increased to 99% and the fatty acid content decreased. The hydrotreated Palm oil solidified at room temperature when the process was carried out at 270°C and the product contained small amounts of triglyceride along with palmitic and stearic acid [60]. The authors also noted that as the temperature increases from 270 to 300°C, the product yield increases from 26.7% to 89.8%. However, as the temperature is further increased to 420°C, the yield falls to 37.9%. Simacek et al. [82] also observed reactant and intermediates in the product when the process was carried out at temperatures below 310°C. In another work of the group, the authors found high acid numbers (0.54-0.65mg$_{KOH}$/g) at 310°C, since more amount of carboxylic acid was formed which reduced to less than 0.06mg$_{KOH}$/g acid number at 360°C.

Heavy atmospheric gas oil (HAGO) was co-processed with waste cooking oil by Bezergianni et al. [96] using NiMo and CoMo at 330, 350, & 370°C, keeping other parameters constant. The sulfur removal rate improved from 89.15% at 330°C to 99.24 at 370°C for pure HAGO, with WCO addition, the removal rate further improved with NiMo catalyst. However, the sulfur removal rate dropped to 87.12% and 80.93% for 10% and 30% WCO addition in HAGO with CoMo as a catalyst. The drop is due to the competition between hydro-desulfurization and HDO which occurs at the same active site. Moreover, the conversion efficiency of NiMo for pure HAGO is small which improves with WCO addition. Similarly, the conversion efficiency improves with WCO addition for CoMo catalyst which is maximum (55%) for 30% addition of WCO. Rajesh et al. [108] used CoMo with carbon as support for hydrotreating a mixture of gas oil (GO) and Jatropha oil (JO). At 330°C, the sulfur content is 40ppm for neat GO, 124ppm at 5% concentration of JO in GO, 154ppm at 10% concentration of JO in GO and 220ppm at 20% concentration of JO in GO. Moreover, with increase in temperature the sulfur content reduced for all percentages of Jatropha in the gas oil.

Waste cooking oil and heavy gas oil (HGO) mixtures were hydroprocessed over NiMo catalyst by Bezergianni et al. [75]. The highest conversion of 48% was observed at maximum temperature of 350°C with 70/30 HGO/WCO mixture. Moreover, the higher the WCO content in the mixture, the higher is the conversion at different temperatures. At low temperature the consumption of hydrogen is low, since only saturation and heteroatom removal takes place whereas at higher temperature cracking also occurs. With HGO/WCO mixture, the consumption of hydrogen is high in comparison to neat HGO which increases with the increase in WCO content in the mixture since hydrogen is also required for deoxygenating and cracking the triglycerides. Pre-hydrotreated and non-hydrotreated vacuum gas oil (VGO) and

Sunflower oil mixtures were hydrocracked by Bezergianni et al. [96]. The authors observed that the conversion efficiency with pre-hydrotreated VGO is higher than non-hydrotreated VGO and VGO conversion efficiency increased with Sunflower oil (SFO) addition. 70/30 hydrotreated VGO/SFO mixture resulted in conversion of 17 wt. % of total mass, whereas, 90/10 hydrotreated VGO/SFO mixture resulted in conversion of 9Twt. % of total mass. With untreated VGO, 12 wt. % is converted with 70/30 VGO/SFO mixture and 6 wt. % is converted with 90/10 VGO/SFO mixture. At a maximum temperature of 390°C, the conversion efficiency approaches a maximum of 70% with 70/30 hydrotreated VGO/SFO mixture. However, the diesel selectivity is adversely affected by the temperature as the large molecules of diesel are cracked into lighter molecules with increase in temperature.

2.4.3. Effect of hydrogen pressure on production

For hydroprocessing the vegetable oil, the hydrogen plays a crucial role, therefore its consumption must be considered for economic evaluation of the process. Bezergianni et al. [90] varied the hydrogen pressure from 8.27 to 9.65 MPa for hydrotreating the WCO. At highest pressure, the maximum yield of 71.36% for diesel like fuel is obtained. Moreover, the yield of gasoline like fuel decreases with increase in pressure. It fell from 5.16% at 8.27MPa to 4.03% at 9.65MPa. Also the oxygen removal efficiency increases with increase in pressure. Nimkarde et al. [81] found that hydrogen pressure strongly affects the hydrogenation, isomerization and cracking reactions. The conversion of karanja oil increased from 60.1% at 1.5 MPa to 85.6% at 3 MPa over CoMo catalyst. Similar result was observed with NiMo catalyst (62.1% and 88.4%). The triglycerides deoxygenation and breaking of glycerol increases with increase in pressure but the operating costs also increases.

The hydrogen pressure was varied in the range of 2 to 8 MPa for hydrotreating a mixture of octadecanoic acid, octadecenoic acid and octadecadienoic acid (5: 77: 18 by weight) as well as an impurity (C_{16-20} fatty acids $\leq$ 3 wt. %) by Yang et al [70]. The authors found that C_{15-18} yield increases till 4MPa, further increase in pressure results in decrease in yield showing that the cracking reaction rate has slowed down. Also, the C_{17} yield reduces from 10.19% at 3MPa to 7.39% at 8MPa while C_{18} yield increased from 7.18% to 10.68%. C_{17} is formed via the HDCN/HDCX reaction route whereas C_{18} is formed via deoxygenation route. The HDO reaction is promoted since large amount of hydrogen is absorbed on the surface of the active sites. Krar et al. [69], Guzman et al. [62] and Anand et al. [111] also observed similar results. Yang et al. [70] also found that the isomerization reactions were reduced at high hydrogen pressure due to lower availability of active sites for the hydrocarbon molecules. Chen et al. [112] found that gaseous product formation is dependent upon both reaction temperature and pressure. At 0.4 MPa approximately 11% C_1-C_4 hydrocarbons, 3% CO_2 and 4% CO is observed. As the hydrogen pressure increases, the gaseous products percentage decreases. With reduction in temperature, the gaseous products further decreases. It can be concluded that at high temperatures due to cracking more gaseous products are formed but high hydrogen pressure inhibits the gaseous products formation.

While hydrotreating crude Palm oil, Palm oil fatty acid distillate and degummed Palm oil, Kiatkittipong et al. [64] observed maximum diesel yield at 40 bar using palm oil fatty acid. Moreover, the pressure has no effect on diesel yield with crude Palm oil and degummed Palm oil, whereas with distillate the yield is affected at higher pressures. This shows that the higher hydrogen pressure along with saturation of dissolved hydrogen pushed the reverse water gas shift reaction towards higher amount of CO formation. CO is a preferential surface adsorber which may deactivate the active sites

of the catalyst. It is also observed that the hydrogen consumption is less for fatty acid distillates as compared to crude and degummed Palm oil. Sotelo-Boyas et al. [91] found that 8-10MPa hydrogen pressure is required for liquid product formation, below 8MPa solid content containing high amount of carboxylic acid is detected. When zeolite catalyst was used, even higher pressures were required for liquid product yield. Sunflower oil and gas oil was co-processed over $NiMo/Al_2O_3$ catalyst incorporating 0, 15 or 30 wt.% zeolite beta (BEA) [71]. For all the catalysts, the conversion efficiency increased with increase in hydrogen pressure from 30 to 60 bar. NiMo-30BEA was the most active catalyst and nearly 93% conversion was observed at 30 bar. HDS activity decreased with vegetable oil addition to the gas oil due to water formation which suppresses the HDS-sites. The zeolites containing catalyst are more active in removing sulfur than alumina bas catalyst. 10% oleic acid addition to the blend also resulted in higher HDS activity, especially at higher pressures.

2.5. Hydroprocessed vegetable oil use in diesel engines

The hydrotreated oil can be used as a neat CI engine fuel, as a blend with commercial diesel or mixed with additives. Researchers have used oil produced by Neste oil refinery which sells the oil under the brand NExBTL. Researchers have tested the oil on bus fleet of Helinski Transport Company, various other buses, cars, and light duty vehicles on roads or by using Braunschweig cycle, NEDC cycle, European stationary cycle and other cycles. This section reviews fuel properties, spray characteristics, combustion, performance, and emission behaviour of HVO as a fuel.

2.5.1. Fuel properties

The density of the hydrotreated vegetable oil (HVO) is slightly lower than fossil diesel but is significantly lower than biodiesel. If an engine has same thermal efficiency with different fuels, then the consumption of fuel will be in direct relation with the

heating value of the fuel, i.e. fuel with lower heating value will be consumed more to produce the same power. HVO has a heating value of nearly 44MJ whereas for petrodiesel it is 43MJ. The cetane number of HVO is in the range of 84-99 as it is a mixture of normal and iso-paraffins. The higher the cetane number the lower is the ignition delay. High cetane number also improves the cold-start ability and reduces noise, white smoke and emissions [83]. For the improvement of cold flow properties, the presence of light hydrocarbons is necessary, however, HVO has limited carbon atom range (C_{15}-C_{18}). Therefore, it is difficult to improve the CFPP with cold flow additives used for petrodiesel. HVO can be isomerized to improve its cold flow behaviour and it is possible to achieve cloud points lower than -40°C [113]. The wax settling tendency of blends of isomerized HVO and diesel in the ratio of 90/10 & 80/20 diesel/iso-HVO was studied by Caprotti et al. [47]. The authors found that the wax crystals did not settle for iso-HVO20 even without adding wax anti-settling additives, due to the dilution effect of iso-HVO and high heat treat rate of the conventional cold flow additives used in the test.

The bulk modulus of compressibility of fuels, affect the start of injection in injection systems that do not operate under constant pressure. For example, a compressibility change of 10% in a pump-nozzle system can affect the start of injection by 0.5° crank angle (CA). If the compressibility of the fuel is less, then the pressure rise will be fast and maximum pressure will be higher [113]. The bulk modulus of compressibility of HVO is high at pressures varying from 5 to 15MPa and it is slightly lower at high pressures in comparison to petrodiesel [114]. A material compatibility study for using HVO as a fuel was conducted by Jaroonjitsathian et al. [115]. The authors found no effect of storing HVO in a zinc coated fuel tank by using a metal cup test. Similar results were obtained by Makinen et al. [45] who found the HVO to be clear even after storing

the fuel in a fuel storage tank for eight months. Due to the aromatic content of the fuel the rubber seals may swell. Since HVO has almost no aromatic content. Some changes in the seal should occur but field trials show that there is no issue with the seals.

2.5.2. Performance Characteristics

The research on spray characteristics with HVO is limited. The influence of spray characteristics with HVO on a common rail engine was studied by Sugiyama et al. [116]. The spray pattern, angle and Sauter mean diameter (SMD) are same for HVO and diesel. The authors also found 3-5% higher fuel quantity of HVO injected than petrodiesel at injection pressures varying from 40 to 200 MPa. However, there is no power loss with HVO even though the energy content on volume basis is nearly less than 5%. Hulkkonen et al. [117] also observed no change in spray pattern while using two orifice diameters of 0.08 and 0.12 mm and injection pressure of 45, 100 and 198 MPa. The authors also did not observe any difference in spray penetration for two orifice diameters, in a fuel injection test with the same injection duration. Bernoulli's equation can be used to explain this phenomenon which states that volume flow rate is inversely proportional to the square root of the fluid density [118]. As the HVO has lower density than diesel its flow rate will be approximately 4% higher. The fuel is pre-metered in the pump barrels of in-line pumps, distributor pumps or pump-nozzle injection systems. These system meter the fuel on volume basis and the quantity of fuel is not varied with change in density. Therefore, for the same amount of fuel less energy content enters the combustion chamber resulting in power loss [113].

The engine performance was compared with biodiesel, HVO and iso-HVO blends with petroleum diesel in various ratios [119]. The results show power loss at the maximum power with HVO, iso-HVO and biodiesel which increases with increase in blending ratio. At full power, biodiesel shows the worst power loss, whereas iso-HVO

shows the least power loss, since the heating value of biodiesel is lowest. The fuel consumption was also lower for HVO blends as compared to biodiesel blends. With the increase in blending ratio the fuel consumption increases with biodiesel whereas the fuel consumption decreases with increase in blending ratio of HVO and iso-HVO. Aatola et al. [120] also reported similar results during the heavy duty engine testing with NExBTL fuel. Makinen et al. [45] conducted a field test for fuel consumption using 11 buses representing EURO II to Enhanced Environmentally friendly Vehicles (EEV) emission certification. Neat HVO reduced the energy consumption by nearly 0.5% in comparison to summer and winter grade diesel, whereas the HVO volumetric consumption increased by 5.2 and 3.5%, respectively. On a chassis dynamometer the acceleration and traction power of the buses was also tested. Buses equipped with inline injection pump takes 17s with summer grade diesel and 18s with 100% HVO to reach 50km/h. The traction power at 50 km/hr is 115kW with diesel and 108 kW with 100% HVO. In the case of common rail injection buses, the buses reach 50 km/hr in 15s and traction power is 150kW.

A Toyota pickup truck was tested using 5% biodiesel and varying blends of iso-HVO in petrodiesel by Caprotti et al. [47]. As the blending ratio of iso-HVO increases the fuel consumption decreases. The cold start ability and drivability of the truck with HVO was also tested in the field. Iso-HVO tested was at least equivalent to base fossil fuel for both start ability and drivability. 20% of HVO blended in diesel can be used in the field with correct cold flow additives at an appropriate treat rate, and its behaviour is harm free in severe driving conditions. NExBTL was utilized by Sugiyama et al. [116] to study the effect of cetane number on combustion with single fuel injection. The ignition delay reduced with HVO due to its high cetane number resulting in lower combustion noise with energy consumption similar to fossil diesel. The rate of heat

release was advanced at low load condition resulting in improvement in combustion which is attributed to lower temperature at the start of injection. The difference in heat release rate and ignition delay is smaller between HVO and diesel fuel at medium load conditions. Moreover, at high load, the ignition delay with HVO is identical to diesel due to higher internal gas temperature at the start of combustion. The ignition delay is same with both the fuels with pilot fuel injection. As the pilot injection causes a rise in gas temperature at the start of combustion thus the difference in heat release rate for both the fuels was lowered at all loads.

A batch process as well as continuous process was used for hydrotreating canola oil derived fatty acids [121]. The tests were performed for jet fuel, biodiesel and baseline diesel. The experimental results show lower brake specific fuel consumption for renewable fuels and shorter ignition delay. With renewable fuels, the peak cylinder pressure is low, the rate of increase in cylinder pressure is low, and the heat release rate is low in comparison to diesel. At a brake mean effective pressure (BMEP) of 1.26 bar the biodiesel has the highest brake thermal efficiency and the renewable diesel made from batch process resulted in a drop of 8% in brake thermal efficiency. At a BMEP of 3.77Tbar the jet fuel has the highest thermal efficiency and the isomerized hydrotreated canola oil has 5% lower efficiency than jet fuel.

Imperato et al. [122] used HVO in large bore CI engines at low loads having marine applications. Miller timing was used to improve the combustion and simultaneously reduce NOx emissions. Up to 70°CA advancing was done for inlet valve timing and the scavenging angle was varied from -45 to 60°CA. With inlet valve timing of 50°CA (Miller timing) and scavenging angle of -30°CA the fuel consumption with HVO is similar to reference timing of 15°CA and 60°CA scavenging. If the scavenging angle is further reduced to -45°CA the fuel consumption shoots up to 230g/kWh. With 70°CA

Miller timing and various scavenging angles the consumption of fuel is almost constant and comparable to standard timing. If the inlet valve closing is more advanced the ignition of mixture is late. With 70°CA Miller timing, the ignition delay is 3°CA longer and the peak pressure is nearly four times higher than reference timing, resulting in creation of high temperature zones which increases the NOx emission. The effect of positive, negative and zero scavenging was also studied with the same Miller timing. The increased exhaust gas residuals resulted in lower peak pressure and earlier ignition. The peak of heat release rate is small in premixed combustion and the overall heat release is lower than positive scavenging. The authors concluded that at low loads, the Miller cycle is not beneficial as the delay in ignition is long and the combustion is not regular. Moreover, the presence of small amount of exhaust gas results in lower NOx emission, slightly higher soot and no penalty on fuel consumption. The same group [123] conducted similar study using high load condition. By implementing only Miller technique the NOx emissions reduced and the fuel consumption improved slightly. The only drawback is the use of high pressure air which means more performing turbocharger. As the Miller rate increases the ignition delay increases and the peak of premixed combustion also increases which makes the combustion less stable. With scavenging the cylinder pressure becomes more stable. 50°CA Miller timing and negative scavenging results in lower NOx emission but the fuel consumption increases. With 70°CA Miller timing, the emissions remain same and the fuel consumption increases by 13%.

2.5.3. Emission Characteristics

Many researchers have studied the emission reduction potential of HVO. The fuel produced by hydrotreating of Jatropha oil was utilized for evaluating the emission produced from a vehicle running on HVO using the thirteen mode European stationary

cycle [124]. The results were compared with Jatropha biodiesel as well. The NOx emissions increased by 26 and 77% with biodiesel and HVO, respectively. Oxygen presence and high degree of unsaturation of biodiesel has a synergistic effect on NOx emission leading to its increase. The CO and HC emission reduced by 16 & 27% and 16% & 41% for HVO and biodiesel, respectively. Since the biodiesel has high oxygen content the emissions reduced, whereas the combustion characteristics improved with HVO due to high cetane number.

Car A having unit injector, car B & C with common rail injection, car A&B with and without catalyst and car C with catalyst was tested with NExBTL blends with ultra-low sulfur diesel using European cycle [125]. As the HVO percentage increases in the blend, particulate matter, CO and HC emissions decreased. No tendency was observed in the formation of nanoparticle. Emissions such as benzene, aldehydes, PAHs, 1, 3-butadiene and mutagenicity decreased with HVO use. However, there was no clear indication on NOx emission reduction with cars. Westphal et al. [120] compared petrodiesel, Rapeseed methyl ester (RME), Jatropha methyl ester (JME) and HVO for their emission and bacterial mutagenicity. The study utilized EURO-III heavy duty diesel engine. The authors observed JME and RME have high mutagenicity whereas HVO has low mutagenicity due to small amount of PAHs produced during combustion. JME and RME engine operation resulted in lowest particulate matter emission. RME engine operations resulted in lower HC and CO emissions than JME. RME and JME engine operation resulted in NOx being higher than EURO III norms whereas HVO operation resulted in lowest NOx emission. NOx, CO, HC, and smoke emissions reduced with HVO without any modifications to the engine [126]. 6% lower NOx and 35% lower PM emissions with default injection timings were observed with HVO in comparison to diesel. When the authors brought the NOx level equal for both the fuels,

the smoke and specific fuel consumption reduced by 37% and 6%, respectively. When the SFC was kept constant, HVO engine operation resulted in NOx and smoke reduction of 16 & 23%, respectively in comparison to diesel.

Pflaum et al. [127] used a four-cylinder CRDi engine and measured the emissions using neat and blends of HVO and diesel on an engine dynamometer and chassis dynamometer. The authors observed reduction in smoke emissions by up to 50% with HVO at low loads due to no aromatic content, they also observed a reduction in particle size but the particle numbers did not reduce. The CO and HC emissions with HVO operation also decreased by nearly 50%. With engine dynamometer testing, the NOx emissions decreased slightly, whereas with chassis dynamometer testing no significant variations were observed. For the regeneration of the diesel particulate filter (DPF), high exhaust gas temperature is required to burn the soot particles collected on the DPF. This can be achieved by post-injecting the fuel which burns late in the power stroke. The injection strategy may result in the fuel hitting the cylinder walls thereby increasing the oil dilution. The authors found that the oil viscosity decreased, after four hours of testing at 1250rpm and 2bar BMEP with increase in HVO percentage, which can be attributed to increase in fuel consumption caused by lower volumetric heating value. The effect of HVO on DPF by testing a passenger car on a chassis dynamometer was studied by Kopperoinen et al. [128]. The soot accumulation rate was lowest with neat HVO and the regeneration of DPF did not start until the car completed 400km. The oxidation characteristics and structure of soot particles was compared between diesel and HVO by Happonen et al. [129]. The characteristics of the soot particles were same although the chemical composition of the soot particles for the two fuels was different. This shows that same after-treatment devices can be used with HVO.

Murtonen et al. [130] used five city buses and three engines to test Fischer-Tropsch oil (GTL), HVO and diesel. The blend of HVO and biodiesel is limited to 30% in diesel. The regulated emissions reduced for most of the cases with GTL and HVO as compared to diesel. 17 city buses with emission certification ranging from EURO II to EEV were tested with HVO by Erkkilam et al. [131]. The average reduction in emissions were 10%, 30%, 29% and 39% for NOx, PM, CO, and HC, respectively with neat HVO. The emission reduction with EURO II and EURO III buses were consistent whereas there was no significant emission reduction in new buses. With HVO, the particulate filter was more effective in comparison to diesel due to favourable NOx to PM ratio which is beneficial for PM reduction. Unregulated emissions were studied using three city buses. Two and three-ring hydrocarbons reduced by 55% with HVO and heavier compounds containing 4 or more rings were reduced by nearly 85%. Hajbabaei et al. [132] used a 2006 engine with no after-treatment and a 2007 engine with DPF for testing with soy and animal-based biodiesel and HVO with blends varying from 5 to 100%. With soy-based biodiesel, NOx emissions increases in the range of 3.9-6.9% for B20, 9.1-18.2% for B50, and 17.4-47.1% for B100 over all the engines and cycles. NOx emission increases in the range of 1.5-5.9% for B20, 6.4-16.3% for B50, and 14.1-39.4% for B100 over the range of engines and cycles for animal based biodiesel. With HVO, the NOx emissions reduced from 2.9%-4.9% for R20, 5.4%-10.2% for R50, and 9.9%-18.1% for R100 over all the cycles. The authors found that on blending biodiesel with CARB diesel fuels, the NOx is effected in comparison to conventional US average diesel at least at B20 or higher levels and some form of mitigation is needed for blending biodiesel with such fuels.

The impact of soy-based biodiesel, animal-based biodiesel, ULSD diesel, and renewable diesel on emissions using a truck with no after-treatment device was tested

on a chassis dynamometer by Na et al. [133]. NOx emissions increased by 10%/20% & 5%/14% for soy B50 (50% of soy biodiesel and 50% of ULSD)/B100 (neat soy biodiesel) and Animal B50 (50% of animal biodiesel and 50% of ULSD)/B100 (neat animal biodiesel), respectively for urban dynamometer driving schedule (UDDS) cycle. Increase in HVO proportion in the blend resulted in decrease in NOx emissions for UDDS cycle. Animal and soy based fuel showed significant reduction in PM emissions for all blends and cycles. Blends having HVO higher than 50% resulted in significant PM reductions. The PM reducing effect is higher with biodiesel in comparison to diesel. The difference in NO and CO emission was lower for HVO/biodiesel blend and CARB ULSD as compared to other regulated emissions.

The effect of blending renewable diesel and FAME with diesel in a passenger car using cold urban phase (UDC) driving cycle on exhaust emissions was studied by Prokopowicz et al. [134]. With the increase in biodiesel percentage in the blend the carbonyl compound emissions increased, however, the emissions decreased with HVO. The acetaldehyde and formaldehyde content is the highest among carbonyl compounds present in the exhaust gas. With the increase in biodiesel content, the emissions of heavy PAH increases. Moreover, the lighter PAH emission increases with HVO blends and pure diesel resulted in increase in nitro-PAH emission. The authors also observed decrease in nitro-PAH emission with biodiesel blend in comparison to HVO blends.

By changing engine parameters or by using additives the engine emissions can be reduced and the engine performance can be improved. Engine setting such as inlet valve closure, inlet timing, injection pressure and EGR were optimized to reduce the emissions [46]. Additive di-n-pentyl ether was also added to HVO. Optimized engine settings for HVO led to reduction in PM and NOx emissions by 41-61% and 31-54%, respectively. The PM emissions decreased with oxygenate and HVO without affect the

NOx emissions, however, the aldehyde emissions increased for some conditions. Happonen et al. [135] also utilized DNPE with neat HVO and blend of 80% HVO with 20% DNPE using a single cylinder research engine. The blend resulted in 25% reduction in PM emissions in comparison to neat HVO, whereas the NOx emission increase is below 5% with neat HVO. NOx and PM emission can also be reduced by utilizing EGR. The hygroscopic nature of the smoke particles by the use of blends was also studied. Due to the combustion of the oxygenate blend, the hygroscopicity of the particles was higher than neat HVO. The authors attributed this trend to the increased organic matter in the exhaust gas which fills some of the cavities of the agglomerated structure of the exhaust particles. Miller timing and EGR was used in a high speed diesel engine by Lehto et al. [136] for reducing NOx emissions. The PM emissions are low with HVO operation in comparison to diesel. To keep the same PM emission level as diesel, high EGR rates (above 20%) can be used with HVO to further reduce the NOx. Miller timing along with advanced injection timing can simultaneously decrease NOx and PM emissions. An optimization study was also conducted by Happonen et al. [137] using a single cylinder diesel engine. By adjusting the engine parameters, the PM and NOx emission reduction was explored for medium to full load. Intake valve closing, injection timing, injection pressure and EGR percentage was varied in the study. Nearly 25% reduction in NOx and PM emission was observed by adjusting engine parameters at all loads.

2.6. Waste cooking oil biodiesel use in a diesel engine

Long chain fatty acid methyl esters produced by the transesterification of vegetable oil are also known as biodiesel. The production of biodiesel takes place in the presence of a homogeneous or a hetergenous catalyst [138]. Although high yield of biodiesel can be obtained by the homogeneous catalyst, it is not economically viable. Since,

expensive chemicals are required, the purification process is complex and the byproducts of the process needs to be safely discharged [139]. Therefore, solid heterogeneous catalyst are strongly recommended for production of biodiesel. The advantage of heterogeneous catalyst are low cost of fabrication, easy separation from liquid phase and recyclable [140]. Zeolite minerals with a functionalized acidic or basic group on their surface have achieved high catalytic performance and realistic biodiesel yields [141,142]. Calcium oxide derived from the eggshells have also achieved higher biodiesel yields [143].

Abed et al. [144] utilized blends of waste cooking oil biodiesel and diesel in a single cylinder diesel engine and studied the engine's performance and emission. The authors observed lower thermal efficiency with the blends in comparison to diesel and the specific fuel consumption of the engine was higher with the blends. The authors observed low CO, smoke and HC emisions with the blends of biodiesel and diesel in comparison to diesel. Moreover, the CO_2 and NOx emissions were higher for the blends in comparison to diesel and as the percentage of the biodiesel increases in the blend, the emissions increases. Wei et al. [145] investigated the effect of the blends of diesel and used cooking oil biodiesel on performance and unregulated emissions using Japanese 13-mode test cycle. The authors observed higher in-cylinder pressure, but lower heat release rate along with early start of combustion. The authors attributed the early start of combustion to higher viscosity and bulk modulus of biodiesel which causes the fuel injection to start earlier. The weighted brake specific emissions of ethene, propene acetaldehyde, formaldehyde, 1, 3-butadiene and benzene were found to increase with biodiesel blends. The probable reason for the observation is the pyrolysis of the long chain molecules in higher pressure and temperature environment. The particle mass concentration, total number concentration and geometric mean

diameter of the particles in the exhaust gas when the engine was operating with biodiesel blends were lower than diesel on account of higher oxygen content that promotes oxidation of the particles. Yesilyurt [146] used blends of waste cooking oil biodiesel and diesel for studying the effect of different fuel injection pressures on the performance and emission of a diesel engine. The author observed that increase in injection pressure to 210 bar resulted in increase in brake power, torque and thermal efficiency with the blends of biodiesel. Decrease in smoke opacity, unburned hydrocarbon emission and increase in CO_2 and NOx emission with the blends was also observed. Kuti et al. [147] simulated the spray combustion characteristics of waste cooking oil biodiesel and diesel using Converge CGD code. The authors found that the experimental data and the simulation data are in agreement at all injection pressures. The authors found from simulation that a cool flame ignition took place before main ignition in which formaledehyde was formed, whereas in the main ignition process, OH radicals were formed. Increase in injection pressure resulted in lower interaction between the spray and the flames. Moreover, the spray flame interaction in waste cooking oil was higher than diesel at all injection pressures. The waste cooking oil resulted in lower smoke formation due to the oxygen content in the fuel. Ternary blends of waste cooking oil biodiesel, propanol and diesel were prepared by Bencheikh et al. [148]. The authors found that addition of propanol resulted in improvement in cold flow properties and decrease in density of the blends. The engine test reveals that propanol addition resulted in increase in energy consumption, and decrease in HC, CO, NOx and smoke emissions.

2.7. Summary

The research work carried out in the past decades on hydroprocessing the vegetable oil was discussed in this chapter. The HVO can be produced from various feedstocks.

It can be used in neat form or blended in biodiesel/diesel and fulfil the bio-mandate without any form of restrictions. The review also discusses the effect of HVO on engine performance and emission. The main conclusion drawn from the review are:

- Diesel selectivity is based mainly upon the type of catalyst and the reaction temperature used. At high temperatures, cracking of the product occurs and the selectivity of diesel is reduced. At high hydrogen pressure the selectivity of diesel is high and less gaseous products are formed but the isomerization process is inhibited.

- When mild hydrocracking of vegetable oil is done, diesel range of products with high cetane index is produced. However, the low temperature properties are poor due to the presence of normal paraffins. The catalytic activity is also affected as the fatty acids present in vegetable are corrosive.

- Co-processing the vegetable oil with petroleum feedstock in small quantities can improve the yield of products. The low-temperature property of the fuel is significantly improved by co-processing as more vegetable oil is added to the blend.

- Since the cetane number of HVO is high, its start of combustion is advanced in medium and low loads, but the influence of cetane number is less at high loads. High cetane number is helpful in increasing the cold-start ability, reducing emissions, noise and white smoke.

- The fuel penetration, size of droplet, and spray angle are same for both HVO and diesel.

- The fuel consumption of an engine with HVO is higher than diesel due to its lower density which tends to reduce the volumetric heating value by 4 to 5%.

- PM, NOx, HC and CO emissions were reduced in heavy duty engines and passenger cars when operated with HVO. The unregulated emissions were also lower.

- In comparison to FAME, engine oil dilution with neat HVO is less as it is chemically compatible with oil.

2.8. Research Gap

On the basis of the exhaustive review of literature, the following research gaps were found.

1. So far, the catalyst used for hydrotreating is a commercial catalyst which is successful in heteroatoms removal but is not fit for the hydrotreating of the biomass based oil.

2. Limited vegetable oils have been utilized for producing diesel like fuel via hydrotreating process technology.

3. Work on testing of fuel for vehicle application is limited, most of the work done is based on European driving cycle conditions and that too with limited vehicles.

4. No work so far is done on use in agricultural engines using steady state cycles.

2.9. Objectives

The following research objectives are envisaged for the present research work.

1. Selection of a suitable catalyst for the process.

2. Selection of a suitable oil for the production of the renewable diesel.

3. Analyzing the properties of the oil produced from the hydrogenation process.

4. Study of effect of various parameters viz. reaction temperature, hydrogen pressure, and reaction time on diesel selectivity.

5. Production of diesel in large quantities using the parameters which gives the maximum diesel selectivity.

6. Comparison of microscopic characteristics of the hydrotreated oil with diesel.

7. Performance, combustion and emission characteristics of a diesel engine using the produced renewable diesel and its blends with diesel/biodiesel in various proportions.

CHAPTER 3
EXPERIMENTAL TECHNIQUES AND TEST PROCEDURES

3.1. Introduction

The basic principles and methodologies used in the present study are described in this chapter. Initially a non-edible oil was identified for the hydrogenation process. Using a suitable catalyst, hydrogenation of the non-edible oil was carried out at different reaction conditions. The reaction parameters were optimized using Taguchi method and Fuzzy logic. With the optimized reaction parameters, the diesel like fuel was produced in large quantities. Comprehensive physico-chemical characterisation of the obtained fuel was carried out. The engine test rig for the engine trials was developed and is described in detail. Blends of the obtained diesel like fuel with diesel/biodiesel were prepared and tested on the developed engine test rig. The procedure for carrying out the engine tests and calculation of heat release rate and mass fraction burnt is also described in the chapter. Lastly, the uncertainties in measurement and the instrument accuracy are also reported. Fig. 3.1 briefly describes flow of the research.
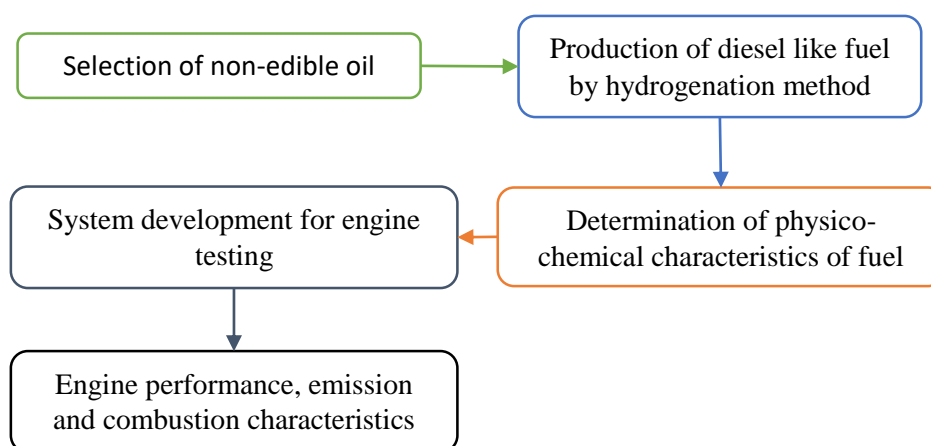
Fig. 3.1 Flow process of the research

3.2. Diesel like fuel production

The waste cooking oil was hydrotreated in a 100ml batch reactor (Amar Equipments) with a maximum pressure and temperature of 100 bar and 450°C,

respectively, the reactor is shown in Plate 3.1. An electric heating mantle along with water flowing through a cooling spiral was used for controlling the temperature of the system. The contents of the reactor were stirred at 1200rpm by a motor operated impeller. The temperature of the reactor was measured and controlled by a PID programmable controller. The schematic of the experimental setup is shown in Fig. 3.2.

The reactor was filled with 20g of waste cooking oil and catalyst was added. The reactor was tightly closed and purged with nitrogen gas. Then the reactor was pressurized with hydrogen at room temperature. The reactor was heated to the required temperature at the rate of 18°C per minute. The pressure during the entire experiment was kept constant by continuously feeding hydrogen. After the reaction time, the reactor was cooled to ambient conditions. The pressure was recorded and the gases were vented by bubbling through water. The liquid product was recovered with the help of a syringe and then weighed. Acetone was added for rinsing the reactor. Then all the solid products along with acetone were filtered, dried and their weight was recorded. The amount of solids subtracted from the initial catalyst amount added was considered as the solids formed during the hydrotreating reaction. The contents of the liquid sample were observed through a gas chromatograph equipment, explained later in the section. The literature study shows that different parameters have different effect on the reaction. Therefore, in this work, the effect of reaction temperature, initial hydrogen pressure, and reaction time on the conversion efficiency and diesel-like fuel selectivity was studied. The range of the parameters was selected according to [149,150]. Table 3.1 shows the process parameters and their range for carrying out the hydrotreating process. The performance of the reaction was evaluated by studying the conversion percentage, diesel like fuel selectivity and naptha (gasoline like fuel selectivity). The parameters were calculated using equation 3.1, 3.2 & 3.3.

Plate 3.1 Test Setup for fuel production

Table 3.1 Process Parameters and their range

Process Parameter	Range
Reaction Temperature (°C)	330 – 390
Reaction Pressure (bar)	30 – 50
Reaction Time (minutes)	80 – 200
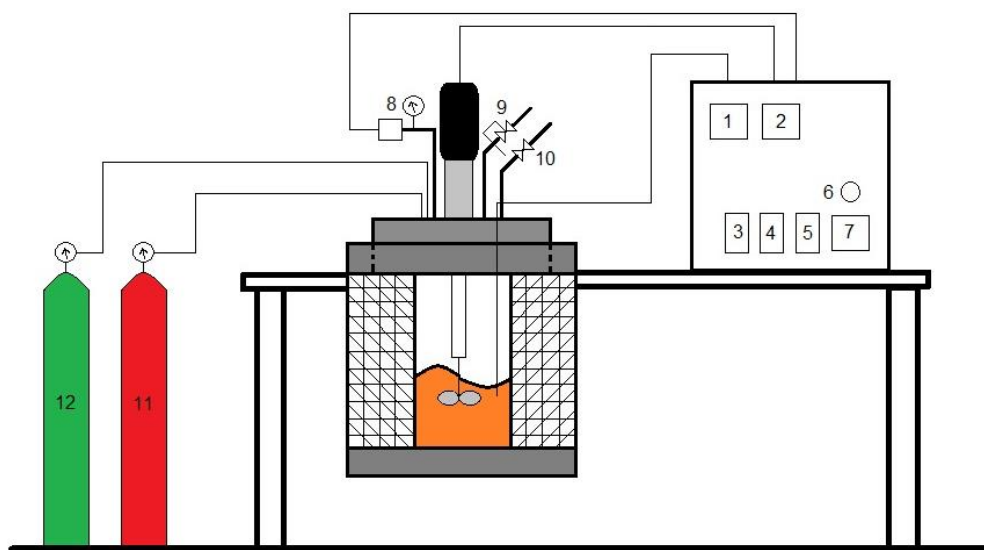
(1) Temperature indicator and controller; (2) Pressure Indicator; (3) Heater Switch; (4) Motor Switch; (5) coolant switch; (6) motor speed controller; (7) motor speed display; (8) pressure sensor; (9) safety valve; (10) purging /gas collection line; (11) hydrogen cylinder; (12) nitrogen cylinder

Fig. 3.2 Schematic of the setup for fuel production

$$\text{Coversion (\%)} = \frac{\text{Initial Oil}_{360+} - \text{Final Product}_{360+}}{\text{Initial Oil}_{360+}} * 100 \qquad (3.1)$$

$$\text{Diesel like fuel Selectivity (\%)} = \frac{\text{Final Product}_{180-360} - \text{Initial Oil}_{180-360}}{\text{Initial Oil}_{360+} - \text{Final Product}_{360+}} * 100 \qquad (3.2)$$

$$\text{Naphtha Selectivity (\%)} = \frac{\text{Final Product}_{40-200} - \text{Initial Oil}_{40-200}}{\text{Initial Oil}_{360+} - \text{Final Product}_{360+}} * 100 \qquad (3.3)$$

Initial oil$_{360+}$ and final product$_{360+}$ are the liquid feed and the product percentage having boiling point higher than 360°C. Initial oil$_{180-360}$ and final product$_{180-360}$ are the feed and product percentage having boiling point in the range of 180-360°C. Similarly, initial oil$_{40-200}$ and final product$_{40-200}$ are the feed and product percentage having boiling point in the rangeTofT40-200°C.

3.3.Optimization of the production process using Taguchi Method

Fisher [151] was the first researcher to develop experimental design methods [152]. However, these methods cannot be easily used and they are too complex. Also, with the increase in number of process parameters, the quantum of experiments to be carried out increases. Therefore, Taguchi designed orthogonal arrays so that all the process parameters can be studied but only a limited number of experiments needs to be carried out. The orthogonal array can be selected on the basis of number of degrees of freedom, which is determined by the number of factors and number of levels in each factor. In the present work, three factors and three levels of each factor was considered based on Table 3.1. Table 3.2 shows the factors and their levels. Based on the factors and levels an L$_9$ orthogonal array was selected, shown in Table 3.3. Then the main factors and the levels are placed in the various columns. After, designing the testing strategy, the tests were carried out randomly.

In the Taguchi method, a signal-to-noise (S/N) ratio is calculated using the experimental results. The ratio measures the deviation in the parameters from their expected values. For analysing the S/N ratio, the performance characteristic is categorized into three categories namely, the nominal-the-better (NTB), the larger-the-better (LTB) and the smaller-the-better (STB). The S/N ratio for LTB and STB is

calculated using equation 3.4 and 3.5, respectively. Using the S/N ratio, the optimal

condition is determined and the influence of individual factors is also studied.

Table 3.2 Factors and their levels

Factors	Level 1	Level 2	Level 3
Reaction Temperature (°C)	330	360	390
Reaction Pressure (bar)	30	40	50
Reaction Time (minutes)	80	140	200

$$\frac{S}{N} = -10log_{10}\left[\frac{1}{n}\sum_{i=1}^{n} y_i^2\right] \qquad (3.4)$$

$$\frac{S}{N} = -10log_{10}\left[\frac{1}{n}\sum_{i=1}^{n} \frac{1}{y_i^2}\right] \qquad (3.5)$$

Where y_i is the value of the performance characteristic measured during the trial, n is

the number of tests in a trial and the S/N ratio has a unit of dB.

Table 3.3 Experimental layout using an L_9 orthogonal array

Test Case	Reaction Temperature (°C)	Reaction Pressure (bar)	Reaction Time (minutes)
T1	1	1	1
T2	1	2	2
T3	1	3	3
T4	2	1	2
T5	2	2	3
T6	2	3	1
T7	3	1	3
T8	3	2	1
T9	3	3	2

3.4. Production of used cooking oil biodiesel

The waste cooking oil collected from the cafeteria of Delhi Technological University

was used to produce biodiesel through the transesterification route. The method used

for the production of biodiesel was similar to the one given by Sidharth and Kumar

[153]. A batch type reactor was selected in which 1L of the sample was heated at 60°C

with a continuous stirring of 300rpm. From the preliminary studies, the optimum

methanol to oil ratio and NaOH concentration was found from to be 5:1 and 0.5% on

weight basis, respectively. Both the chemicals were mixed separately and stirred till

NaOH completely dissolves in methanol. The used cooking oil was first filtered to remove impurities and then heated for removing the moisture content. The temperature of the used oil was then brought down to 60°C and then the mixture of NaOH and methanol was added. After 1 hour, the reactions were complete as the mixture became transparent. In a separator the resultant mixture was allowed to settle for 10-12 hours. Two layers were visible after the settlement period, the lower layer contained glycerol and the upper layer contained the waste cooking oil biodiesel. Both layers were separated and the biodiesel was washed with water for removing the excess of the catalysts. The biodiesel was then heated above the boiling point of water for removing the left over water. The yield of the biodiesel through this process was nearly 90%.

3.5. Test fuels used

The HVO obtained from the hydrogenation process was blended with diesel in various proportions. The present study considered 10%, 20%, 30%, 40% and 50% blends of HVO in diesel. The test fuel samples were prepared on volume basis i.e. in a one litre of the test fuel, say 100ml of HVO was added to 900ml of diesel resulting in the formation of 10% blend of HVO in diesel. Similarly other blends were formed. The prepared fuel samples are shown in Plate 3.2. Blends of the hydrotreated oil, biodiesel and diesel were also prepared. The nomenclature and composition of various test fuels is shown in Table 3.4. The blending of the sample was carried out by rigorous agitation at high speed using a hand blender. The test samples were monitored for 60 days for homogeneity and phase separation. No signs of separation were observed.

Plate 3.2 Fuel Samples

Table 3.4 Composition of various test fuels and nomenclature

Test Fuel Composition	Nomenclature
100% Diesel	D100
100% HVO	H100
10% HVO and 90% Diesel	H10D90
20% HVO and 80% Diesel	H20D80
30% HVO and 70% Diesel	H30D70
40% HVO and 60% Diesel	H40D60
50% HVO and 50% Diesel	H50D50
20% HVO, 5% Biodiesel and 75% Diesel	H20B5
20% HVO, 10% Biodiesel and 70% Diesel	H20B10
20% HVO, 15% Biodiesel and 65% Diesel	H20B15
30% HVO, 5% Biodiesel and 65% Diesel	H30B5
30% HVO, 10% Biodiesel and 60% Diesel	H30B10
30% HVO, 15% Biodiesel and 55% Diesel	H30B15

3.6. Test methods for determination of physico-chemical characteristics

Determining the properties of the test samples is important for a better understanding of the trends obtained during the engine trials. Therefore, 500ml of the test samples were prepared for finding the physico-chemical characteristics of the fuel. In the subsequent sub-sections, the various properties of the fuel and their test methods is described.

3.6.1. Density

The density of the test fuels was measured using an Anton Paar density meter, model DMA 4500. Plate 3.3 shows the test equipment. The instrument measures the specific gravity of the test fuel in accordance with the ASTM D-4052 standard. The

temperature set for measuring the specific gravity is fixed at 15°C. First toluene is used to rinse the test fuel line by injecting 10ml of it through the sample injection port. Then 10ml of the test sample is injected through the same port. The same sample was checked thrice for repeatability which was found satisfactory. The three readings were averaged and was taken as the final value.

Plate 3.3 Instrument used for finding the density

3.6.2. Kinematic Viscosity

A Petrotest make viscometer, shown in Plate 3.4 was used for the measurement of the kinematic viscosity of the test samples. The viscosity of the samples was measured at 40°C as per the ASTM D-445 standard. A capillary tube having a lower level and an upper level mark was filled with the test sample. The time taken for the fuel to flow from the upper level mark to the lower level mark was measured using a stop watch. The kinematic viscosity of the sample was calculated by multiplying the time in seconds with the capillary constant. The formula used for finding kinematic viscosity is given by equation 3.6.

$$v = k * t \qquad\qquad (3.6)$$

Where k = 0.005675mm^2/s^2, t is in seconds and v is the kinematic viscosity in mm^2/s.

Plate 3.4 Instrument used for finding the kinematic viscosity

3.6.3. Calorific Value

The calorific value of a liquid fuel is measured using an isothermal bomb calorimeter. The calorific value is the amount of heat released by the combustion of a certain amount of fuel in the presence of oxygen. In the present work, a Parr 6100 oxygen bomb calorimeter, shown in Plate 3.5, was used which works in accordance with the ASTM D-240 standard. A certain amount of fuel is filled in the crucible which is then placed in between the electrodes. To complete the circuit a nichrome wire is placed in the ends of the electrode and the wire is dipped in the fuel. The electrodes are then placed in the bomb and they are tightened completely which is now filled with oxygen. The bomb is then placed in the bucket containing water and the whole setup is kept in the calorimeter which then calculates the calorific value.

Plate 3.5 Instrument for finding the calorific value

3.6.4. Flash Point

Flash point of the fuel is the minimum temperature at which the vapours of the fuel when mixed with air forms an ignitable mixture that gives a momentary flash when a small flame is brought near it. The flash point was measured using a Pensky Martens Automatic Flash Point Apparatus made by Dott Gianni Scavini and Co. as shown in Plate 3.6. The instrument works in accordance to ASTM D-93 standard. In this method, the sample is placed in a test cup which is heated at a specified rate with continuous stirring. A small flame is directed to the cup at regular intervals with the interruption of stirring. The flash point is the lowest temperature at which the vapours formed above the sample ignite momentarily when a test flame is brought near the cup.

Plate 3.6 Instrument for measuring the flash point

3.6.5. Distillation

The distillation of 100ml of the test sample is carried out according to ASTM D-86 test method. The instrument used for the distillation process is shown in Plate 3.7. The sample is placed in a distillation flask and under prescribed conditions the distillation is carried out. The temperature at the instant of the first drop of the condensate falling from the lower end of the condenser is observed. At specified intervals, the temperature of the condensate against volume of condensate is measured. Also the maximum temperature at which all the fuel is condensed is also recorded.

These observed temperature readings are then corrected against normal atmospheric pressure.

Plate 3.7 Instrument for the distillation of the test fuels

3.6.6. Cetane Index

The cetane index is determined as per the calculations given in ASTM D-4737 which requires density and boiling point temperatures of the test fuel. It is useful when the test engine is not available or the sample quantity is low. It is calculated according to the equation 3.7.

$$CI = 45.2 + 0.0892 * T_{10N} + (0.131 + 0.901 * B) * T_{50N} + (0.0523 - 0.42 * B) * T_{90N} + 0.00049 * ((T_{10N})^2 - (T_{90N})^2) + 107 * B + 60 * B^2$$

$$(3.7)$$

Where

$$T_{10N} = T_{10} - 215 \qquad (3.8)$$

$$T_{50N} = T_{50} - 260 \qquad (3.9)$$

$$T_{90N} = T_{90} - 310 \qquad (3.10)$$

T_{10} is 10% (V/V) distillation recovery temperature in °C

T_{50} is 50% (V/V) distillation recovery temperature in °C

T_{90} is 90% (V/V) distillation recovery temperature in °C

$$B = [\exp(-0.0035 * D_N)] - 1 \qquad (3.11)$$

$$D_N = D - 850 \tag{3.12}$$

D is the density at 15°C, in kg/m^3

3.6.7. Cloud point

The temperature at which a test sample upon cooling forms a cloud of wax crystals first is called cloud point. Pour point is another measure of the low temperature performance of fuels. It is the lowest temperature at which the fuel sample can flow. The pour point also has implications on the handling of fuel during cold weather conditions. It tells about the pumping ability of the fuel. The cloud point is measured using a Koehler make instrument given in Plate 3.8. Cloud Point is determined by ASTM D-2500 test methods. For determining the cloud point, the sample is cooled at a specified rate and periodically examined. The temperature at which the bottom of the jar becomes cloudy or hazy is recorded as cloud point.

Plate 3.8 Instrument for finding the cloud point

3.6.8. Cold Filter Plugging Point

The minimum temperature at which the fuel cannot flow through the fuel filter is known as cold filter plugging point (CFPP). The test is carried out in accordance with ASTM D-6371 standard test method. The instrument used for measuring the CFPP is shown in Plate 3.9, it is manufactured by Linetronic technologies. The sample was cooled in a bath at -34°C and vacuum was maintained for the fuel suction in a capillary connected to a filter of 10 microns. The fuel is allowed to come to the filter through the

capillary and fall back after passing through the filter, the process should be finished within 60 seconds. The procedure is carried out for every degree fall in temperature. The temperature at which the fuel fails to complete the process within 60 seconds is the cold filter plugging point of the fuel.
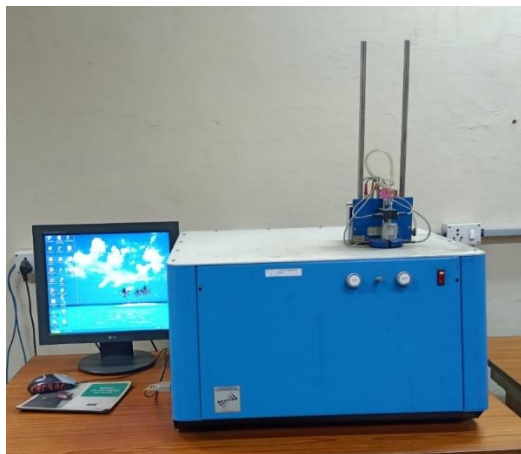
Plate 3.9 Instrument for finding the cold filter plugging point

3.6.9. Lubricity

Friction is always present between surfaces moving relative to each other. A lubricant can reduce the friction between the surfaces. The fuel injection pump in a diesel engine can be lubricated only by the fuel. Therefore, the fuel has to have some lubricity. A High-Frequency Reciprocating Rig (HFRR) (Plate 3.10) can be used to measure the lubricity of a fuel. The test method for finding the lubricity is given in ASTM D-6079 standard. In this test, 2ml of the sample is placed in the reservoir and maintained at a standard temperature. A vibrator arm holds a non-rotating steel ball. The arm is loaded with a 200gm weight. The arm is then lowered until it comes into contact with a test disk which is submerged in the test fuel. The arm vibrates with a 1mm stroke at a 50Hz frequency for 75 minutes causing the ball to rub against the disk. The dimensions of the wear scar formed is measured under 100x magnification and recorded. The size of the wear scar is the measure of the lubricity of the sample.

Plate 3.10 Instrument for finding the Lubricity

3.6.10. Fourier Transform Infra-Red (FTIR) Spectroscopy

It is a study of the interactions between the matter and electromagnetic fields in the infrared (IR) region. The spectrum obtained represents the molecular absorption and transmission of the infrared rays. If the photon energy of a particular frequency is similar to the vibrational energy of the molecule then its probability of being absorbed is high. The rest of the frequency may pass through the sample without being absorbed thus providing a spectrum. IR spectroscopy is therefore a powerful technique in creating a molecular fingerprint of the sample.

Thermo Fisher Scientific make, Nicolet 380 model was used in the present study for carrying out the FTIR analysis of the test sample. The instrument is shown in Plate 3.11. The instrument is a Fourier transform infrared spectrometer wherein a beam of IR radiation is split into two components which after passing through an optical system produce an interference pattern on recombination.

Two parallels beams after passing through an opaque mirror, splits into two. Half of the split beam moves to the movable mirror and half is passed to the fixed mirror. The fixed mirror send the beam back, whereas the moving mirror reflects a portion of the light to the splitter. When the two reflected beams are recombined at the splitter, they interfere either constructively or destructively depending upon whether they are

out-of-phase or in-phase. This situation depends upon the position of the moving mirror when the reflection is occurring. The result is an interference pattern, or inter-ferrogram, which can be subsequently Fourier transformed mathematically on a micro-computer to produce an IR spectrum.

A compound's IR spectrum can be obtained in a matter of seconds. First the spectrum of the optical path is obtained in the absence of a sample to understand the associated background, then the sample is positioned in the beam path to find its spectrum. The resulting, co-added inter-ferrograms of the sample and the background are then Fourier transformed thereby producing the desired FTIR spectrum.

Plate 3.11 Infrared spectroscopy test setup

3.6.11. Gas Chromatograph and Mass Spectrometer (GC-MS)

The most widely used method for finding the chemical composition of the volatile organic mixtures is gas liquid chromatography. A capillary column which is essentially a flow through thin tube is used in the apparatus. In a gas medium different components of the sample are passed through the column at different rates based upon their physical and chemical properties. The mobile phase for carrying the sample through the column is an inert gas namely nitrogen or helium. An immobilized stationary phase is also present in the column. A liquid is immobilized on the surface of a solid support by either adsorption or by chemical bonding to form the stationary phase. The gaseous

phase and the immobilized liquid phase separates the sample into individual components by distributing between them. Due to the discretization of the components by the immobile phase, they exit the column at different time. Hence they can be easily recognized electronically.

The GC setup consists of a carrier gas cylinder with regulator, a flow controller for the gas, an injection port for introducing the sample, the column, the detector and the recorder. The injection port, column and detector are heated to a pre-specified temperature. As the mobile phase is a gas, the components of the sample should be in vapour form so that they can be easily carried through the column. To successfully find the components of a mixture through this technique the selection of appropriate column and the correct temperature of the components is necessary. In the mass spectrometer, the components of the gas is converted into ions and then measured.

In the present study, a Shimadzu QP – 2010 instrument equipped with Agilent DB-2887 column with a flame ionization detector was used. Plate. 3.12 shows the instrument. 0.1µl liquid samples were injected and the injector temperature was maintained at 350ºC. A programmable temperature controller with a ramp rate of 15ºC/min was used to maintain the oven temperature. The test procedure was in accordance to ASTM D-6584 test standard.

Plate 3.12 GC-MS test setup

3.7. Hot plate test setup

In the present work, a hot plate test method was used for understanding the ignition delay. In this method a droplet of fuel is dropped in the middle of the plate heated to a fixed temperature and the time taken for the fuel to evaporate is measured. The schematic of the experimental setup is shown in Fig. 3.3. A steel plate having 152mm diameter and 8mm thickness was used in the present work. The plate was heated by a nichrome wire electrical heater. The plate temperature was measured using a k-type thermocouple. To change the temperature given by the electrical heater, the voltage supply to the heater was varied using a variac. The plate was directly placed above the heater and to minimize the heat loss to the surroundings, the empty space between the heater and the plate was filled with glass wool. The centre of the plate had a small concave depression so that the droplet stays in the middle of the plate. A pipette placed 20mm above the steel plate was used to drop the fuel droplet on the plate's centre. The distance was so chosen such that the flame produced on the plate doesn't ignite the fuel present in the pipette, another reason was the droplet not breaking off while falling from the pipette. The droplet average size was determined on the basis of the number of droplets generated for a specified fuel volume. The average droplet size was 2.6mm and the size was same for all the test samples.

For finding the evaporation time, ten tests were carried out with each fuel sample and three readings were taken for each surface temperature. The temperature was varied from 150-600°C. In the ignition delay test, after dropping the fuel droplet two events namely no ignition of droplet and droplet ignition was recorded. Ten readings were taken at a particular temperature and averaged. The temperature for the test was varied from 280 to 640°C in steps of 20°C. Time (in seconds) was measured from the moment the drop landed on the plate till it ignited. A camera with 90 frames per second was

used for finding out the time. The steel plate was glazed after every experiment using a sand paper of 90 grit size. The test were performed in a closed room at atmospheric pressure. The environmental conditions such as atmospheric pressure, temperature and fuel temperature play an important role in the experiment. Therefore, in this study these conditions were kept constant.
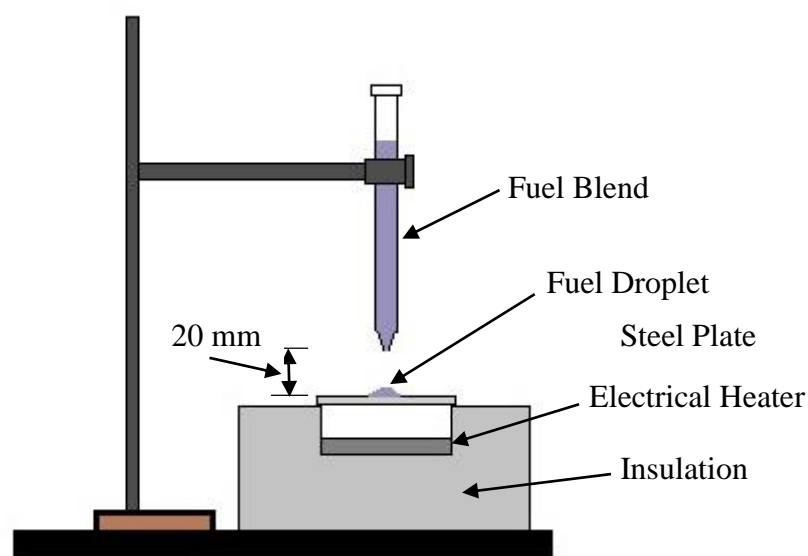
Fig. 3.3 Schematic of hot plate test setup

3.8. Test for finding the average particle size of the fuel spray

The atomization of the fuel plays a major role in its combustion. The atomization is affected by the fuel injection pressure, density and viscosity of the fuel. If the fuel's viscosity is low and if the injection pressure is high then very fine particles will be formed during the spray. These fine particles reduce the ignition delay due to high surface area. However, the penetration of these particles will be low as they have less momentum and low velocity relative to air resulting in reduced utilization of air. As a result during the diffusion combustion phase, the heat release will be more and more pressure rise will take place. Whereas with larger droplet size and low injection pressure, the pressure rise is low during the second stage of combustion and the engine runs smoother. Therefore, it is necessary that the particle size is optimum for efficient

running of the engine [154]. The average particle size of the fuel spray can be measured using a laser diffraction system. In the present work, Spraytec made by Malvern was used to measure the Sauter mean diameter (SMD) of the fuel spray. Its specifications are given in Appendix – I.

The system works on the principle of laser Doppler Effect, wherein the particles are passed through a laser beam and the scattering of the beam caused by the particles is predicted. From one end of the analyser the beam is projected and the other end receives the beam. Plate 3.13 shows the Malvern Spraytec instrument. The particle is considered to be spherical in shape and based on the scattering pattern its size and concentration is determined. An injection system was developed for spraying the fuel in between the laser beam. The system comprises of a fuel tank wherein the test fuel sample is stored, shown in Plate 3.14. A high pressure fuel pump takes the fuel from the tank and pumps it to a common rail. The high pressure pump is operated by a motor through a v-belt, shown in Plate 3.15. The injector was connected to the common rail through a high pressure fuel line. The fuel injector has three holes, two of which were closed so that the fuel could be sprayed through a single hole. Plate 3.16 shows the injector used for the experiment. The opening pressure of the fuel injector was fixed at 200bar throughout the experiments. The pressure was so chosen because the engine used in the present study operates on the same injection pressure. Fig. 3.4 shows the schematic of the test setup. The experiments for each test fuel was repeated five times and the values were averaged. Throughout the experiments the distance between the injector and laser beam was fixed at 60mm. The data was collected for 200ms although a single injection lasted about 12ms. The data reported in his work is displayed at 6ms, so that a clear comparison can be made of the droplet distribution in the middle of the injection. To minimize the effect of sunlight, the tests were carried out in a low-light

room at atmospheric conditions. These conditions were chosen since the primary atomization of the fuel needs to be studied. The primary atomization is dependent upon the fuel properties, the geometry of the injector and the density of air in which the fuel is sprayed. Since the injector geometry and air density is constant, the fuel properties will play a major role in the fuel spray characteristics.

Plate 3.13 Malvern Spraytec instrument

Plate 3.14 Fuel tank for the setup

Plate 3.15 Fuel pump connected to the motor

Plate 3.16 Injector used in the setup
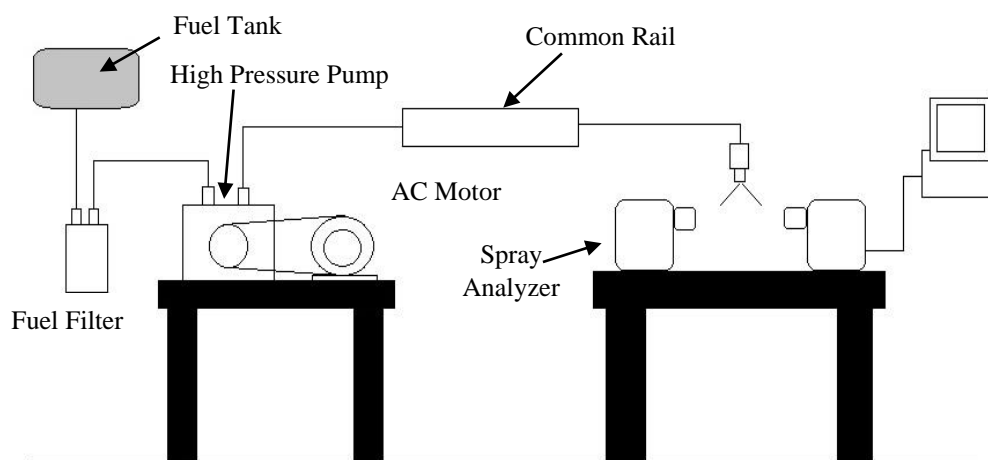
Fig. 3.4 Schematic of the spray analysis setup

3.9. Selection of the test engine

In the present work, a single-cylinder, water-cooled, direct-injection, diesel engine developing 3.5kW at the rated speed of 1500rpm was used, shown in Plate 3.17. Such engines are an integral part of the rural agrarian economy of India, they also double up as power backups when required. The specifications of the engine is given in Appendix – II. The engine cylinder was made of cast iron and fitted with a hardened high-phosphorus cast iron liner. The lubrication system used in the engine was wet-sump type. The overhead inlet and exhaust valves and the fuel pump were driven by the camshaft. The combustion chamber was hemispherical in shape and placed in the piston. To measure the in-cylinder pressure, the piezoelectric transducer was placed in the cylinder head surface and the crank angle encoder was placed at the end of the eddy current dynamometer which was used to load the engine. These sensors send the signal to a personal computer with the help of a data acquisition system (NI USB 6210 (Plate 3.18)). 'Enginesoft' software installed on the computer was used to read the data given by the data acquisition system and further analysis was carried out using the data. The data acquisition system, the engine loading system, the fuel and air flow measurement system was house in the control panel, shown in Plate 3.19. The schematic of the test setup is shown in Fig. 3.5. A central water cooling system was used to cool the engine and the eddy current dynamometer. The flow rate of the water to the engine was maintained at 250l/h whereas for the dynamometer it was maintained at 120l/h.
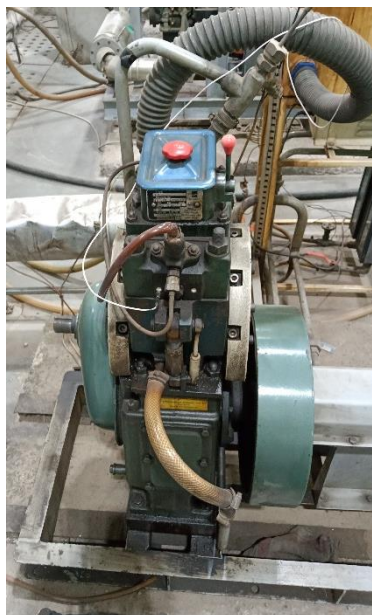
Plate 3.17 Test engine

Plate 3.18 NI Data acquisition system

Plate 3.19 Control panel
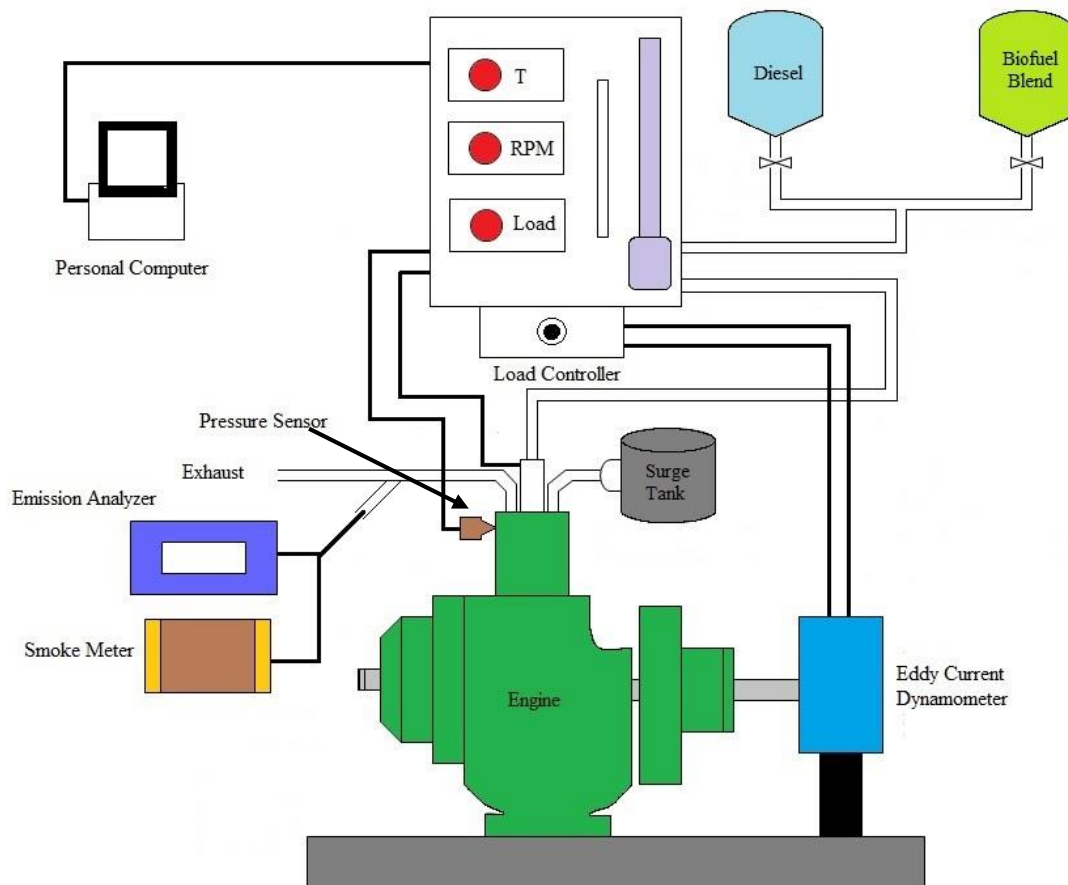
Fig. 3.5 Schematic of the engine experiment setup

3.10. Selection of the engine test parameters

Selecting the appropriate test parameters is essential for the testing of the engine and in this study the parameters were judiciously selected. The testing of the engine was performed in accordance with IS: 10000. The various observed parameters during the test and the calculated parameters are given below.

The various observed parameters are:

1) Engine load

2) Engine speed

3) Air flow rate

4) Fuel consumption rate

5) Temperature

6) In-cylinder pressure

7) Exhaust emissions of HC, CO, CO_2, and NOx

8) Smoke Opacity

The parameters that were calculated are:

1) Brake thermal efficiency (BTE)

2) Brake specific energy consumption (BSEC)

3) Pressure rise rate

4) Heat release rate

5) Ignition delay

6) Combustion duration

3.10.1. Measurement of brake power

The most important parameter in the testing of an internal combustion engine is brake power (BP). The engine was coupled to an eddy current dynamometer through a flexible coupling. The water cooled eddy current dynamometer was used for loading the engine and measuring the brake power at each load, shown in Plate 3.20. An eddy current dynamometer consists of a stator and rotor. Permanent electromagnets are placed in the stator whereas rotor consists of a disc of copper or steel. The rotor is connected to the engine shaft through the coupling. While loading the engine, the electromagnets are energized by passing the current through them. As the rotor rotates, eddy current is produced in the electromagnets. This eddy current produces a magnetic field which opposes the movement of the rotor thus loading the engine. The heat generated during the loading is dissipated by the passing water through the dynamometer. The load was measured by the help of a moment arm which applied force on a load cell, shown in Plate 3.21. The load was measured in kg. The brake power was calculated according to the equation 3.13.

$$\text{BP (kW)} = \frac{2*\pi*\text{N(rpm)}*\text{Load(kg)}*9.81*\text{Dynamometer arm length (m)}}{60*1000} \quad (3.13)$$

The arm length of the dynamometer was 0.185m.

Plate 3.20 Eddy current dynamometer

Plate 3.21 Load cell placed on the dynamometer

3.10.2. Measurement of engine speed

On the dynamometer end of the shaft a disc with teeth was placed. A magnetic pickup type rpm sensor was mounted close to the toothed disc, shown in Plate 3.22. The sensor consists of a permanent magnet, a yoke and a coil. As each tooth passed the sensor, a pulse was induced in the coil. With the increase in speed more pulses were produced by the sensor. These pulses were sent to the digital acquisition system which calculated the engine rpm. The engine rpm was displayed both on the control panel and the software loaded on the personal computer.

Plate 3.22 Instrument for engine speed measurement

3.10.3. Measurement of fuel flow

At each load, the quantity of fuel consumed by the engine was measured using a differential pressure transmitter (Yokogawa, Japan make) which works on the hydrostatic head principle. The transmitter was placed at the end of the burette and it produced an output voltage which is proportional to the weight of the fuel in the column, shown in Plate 3.23. The fuel flow rate was calculated by measuring the difference in transmitter output at specific intervals and multiplying it with fuel factor. The fuel factor is the amount of fuel (in kg) that comes out from the burette per unit change in the output voltage of the transmitter (kg/V). The fuel factor is given by equation 3.14.

$$\text{Fuel Factor} = \rho * g * h * A \qquad (3.14)$$

The sensor provided direct signal to the data acquisition system which in turn gave the fuel flow rate. The data from the sensor was ascertained by simultaneously taking manual readings from the burette. From the fuel flow rate, brake thermal efficiency and brake specific energy consumption (BSEC) of the engine at a particular load can be calculated.

The brake thermal efficiency is the conversion efficiency of the heat stored in the fuel into useful work available at the brakes. The formula for brake thermal efficiency is given in equation 3.15. Similarly, BSEC is amount of energy in the fuel consumed to produce a unit shaft power. It is calculated by the equation 3.16.

$$\text{BTE } (\%) = \frac{\text{BP (kW)}}{\text{mass flow rate (kg/s)} * \text{Calorific value(kJ/kg)}} \quad (3.15)$$

$$\text{BSEC } (\text{MJ/kWh}) = \frac{\text{mass flow rate } \left(\frac{\text{kg}}{\text{s}}\right) * \text{Calorific value } \left(\frac{\text{kJ}}{\text{kg}}\right) * 3600}{\text{BP (kW)}} \quad (3.16)$$

Plate 3.23 Fuel flow sensor

3.10.4. Measurement of air flow

Measuring accurate amount of air flow is not easy, as the engine requirement of air is pulsating since the air flows once in two revolutions of the crankshaft and air is also compressible. Therefore using only an orifice in the induction pipe is not feasible as the data won't be reliable. So an air box of suitable size was used which had a sharp edged circular orifice for measuring the air flow. The pressure difference between the atmosphere and the air box was measured using a U-tube manometer, shown in Plate 3.19. The mass flow rate of air was calculated using equation 3.17.

$$\text{Mass of air } \left(\frac{\text{kg}}{\text{h}}\right) = c_d * A * \sqrt[2]{2 * g * h_w * \frac{\rho_w}{\rho_a}} \quad (3.17)$$

Where C_d = coefficient of discharge (0.6), A = orifice area, g= acceleration due to gravity, h_w = height of water column, ρ_w / ρ_a = density of water/density of air.

An air sensor was also installed in the air box to measure the air flow rate, shown in Plate 3.24. The air sensor consists of a rotor with blades installed on it. As the air flows through the blades, they start rotating which is detected magnetically as each blade is embedded with a piece of metal thus a pulse is generated. The transmitter processes the signal and determines the flow rate of air. The data was available on the software installed on the computer.

Plate 3.24 Air flow sensor

3.10.5. Measurement of temperature

In the present work, K-type thermocouples made of chrome-alumel, were connected to a six channel digital panel meter for measuring temperature of the intake air, exhaust gas, coolant water in and out temperature, and calorimeter water inlet and outlet temperature. The meter was calibrated by a millivolt source up to 800°C.

3.10.6. Measurement of in-cylinder pressure

A piezoelectric transducer of 'Kubeler' make was used for the in-cylinder pressure measurement. The signals from the transducer was send to a charge amplifier which amplified the signals and reduced the signal noise. The signals were then sent to the data acquisition system which along with the signals from crank angle encoder produced the pressure versus crank angle graph in the software installed on a personal

computer. The pressure data was produced for each degree of crank angle rotation. In the present study, fifty continuous cycles were averaged for producing the in-cylinder pressure versus crank angle data. Plate 3.25 shows the pressure sensor placed on the engine head.

Plate 3.25 Pressure sensor installed on the engine head

3.10.7. Measurement of exhaust emissions

The major pollutants in the exhaust emissions of a diesel engine are unburnt hydrocarbons, carbon monoxide, carbon dioxide, oxides of nitrogen and smoke, etc. The smoke emissions are indirectly measured by measuring the opacity of the exhaust gas i.e. if the smoke emissions are high then the smoke opacity will be more and vice versa. In this work an AVL smoke meter (Plate 3.26) was used in which light beam is projected from a source and the receiver receives the light beam. As the stream of exhaust gas is passed through the light beam due to the presence of smoke particles some part of the light beam is scattered or absorbed. The receiver receives rest of the light beam which is a measure of the opacity of the smoke. The receiver is a photocell, which generates photoelectric current when light falls on it. The unburnt hydrocarbon emissions, carbon monoxide and oxides of nitrogen emission was measured using an AVL di-gas analyser (Plate 3.27). The technical specifications of the smoke meter and the di-gas analyser are given in Appendix – III and IV, respectively. The emission data of CO, HC and NO were converted to brake specific emission values offline.

| **Plate 3.26** Smoke meter | **Plate 3.27** Five gas analyzer |

3.11. Calculation of heat release rate

Evaluating the heat release during the combustion of a fuel in a compression ignition is of great significance. Since the heat release affects the engine efficiency, power output as well as emissions. Various models have been proposed by researchers for determining the heat release rate. The method described in Heywood [154] was used in the present work. This method is based on the first law of thermodynamics. The model is a single zone model and does not distinguish between burned and unburned zones present in the cylinder during combustion. Although multi zone models exist, but the developer has to keep track of unburned and burned areas for calculating the heat transfer. It was found that using a multi-zone model does not have large benefits due to the uncertainties in defining the evolution of zones [155]. The heat release rate is given by equation 3.18.

$$\frac{dQ}{d\theta} = \frac{\gamma}{\gamma-1} * P * \frac{dV}{d\theta} + \frac{1}{\gamma-1} * V * \frac{dP}{d\theta} - \frac{dQ_w}{d\theta} \qquad (3.18)$$

Where $dQ/d\theta$ = Rate of net heat release inside the engine cylinder (J/°CA); $dQ_w/d\theta$ = Rate of heat transfer from wall (J/°CA), γ = ratio of specific heats; P = Cylinder pressure (bar); V = Gas volume (m³); θ = Crank angle (°)

Many researchers have used this model [155–158]. The ignition delay was also computed in this study, it was calculated as the interval in terms of crank angle from

the moment the fuel is injected to the start of rapid rise in heat release. The combustion duration is the interval from the start of the heat release to the end of heat release.

3.12. Predicting the cyclic variation using artificial neural network

It is well known that there is a variation in the combustion process for every cycle which has made it a topic of research as it adversely affects the engine performance that may lead to lower efficiency and higher emissions [159]. The cyclic variation can be caused by air motion in the cylinder due to variation in swirl and turbulence. Also, the cyclic changes in the fuel and air entering into the cylinder and mixing of the two before start of combustion can also cause variation in combustion process for every cycle [160,161]. The cyclic variability is evaluated by indicated mean effective pressure (IMEP) as it reflects extensive pressure information of a cycle [162]. The variation in IMEP can be understood by using proper orthogonal decomposition method [163], wavelet transform method [164] and coefficient of variance (COV) [165] method. In this study, the COV of indicated mean effective pressure was used to investigate the cyclic variability as given in eq. 3.19.

$$COV_{imep} = \frac{\sigma_{imep}}{\overline{imep}} * 100 \qquad (3.19)$$

Where σ_{imep} (eq. 3.20) is the standard deviation of IMEP of 50 sequential cycles and $\overline{imep}$ (eq. 3.21) is the mean of IMEP values.

$$\sigma_{imep} = \sqrt{\frac{\sum_{i=1}^{n}(\overline{imep}-imep_i)^2}{n-1}} \qquad (3.20)$$

$$\overline{imep} = \frac{1}{n}\sum_{i=1}^{n} imep_i \qquad (3.21)$$

Controlling the cyclic variations is important, as it will improve the engine efficiency and reduce emissions. To achieve low cyclic variations a strategy needs to be developed. For developing the strategy a model is required that can predict the cyclic

variability for every load. Artificial neural network (ANN) is one such tool that is useful in modelling the cyclic variability. ANN is a non-linear tool that can work on multiple inputs and predict multiple outputs. It can be modelled without any prior knowledge of the processes. A well-trained neural network can predict faster than conventional models since no lengthy iterative calculations are required. However, selecting the network topology in terms of model simplicity and accuracy is important [166,167].

The neural network contains neurons which are highly interconnected processing elements. The network contains input layer, hidden layer and an output layer. Input is provided by the source to these neurons in the hidden layer which perform non-linear operations by using bias, weights, and activation functions and then provide the output. There can be more than one hidden layer in the network that send output to the next layer and finally to the output layer. The external world then receives the data from the output layer. The network can approximate a function of any complexity with enough hidden neurons. However, there is a limit to the number of neurons as the network may tend to over fit during training resulting in the introduction of random noise [168].

3.12.1. Network parameters

A continuous differential log-sigmoid activation function was used for both the hidden and the output layer. A non-linearity is introduced in the neural network which makes it stronger than linear fucntions. A form of automatic gain control is produced by the function and it produces values between 0 and 1 [169]. Equation 3.22 gives the activation function.

$$F_i = \frac{1}{1+e^{-x}}$$

(3.22)

Where 'x' is the wieghted sum of inputs.

3.12.2. Normalization of input and output data

Scaling of input and output parameters can drastically improve the network's performance. Hence the input and output parameters were normalized in the present study. For normalization, eq. 3.23 was used as it gives values in the range of 0.1 and 0.9 which is within the range of log-sigmoid function [170].

$$nv_i = 0.8 * \left(\frac{v_{min} - v_i}{v_{min} - v_{max}} \right) + 0.1 \qquad (3.23)$$

3.12.3. Learning algorithm

An appropriate learning algorithm is required by the network which adjusts the weight of the layers so that the desired response can be achieved. Many algorithms exists for training the network, some of them are gradient descent with momentum and adaptive learning rule, gradient descent with adaptive learning rule [171], Levenberg – Marquardt (LM) [168], and scaled conjugate gradient (SCG) [170]. In the present study, both LM and SCG were used to train the network and their outputs were compared.

3.12.4. Training and testing data

In this study two input parameter and one output parameter was used for training the network. Engine load and blends of hydrotreated oil and diesel were used as input whereas coefficient of variance of IMEP was used as output parameter. In total thirty five tests were conducted. The test data was randomly divided into three datasets: training, validation and test set. The training set is used to only train the network, the validation set prevents the overfitting of the training set whereas the test set determines the performance of the model. The training of the network was carried out using 70% of the experimental data, validation was carried out using 15% of the data and the rest of the 15% data was used for testing the network.

3.12.5. Network structure

In the present study, the number of neurons in the hidden layer were varied from 3 to 20. The iterations for each network topology was performed according to a loss criteria function which should be minimized. Mean square error was used as the loss criteria function due to differentiability, symmetry and convexity of the function. The training of the network stopped when the validation error started increasing; this prevents over-training of the network. Fig. 3.6 shows the neural network structure. MATLAB was used for the development of the model.
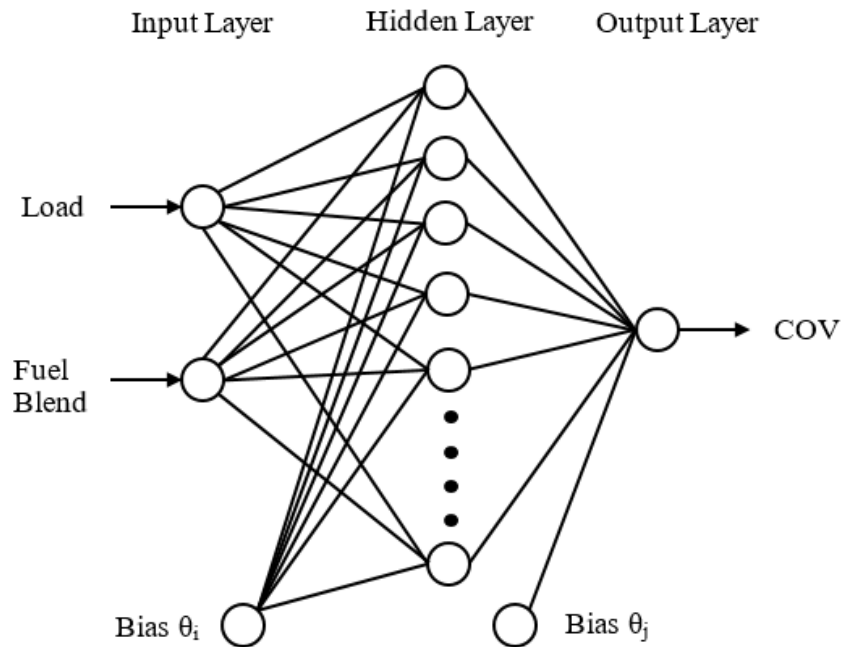
Fig. 3.6 ANN structure with one hidden layer

3.12.6. Output Evaluation

The statistical methods used for evaluating the prediction performance of the network are coefficient of determination (eq. 3.24) (R^2), Root Mean Square Error (eq. 3.25) (RMSE) and Mean Absolute Percentage Error (eq. 3.26) (MAPE) [172–174].

$$R^2 = 1 - \left(\frac{\sum_{i=1}^{n}(t_i - o_i)^2}{\sum_{i=1}^{n}(o_i)^2} \right) \tag{3.24}$$

$$RMSE = \sqrt{\frac{1}{n}\sum_{i=1}^{n}(t_i - o_i)^2} \tag{3.25}$$

$$\text{MAPE} = \frac{1}{n}\sum_{i=1}^{n}\left(\left|\frac{t_i - o_i}{t_i}\right|\right) * 100 \qquad (3.26)$$

3.13. Engine trial procedure

The engine was started in no load condition with neat diesel. After the engine attained steady state condition, then the fuel supply was switched to the test fuel and the engine was operated for nearly thirty minutes for stabilizing with the test fuels. All the readings at each load was observed only when the engine reached stability. All the instruments were calibrated periodically. The injector opening pressure was kept at the rated value throughout the experiments.

The load on the engine was varied in steps from no load to full load. The readings were observed at no load, 20% of full load, 40% of full load, 60% of full load, 80% of full load and full load. At each load, the air flow rate, the fuel flow rate, exhaust gas temperature, emissions of CO, HC, NOx and smoke opacity were recorded. The pressure crank angle history of 50 consecutive cycles was also recorded by using the data acquisition system and the personal computer. This data was processed to get the average pressure crank angle variation.

3.13.1. Experiments

- The tests were conducted with neat diesel, neat hydrotreated waste cooking oil, and their blends in proportions, given in Table 3.4. The engine performance and emission characteristics of the blends were compared with the base fuels.

- The blend of hydrotreated waste cooking oil and diesel that gave the best engine performance in terms of brake thermal efficiency and emissions was selected and different percentages of waste cooking oil biodiesel on volume basis was added to further improve the engine performance and emissions.

3.14. Accuracy of instruments and uncertainty in measurement

The range and accuracy of the instruments used in the present study is given in Table 3.5. All the instruments exhibited higher accuracy.

Table 3.5 Accuracy of instruments

Measurement	Measuring Principle	Range	Accuracy
Engine Load	Strain gauge type load cell	0-25kg	±0.1kg
Engine Speed	Magnetic pick-up type	0-2000rpm	±20rpm
Time	Stop-watch	-	±0.5%
Exhaust Temperature	K-type thermocouple	0-1000°C	±1°C
Crank angle encoder	Optical	0-720°CA	±0.2°CA
Pressure	Piezoelectric	0-200bar	±1bar

When any quantity is measured the results are always different from their true values even when the experiments are carried out carefully. This error in measurement may be either systematic or random. The systematic error can be removed by adding a correction factor. Whereas, random error cannot be predicted in advance, therefore it can be only statistically estimated. Its presence can be detected when the same quantity is measured a number of times under the same conditions and with same care. Gaussian distribution method with confidence level of $\pm 2\sigma$ (i.e. 95.45% of the measured data lie within these limits) can be used to estimate the uncertainty. The uncertainty is estimated using equation 3.27.

$$\text{Uncertainty of any measured parameter } (\Delta X) = 2\sigma_i/\bar{X} * 100 \qquad (3.27)$$

Experiments were conducted to obtain the mean $(\bar{X})$ and the standard deviation (σ_i) of any measured parameter. From the measured parameters, the uncertainty is computed by the method given by Kline and McClintock [175].

Let R be the computed quantity from 'n' independent measured parameters.

$$X_1, X_2, X_3, X_4 ....X_n$$

Thus $\qquad R = R(X_1, X_2, X_3, X_4....X_n) \qquad (3.28)$

Let uncertainty limits for the measured parameters be

$$X_1 \pm \Delta X_1, X_2 \pm \Delta X_2, X_3 \pm \Delta X_3, X_4 \pm \Delta X_4 ....X_n \pm \Delta X_n$$

And the uncertainty limit for the computed parameter be $R \pm \Delta R$

In order to get realistic error limits for any computed quantity based on several measured quantities the principle of root-sum-squared method is used and the magnitude of error is given by equation 3.20.

$$\Delta R = SQRT\ ((\partial R/\partial X_1 * \Delta X_1)^2 + ((\partial R/\partial X_2 * \Delta X_2)^2 + \ldots ((\partial R/\partial X_n * \Delta X_n)^2)(3.29)$$

Using equation 3.29 the uncertainty for a given operating condition can be computed. A sample calculation is given in Appendix – V. The overall uncertainty of the experiments was found to be $\pm 3.7\%$.

CHAPTER 4
FUEL PRODUCTION AND CHARACTERIZATION

4.1. Introduction

For the hydrotreating process conventional catalysts such as sulfided nickel-molybdenum and cobalt-molybdenum are used. However, the reactions take place under harsh conditions and the catalyst requires to be leached with sulfur which hinders their applications [49,82,85,91,176–178]. For sulfidation hydrogen sulfide gas [36,179] can be passed over the catalyst or elemental sulfur or a sulfur rich compound, such as dimethyl-disulfide (DMDS) can be added to the feed [91,180]. However, the catalyst activity reduces over a period of time due to sulfur leaching and also the product stream is contaminated with sulfur [181,182]. During sulfidation, there is a possibility of sulfur being released into the atmosphere, which is detrimental for the atmosphere. These drawbacks of catalyst sulfidation can be circumvented by using catalyst which do not require sulfidation pre-treatment. Several noble metals such as palladium (Pd), platinum (Pt) and ruthenium (Ru) on different supports have been used in the past for hydrotreatment and they have shown high activity in converting vegetable oil into alkanes [183]. Generally, Pt catalysts support decarbonylation reaction, whereas Pd catalyst support decarboxylation reaction process [184]. Moreover, Ru based catalyst are also active for HDO reactions [185,186].

Sunflower oil was hydroprocessed by Kikhtyanin et al. [68] using Pd/SAPO-31 catalyst. As the authors increased the temperature from 320 to 360°C the C_{17}/C_{18} ratio increased from 1-4 to 8-10 indicating the dominance of HDCN/HDCX reaction over HDO reaction process. The cloud and pour points of the produced fuel was less than -50°C. Liu et al. [181] hydroprocessed waste cooking oil using Ru/Al_{13}-montmorillonite catalyst. The triglycerides and free fatty acids (FFA) containing high acid value cooking

oil was deoxygenated to form hydrocarbon products. The authors observed the pour point to be 20°C with SiO_2 support whereas with montmorillonite support the pour point reduced to -15°C. Murata et al. [179] also hydrotreated Jatropha oil using Pt-Re catalyst supported on HZSM-5. With a 10 oil to catalyst ratio, the optimum Re-Pt/HZSM-5 catalyst resulted in C_{15}-C_{18} yield of 67%. The authors found that initially the cleavage of double bond occurs followed by HDO, HDCN and HDCX reaction to form C15-C18 alkane mixture. Jatropha oil and a model compound (stearic acid) was hydrotreated under mild conditions by Guo et al. [149] using ruthenium with different supports. Ru supported on $La(OH)_3$ resulted in 100% conversion of Jatropha with 98% long chain selectivity at 200°C and 4MPa. The authors also checked the recyclability of the catalyst and found that up to four times nearly 70% alkanes were obtained under the same conditions. The effect of addition of cerium to palladium and ruthenium with $La(OH)_3$ support on the hydrocarbon yield was studied by Patil and Vaidya [187]. The authors in a fixed-bed reactor deoxygenated Jatropha oil. At optimized reaction conditions, the yield and oil conversion for Pd-Ce and Ru-Ce were 81 & 97.3% and 75.3 & 91.8%, respectively. The catalyst efficiency was not affected for more than 40 hours of on-stream time. In another study [188], the same authors used hydrotalcite-like (HTlc) supports for palladium and ruthenium catalyst and they studied the effect of various parameters such as pressure, temperature and H_2/oil ratio. At optimum reaction conditions, the yield with Pd is 91.2% and with Ru the yield is 85.6%. Both the catalyst were stable for over 30 hours of on-stream time.

The literature show that different catalysts can be used for hydrotreating waste cooking oil. However, mostly nickel or cobalt based catalysts has been used by the researchers and few studies have used noble metals based catalyst for the hydrotreating of waste cooking oil. Moreover, sulphidation is necessary for the former catalysts which

is carried out by using H_2S gas or by adding dimethyl disulphide (DMDS), whereas no suplidation is required for noble metals. Also the energy requirement is less with the noble metals. Therefore, in the present work a cerium and manganese promoted catalyst containing ruthenium supported on Al_2O_3 was used for hydrotreating the waste cooking oil. To reduce the time and cost of the experimentation Taguchi and Fuzzy logic was used for optimizing the process parameters. The used cooking oil was collected from cafeteria of Delhi Technological University.

4.2. Catalyst Preparation and Characterization

The catalyst was prepared by a wet impregnation method. An aqueous solution of cerium nitrate hexahydrate was prepared and it was slowly dropped with the help of a dropper on the calcined Al_2O_3 support till the support was just wet. The process was repeated for impregnating an aqueous solution of manganese acetate and ruthenium chloride. A solid sample was then obtained by drying the support at 100°C and calcined at 500°C for 3 hours. The support contained 5% of cerium and 5% of magnesium, whereas the ruthenium loading was 2% of the catalyst weight. For this, 0.62gm of cerium nitrate hexahydrate was dissolved in 15ml of distilled water, 0.274gm of manganese acetate was separately dissolved in 50ml of distilled water and 0.248gm of ruthenium chloride was separately dissolved in 50ml of distilled water. The three aqueous solutions were then added to a 5gm calcined support. The prepared catalyst, before every reaction, was reduced in a hydrogen (2MPa) environment at 220°C for 3 hours.

Fig. 4.1 shows the XRD pattern of the catalyst. The visible peaks at $2\theta=38.5°$, $46.7°$ and $66.9°$ are typical of Al_2O_3 which is prepared from microcrystalline boehmite. Similar peaks were observed by Sankaranarayanan et al. [71]. The pattern reveals that the metals are highly dispersed on the support surface and due to lower percentage of

the metals their individual peaks are not visible [189]. It also indicates that the nature of Al_2O_3 is not affected significantly by the method used for the impregnation of the metals. Even with higher percentage of ruthenium loading similar XRD pattern was observed by Mishra et al. [190].

The scanning electron microscope was used to study the morphology of the freshly prepared catalyst. The SEM analysis, shown in Fig. 4.2, was carried out before the catalyst reduction. The EDS analysis confirms the presence of ruthenium, cerium and manganese in the catalyst. The mass percentage of ruthenium, cerium and manganese in the catalyst are 6%, 2% and 0.03%, respectively.
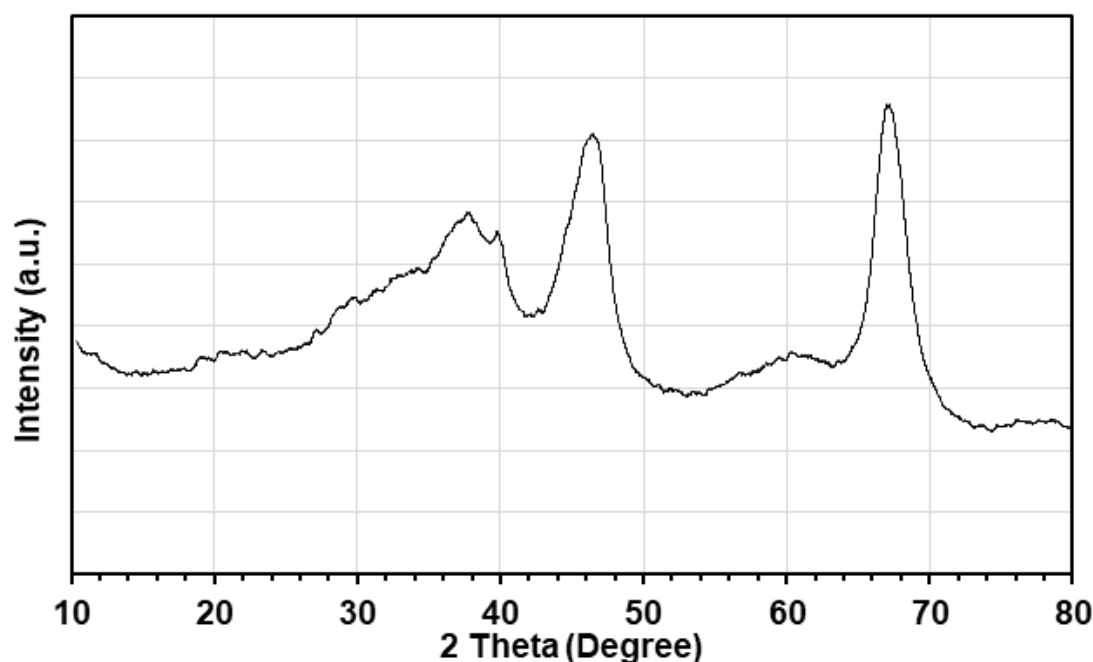

Fig. 4.1 XRD pattern of the catalyst
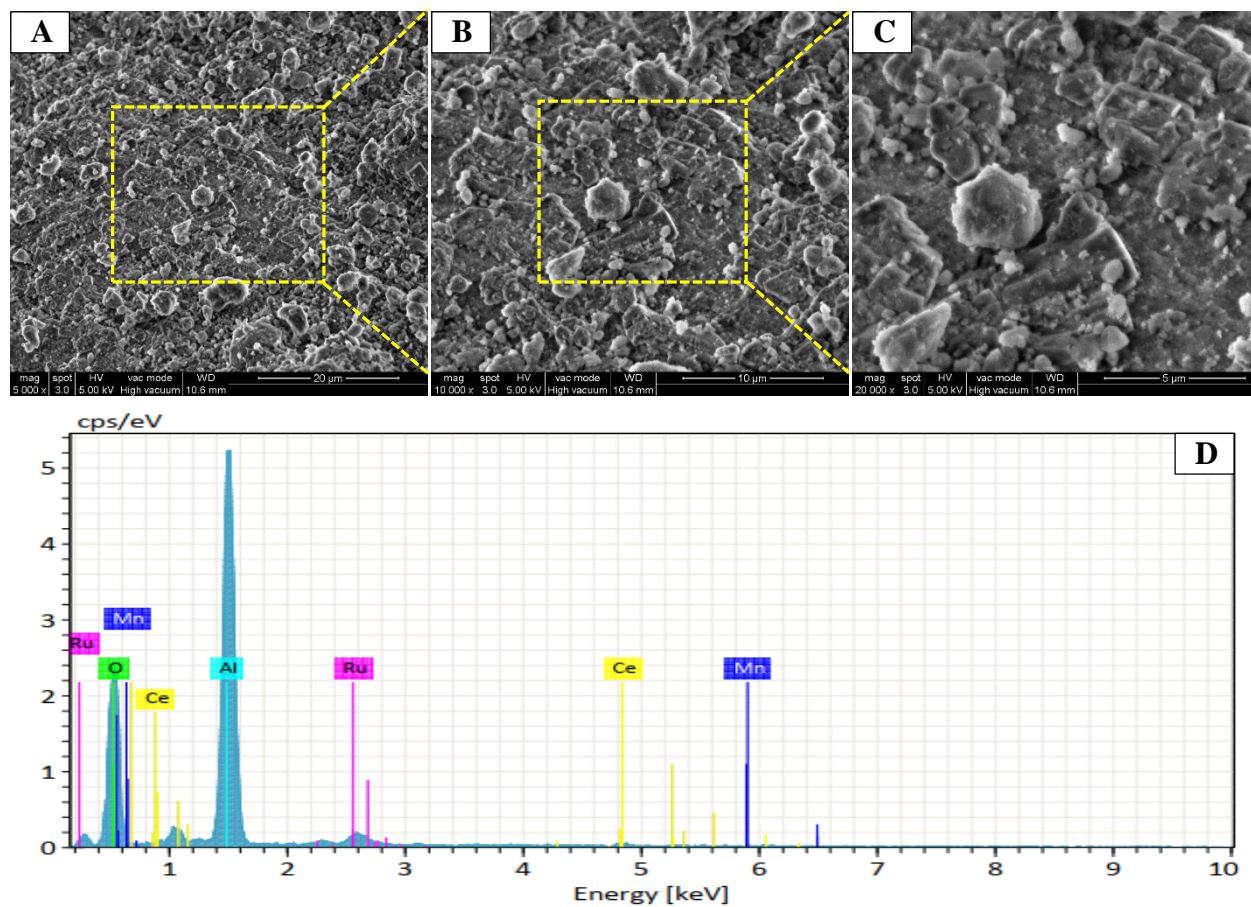
Fig. 4.2 SEM images of the catalyst at (a) 20μm, (b) 10μm, (c) 5μm and (d) EDS analysis

4.3. Discussion on the results

As previously discussed in Section 3.3, the experiments were carried out in a 100ml batch reactor filled with 20g of used cooking oil and the reduced catalyst. Instead of a full factorial experimental work, Taguchi method was used and the experiments were carried out as per the discussion in Section 3.4.

4.3.1. Composition of used cooking oil

GC-MS (HP-624 column) analysis was carried out for determining the composition of used cooking oil. The results show that the used cooking oil contains palmitic acid (17.47%), linoleic acid (58.51%), oleic acid (16.75%), and stearic acid (4.85%). The unsaturated fatty acids in the used cooking oil were palmitoleic, oleic, linoleic, and linolenic acids whereas the saturated acids were palmitic acid, stearic acid. The saturated fatty acids were about 22.47% whereas the unsaturated fatty acids were 77.53% in the total acids of used cooking oil. All the fatty acids had even carbon atoms in the carbon chain i.e. C_{16}, C_{18} and C_{20}. The sixteen chain carbon atoms occupy 17.5%, eighteen chain carbon atoms occupy 80.7% whereas carbon chains with twenty carbon atoms occupy 1.79% of the fatty acids of used cooking oil.

4.3.2. Hydrotreating of used cooking oil

During the hydroprocessing of unsaturated fatty acid methyl ester, complicated reactions are involved such as dehydration, cracking, hydrogenation, decarbonylation or decarboxylation and carbon deposits. These reactions may occur simultaneously or consecutively. The intermediate products formed are alcohols, relative fatty acids and olefins and the final products are carbon monoxide, carbon dioxide and alkanes [71,191]. The $C_1 - C_4$ alkanes are in gaseous form whereas alkanes containing greater than five number of carbon atoms are in liquid form and may be normal or isomeric in nature. The reaction can take place via hydrodeoxygenation route with water as by-

product and through decarbonylation or decarboxylation route with CO or CO_2 as by-product [192]. The carbon chain has same number of atoms with hydrodeoxygenation route whereas with decarbonylation or decarboxylation route, the carbon chain reduces by one carbon atom [193]. The selectivity of diesel like fuel and the conversion percentage for all the tests cases is depicted in Fig. 4.3.

It is seen that all the three parameters considered in the study namely, reaction temperature, reaction pressure and reaction time affect the overall conversion efficiency as well as the diesel selectivity. Moreover, the reaction temperature has a stronger influence in comparison to the other two parameters. The general trend shows a decrease in conversion efficiency with high temperatures. The highest conversion efficiency was observed at 330°C and the lowest at 390°C. The selectivity of diesel like fuel was higher than naphtha at all the temperatures, and at 330°C the diesel like fuel selectivity was highest. With increase in temperature the diesel like fuel selectivity decreases. Moreover, as the temperature increases the naphtha selectivity increases and it is highest at 390°C since cracking of the product takes place at higher temperatures and lighter molecules are formed [112].

The hydrogen pressure determines the pathway of the used cooking oil conversion into alkanes. As the hydrogen pressure increases the conversion efficiency increases because the acid-catalyzed reaction rate increases as more hydrogen is adsorbed on the catalyst surface thus producing more acid sites for the reaction [194]. This facilitates triglycerides deoxygenation along with the breaking of the glycerol backbone. Fig. 4.3 shows that the pressure and reaction time both affect the conversion percentage as well as the diesel selectivity. It is seen that at 330°C as the pressure and reaction time increases the conversion percentage increases but the diesel like fuel selectivity decreases. At 330°C, 40 bar pressure and 140 minutes reaction time, the conversion

efficiency increases from 88.6% to 89.9% at 50 bar pressure and 200 minutes. Whereas the diesel like fuel selectivity decreases from 86.7% to 84.2% as the amount of time available for the reaction increases and also more amount of triglycerides are converted into alkanes. Also, as large amount of hydrogen is present in the reactor, the formation of lighter products (water, propane, and methane) is enhanced. The energy consumption is also increased by increasing the hydrogen pressure [81,91]. At 390°C, 30bar and 200 minutes, the conversion efficiency is 78.2% and diesel like fuel selectivity is 67.8% which increases to 80.9% and 71.1% respectively at 40bar and 80 minutes reaction time. As the reaction pressure increases and time decreases, the relative conversion of waste cooking oil into lighter carbon chains and gas reduces and high amount of hydrogen is utilized in only forming long chain alkanes. Whereas at 50bar and 140 minutes reaction time, the diesel like fuel selectivity and the conversion efficiency is 66.5% and 76.6%, respectively. Since at high hydrogen pressure and more reaction time, the longer chain carbon atoms may have cracked to smaller chain atoms.

To understand the reaction route, it is necessary to estimate the ratio of the amount of odd number of carbon atoms (C_{17}) to even number of carbon atoms (C_{18}) in the liquid product. The C_{17}/C_{18} ratio, shown in Fig. 4.4, indicates the relative activity as the long-chained used cooking oil consists mainly of C_{18} carbon atoms. It is seen that high amount of heptadecane was formed with the increase in temperature. This is most likely because of endothermic nature of the decarbonylation and decarboxylation reactions whereas the hydrodeoxygenation reaction is exothermic in nature [112,184]. At 330°C, with the increase in reaction time and pressure the amount of odd number of carbon atoms decreases. The primary reason for the trend is the increase in the adsorption of hydrogen on the catalyst's active sites which increases the deoxygenation activity and reduces the decarboxylation and decarbonylation reaction [70]. Similar trend is

observed at 360°C and 390°C. Moreover, the reaction time has little effect on the heptadecane formation as the effect of hydrogen adsorption on active sites is more dominant.
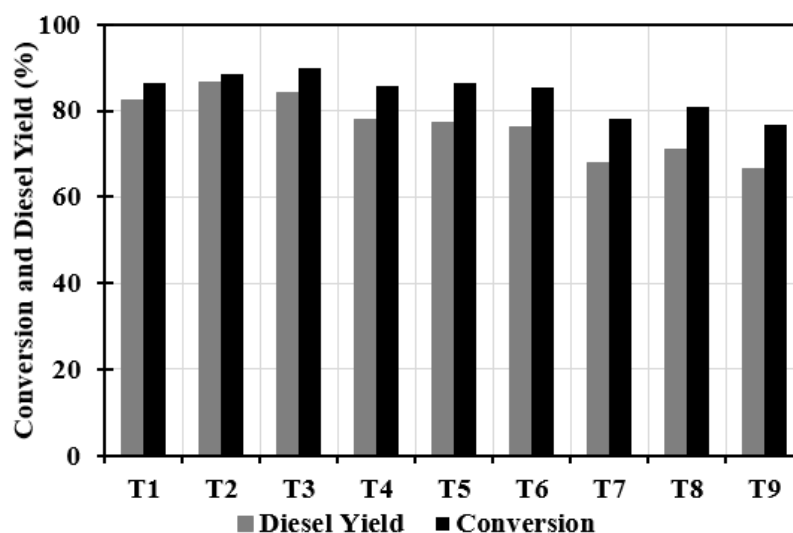
Fig. 4.3 Conversion and Diesel yield at various test conditions
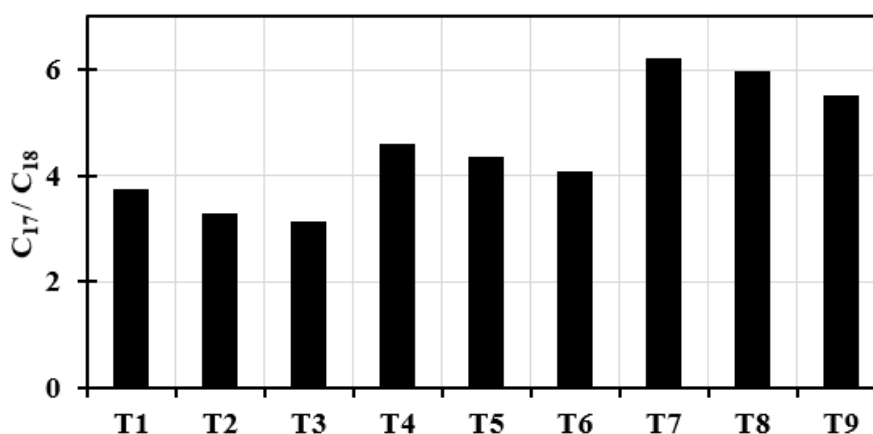
Fig. 4.4 Molar ratio of C_{17}/C_{18} at different test conditions

4.4. Optimization of the production process

In the present study, the effect of the three factors on the conversion efficiency of the process, diesel like fuel selectivity and naphtha selectivity of the process is studied. However, the Taguchi method is designed for optimizing a single performance characteristic. Therefore, other theories such as grey relation theory [195,196], utility theory [197] and desirability function [198] approach have been combined with Taguchi method for optimization of multiple performance characteristics. Deng

proposed grey system theory in the year 1982. This system can solve problems having complicated relationships between variables and their factors. In this system all the objectives of a multi objective problem are combined into one single objective thereby reducing the complexity and increasing the system's efficiency. All the output responses are normalized between 0 and 1 which are in turn used to calculate grey relational coefficient for each response. The coefficient is then averaged for each experiment to calculate grey relational grade. The optimal solution is attributed to the maximum grey relational grade [199,200]. Derringer and Suich popularized a multi response optimization technique in 1980. The technique was known as desirability function that transforms a response into a scale free value known as desirability. The range of desirable is from 0 to 1 and the factor settings that gives the maximum total desirability are considered to be the best parameters. In this technique the desirability index is calculated first from the responses and then based on the index the composite desirability is calculated. The optimal parameters and the combination of the levels are found using the composite desirability value [201]. According to utility theory, a product is evaluated by a customer based upon on its qualities. To make the choice rational, the characteristics of the products are evaluated and assigned a utility value. The utility value represents the product's utility. A preference scale for each quality is constructed and is used to determine the utility value for a number of quality characteristics. These scales are then weighted for obtaining an overall utility. The weighting is carried out for satisfying the test of indifference in the quality characteristics. The preference scale for each characteristic is set between 0 and 9 [197]. In all these theories each response is allocated with weights. Since these weights are assigned on the basis of some assumptions that results in uncertainty and indistinctness

in the solution. Therefore fuzzy based Taguchi method can be used for optimization of multiple objectives.

In fuzzy control, the logic of human thought in controlling a process is represented as fuzzy rules or relations. The fuzzy logic unit consists of a fuzzifier, membership functions, a fuzzy rule base, an inference engine and a defuzzifier [202]. The S/N ratios obtained from the Taguchi method are normalized in the range 0-1 so that the quality characteristic of the performance parameter with smaller S/N ratio is present. The normalization of the S/N ratio is carried out using equation 4.1.

$$X_{normalized} = (X_i - X_{min})/(X_{max} - X_{min}) \qquad (4.1)$$

Where i varies from 1,2,3,..etc. X_i denotes the S/N ratio at the ith position, X_{min} is the minimum S/N ratio and X_{max} is the maximum S/N ratio.

The fuzzifier then fuzzifies the normalized S/N ratio using the membership functions. The inference engine then generates a fuzzy value by applying fuzzy reasoning using the fuzzy rules. Lastly, the fuzzified value is defuzzified and converted into multi performance characteristics index (MPCI). The highest value of MPCI dictates the best parameters for the process.

The input and the output variables were divided using the triangular membership function, which were then used for finding the MPCI. The three input variables, reaction temperature, reaction pressure, and reaction time have three level, small (S), medium (M), large (L), shown in Fig. 4.5. The output MPCI has seven levels namely, very-very small (VVS), very small (VS), small (S), medium (M), large (L), very large (VL), very-very large (VVL), shown in Fig. 4.6. Table 4.1 shows the fuzzy rules for all the inputs and the outputs. The defuzzification is carried out using the centre of gravity method. Table 4.2 shows the inferred MPCI using the experimental combinations given in Table 3.4.

Since the design of experiments is orthogonal, the effect of all variables at different levels on the MPCI can be studied. The mean of the MPCI for each process parameter level was calculated and given in Table 4.3. The mean of MPCI for the reaction temperature at first level is calculated by averaging the mean performance characteristic indexes for the test cases 1-3. Similarly, the mean MPCI for each level of other variables can be found. The total mean of the test cases is also given in Table 4.3. The effect of individual parameters is shown in the MPCI graph (Fig. 4.7), and the total mean of MPCI is indicated by the dashed line. Basically, the highest value of MPCI dictates the best parameters for the process as the variance of performance characteristics around the required value is small. However, it is still required to know the relative importance of each parameter such that the optimized combinations of the variable's level can be accurately determined.
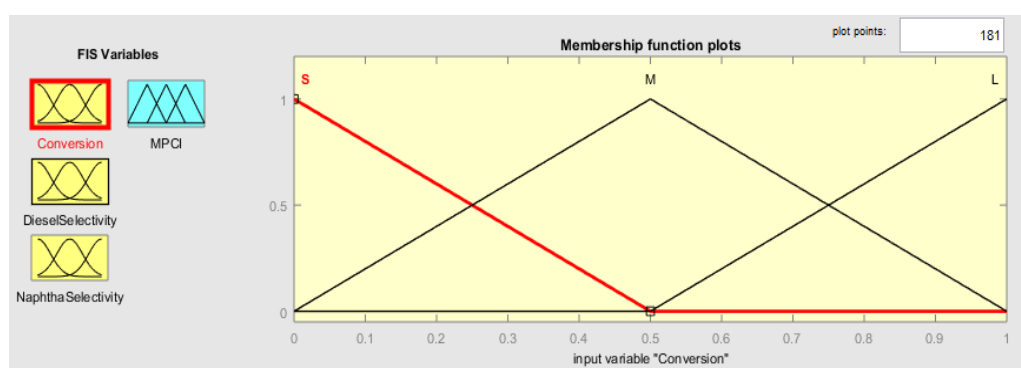
Fig. 4.5 Membership function for conversion
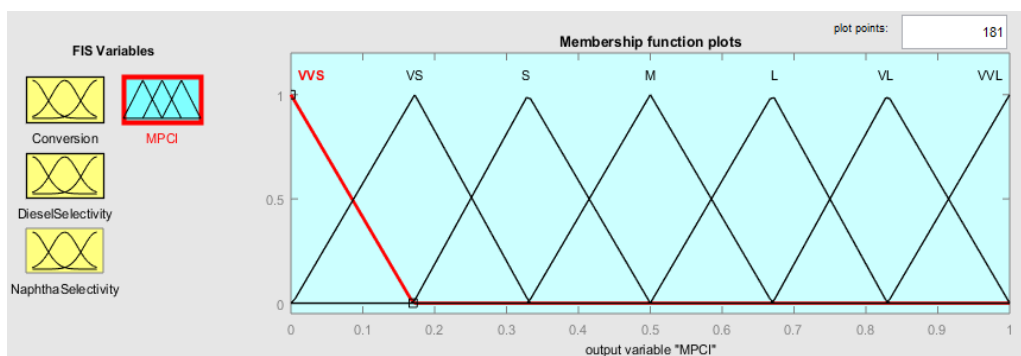
Fig. 4.6 Membership function for multi performance characteristics index

Table 4.1 Fuzzy rule matrix

S. No.	Conversion (%)	Diesel Selectivity (%)	Gasoline Selectivity (%)	Output
1	S	S	S	VVS
2	S	S	M	VS
3	S	S	L	S
4	S	M	S	VS
5	S	M	M	S
6	S	M	L	M
7	S	L	S	S
8	S	L	M	M
9	S	L	L	L
10	M	S	S	VS
11	M	S	M	S
12	M	S	L	M
13	M	M	S	S
14	M	M	M	M
15	M	M	L	L
16	M	L	S	M
17	M	L	M	L
18	M	L	L	VL
19	L	S	S	S
20	L	S	M	M
21	L	S	L	L
22	L	M	S	M
23	L	M	M	L
24	L	M	L	VL
25	L	L	S	L
26	L	L	M	VL
27	L	L	L	VVL

Table 4.2 S/N ratio for the three variables and the inferred MPCI

Test Case	Conversion (%)	S/N Ratio (Conversion)	Diesel Selectivity (%)	S/N Ratio (Diesel selectivity)	Naphtha Selectivity (%)	S/N Ratio (Naphtha selectivity)	MPCI
T1	86.4	38.73	82.5	38.33	1.8	-5.11	0.704
T2	88.6	38.95	86.7	38.76	1.2	-1.58	0.899
T3	89.9	39.08	84.2	38.51	1.4	-2.92	0.838
T4	85.8	38.67	77.8	37.82	3.1	-9.83	0.612
T5	86.4	38.73	77.2	37.75	3.3	-10.37	0.600
T6	85.4	38.63	76.1	37.63	4.1	-12.26	0.518
T7	78.2	37.86	67.8	36.62	8.0	-18.06	0.187
T8	80.9	38.16	71.1	37.04	7.6	-17.62	0.263
T9	76.6	37.68	66.5	36.46	8.4	-18.49	0.053

Table 4.3 MPCI Table

Process Parameter	MPCI			
	Level 1	Level 2	Level 3	Max-Min
Reaction Temperature (°C)	0.814	0.577	0.167	0.647
Reaction Pressure (bar)	0.501	0.587	0.469	0.118
Reaction Time (minutes)	0.495	0.521	0.542	0.047
				Mean Value of MPCI = 0.519
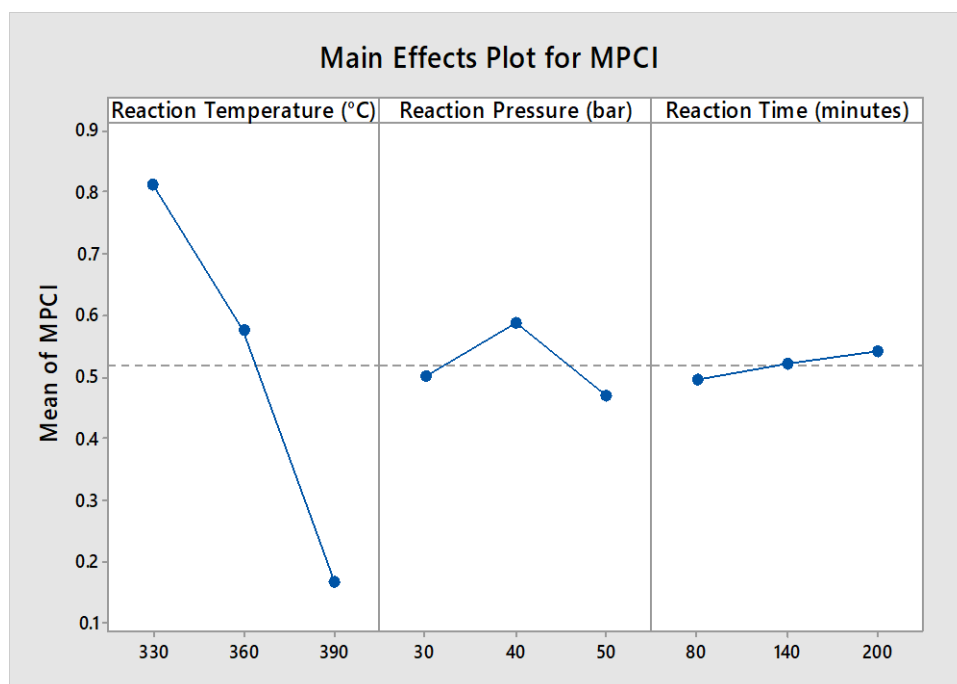
Fig. 4.7 MPCI graph

4.4.1. Analysis of Variance (ANOVA)

To identify the most significant process variables and their effect on the output parameters the analysis of variance was conducted. By summing up and squaring the deviations from the total mean of multiple performance characteristics indexes, the variability of MPCI can be separated into contribution by each variable and error. Equation 4.2 is used to calculate the total sum of squared deviations (SDT).

$$SD_T = \sum_{i=1}^{q}(\eta_i - \eta_m)^2 \tag{4.2}$$

Where q is the number of test cases, η_m is the mean of MPCI and η_i is the mean of MPCI for i^{th} test case.

The total sum of squared deviation consists of two parts: one the sum of squared deviation due to each variable SD_D and second the sum of squared error SS_E. Table 4.4 tabulates the results after applying analysis of variance. The percentage contribution of each variable in the total sum of squared deviations is calculated by equation 4.3. The percentage contribution signifies the importance of change in each variable on the output. In addition F-test with 95% confidence was used to determine the significant contribution of each variable on the output. Large F value signifies that the change in a particular process parameter significantly affects the output.

$$\text{Contribution (\%)} = \frac{SD_D(\text{for each process parameter})}{SD_T} \qquad (4.3)$$

The F-test and the contribution percentage shows that MPCI is significantly affected by the reaction temperature, followed by reaction pressure with reaction time having the least effect on the MPCI. The outcomes are reasonable enough as the increase in reaction temperature decreases the conversion efficiency and diesel like fuel selectivity and increases naphtha selectivity as the long chain carbon atoms are broken into small chain carbon atoms. Based on the discussions, the optimal process parameters are 330°C reaction temperature, 40bar reaction pressure and 200minutes of reaction time.

Table 4.4 ANOVA results

Process Parameter	Degrees of Freedom	Sum of Squares	Mean Squares	F-test	Contribution (%)
Reaction Temperature (°C)	2	0.6407	0.32035	28.89	93.1
Reaction Pressure (bar)	2	0.0222	0.0111	1	3.23
Reaction Time (minutes)	2	0.0032	0.0016	0.15	0.46
Error	2	0.0221	0.01105		3.21
Total	8	0.6882			100

4.4.2. Confirmation experiment

After fixing the optimal process parameters, prediction and verification of the improvement in the performance characteristics is necessary. For the optimized process parameters, the MPCI is predicted using equation 4.4.

$$\eta = \eta_m + \sum_{i=1}^{q}(\eta_i - \eta_m) \tag{4.4}$$

Where η is the estimated MPCI, η_m is the total mean MPCI, η_i is the mean of MPCI at the optimal level and q is the number of parameters that affect the MPCI.

With the optimal process parameters, the hydrotreating of used cooking oil was carried out and the conversion efficiency, diesel selectivity and naphtha selectivity was found. The predicted MPCI and the experimental results with the optimal process parameters is given in Table 4.5. As compared to the initial process parameters, the conversion efficiency, diesel selectivity has increased whereas the naphtha selectivity decreased. The signal-to-noise ratio and the MPCI has also improved for the optimized process parameters.

Table 4.5 Result of confirmation experiment

Setting Level	Initial Process Parameters		Optimal Process Parameters			Improvement in S/N Ratio	Improvement in MPCI
			Prediction	Experiment			
	390°C, 50bar & 140minutes	S/N ratio	330°C, 40bar & 200minutes	330°C, 40bar & 200minutes	S/N ratio		
Conversion (%)	76.6	37.68		89.7	39.056	1.376	
Diesel Selectivity (%)	66.5	36.46		88.2	38.91	2.45	
Naphtha Selectivity (%)	8.4	-18.49		1.1	-0.82	17.67	
MPCI	0.053		0.944	0.940			0.887

4.5. Physico-chemical properties

In a one liter capacity test setup (similar to the one described in Section 3.3), the optimized parameters were used to produce the hydrotreated waste cooking oil in large quantities. Blends of the hydrotreated oil & diesel and ternary blends of hydrotreated oil, biodiesel & diesel were prepared as previously described in Section 3.5. In this section the properties of the fuel blends and neat fuel samples which were evaluated using the equipment and methods described earlier is discussed in detail.

4.5.1. Composition of the fuel

The gas chromatography was carried out to find the composition of the neat hydrotreated oil using a Shimadzu QP-2010 instrument. The GC profile shows (Fig. 4.8) that the fuel has carbon atoms in the range of C_{11} to C_{20} and heptadecane is the predominant hydrocarbon. The other major straight chain hydrocarbons observed are decane, undecane, dodecane, tetradecane, hexadecane, octadecane, nonadecane and tricosane. The straight chain carbon atoms present in the fuel improves its energy density and volatility which increases as the chain length increases. This tends to improve the ignition quality and combustion of the fuel [121].

Initially, the waste cooking oil had nearly 77% unsaturation which reduced to 40% after the hydrotreating process whereas the saturation of the fuel increased to nearly 60%. The unsaturation is caused by the presence of the methyl esters in the fuel sample. The mass spectroscopy also shows that the isomerization of the fuel has taken place and significant amounts of isomers are present in the fuel sample. It is expected that the isomers help in improving the cold flow properties of the fuel [78].

4.5.2. Infrared Spectroscopy

The infrared analysis of the fuel was carried out to analyse its molecular structure which is based upon the vibration of the molecules and the energy associated with it.

The data of the infrared spectroscopy is shown in Fig. 4.9. The infrared absorption frequencies for the hydrocarbons is given in Table 4.6. The peaks at 2854, 2923 and 2956 wave number are of straight chain alkanes and the peaks at 1378 and 1463 wave number are of –CH_3 bending i.e. of methyl groups. These peaks show that the fuel contains large amount of straight chain hydrocarbons and small amount of isomeric hydrocarbons. The peaks at wave number 1170 and 1742 represent the presence of ester compounds in the fuel, however, these peaks are small which shows that the amount of these compounds is less in the fuel. The GC-MS analysis confirms these findings. This data shows that the hydrotreating process has considerably reduced the amount of oxygen in the fuel and it contains large amount of straight chain hydrocarbons. Similar results were also observed by Satyarthi and Srinivas [203].
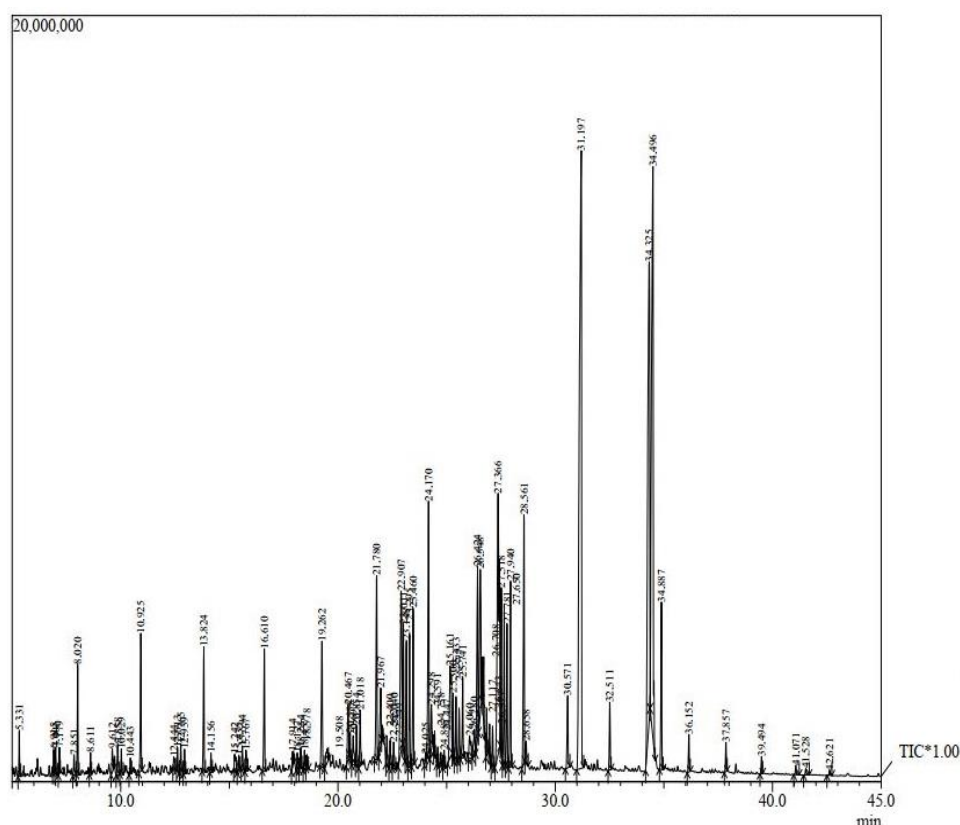

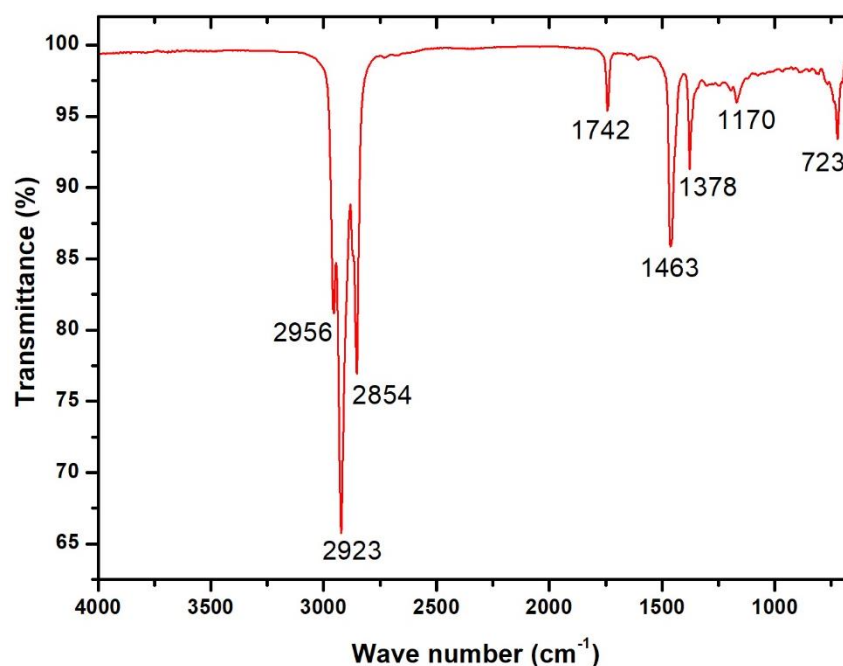**Fig. 4.8** GC-MS profile of hydrotreated used cooking oil

Fig. 4.9 FTIR test of neat hydrotreated used cooking oil

Table 4.6 Infrared absorption frequencies

S. No.	Functional Group	Wave Number (cm^{-1})
1	-O-H stretching (alcohol)	3300-3400
2	=C-H stretching (alkene)	3265-3335
3	-C-H stretching (alkane)	2850-3000
4	-C-H stretching (aliphatic)	4200-4600
5	-C=O stretching (ester)	1730-1750
6	-C=C stretching (alkyne)	1600-1680
7	-CH$_3$ bending	1450-1375
8	O=C-O-C aliphatic (ester)	1160-1210
9	-C-O stretching (ester)	1000-1300
10	Alcohols free	3600-3650
11	Alcohols H-bonded	3200-3500
12	Out of plane bend	>1000

4.5.3. Density

Density is one of the key properties for understanding the applicability of a fuel in a compression ignition engine. Important fuel characteristics such as cetane rating and heating value is related to density. The engine power output is also affected by the fuel density [204]. As per ASTM D1298 and EN 590 standard for diesel fuel, the density should be in the range of 820-860kg/m^3 and 820-845kg/m^3, respectively. As discussed previously, the density of the test samples was determined using an Anton Parr

oscillating U-tube density meter. Fig. 4.10 shows the density of the blends of hydrotreated oil and diesel. It is seen that the density of H100 was lowest and neat diesel had the highest density. As the percentage of hydrotreated oil increased in the blend, the density decreased. The density was observed to be 835.1, 817.7, 832.4, 829.7, 829.1, 828.5 and 827.7kg/m^3 for D100, H100, H10D90, H20D80, H30D70, H40D60 and H50D50, respectively.

Fig. 4.11 shows the density of the ternary blends of diesel, hydrotreated oil and biodiesel. It is seen that the density of the biodiesel is the highest and the ternary blends had lower density and as the percentage of biodiesel increases in the blend of diesel and hydrotreated oil, the density increases. The density for B100, H20B5, H20B10, H20B15, H30B5, H30B10, and H30B15 is 863.7, 833, 834.46, 835.89, 831.29, 832.72, and 834.15 kg/m^3, respectively.
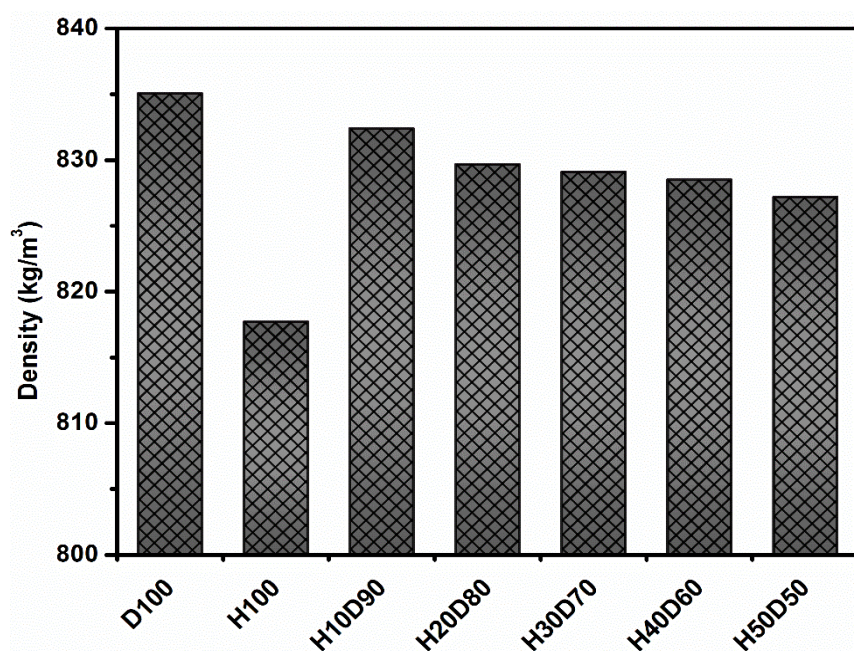

Fig 4.10 Variation in density for blends of hydrotreated oil and diesel
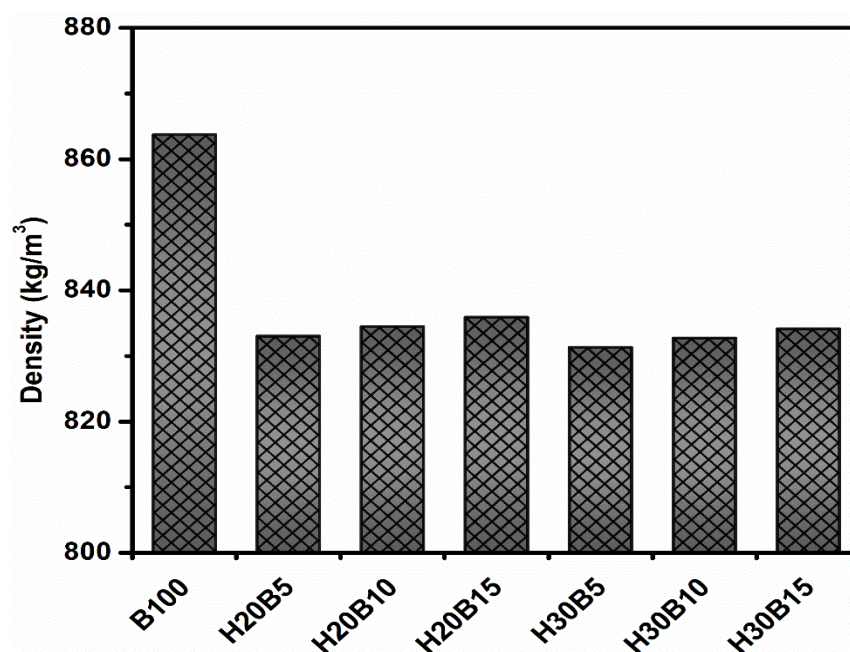
Fig 4.11 Variation in density for blends of biodiesel, hydrotreated oil and diesel

4.5.4. Kinematic viscosity

Kinematic viscosity is known as the resistance to the flow of fluid. It affects the operation of the fuel injection system and the atomization of the spray. Its affects are more visible on low temperatures as the viscosity of the fluid increases thereby affecting the combustion of the fuel. Moreover, soot formation and deposits in the engine may also increase due to insufficient atomization of fuel [205]. According to ASTM D445 and EN 590 standard, to utilize diesel like fuels in a compression ignition engine the kinematic viscosity should be in the range of 2 – 4.5cSt. Figs. 4.12 & 4.13 shows the kinematic viscosity of all the fuel samples. The kinematic viscosity of D100, H100, H10D90, H20D80, H30D70, H40D60, H50D50, B100, H20B5, H20B10, H20B15, H30B5, H30B10 and H30B15 was observed to be 2.51, 2.9, 2.54, 2.59, 2.62, 2.66, 2.69, 5.82, 3.29, 3.44, 3.62, 3.32, 3.47 and 3.64cSt, respectively. The kinematic viscosity of neat hydrotreated oil and biodiesel is higher than pure diesel as the fuel contains some amount of oxygen. Manchanda et al. [206] in their study observed that the presence of oxygen in the fuel affects its kinematic viscosity, i.e. the higher the amount of oxygen the higher is the viscosity.
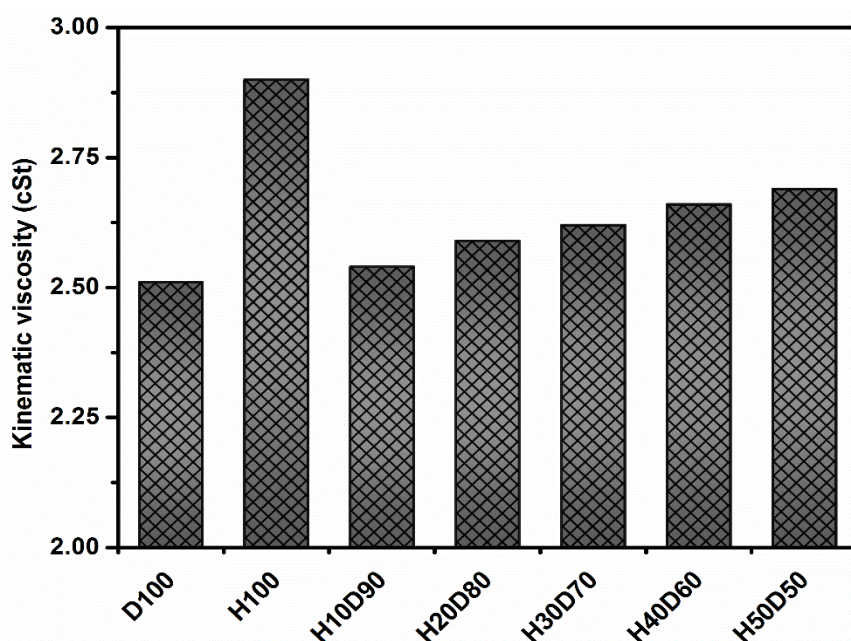
Fig 4.12 Variation in kinematic viscosity for blends of hydrotreated oil and diesel
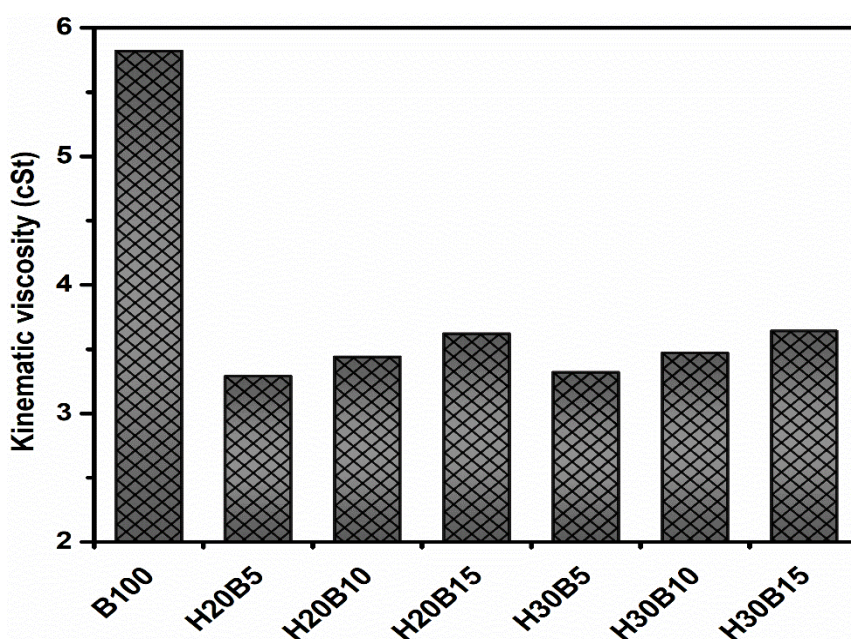
Fig 4.13 Variation in kinematic viscosity for blends of biodiesel, hydrotreated oil and diesel

4.5.5. Calorific value

It represents the energy released by burning a unit mass of fuel resulting in the formation of water and CO_2. The power of the engine is directly affected by this property. As previously discussed, a bomb calorimeter was used for measuring the energy content of the test samples. Fig. 4.14 shows that diesel has the highest calorific

value of 42.57MJ/kg. Neat H100 has the lowest calorific value of 41.79MJ/kg. Fig. 4.15 shows calorific value of the ternary blends of the hydrotreated oil, diesel and biodiesel. The calorific value of a fuel is affected by its oxygen content, since neat H100 has some oxygen content its calorific value is lower than diesel. Similarly, B100 has high oxygen content, therefore, its calorific value is also lower than diesel. For the blends, as the content of the hydrotreated oil increases in the mixture the calorific value decreases. For H10D90, H20D80, H30D70, H40D60 and H50D50 the calorific was found to be 42.41, 42.29, 42.08, 41.92 and 41.86 MJ/kg, respectively. For the ternary blends also as the percentage of the biodiesel in the blend increases, the calorific value decreases. The calorific value of B100, H20B5, H20B10, H20B15, H30B5, H30B10 and H30B15 is 41.27, 42.35, 42.28, 42.22, 42.27, 42.21, and 42.14MJ/kg, respectively.

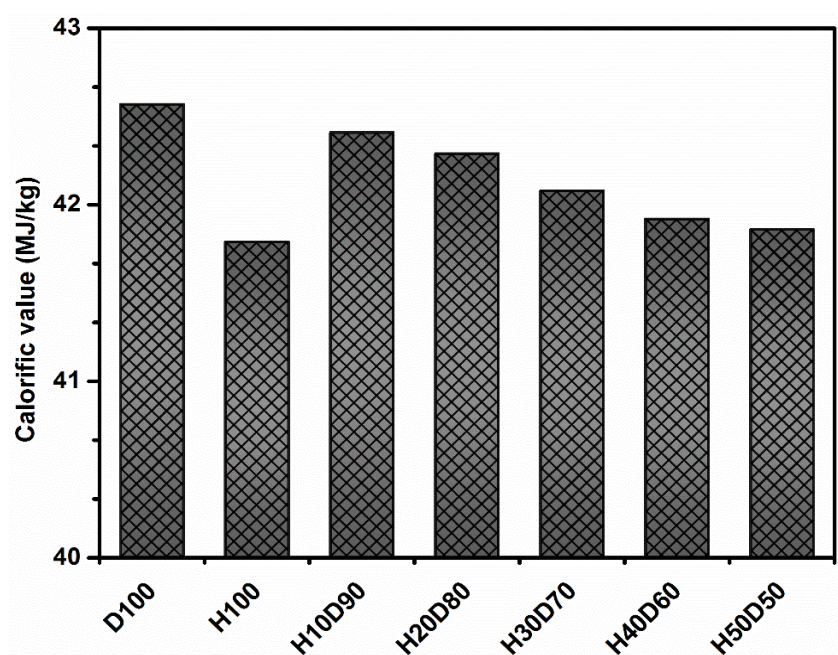**Fig 4.14** Variation in calorific value for blends of hydrotreated oil and diesel
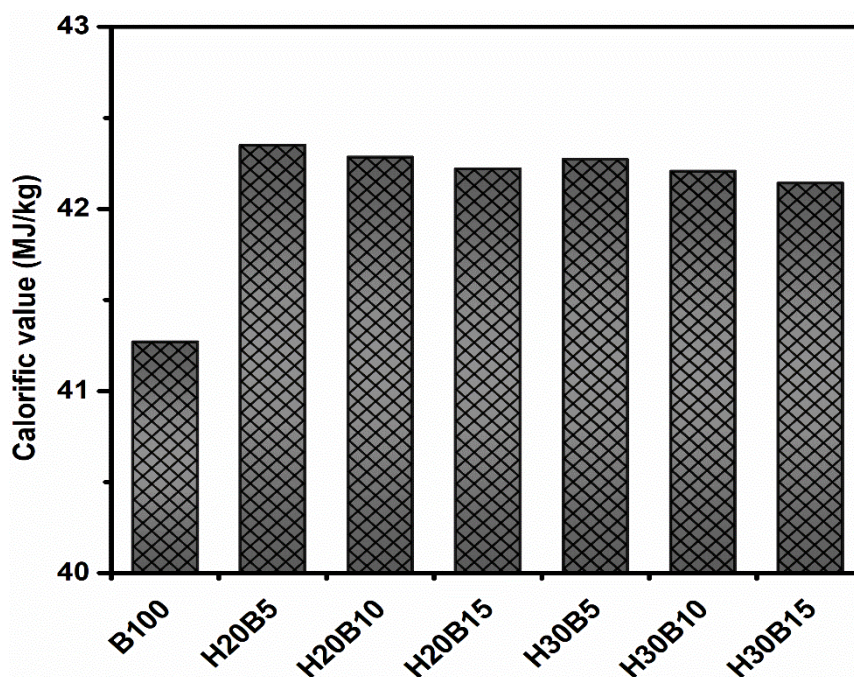
Fig 4.15 Variation in calorific value for blends of biodiesel, hydrotreated oil and diesel

4.5.6. Flash point

The minimum temperature at which the produced vapours on heating the fuel are flammable in nature. At this temperature when a source of ignition is brought near the surface of the fuel, the vapours combine with the oxygen in air and flash for a fraction of second. It is seen in Fig. 4.16 that H100 has a flash point of 68°C, whereas, diesel has flash point of 58°C. Blending of the hydrotreated oil with diesel resulted in increase in flash point as the percentage of the hydrotreated oil increased in the blend. The flash point of H10D90, H20D80, H30D70, H40D60 and H50D50 was observed to be 59°C, 60°C, 61°C, 62°C, and 63°C, respectively. Fig. 4.17 shows that B100 has the highest flash point of 165°C. The addition of the biodiesel to the blends of the hydrotreated oil resulted in increase in flash point and as the percentage of biodiesel increases the flash point increases. The flash point of H20B5, H20B10, H20B15, H30B5, H30B10 and H30B15 is 70, 77, 83, 73, 78 and 84°C, respectively.
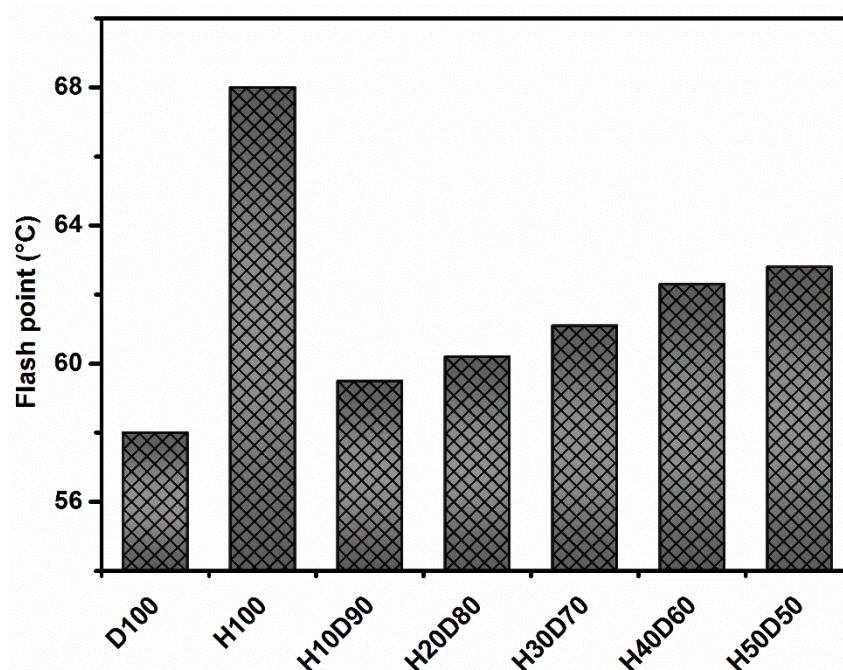
Fig 4.16 Variation in flash point for blends of hydrotreated oil and diesel
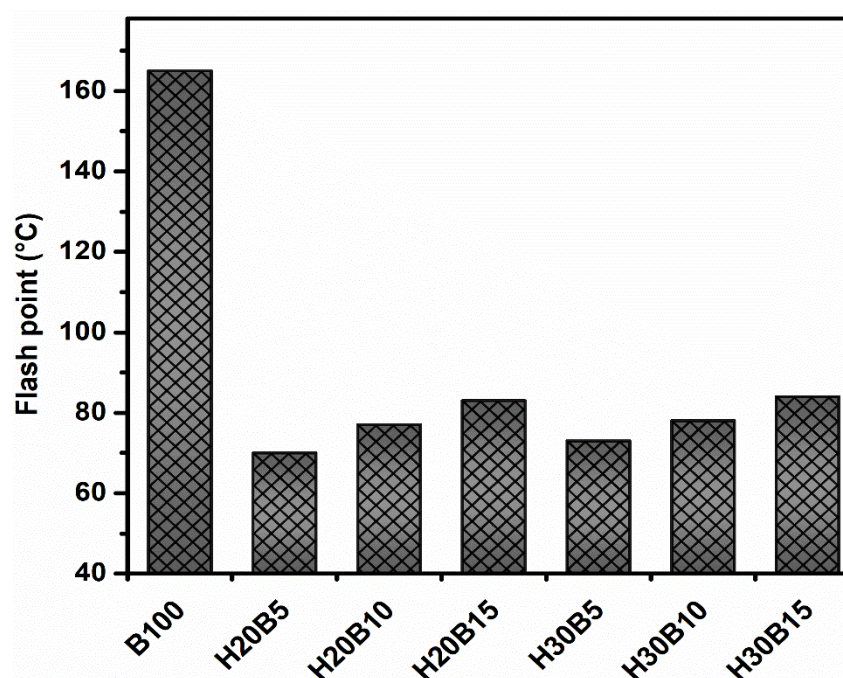
Fig 4.17 Variation in flash point for blends of biodiesel, hydrotreated oil and diesel

4.5.7. Distillation Data

The distillation of the test samples was carried out using the method given in Section 3.6.5. Figs. 4.18 shows the distillation temperature when 10%, 50% and 90% of the fuel sample was recovered. The boiling temperature when 10% of the fuel fraction is recovered indicates the ease with which vaporization takes place i.e. the

volatility of fuel is high. While the temperature when 90% of the fuel is recovered indicates that high molecular weight compounds are present which are difficult to vaporize thereby increasing the particulate emissions and engine deposits [74]. It is seen that H100 has a higher distillation temperature than diesel when 10% and 50% of the fuel sample was recovered. Whereas, H100 has lower distillation temperature than diesel when 90% of the sample was recovered. This shows that the engine operation with H100 will result in lower emissions than diesel as it has low amount of compounds with high molecular weight.

Neat biodiesel has the highest distillation temperature at 10%, 50% and 90% recovery of the fuel due to its low volatility. When biodiesel is added to 20% and 30% of the hydrotreated oil, the recovery of fuel at 10%, 50% and 90% increases and is higher than the hydrotreated blends without biodiesel. As the percentage of biodiesel increases in the blend, its distillation temperature increases. Moreover, the maximum temperature is lower than the ASTM D6751 standard limit.

4.5.8. Cetane index

Cetane number helps in understanding the self-ignition characteristics of the fuel after it is injected into the combustion chamber. Since cetane number is difficult to estimate another parameter cetane index helps in understanding the ignition characteristics of the fuel. Cetane index is determined by the distillation of the fuel and its density. The method for finding out the cetane index was discussed in detail in Section 3.6.6. Figs. 4.19 & 4.20 shows the cetane number of the test fuels. It is seen that the cetane index of H100 is higher than diesel and as the content of the hydrotreated oil in the blends increases the cetane index increases. As seen in Fig. 4.29, the ignition probability of H100 is higher than diesel at any temperature and the probability rises to 100% at lower temperatures for H100 as compared to other test samples. This shows

that the higher cetane index of H100 helps in the earlier ignition of the fuel. B100 has a higher cetane index than diesel but lower cetane index than H100. The ternary blends prepared by mixing biodiesel in the blends of the hydrotreated oil and diesel resulted in increase in cetane index of the samples as the biodiesel replaces diesel. Also as the percentage of biodiesel increases in the blend, the cetane index increases. The cetane index of D100, H100, H10D90, H20D80, H30D70, H40D60, H50D50, B100, H20B5, H20B10, H20B15, H30B5, H30B10 and H30B15 was observed to be 45.7, 65.2, 47.9, 49.9, 51, 52.2, 53.9, 46.9, 50.2, 51.6, 52.7, 52.1, 53.15, and 54.17, respectively.
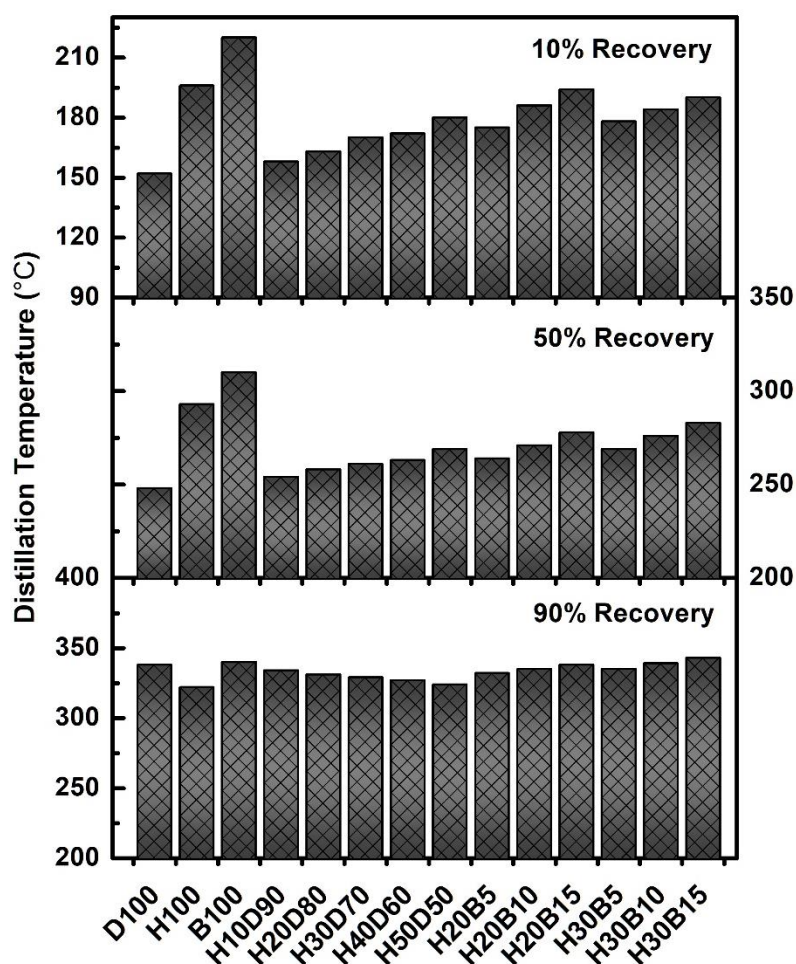
Fig. 4.18 Distillation data for blends of hydrotreated oil and diesel and ternary blends of hydrotreated oil and diesel and biodiesel at 10%, 50% and 90% recovery
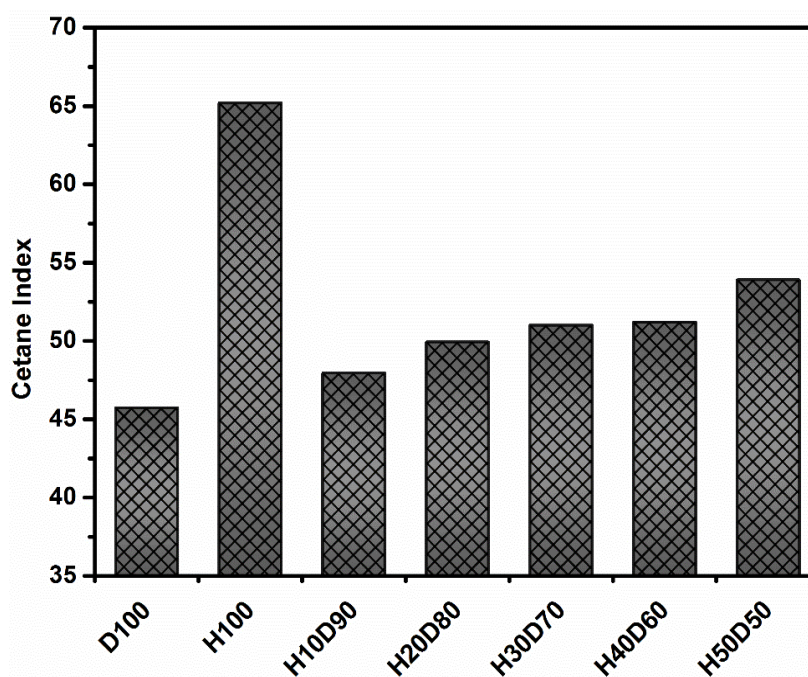
Fig. 4.19 Variation in cetane index blends for blends of hydrotreated oil and diesel

Fig. 4.20 Variation in cetane index for blends of biodiesel, hydrotreated oil and diesel

4.5.9. Cold flow properties

To understand the suitability of the fuel at low temperatures, it is important to study its cold flow properties. Paraffinic hydrocarbons are more suitable as fuel as they have good auto-ignition characteristics but their cold flow properties are poor resulting in the

formation of wax crystals [207]. This affects the fuel pump pumping capacity by clogging the fuel filter resulting in engine failure [208]. Cold flow properties are mainly dependent upon the contents of the fuel. Cloud point and cold filter plugging point (CFPP) are the two properties that were determined in this study. Cloud point is the lowest temperature at which the fuel molecules start agglomerating and crystal formation can be seen. CFPP is the temperature at which a given volume of fuel ceases to flow through a fuel filter. At this temperature the crystals formed are big enough to clog the fuel filter thereby stopping the flow of the fuel to the fuel injector. The method and the equipment used for finding the cloud point and CFPP is given in Section 3.6.7 and 3.6.8, respectively. Figs. 4.21, 4.22, 4.23 and 4.24 shows the cloud point and CFPP of the test fuels. It is seen that H100 has lower cloud point and CFPP than diesel and B100. Moreover, as the percentage of the hydrotreated oil in the blend increases the temperatures of both the properties decreases. The GC-MS profile of H100 (Fig. 4.8) shows that the fuel has some isomeric content which improves its cold flow property [78]. Therefore, the fuel can be easily used in the Indian winter conditions. Due to high viscosity of biodiesel, its cloud point and cold filter plugging point are high. With biodiesel addition to the blends of the hydrotreated oil, the cloud point and CFPP increases. This shows that the cold flow properties of the biodiesel blends have deteriorated and additives that can enhance the cold flow properties are required.
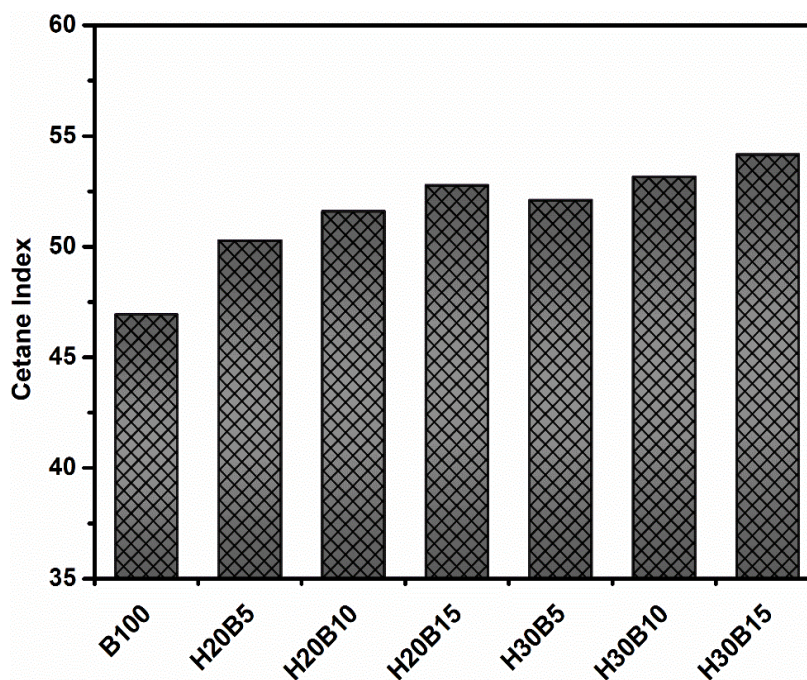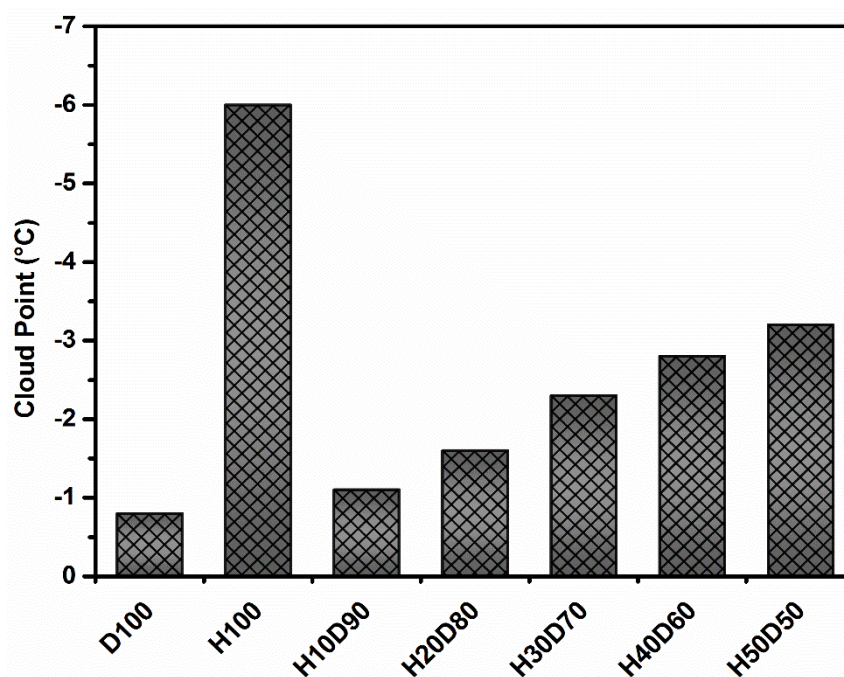
Fig. 4.21 Variation in cloud point for blends of hydrotreated oil and diesel
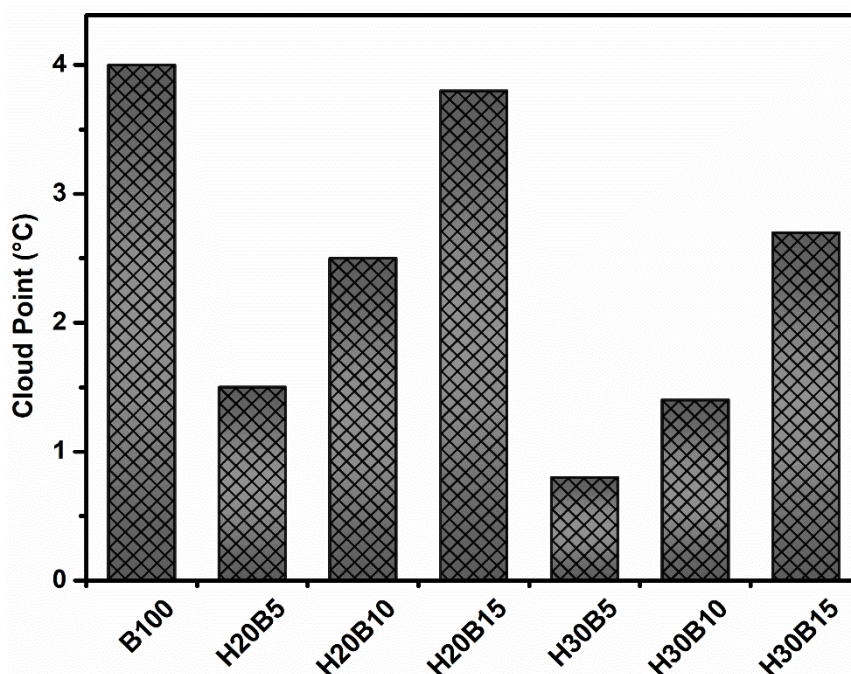
Fig. 4.22 Variation in cloud point for blends of biodiesel, hydrotreated oil and diesel
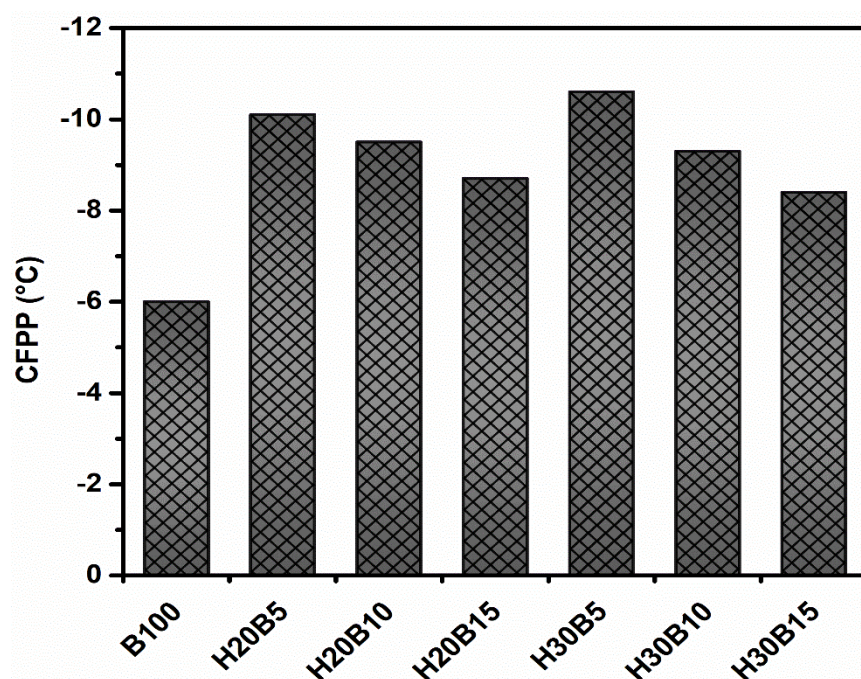
Fig. 4.23 Variation in cold filter plug point for blends of hydrotreated oil and diesel
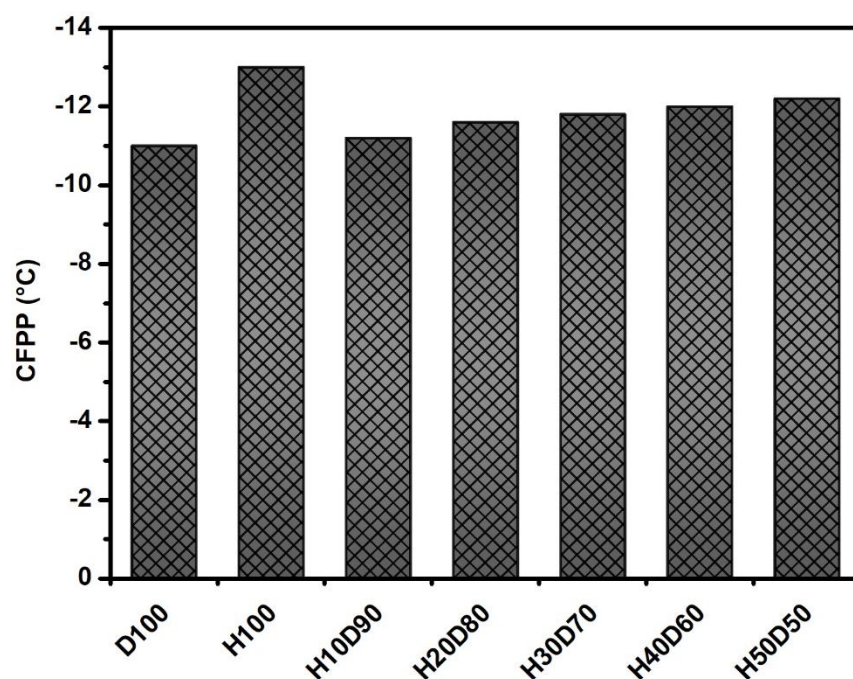
Fig. 4.24 Variation in cold filter plug point for blends of biodiesel, hydrotreated oil and diesel

4.5.10. Lubricity

The fuel pump in a compression ignition engine is lubricated only by the fuel.

Therefore, the fuel should have good lubricating properties. To evaluate the lubricating

properties, the wear scar diameter on the ball rubbing on a disk filled with the fuel can

be found out using an HFRR test rig (Section 3.6.9). The lower the scar diameter on the ball, the better the lubricating properties of the fuel. The experiment is based on ASTM D6079 standard. The experimental results are shown in Figs. 4.25 and 4.26. It is seen that H100 has lower wear scar diameter than diesel. This is mainly due to its high viscosity which helps in forming a layer on the disk thereby reducing the scar formation on the ball, which shows that the lubricating properties of H100 is better than all the other test samples. The scar diameter with the other blends were observed to be in between H100 and diesel. As the percentage of the hydrotreated oil increases in the blend, the wear scar diameter is reduced. B100 has the lowest wear scar diameter, as its viscosity is highest. As the biodiesel is added to the blends of 20% and 30% of the hydrotreated oil, the wear scar diameter is observed to decrease for all the blends and as the percentage of the biodiesel increases the wear scar diameter decreases, i.e. the lubricity of the test blends increases. Table 4.7 and Table 4.8 compares the properties of the blends.
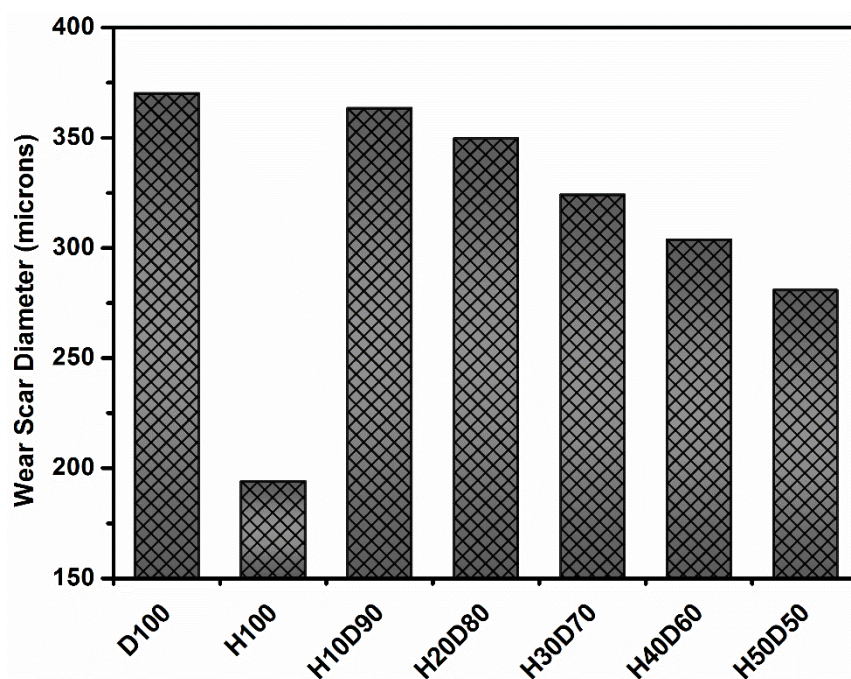
Fig. 4.25 Variation in wear scar diameter for blends of hydrotreated oil and diesel
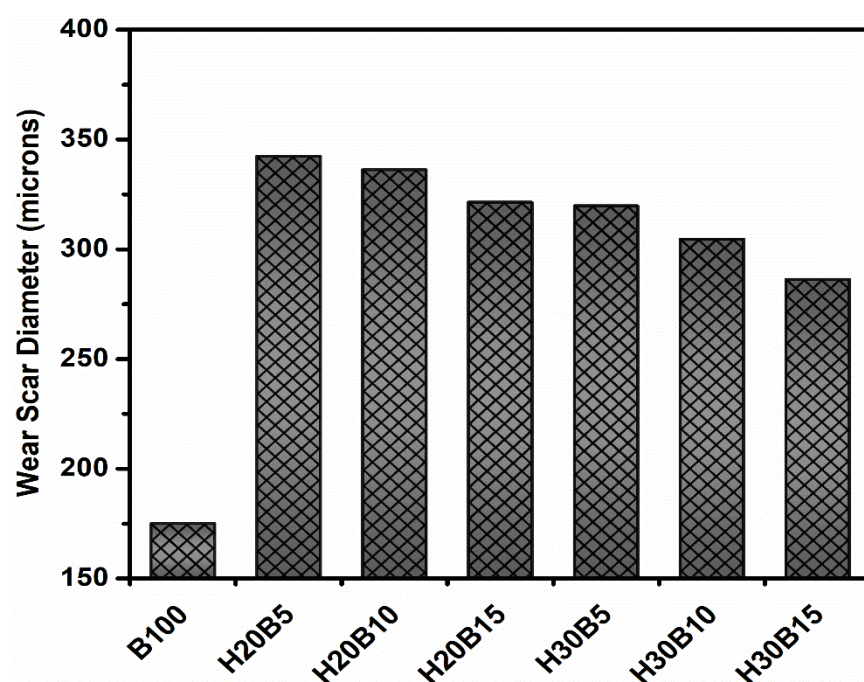
Fig. 4.26 Variation in wear scar diameter for blends of biodiesel, hydrotreated oil and diesel

Table 4.7 Properties of the neat diesel, HVO and their blends

Property	D100	H100	H10D90	H20D80	H30D70	H40D60	H50D50
Density at 15°C (kg/m^3)	835.07	817.7	832.4	829.68	829.1	828.5	827.19
Kinematic viscosity at 40°C (cSt)	2.51	2.9	2.54	2.59	2.62	2.66	2.69
Calorific value (MJ/kg)	42.57	41.79	42.41	42.29	42.08	41.92	41.86
Flash point (°C)	58	68	59.5	60.2	61.1	62.3	62.8
Cetane Index	45.73	65.2	47.95	49.93	51.0	52.2	53.9
Cloud point (°C)	-0.8	-6	-1.1	-1.6	-2.3	-2.8	-3.2
CFPP (°C)	-11	-13	-11.2	-11.6	-11.8	-12	-12.2
Lubricity, HFRR (microns)	370.2	194	363.4	349.6	324.1	303.6	280.8

Table 4.8 Properties of the neat biodiesel, HVO and their blends

Property	B100	H20B5	H20B10	H20B15	H30B5	H30B10	H30B15
Density at 15°C (kg/m^3)	863.71	833.02	834.46	835.89	831.29	832.72	834.15
Kinematic viscosity at 40°C (cSt)	5.82	3.29	3.44	3.62	3.32	3.47	3.64
Calorific value (MJ/kg)	41.27	42.35	42.28	42.22	42.27	42.21	42.14
Flash point (°C)	165	70	77	83	73	78	84
Cetane Index	46.93	50.28	51.6	52.77	52.1	53.15	54.17
Cloud point (°C)	4	1.5	2.5	3.8	0.8	1.4	2.7
CFPP (°C)	-6	-10.1	-9.5	-8.7	-10.6	-9.3	-8.4
Lubricity, HFRR (microns)	175	342.3	336.2	321.4	319.8	304.6	286.2

4.6. Evaporation time and ignition probability

The hot plate setup was used for finding the evaporation time and ignition probability. Fig. 4.27 shows the evaporation time of the fuel samples at various temperatures of the plate surface. The experiments were conducted as discussed in the previous chapter. The trends can be broadly classified into four regions namely evaporation of the fuel, nucleate boiling, transition boiling and film boiling [209]. The droplet and the plate surface are in direct contact with each other in the evaporation region. As the surface temperature increases, the heat transfer through conduction increases resulting in decrease in evaporation time. Further increase in surface temperature leads to formation of bubbles known as nucleate boiling. Due to the formation of bubbles, the mixing of the fluid increases thereby increasing the heat transfer rate through the surface of the plate and as the temperature increases the evaporation time decreases further. The bubble formation of H100 and D100 started at 195 and 250°C, respectively. The boiling point of a liquid is dependent upon its heat capacity and boiling temperature. Therefore, the liquid having shortest boiling temperature will evaporate first [210]. The trends also shows that as the percentage of the hydrotreated oil in diesel increases the evaporation time decreases.

The surface temperature at which the evaporation time is lowest is called as critical temperature. At this temperature, the droplets are disintegrated after significant boiling and the evaporation of the test sample is almost instantaneous. H100 and D100 had a critical temperature of 270 and 360°C, respectively. The lowest critical temperature was observed for H100 and with its increase in percentage in diesel the critical temperature was found to increase. As the surface temperature is further increased the trend moves towards the region of transition boiling. In this region, the vapor film surrounds the droplet due to excessive bubble formation and the direct contact between the droplet

and the hot surface is broken. The evaporation time increases in this region due to low thermal conductivity of the vapor film thereby reducing the heat transfer. With further increase in surface temperature, the trend enters the film boiling region, wherein Leidenfrost phenomenon occurs i.e. the droplets surrounded by a vapor film starts levitating on the plate surface. The heat transfer in this region takes place through both thermal conduction and radiation resulting in slight decrease in evaporation time. Further increase in surface temperature lead to the ignition of the fuel sample.

Another study was conducted for finding the ignition probability using the hot plate test setup. The ignition probability was calculated using Logistic regression and the fit quality was determined using Chi-squared goodness fit test [211]. The surface temperature for the tests were varied in the range of 280 to 640°C since the film boiling for the test fuels occurs in this region. Previous studies [212–214] also show that the film boiling region has the highest ignition probability. Fig. 4.28 shows that the ignition probability of H100 is higher than the other test fuels at all the temperatures. At 560°C the ignition probability was 100% with H100, whereas the ignition probability was 100% for diesel at 600°C. The ignition probability of the blends was found to vary in between the two test fuels. The fuels' chemistry plays a major role in improving its ignition chances. The large paraffinic and low aromatic content of hydrotreated oil improves its cetane number, thereby improving its ignition probability [193,215]. Also, H100 has carbon atoms in range of C_{11} to C_{18} whereas the carbon atoms in a typical diesel fuel varies from C_8 to C_{22} [121]. If small quantity of long chain carbon atoms is present in a fuel then its boiling point is relatively less and its volatility is higher in comparison to fuels having large quantity of long chain carbon atoms [216]. Since, H100 contains smaller carbon atom chains than diesel, therefore its boiling point is lower and volatility is higher than diesel which increases its ignition probability.
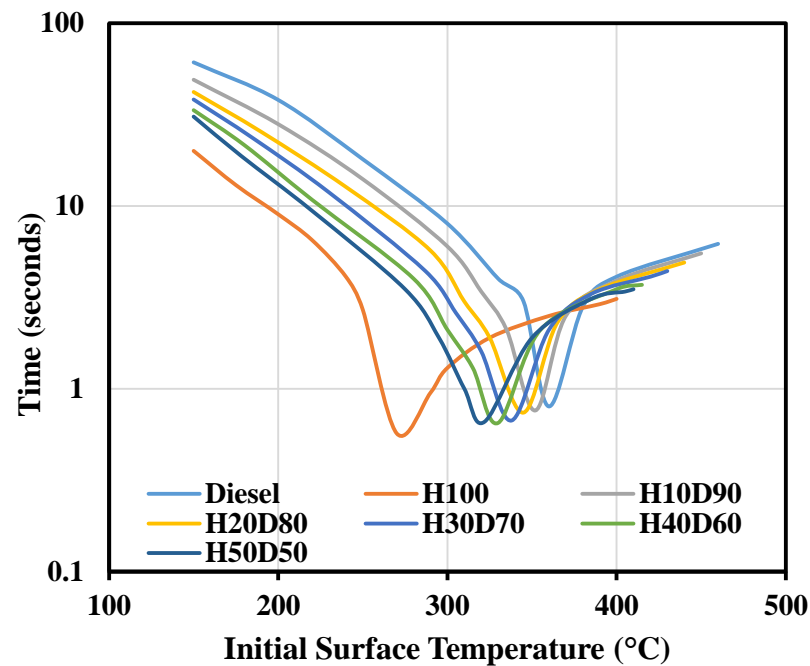
Fig. 4.27 Variation of evaporation time with surface temperature of plate
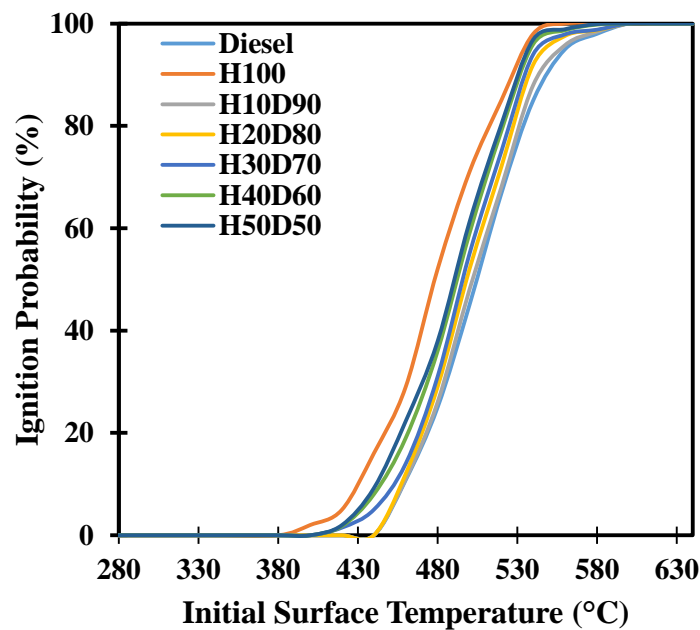
Fig. 4.28 Variation of ignition probability with surface temperature of plate

4.7. Sauter mean diameter

Whenever, the fuel is injected, the spray consists of particles of varying sizes, therefore, the average size of the particles is statistically calculated which is known as Sauter mean diameter (SMD). The particle size depends upon the fuel properties such as surface tension, density, and viscosity. The fuel injection pressure also plays a role

in the particle size. The SMD of neat diesel, hydrotreated oil and their blends is shown in Fig. 4.29. The SMD of the hydrotreated oil is higher than diesel on account of its higher viscosity. Due to instabilities present in the sprayed fuel its breaks up into fine particles [217]. However, the molecules of high viscosity fuel are closely packed and the collision force of the molecules is less. Therefore the fuel molecules are unable to move with respect to each other within the spray hence the fuel jet is stable and unable to break, thereby increasing the particle size. Biodiesel produced from various inedible oils also has higher SMD than diesel due to their higher viscosity [218].

Fig. 4.30 shows the specific surface area of the fuel samples. It is the ratio of the surface area of the particle to its volume. Particles having high surface area will be surrounded by more amount of oxygen resulting in lesser ignition delay thereby improving the combustion [219]. Diesel has the highest while H100 has the lowest surface area. As seen in Fig. 4.30, the particles having the lowest SMD has the highest surface area. Also H10D90 has surface area similar to that of diesel whereas with the increase in the percentage of hydrotreated oil, the surface area keeps decreasing.
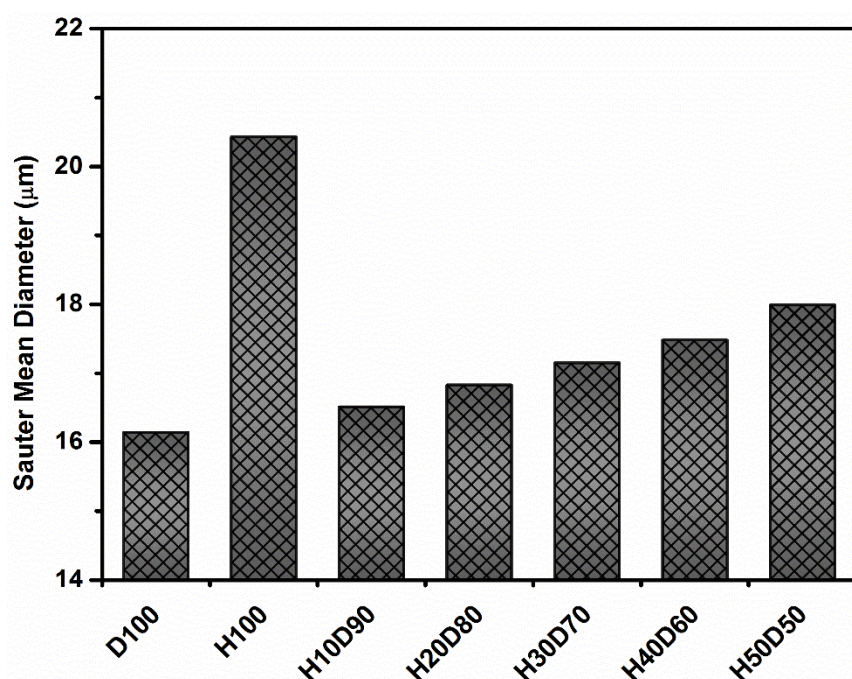
Fig. 4.29 Sauter mean diameter for blends of hydrotreated oil and diesel

Performance, Emission and Combustion Studies of a Modified Vegetable Oil in a Compression Ignition Engine
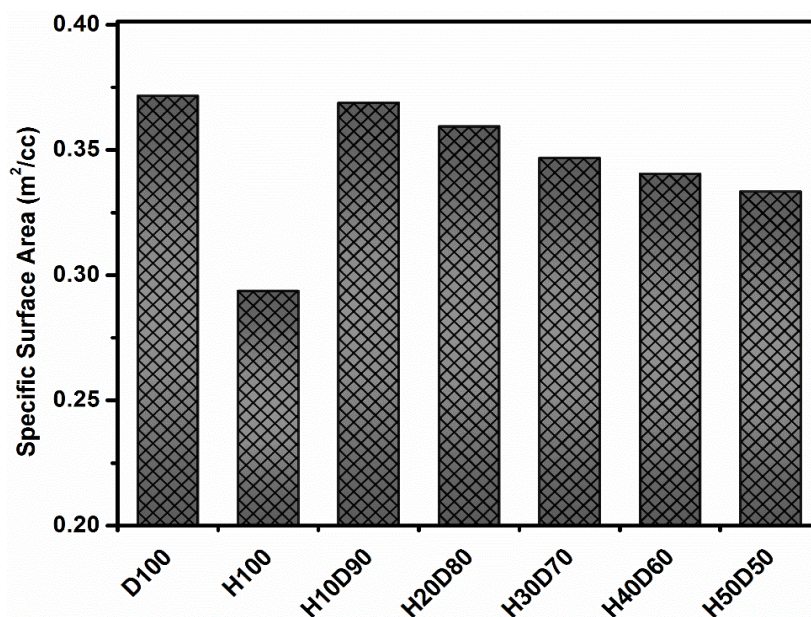
Fig. 4.30 Specific surface area for blends of hydrotreated oil and diesel

4.8. Effect of storage on fuel properties

When the fuel is stored for a long time there is a possibility of the degradation of the fuel. In this work, three key properties namely, density, kinematic viscosity and calorific value were evaluated every month to understand the change in fuel stored for one year. The samples were stored in an air tight glass container where no direct sunlight enters.

Fig. 4.31 shows that the density of the test fuels changed slightly over a period of twelve months. The rate of increase of density of H100 was higher than the blends. This is probably due to the presence of small amount of oxygen which may have resulted in the formation of oxygenated products. As the blends contain less amount of hydrotreated oil, the oxygen content is less therefore the change in properties of the blends is less. As compared to freshly prepared fuel, the density of the stored fuel with H10D90, H20D80, H30D70, H40D60, H50D50 and H100 increased by 0.48%, 0.51%, 0.49%, 0.49%, 0.48% and 0.68%, respectively.

The change in kinematic viscosity of the test fuels stored for twelve months is shown in Fig. 4.32. The viscosity of the fuel greatly affects the fuel injection system of a diesel engine. The fuel injected by the injector will not be atomized properly if its viscosity is high resulting in poor engine performance characterized by high fuel consumption and emissions [220]. High viscosity of the fuel can plug the fuel filters as well. With increase in storage period an increasing trend in the viscosity is observed. The viscosity of freshly prepared H100 was 2.9cSt which increased to 3.33cSt in one year of storage. It is also seen that the kinematic viscosity of the blends also increased but they were lower than H100.

The variation of calorific value of H100, H10D90, H20D80, H30D70, H40D60 and H50D50 stored over twelve months is indicated in Fig. 4.33. As the storage period increases the calorific value decreases for all the test samples. The rate of decrease of calorific value for H100 was higher than the other fuel samples. The calorific value of freshly prepared H100 was 41.79MJ/kg which decreased to 40.58MJ/kg after twelve months, a decrease of 0.51%.

The three figures show that the properties of fuel are affected when stored for twelve months, but the variation in properties is not significant and the values are still lower than that specified in the standards of diesel. This shows that the fuel can be used in a CI engine without any difficulty even if it is stored for twelve months.
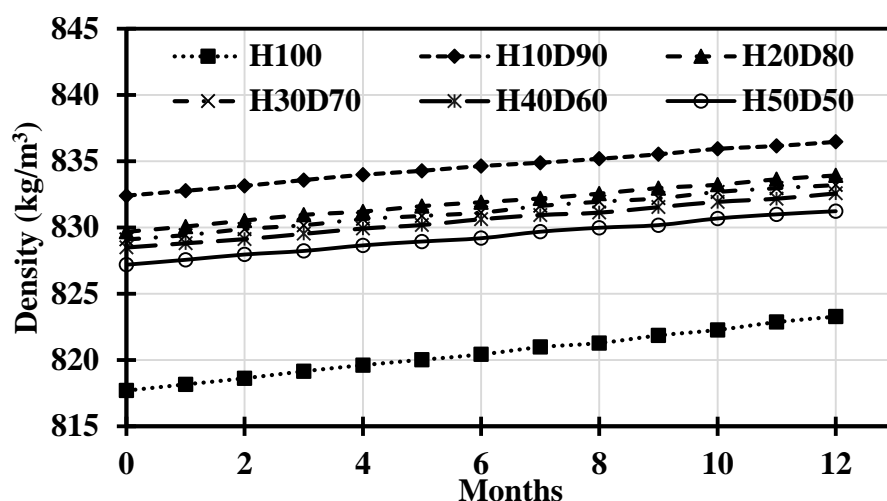
Fig. 4.31 Variation in density for blends of hydrotreated oil and diesel stored for 12 months
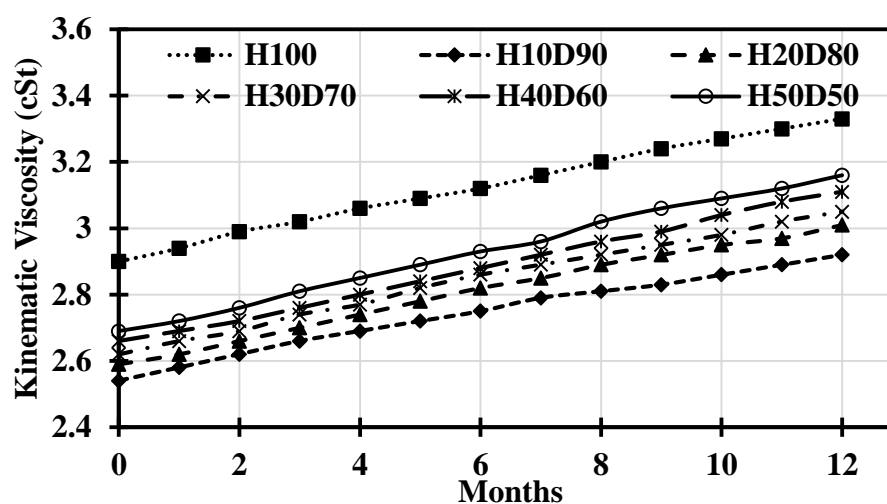
Fig. 4.32 Variation in kinematic viscosity for blends of hydrotreated oil and diesel stored for 12 months
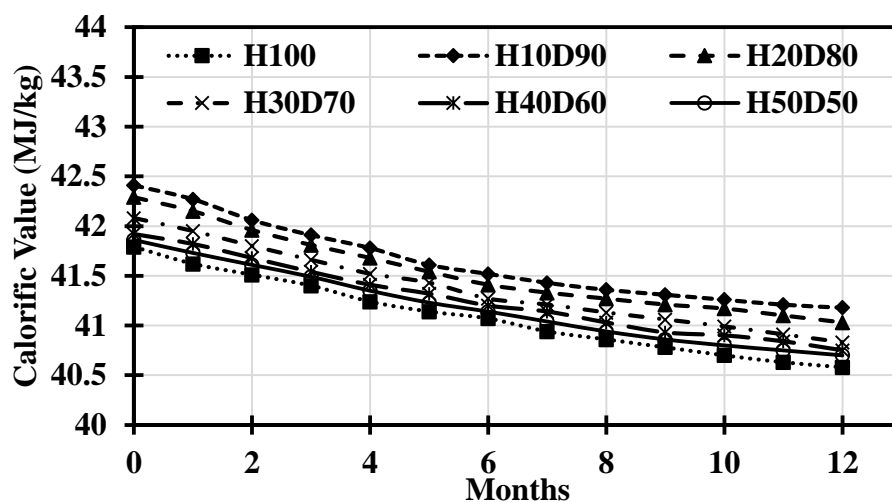
Fig. 4.33 Variation in calorific value for blends of hydrotreated oil and diesel stored for 12 months

CHAPTER 5

ENGINE PERFORMANCE, COMBUSTION AND EMISSION STUDY

5.1. Introduction

Renewable diesel can be a prospective alternative fuel for compression ignition engines. As discussed earlier, hydrogen breaks the double bond and removes oxygen present in the triglycerides with the help of a catalyst. The physical and chemical properties of the produced fuel is similar to diesel and its storage and transportation can be carried out using the existing infrastructure of diesel [193].

The in-cylinder peak pressure and rate of rise of pressure is low for hydrotreated oil fueled engines fueled [121]. The reason for the trend is reduced ignition delay caused by the burning of smaller premixed fraction thereby lowering the initial heat release rate. A light-duty, EURO-V diesel engine was operated with hydrotreated waste cooking oil by Kousoulidou et al. [221]. At low load the in-cylinder pressure with the hydrotreated oil was slightly higher than diesel which narrowed down at high loads. Since, the cetane number of the hydrotreated oil is high, the delay in ignition is less which slows down the heat release rate. Aatola et al. [126] and Sugiyama et al. [116] also observed similar results. Sugiyama et al. [116] also found small difference in heat release rate and ignition delay with hydrotreated oil and diesel at medium load condition.

Many researchers have used hydrotreated oil or its blends for studying the emissions from diesel engines. Aatola et al. [126] studied the smoke, HC, CO and NOx emissions from the exhaust of an unmodified engine operated with the fuel. The NOx and PM emissions reduced by 6 and 35%, respectively with the hydrotreated oil in comparison to diesel. The authors brought the NOx level with the hydrotreated oil equal to that with diesel and found 37% and 6% reduction in smoke and specific fuel

consumption. When the fuel consumption was kept same for both diesel and hydrotreated oil, reduction of 16% and 23% in NOx and smoke, respectively was observed for hydrotreated oil in comparison to diesel. Rapeseed methyl ester (RME), Jatropha methyl ester (JME), HVO and fossil diesel were compared for their bacterial mutagenicity and emission using a EURO-III heavy duty diesel engine [120]. The mutagenicity of JME and RME was found to be higher than hydrotreated oil. JME and RME engine operation resulted in lowest PM emission, while, RME engine operation has lower HC and CO emission. Moreover, RME and JME had higher NOx emissions in comparison to hydrotreated oil operation.

As seen in literature review (Chapter 2), calorific value and cetane number of hydrotreated oil influences its combustion that has an affect on the engine out emissions except for oxides of nitrogen emission. Since NOx emission is also dependent upon type of engine (light-duty or heavy duty), type of injection system, injection timing, combustion chamber design and test cycle [222]. This chapter discusses the experimental investigation for evaluating the hydrotreated used cooking oil fuel. The research was carried out on a single cylinder diesel engine which is used in agriculture as well as a power backup. The engine's performance, emission and combustion characteristics was evaluated at different loads. The effect of adding small percentages of used cooking oil biodiesel in the blends of the hydrotreated oil and diesel was also studied.

5.2. Engine performance characteristics for blends of hydrotreated oil and diesel

In the first phase, the engine experiments were first conducted with blends of neat hydrotreated oil and diesel. The tests were also carried out with neat hydrotreated oil and diesel. The load was varied in steps of 25% of full load. This section discusses the

combustion, performance and emission characteristics of the engine when operated with the test fuels.

5.2.1. Combustion Characteristics

In Fig. 5.1, the heat release rate at full load is compared for diesel, H10D90, H20D80, H30D70, H40D60, H50D50 and H100. The peak heat release for diesel is 56.13J/°CA whereas it is 45.96J/°CA for H100. The peak heat release of the blends was observed to be in between the two fuels and a decrease in the peak heat release is observed with increase of the hydrotreated oil in the blend. It is also seen that the hydrotreated oil and its blends had an earlier heat release due to reduced ignition delay caused by higher cetane number. Moreover, for H100 and the blends the heat released in diffusion combustion phase is high. The reason for small premixed combustion is burning of low amount of fuel because of shorter ignition delay. Similar results were obtained by Aatola et al. [126], McDaniel et al. [223], Sugiyama et al. [116], Mattson et al. [224] and Singh et al. [225].

Fig. 5.2 presents the in-cylinder pressure for the test fuels at full load. The peak in-cylinder pressure for diesel, H10D90, H20D80, H30D70, H40D60, H50D50 and H100 is 75.8bar, 73.41bar, 72.78bar, 71.4bar, 70.48bar, 68.6bar and 66.8bar, respectively. Due to lower heat release in the premixed stage, H100 and its blends with diesel resulted in lower peak pressures in comparison to diesel. Higher cetane index of the hydrotreated oil is the probable reason for the trend. With the increase in the hydrotreated oil in the blend the peak pressure reduces due to the rise in cetane number. Another interesting point to note is that the rate of pressure rise is slow for the neat hydrotreated oil and its blends. The gentle slope of the pressure curve indicates this phenomenon.
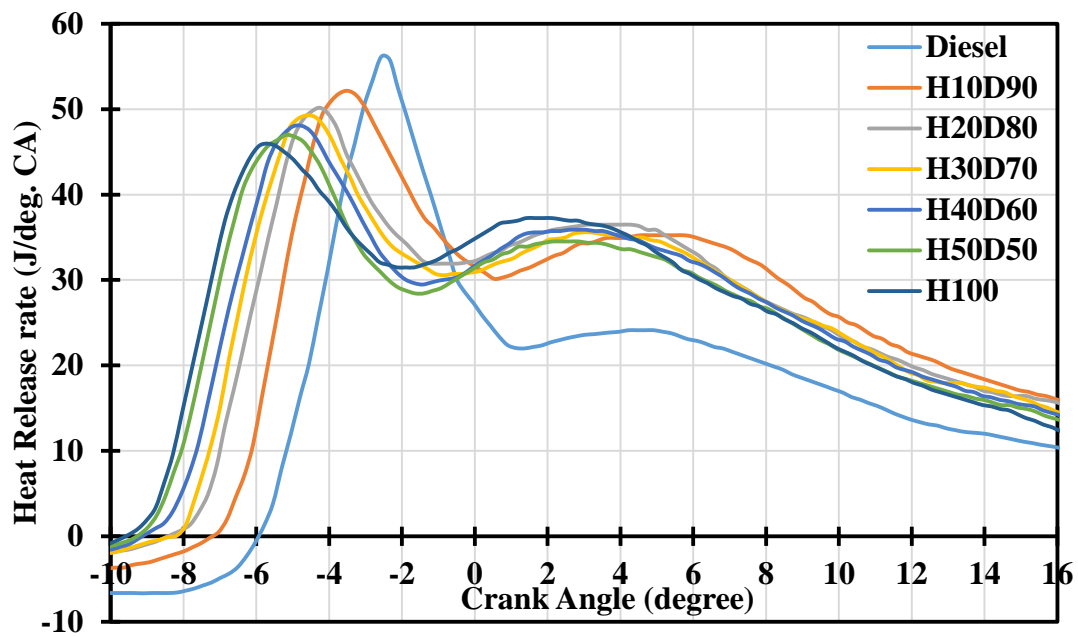
Fig 5.1 Variation in heat release rate at full load
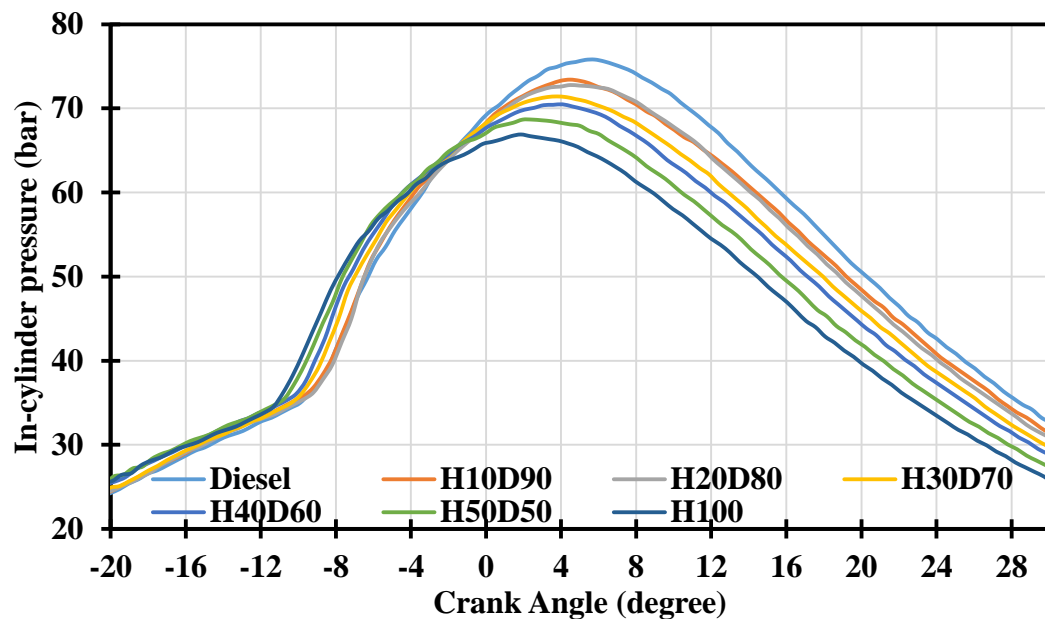
Fig 5.2 Variation in in-cylinder pressure at full load

The variation in peak pressure at different loads for all the test samples is shown in Fig. 5.3. It is seen that the peak pressure increases as the load on the engine increases. With the rise in load, the heat released increases as the amount of fuel injected is higher thereby increasing the in-cylinder pressure [226]. Moreover, the peak pressure at all the loads is lower for the test fuels in comparison to diesel. Also the increase of the hydrotreated oil in the blend decreases the in-cylinder pressure and neat hydrotreated

oil showed the lowest peak pressure. As stated earlier, cetane index influences the combustion causing the fuel to combust earlier than diesel and as less fuel is prepared to burn, the heat released in pre-mixed combustion is less thereby decreasing the in-cylinder pressure.
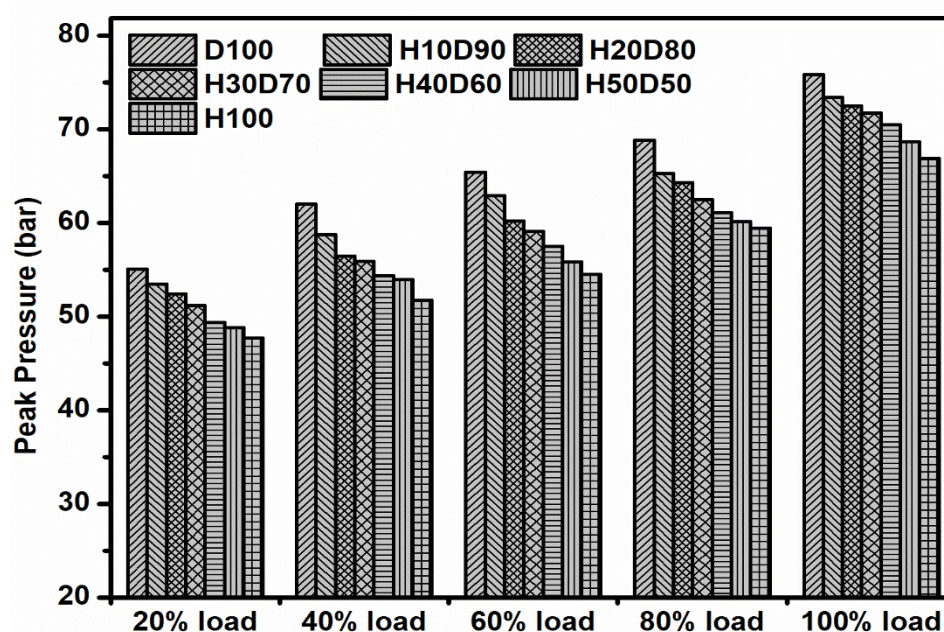
Fig 5.3 Variation in peak pressure at various loads

Fig. 5.4 presents the variation of ignition delay for all the test fuels with increasing load. The ignition delay in a diesel engine is defined as the difference in time (in terms of degree crank angle) when the fuel is injected to the time when the combustion begins [227]. The onset of combustion was considered when the heat release became positive in Fig. 5.1. For all the blends as the load on the engine increased, the ignition delay reduced. As the load increases, the in-cylinder temperature along with pressure increases which provides the necessary heat for the reaction to start earlier thereby decreasing the ignition delay. It is seen that the engine operation with diesel resulted in higher ignition delay than the hydrotreated oil blended samples at all the loads. Due to high cetane index of the hydrotreated oil and its blends (Fig. 4.15), the ignition delay is shorter. These results also conform to the ignition probability test (Fig. 4.20) which

shows that the ignition probability of the hydrotreated oil and its blends is higher than

diesel.
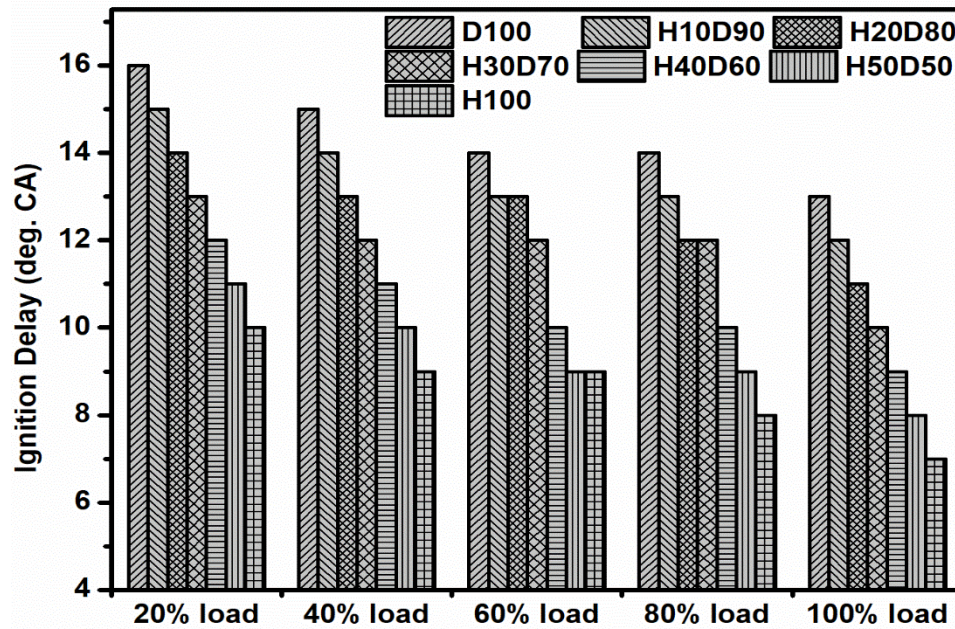
Fig 5.4 Variation in ignition delay at various loads

Fig. 5.5 indicates the combustion duration of the test fuels at 20%, 40%, 60%, 80%

and full load. The combustion duration with diesel varied from 42°CA at 25% load to

57°CA at full load, with H100 the combustion duration varied from 35°CA at 25% load

to 45°CA at maximum load. The trends show an increase in combustion duration with

the increase in power output of the engine for all the test fuels. As the engine's power

output increases, the fuel requirement also increases which requires more time to burn

thereby increasing the combustion duration [228]. Moreover, the combustion duration

with the fuel samples containing the hydrotreated oil was low as compared to diesel.

As the percentage of the hydrotreated oil increases the combustion duration decreases.

As seen in Fig. 5.1 the heat released in diffusion combustion phase for the blends is

rapid and higher than diesel. In the second combustion phase, the accumulated fuel

burns earlier because of its higher cetane number. Due to this rapid release of heat the

time required in terms of crank angle for burning of the fuel is less thereby reducing the

combustion duration. Thiyagarajan et al. [229] also observed similar results while operating a similar engine with a blend of Karanja oil methyl ester and orange peel oil.
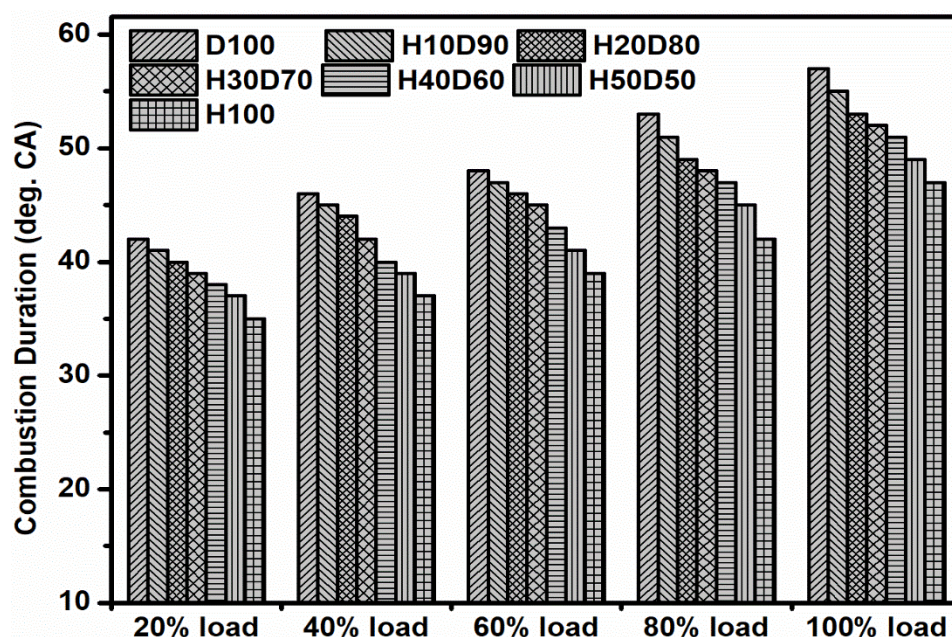
Fig 5.5 Variation in combustion duration at various loads

The crank angle at which 50% of the heat is released for all the test fuels at all the loads is shown in Fig 5.6. It is seen that the CA50 increases as the load on the engine increases. Zhang et al. [230] also observed similar results, while operating an engine with blends of the hydrotreated oil and gasoline. Moreover, it is highest for diesel and as the percentage of the hydrotreated oil in the blend increases, the CA50 decreases for all the loads. The decrease of CA50 for all the blends is due to the reduction in ignition delay. The decrease in crank angle for CA50 leads to a uniform heat release as shown in Fig. 5.1. This gives higher combustion stability, specifically at low loads, which can be seen in Fig. 5.7 wherein the coefficient of variation of IMEP for the blended samples is lower than diesel.
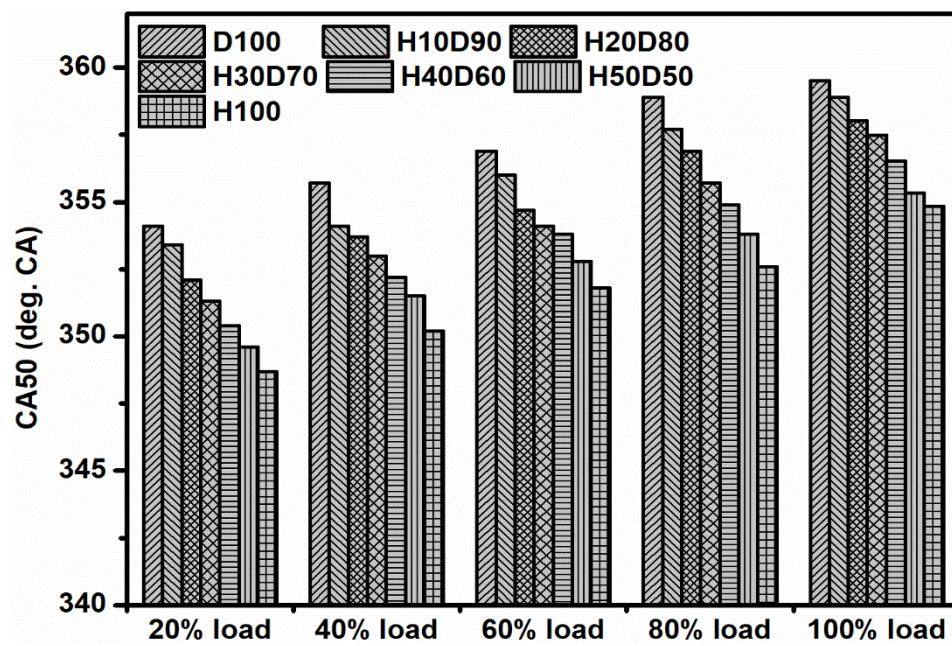
Fig 5.6 Variation in CA50 at various loads

5.2.2. Prediction of Coefficient of variance

To understand the cyclic variability of the engine for all the test fuel samples, the coefficient of variance (COV) of indicated mean effective pressure was calculated (eq. 3.18). It shows the extent to which the data in a sample varies in relation to the mean of the sample population [231]. The coefficient of variance for all the test fuel samples at all the loads was calculated and shown in Fig. 5.7. It is seen that the cyclic variation in the engine when operated with diesel was highest and as the hydrotreated oil replaces diesel the cyclic variation reduces and it was observed to be lowest with neat hydrotreated oil engine operation. At full load, the COV for diesel, H10D90, H20D80, H30D70, H40D60, H50D50 and H100 is 2.46, 2.18, 2.04, 1.97, 1.83, 1.78 and 1.63, respectively. The decrease in variability with the increase of the hydrotreated oil in the blend is due to the higher cetane number of the blend which tends to reduce the ignition delay and improve the combustion process. As the load increases the air-fuel mixing process improves which in turn improves the combustion process thereby reducing the cyclic variability. It was observed during engine operation with the blends that the

engine noise was less and the vibrations were also less as compared to diesel fuel operation.
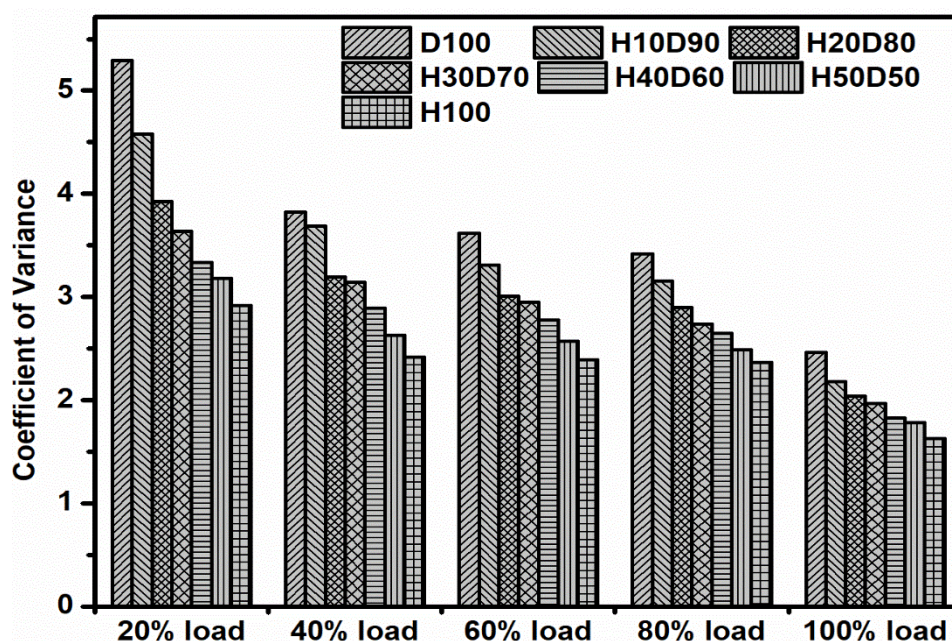
Fig 5.7 Variation in coefficient of variance at various loads

The data of the coefficient of variance was used in this study to develop a neural network. For developing the network, engine load and fuel blends were taken as input parameters, whereas the cyclic variability was used as the output parameter. The details of the network is described in section 3.12. The neurons in the hidden layer were varied from 3 to 20 and both Levenberg – Marquardt (LM), and scaled conjugate gradient (SCG) were used for training the network. Table 5.1 shows the coefficient of determination (R^2), Root Mean Square Error (RMSE) and Mean Absolute Percentage Error (MAPE) for the various neurons. It is seen that sixteen neurons and LM training algorithm resulted in the neural network model with highest R^2 value of 0.9996 and lowest RMSE and MAPE value of 0.0699 and 1.4245, respectively.

Fig. 5.8 shows the regression graphs of the neural network having sixteen neurons. The regression graph is drawn between the COV predicted by the neural network and the COV calculated from the experimental data. The correlation coefficient of the training, validation and test data set are 0.99974, 0.99991 and 0.99994, respectively.

All the data set consisting of training, validation and test data had a correlation of 0.9998 which is very close to 1. This shows that the predicted and actual values are well correlated and the network can predict the values with high accuracy. The equation obtained from the optimized neural network for predicting the CoV is given in Appendix – VI.

Table 5.1 Statistical data and training algorithm

No. of Neurons	Training Algorithm	R^2	RMSE	MAPE
3	trainlm	0.99903	0.1097	2.5729
	trainscg	0.99597	0.2225	6.3126
4	trainlm	0.99909	0.1059	2.4366
	trainscg	0.99236	0.3111	9.0507
5	trainlm	0.99932	0.0922	2.1827
	trainscg	0.99685	0.1983	6.0480
6	trainlm	0.99935	0.0897	1.7840
	trainscg	0.99653	0.2083	6.7976
7	trainlm	0.99940	0.0863	2.0569
	trainscg	0.99675	0.2011	6.2348
8	trainlm	0.99920	0.0994	2.1464
	trainscg	0.99301	0.2970	8.7171
9	trainlm	0.99871	0.1268	2.8719
	trainscg	0.99277	0.2999	8.5528
10	trainlm	0.99932	0.0919	2.0271
	trainscg	0.99560	0.2349	6.7508
11	trainlm	0.99944	0.0838	2.0738
	trainscg	0.99147	0.3263	9.7434
12	trainlm	0.99834	0.1429	2.4583
	trainscg	0.99254	0.3042	8.9287
13	trainlm	0.99944	0.0830	1.8641
	trainscg	0.99188	0.3150	8.7220
14	trainlm	0.99944	0.0834	1.6558
	trainscg	0.99267	0.3011	8.8080
15	trainlm	0.99882	0.1219	1.8634
	trainscg	0.99208	0.3093	8.2816
16	**trainlm**	**0.99960**	**0.0699**	**1.4245**
	trainscg	0.99175	0.3196	9.2935
17	trainlm	0.99896	0.1133	2.5551
	trainscg	0.99172	0.3206	7.9569
18	trainlm	0.99903	0.1090	2.2621
	trainscg	0.99095	0.3328	9.8846
19	trainlm	0.99927	0.0947	2.4856
	trainscg	0.99241	0.3095	8.5175
20	trainlm	0.99831	0.0875	2.1960
	trainscg	0.99178	0.3195	9.1614
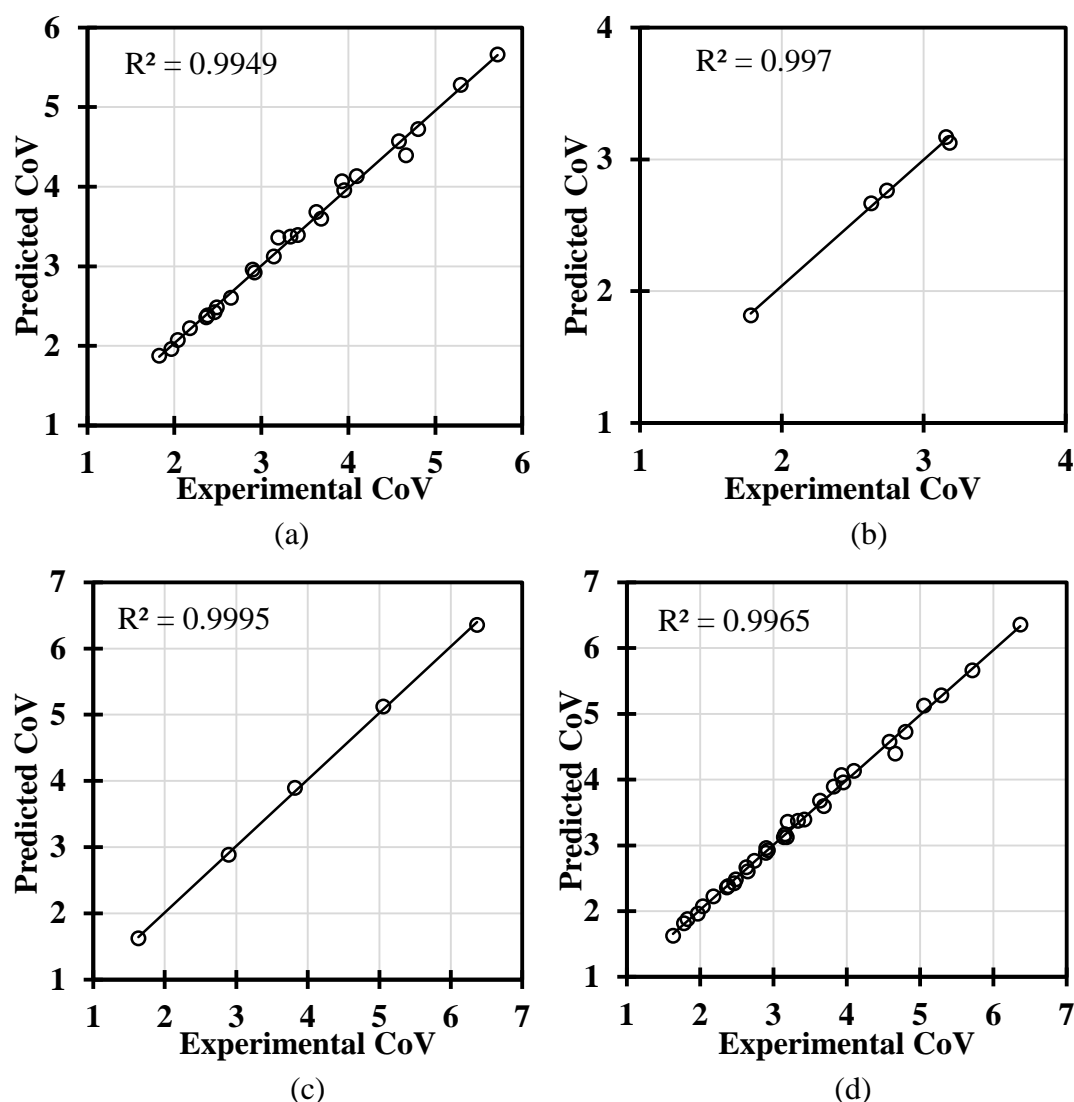
Fig. 5.8 Regression graphs of the developed network (a) Training data set (b) validation data set (c) testing data set (d) all data set

5.2.3. Performance Characteristics

The influence of the test fuels on the engine brake thermal efficiency is shown in Fig. 5.9. The engine's ability in converting the fuel's chemical energy into useful shaft work is known as brake thermal efficiency. As the load on the engine increases more fuel is injected which releases more energy resulting in increase in power production and hence increase in BTE. All the test fuels had trend similar to diesel. Moreover, as hydrotreated oil increases in the blend, the brake thermal efficiency decreases. The BTE at full load for H100, H50D50, H40D60, H30D70, H20D80, H10D90 and diesel is 27%, 27.6%, 28.2%, 28.9%, 29.6%, 30.17% and 31.18%, respectively. The thermal

efficiency decreases due to lower calorific value of the hydrotreated oil along with the slightly higher viscosity of the oil. Fig. 4.21 shows larger particle size of test fuels spray than diesel caused by higher viscosity of the fuel. Larger particle size fuel may affect the mixing tendency of air and fuel thereby delaying the ignition process [227,232]. However, Fig. 5.1 shows earlier heat release for the blends at full load, suggesting low influence of particle size on the ignition delay.
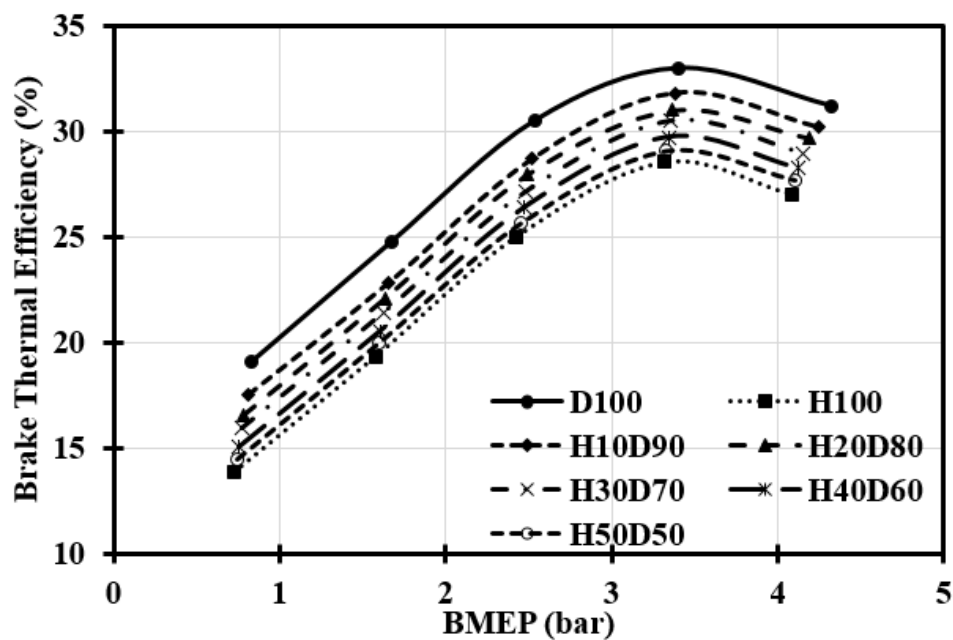
Fig. 5.9 Variation in brake thermal efficiency at various loads

Comparative assessment of volumetric consumption of fuel is an important parameter in explaining the engine performance of different test fuels. In this context, brake specific fuel consumption (BSFC); which is a ratio between mass flow rates of fuel to the brake power has been used as a conventional parameter. However, BSFC has not been considered as a reliable parameter when the calorific values and densities of test fuels vary considerably [233]. Therefore, brake specific energy consumption (BSEC) is considered as more reliable assessment method for comparison of volumetric fuel consumption.

Brake specific energy consumption for the test fuels at 20%, 40%, 60%, 80% and full load is shown in Fig. 5.10. The BSEC decreases as the load increases for all the test fuels due to the improvement in thermal efficiency. The energy consumption at all the loads is higher than diesel for all the blends and it increases with the increase in the hydrotreated oil in the blend. At full load the BSEC is 11.54, 11.93, 12.13, 12.43, 12.74, 13 and 13.32MJ/kWh for diesel, H10D90, H20D80, H30D70, H40D60, H50D50 and H100, respectively. As the hydrotreated oil replaces diesel on volumetric basis, the test samples heating value decreases and the air-fuel mixture becomes leaner resulting in more energy requirement which is fulfilled by injecting more fuel.
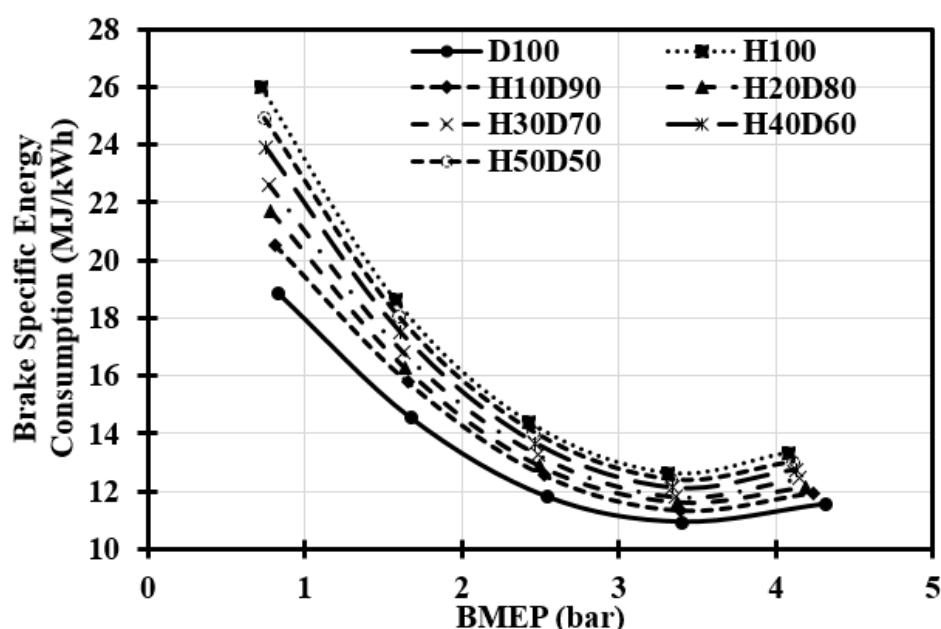
Fig. 5.10 Variation in brake specific energy consumption at various loads

Fig. 5.11 shows the exhaust gas temperature (EGT) with load for different test fuels. It was observed that as the engine load increases, the EGT increases. Diesel fuel engine operation resulted in lowest EGT at all the loads. Further, with the increase in the hydrotreated oil in the blend the EGT increases. At full load, diesel, H10D90, H20D80, H30D70, H40D60, H50D50 and H100 had 416, 420, 426, 431, 437, 442, and 446°C, respectively as the exhaust gas temperature. When more heat is released in the diffusion combustion phase, the exhaust gas temperature is higher. As the energy leaves

the cylinder as waste heat and is not utilized in producing useful work [228,234]. Fig. 5.1 shows higher heat release in the diffusion combustion phase for the hydrotreated oil and its blends, resulting in higher EGT.
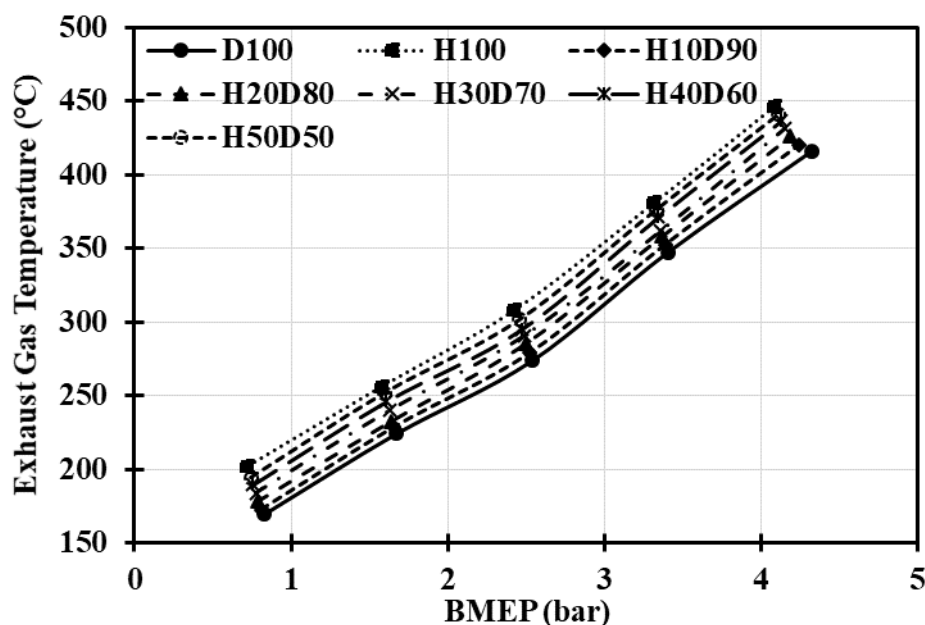
Fig. 5.11 Variation in exhaust gas temperature at various loads

5.2.4. Emission Characteristics

Fig. 5.12 portrays the unburned hydrocarbon emission for the test fuels. At low loads, the HC emission is high and the emission level decreases as the engine load increases. All the tested fuel samples followed the same trend. Due to the quenching of the charge present near the cylinder wall, the hydrocarbon emission increases. At low loads, the quenching effect is more dominant due to lower cylinder temperature and flame speed as the flame cannot reach the far ends of the combustion chamber [235]. As compared to diesel, the HC emissions at full load reduced by 5.5%, 10.3%, 14.4%, 7.4%, and 2.5% with H10D90, H20D80, H30D70, H40D60, and H50D50, respectively. Whereas, with H100, the HC emission increases by 9.7%. Although the heat released during the combustion of the hydrotreated oil and its blends is lower than diesel the HC emission decreases. High paraffinic nature and low aromatic content of the fuel resulted

in improvement in the combustion. Since, the energy requirement for breaking straight chain carbon atoms is less in comparison to fuel having large amount of aromatic rings [121]. Also the presence of shorter chain carbon atoms in the hydrotreated oil resulted in lower energy requirement. Moreover, till 30% blending of the hydrotreated oil the HC emissions were found to decrease. As the hydrotreated oil was further added in the blend the HC emissions were found to increase at all the loads. The HC emissions reduced till H30D70 as the cylinder temperature was high enough to sustain proper combustion. Further increase in hydrotreated oil percentage leads to reduced heat release such that the combustion is unable to sustain. Hence, an increase in HC emissions is observed and H100 engine operation resulted in highest HC emission.

The effect on CO emission under the influence of test fuels and various loads is shown in Fig. 5.13. It is seen that up to 50% engine load, a decrease in the emission level is observed. As the load is further increased, the CO emission increases and at full load the CO emission is highest. At high loads, the relatively rich mixture may not find enough oxygen to be completely converted into carbon dioxide [236]. The CO emissions at full load for diesel, H10D90, H20D80, H30D70, H40D60, H50D50 and H100 is 31.9, 29.7, 27.9, 26.55, 27.41, 30.7 and 34g/kWh, respectively. The CO emissions also decreases till 30% blend of the hydrotreated oil mixed in diesel. Further increase in the hydrotreated oil ratio in the blend resulted in increase in CO emission and H100 fuel operation resulted in highest CO emission. The CO emissions are formed due to incomplete combustion of the carbon containing compounds. Due to high paraffinic content and cetane number of the blends, their combustion is proper, resulting in a decrease in carbon monoxide emission. Also, the hydrotreated oil contains small amount of oxygen which aids the conversion of carbon monoxide to carbon dioxide.

The CO emission increases with H100 due to lower combustion temperature resulting in incomplete combustion.
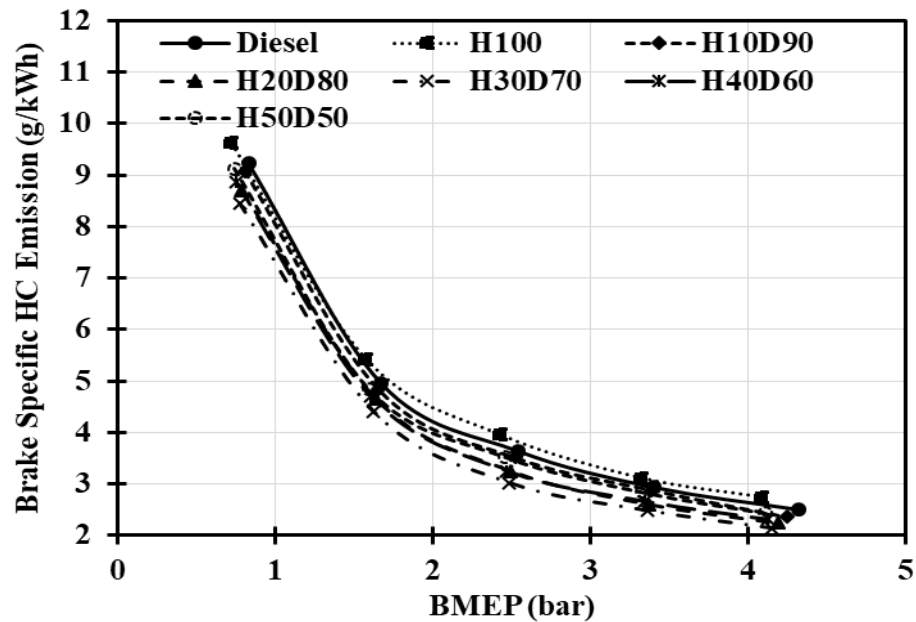
Fig. 5.12 Variation in brake specific unburned hydrocarbons emission at various loads
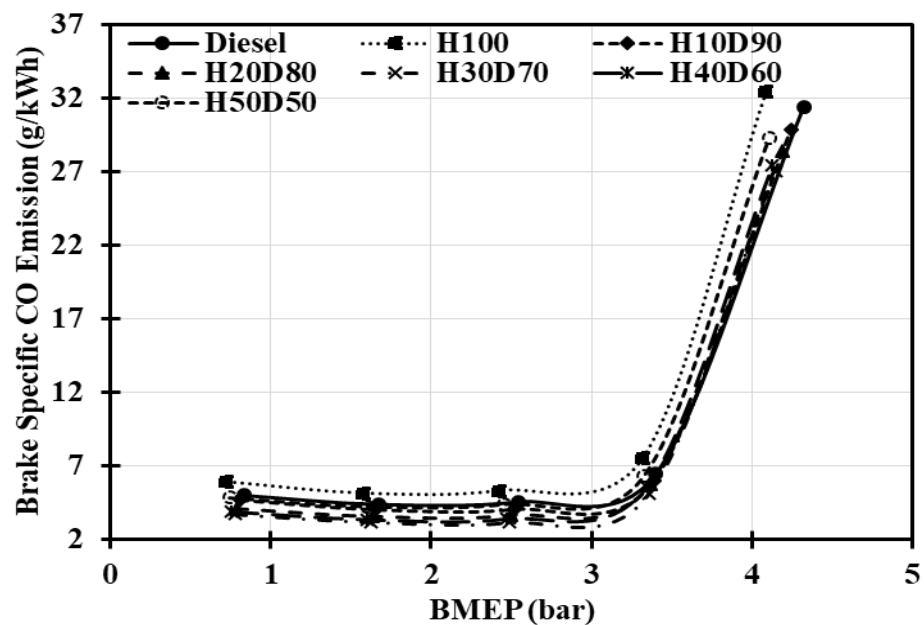
Fig. 5.13 Variation in brake specific carbon monoxide emission at various loads

The combustion temperature, availability of time for chemical reaction and availability of oxygen rich zones plays a major role in the NO emission. The oxides of nitrogen emission can also form when the molecular nitrogen reacts with hydrocarbon

radicals in fuel rich flame zone. Fuels containing nitrogen are also responsible for NO formation. However, the main reason for NO formation in a CI engine is high combustion temperature. The oxides of nitrogen formation can be explained through the extended Zeldovich mechanism [124,154]. The brake specific NO emission is shown in Fig. 5.14. The NO emission at full load is 4, 3.9, 3.6, 3.5, 3.4, 3.3 and 3.1g/kWh for diesel, H10D90, H20D80, H30D70, H40D60, H50D50 and H100, respectively. The premixed combustion phase with the test fuels is lower than diesel that tends to decrease the combustion temperature resulting in decrease in NO emissions. The decrease in the premixed combustion phase is caused by the higher cetane number of the test fuels that reduces the delay in ignition. Singh et al. [225] utilized a single cylinder diesel engine with 19:1 compression ratio and observed NO to be lower than diesel. In another study Singh et al. [124] used a turbocharged diesel engine with 17:1 compression ratio and observed higher NO emission than diesel. The compression ratio of the turbocharged engine was lower therefore, the delay in ignition for the engine will be higher than the naturally aspirated engine. This increases the time available for fuel to mix with air and release more heat in the initial combustion phase resulting in higher NO emission. As an engine with 17.5:1 compression ratio is used in the present study, therefore it is expected that due to shorter ignition delay and small heat release with the hydrotreated oil and the blends the NO emissions are lower in comparison to diesel.
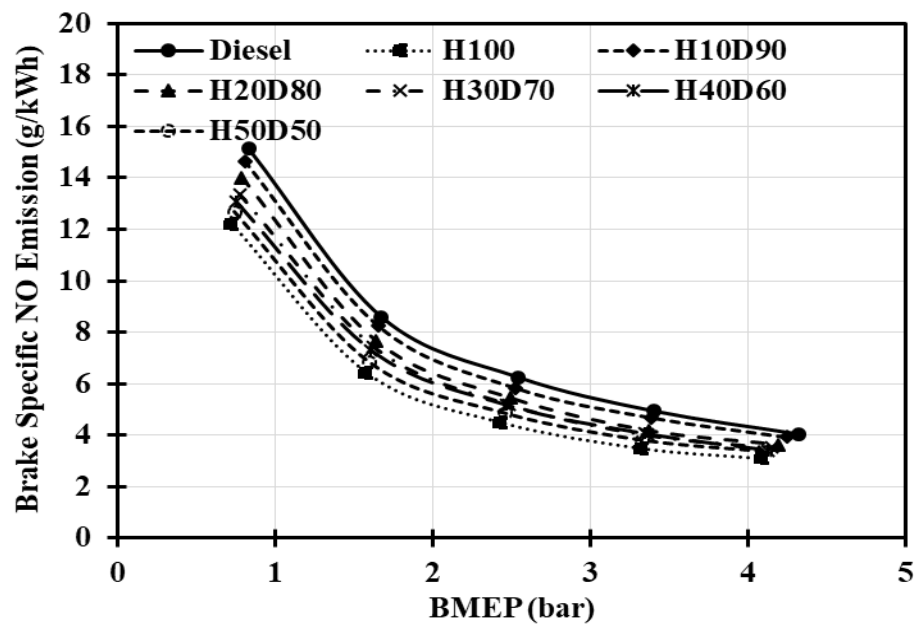
Fig. 5.14 Variation in brake specific NO emission at various loads

The effect of load on the exhaust smoke for the test fuels is shown in fig. 5.15. The phenomenon of soot formation is complex and is dependent on various factors like the air-fuel ratio, ignition delay and fuel composition. For all the test fuels it is observed that the soot emission increases as the load on the engine increases. The smoke opacity of H100 and its blends were lower as compared to diesel. The smoke opacity at full load is 61.4%, 59.1%, 55.9%, 54.1%, 55.8%, 56.3% and 62.8% with diesel, H10D90, H20D80, H30D70, H40D60, H50D50 and H100, respectively. The main reason for soot formation is the aromatic content of the fuel. The soot formation tendency with the hydrotreated oil is low due to less aromatic content. Moreover, air and fuel have enough time to mix because of lower premixed combustion phase, resulting in the improvement of the combustion quality leading to complete combustion. The reduction in smoke emissions was also observed by Singh et al. [237], Prokopowicz et al. [134], Singh et al. [225] and Ogunkoya et al. [121]. It is also possible to further reduce the PM emission by blending oxygenates with the hydrotreated oil [135]. Further, it is seen that the emission starts increasing when the percentage of the hydrotreated oil in the blend is

higher than 30%. Since, the combustion temperature required for the chemical reactions to sustain is less.
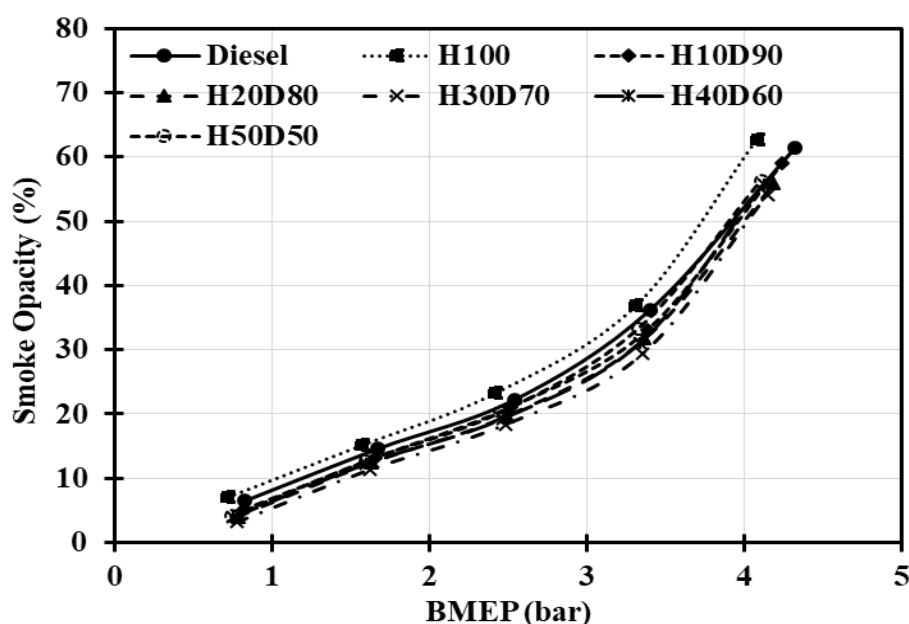
Fig. 5.15 Variation in smoke opacity at various loads

5.3. Engine performance characteristics for blends of hydrotreated oil, biodiesel and diesel

In the previous section results of the engine tests carried out with various blends of the hydrotreated oil and diesel were discussed. It was observed that 30% blend of hydrotreated oil resulted in lowest emissions but the thermal efficiency was low. The efficiency with 20% blend of hydrotreated oil was higher than 30% blend but the emissions with 20% blend were higher. To improve the shortcomings of the two samples, addition of biodiesel can be explored. Therefore, experiments were carried out by blending waste cooking oil biodiesel in 20% and 30% blend of the hydrotreated oil. This section discusses the effect of the biodiesel blending in the 20% and 30% blend of the hydrotreated oil.

5.3.1. Combustion Characteristics

In 20% and 30% blend of hydrotreated oil, 5%, 10% and 15% of the waste cooking oil biodiesel was added and abbreviated as H20B5, H30B5, H20B10, H30B10, H20B15

and H30B15, respectively. Figs. 5.16, 5.17 and 5.18 compares the heat release rate of 5%, 10% and 15% blending of biodiesel with H20D80, H30D70 and diesel. In the graphs it is seen that as the percentage of the biodiesel increases in the blend the heat released increases. Among the blends, the maximum heat release is observed with 15% blending of biodiesel and H30B15 showed the highest heat release, but this heat release was lower than neat diesel engine operation. It is also seen that due to the addition of biodiesel the heat release curve shifts towards the top dead centre and as the percentage of biodiesel increases in the blend, the shifting of the curve towards the TDC increases. As the biodiesel is added to the blends, due to their higher viscosity the ignition delay increases that tends to give more time for larger quantity of fuel to prepare for combustion and when the combustion starts the heat released is higher than the blends of the hydrotreated oil. Thiyagarajan et al. [238] also reported higher ignition delay with wheat germ oil and pine oil. It can be argued that as the biodiesel replaces diesel, the calorific value of the fuel sample decreases and the heat released should decrease. However, the trends suggest otherwise, because the effect of ignition delay on providing sufficient time for large amount of injected fuel to burn is more dominant.
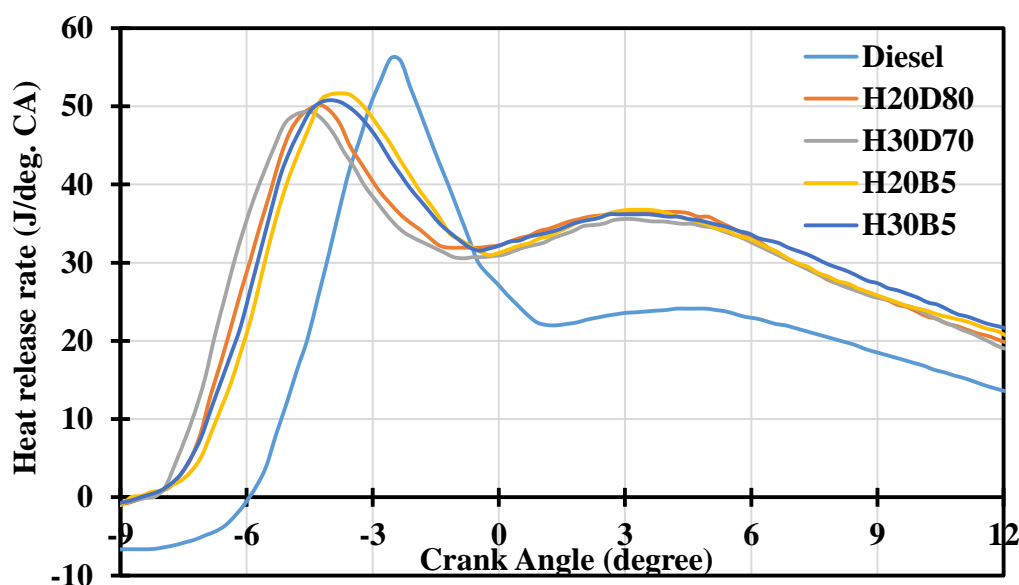
Fig. 5.16 Variation in heat release at full load with 5% blending of biodiesel
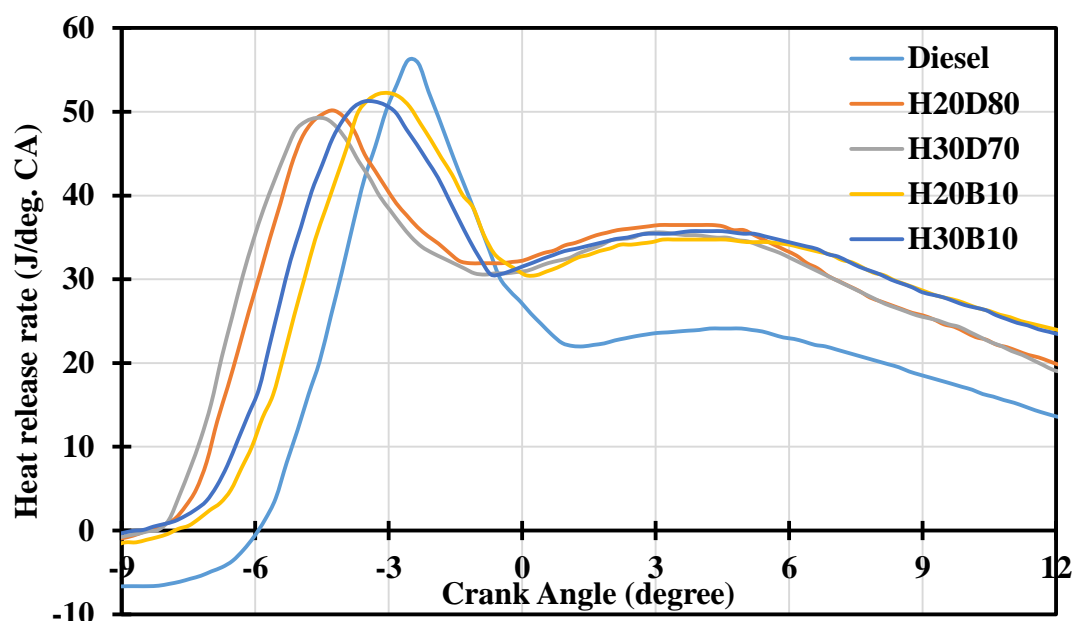
Fig. 5.17 Variation in heat release rate at full load with 10% blending of biodiesel
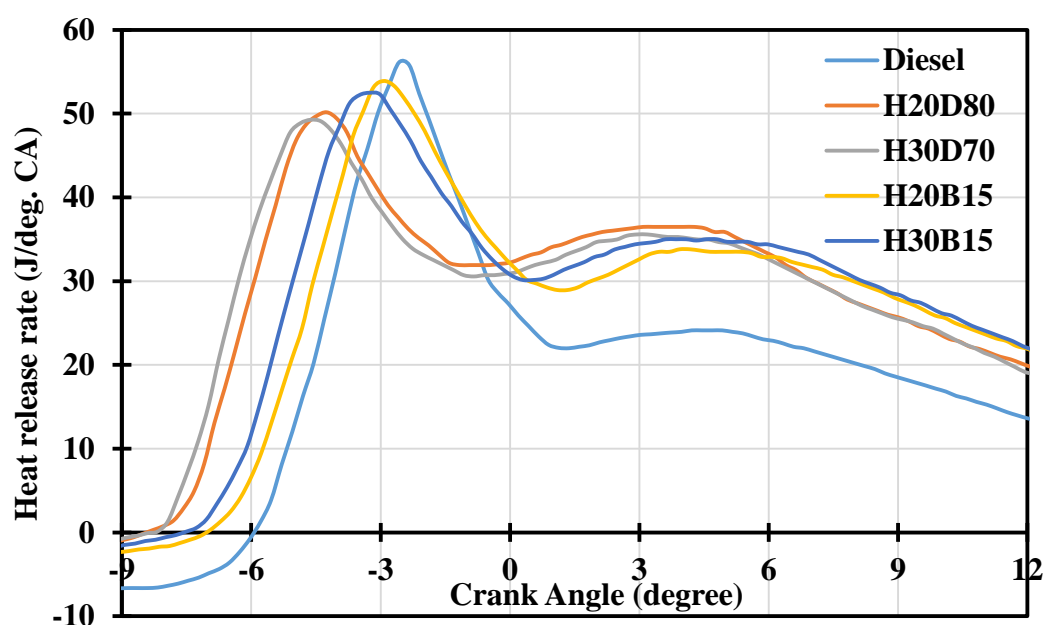
Fig. 5.18 Variation in heat release rate at full load with 15% blending of biodiesel

The in-cylinder pressure at full load for 5%, 10% and 15% biodiesel blending with H20D80 and H30D70 is compared in Figs. 5.19, 5.20 and Figs. 5.21, respectively. It is generally seen that if the heat released in the premixed combustion stage is low then the cylinder pressure is also low [239]. Figs. 5.16 – 5.18 shows that the heat released in the premixed stage is low for all the blend samples that leads to lower peak pressure in comparison to diesel. The heat released in the premixed stage is low due to higher

cetane index of the samples that reduces the delay in ignition. This causes the combustion to start earlier and as less fuel is prepared for burning, the quantity of fuel burnt is less thereby reducing the heat release and hence the peak pressure [225]. It was observed that the addition of biodiesel to the blends resulted in higher cylinder pressure as compared to blends without biodiesel. Also, due to higher ignition delay the cylinder pressure was observed to shift away from the TDC [228].
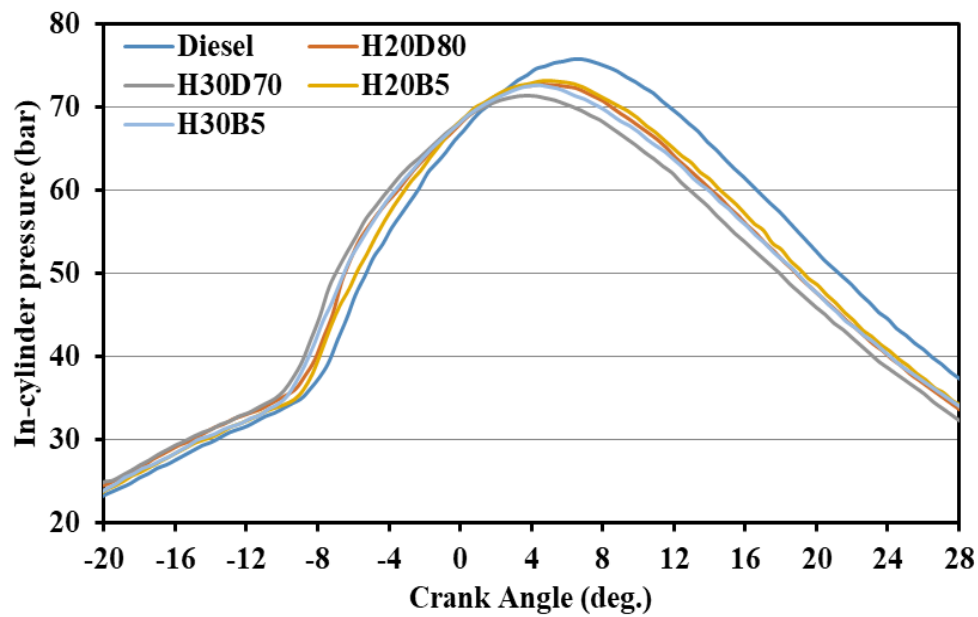
Fig. 5.19 Variation in in-cylinder pressure at full load with 5% blending of biodiesel
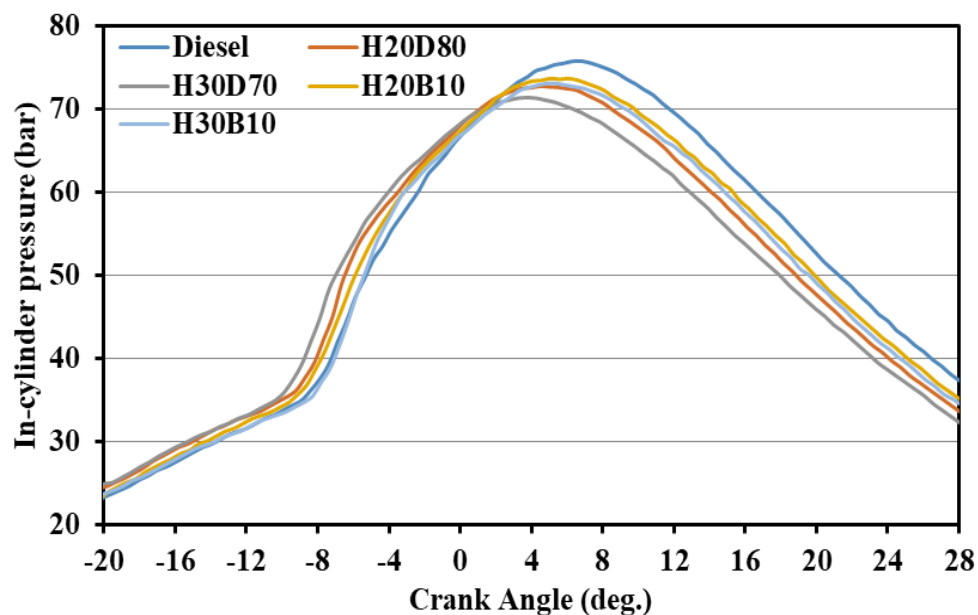
Fig. 5.20 Variation in in-cylinder pressure at full load with 10% blending of biodiesel
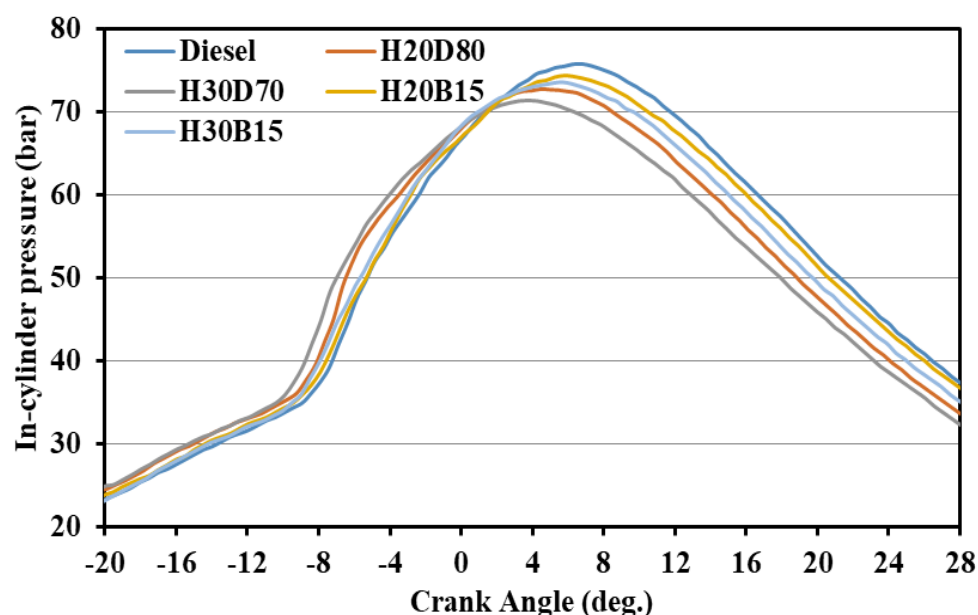
Fig. 5.21 Variation in in-cylinder pressure at full load with 15% blending of biodiesel

The variation in peak pressure at different loads for diesel, H20D80, H30D70, H20B5, H30B5, H20B10, H30B10, H20B15 and H30B15 is given in Fig. 5.21. It is seen that the peak pressure for the blends is lower than diesel. The peak pressure for H30D70 is lower than H20D80 blend as the heat released for the blend is low. With the addition of biodiesel, the peak pressure for all the blends increases and as the percentage of the biodiesel increases the peak pressure increases. At full load, the peak pressure for diesel, H20D80, H30D70, H20B5, H30B5, H20B10, H30B10, H20B15 and H30B15 is 75.8, 72.47, 71.72, 73.2, 72.67, 73.7, 73.1, 74.4, and 73.6bar, respectively. Due to the higher viscosity of biodiesel, the atomization of the sprayed fuel is slow, which increases the delay in ignition, thereby increasing the heat release and hence higher pressure [229]. Also, the peak pressure of the biodiesel mixed in 30% of the hydrotreated oil blend was lower than blend containing 20% of hydrotreated oil. As biodiesel replaces diesel in both the blends the ignition delay of the sample increases and more so for H20 blend, which causes the fuel to burn late and hence release more heat thereby increasing the cylinder pressure.
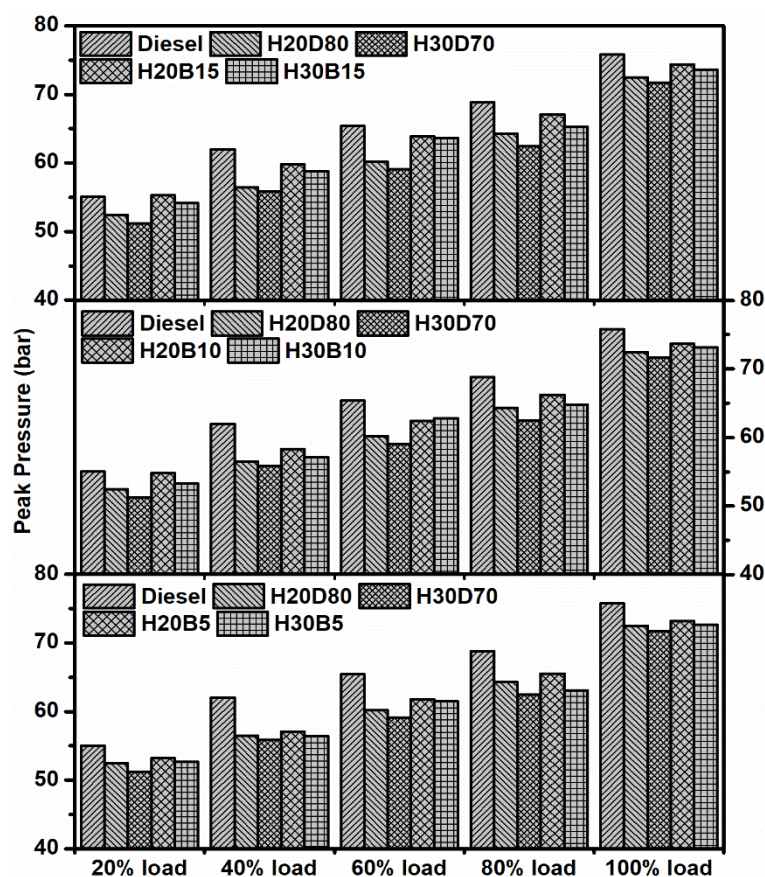
Fig. 5.22 Variation in peak pressure with biodiesel mixed in the blends

The variation in ignition delay for the different test fuels with increasing load is presented in Fig. 5.23. The ignition delay was calculated as discussed earlier in section 5.2.1. It is seen that the ignition delay reduces as the load on the engine increases. The ignition delay with the hydrotreated oil blends is found to be lower than diesel. With the addition of biodiesel to the blends, an increase in ignition delay is observed for all the blends at all the loads. Agarwal and Dhar also observed an increase in ignition delay while operating a similar engine with Karanja oil [240]. It can be argued that the addition of biodiesel will increase the cetane index of the sample as its cetane index is higher than diesel that may reduce the ignition delay. However, the trends show that the ignition delay increases, this is caused by the higher viscosity of the biodiesel which affects its atomization and slows the fuel-air mixing process. Moreover, the ignition

delay with the biodiesel samples is lower than diesel, since the effect of high cetane

index hydrotreated oil is more dominant.
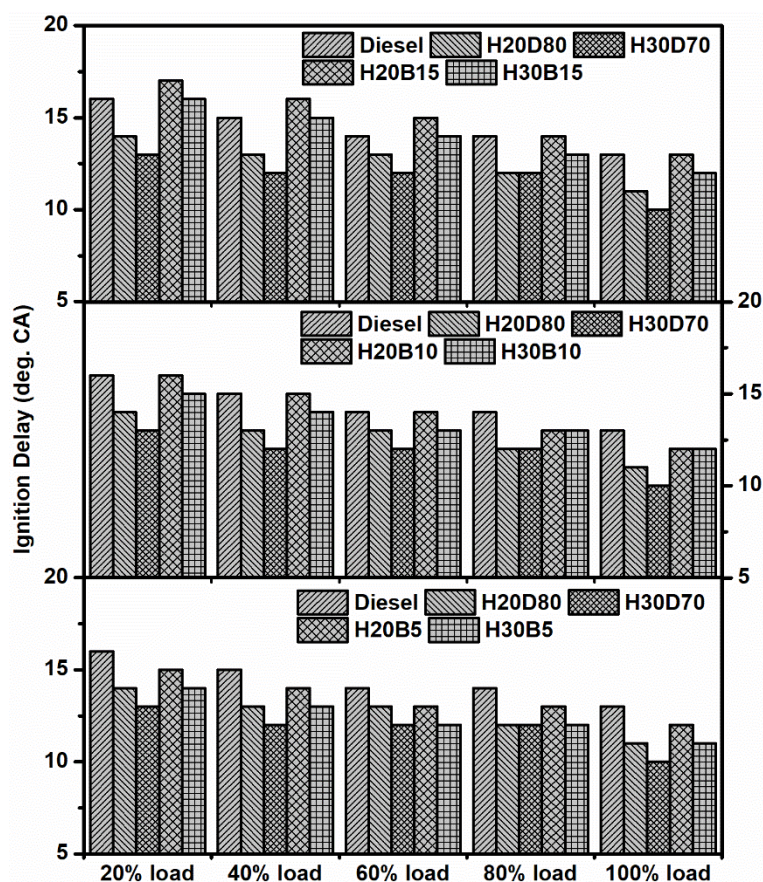
Fig. 5.23 Variation in ignition delay with biodiesel mixed in the blends

The combustion duration with diesel, H20D80, H30D70, H20B5, H30B5,

H20B10, H30B10, H20B15 and H30B15 at 20%, 40%, 60%, 80% and full load is

depicted in Fig. 5.24. The combustion duration for the blends containing biodiesel was

found to be higher than the blends without biodiesel. Thiayagarajan et al. [241] also

observed higher combustion duration with biodiesel blends. As seen in Figs. 5.16 –

5.18, with the biodiesel blends engine operation, the heat release rate in the diffusion

combustion phase is slower than the blends without biodiesel, which increases the time

for combustion in terms of crank angle. The probable reason for the slowness in the

heat release is due to higher viscosity of biodiesel molecules which affects their

atomization thereby slowing their ability to find oxygen and burn.
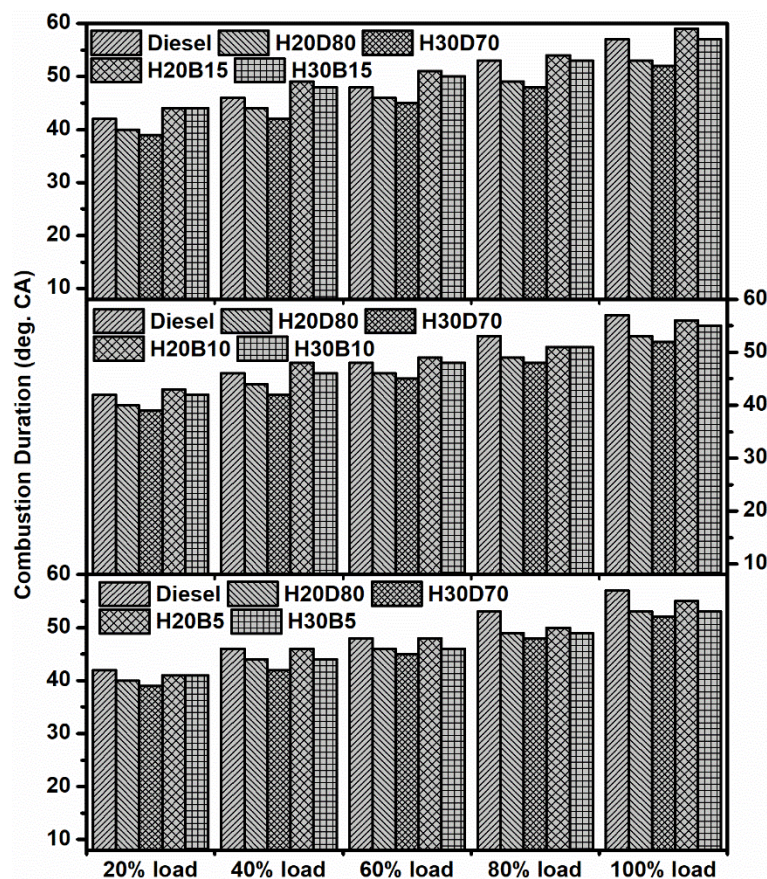
Fig. 5.24 Variation in combustion duration with biodiesel mixed in the blends

For all the test fuels at different loads, Fig. 5.25 shows the crank angle at which 50% of the heat is released. It is seen that as the load on theTengine increases, CA50 increases and moves towards the top dead center. However, at full load the CA50 crosses top dead center with 10% and 15% blending of biodiesel in both the blends of hydrotreated oil and diesel. Fig. 5.25 also shows that the CA50 with the 10% and 15% biodiesel blended fuel samples was higher than diesel, H20D80 and H30D70. Due to the addition of biodiesel, the rate of heat released is reduced because of its higher viscosity and density thereby increasing the CA50. Moreover, the combustion duration (Fig. 5.24) for the biodiesel blends was lower than diesel but higher than H20D80 and H30D70, since the hydrotreated oil improves the combustion process and as seen in Fig. 5.1, the heat released in the diffusion phase is rapid and the combustion ends earlier thereby reducing the combustion duration.
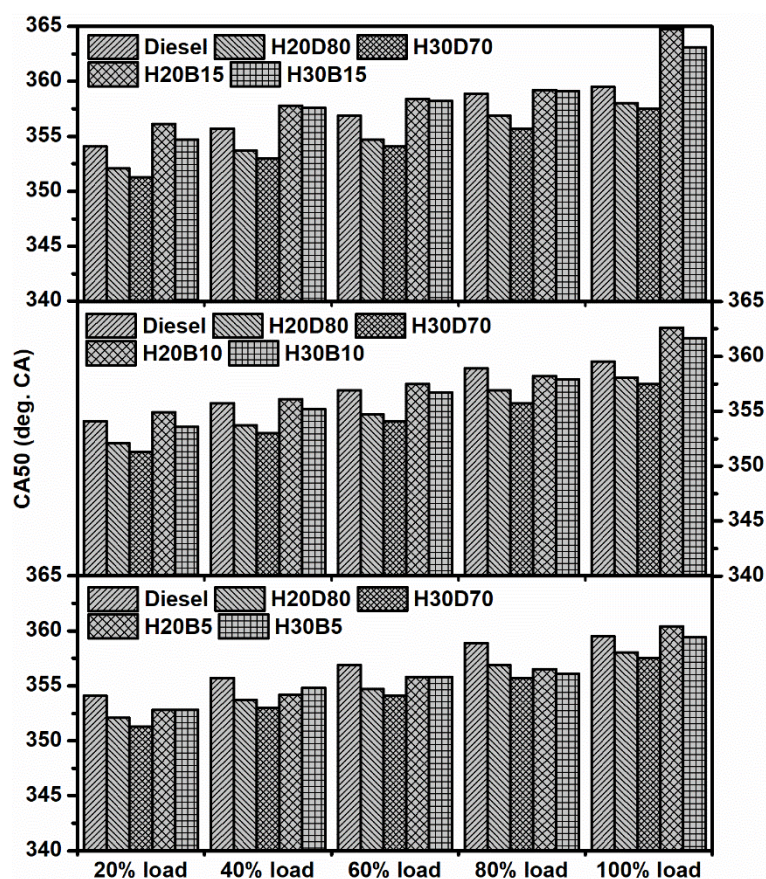
Fig. 5.25 Variation in CA50 with biodiesel mixed in the blends

5.3.2. Performance Characteristics

The brake thermal efficiency of the engine operating with the test fuel samples at different loads is shown in Fig. 5.26. The results show that the addition of biodiesel to the blends, resulted in increase in brake thermal efficiency at all the loads and as the percentage of biodiesel increases the efficiency further increases. At full load, the efficiency with diesel, H20D80, H30D70, H20B5, H30B5, H20B10, H30B10, H20B15 and H30B15 is 31.18%, 29.67%, 28.94%, 29.9%, 29.75%, 30.5%, 30.1%, 30.96% and 30.41%, respectively. Due to the addition of biodiesel the heat released in the premixed phase is higher than the blends without biodiesel since the oxygen content of the blend increases. This causes higher combustion pressure and temperature and the slight shift of the heat release towards the TDC makes combustion process approach constant volume combustion, thereby increasing the thermal efficiency [242].
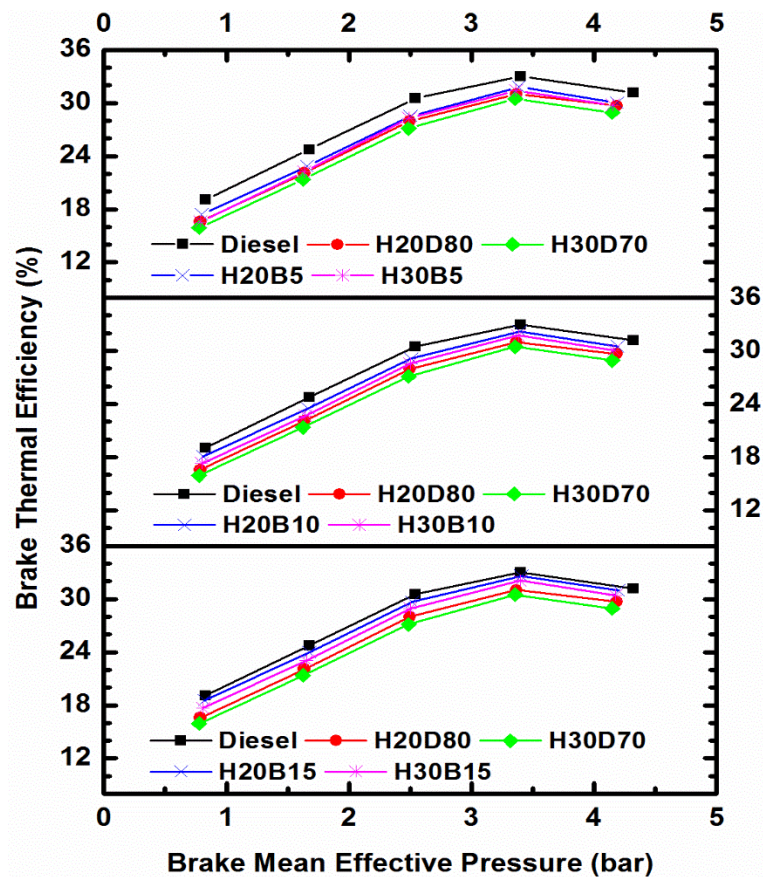
Fig. 5.26 Variation in brake thermal efficiency with biodiesel mixed in the blends

The brake specific energy consumption for diesel, H20D80, H30D70, H20B5, H30B5, H20B10, H30B10, H20B15 and H30B15 at different loads is shown in Fig. 5.27. The energy consumption of H20D80 and H30D70 is higher than diesel as the thermal efficiency of the two fuel samples was lower than diesel. Biodiesel addition in various proportions to the blends resulted in decrease in energy consumption, but it was still higher than diesel. Chelladurai and Geo [243] in their study observed that the engine operation with methyl ester resulted in higher energy consumption than diesel. Also, as the percentage of biodiesel increases in the blend the energy consumption decreases. At full load the BSEC is 11.54, 12.13, 12.43, 12, 12.1, 11.8, 11.96, 11.62, and 11.84MJ/kWh for diesel, H20D80, H30D70, H20B5, H30B5, H20B10, H30B10, H20B15 and H30B15, respectively. The energy consumption with biodiesel blending decreases since the combustion efficiency of the engine increases, therefore less amount

of fuel is required to produce the same power. With increase in percentage of biodiesel the efficiency of the combustion further increases that results in decrease in energy consumption.
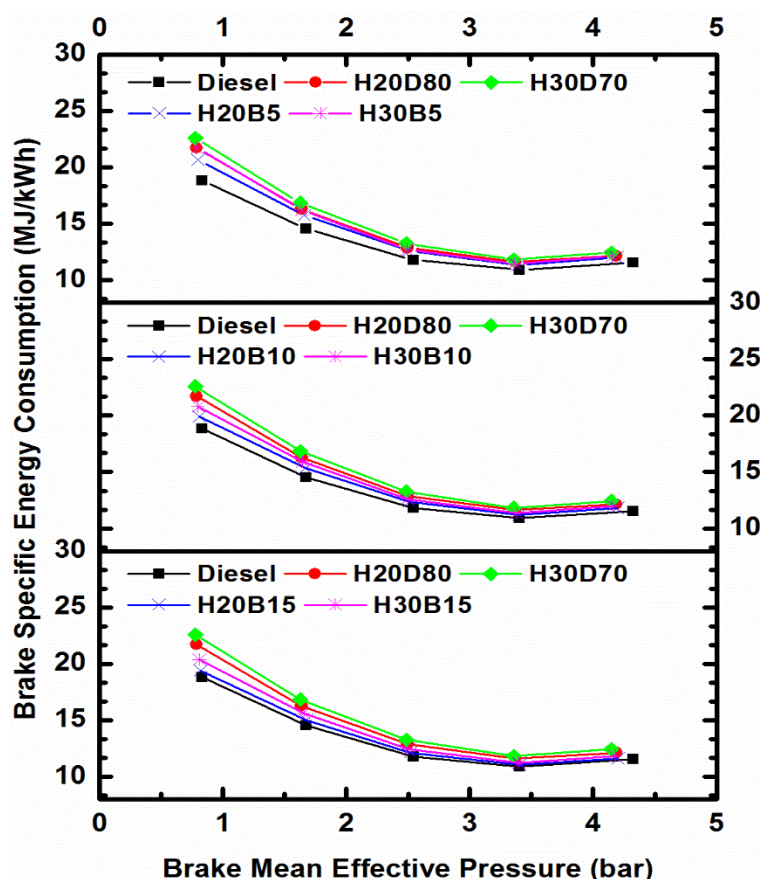
Fig. 5.27 Variation in brake specific energy consumption with biodiesel mixed in the blends

The variation in exhaust gas temperature with load for the test fuels is shown in Fig. 5.28. Engine operation with all the blends resulted in higher exhaust gas temperature as compared to diesel. The EGT with H30D70 was higher than the EGT with H20D80. Blending of biodiesel resulted in higher EGT than H20D80 & H30D70 and as the percentage of biodiesel increases the EGT increases. The EGT at full load with diesel, H20D80, H30D70, H20B5, H30B5, H20B10, H30B10, H20B15 and H30B15 is 416, 426, 431, 431, 434, 436, 441, 440, and 448°C, respectively. As the heat released in diffusion combustion phase is higher with the blends, the EGT is higher. With the biodiesel mixed in the blends, the heat release in the second stage of

combustion starts later than the hydrotreated blends. Hence the heat is released in the later part of the expansion stroke, which provides less useful work and leaves the engine as waste heat.
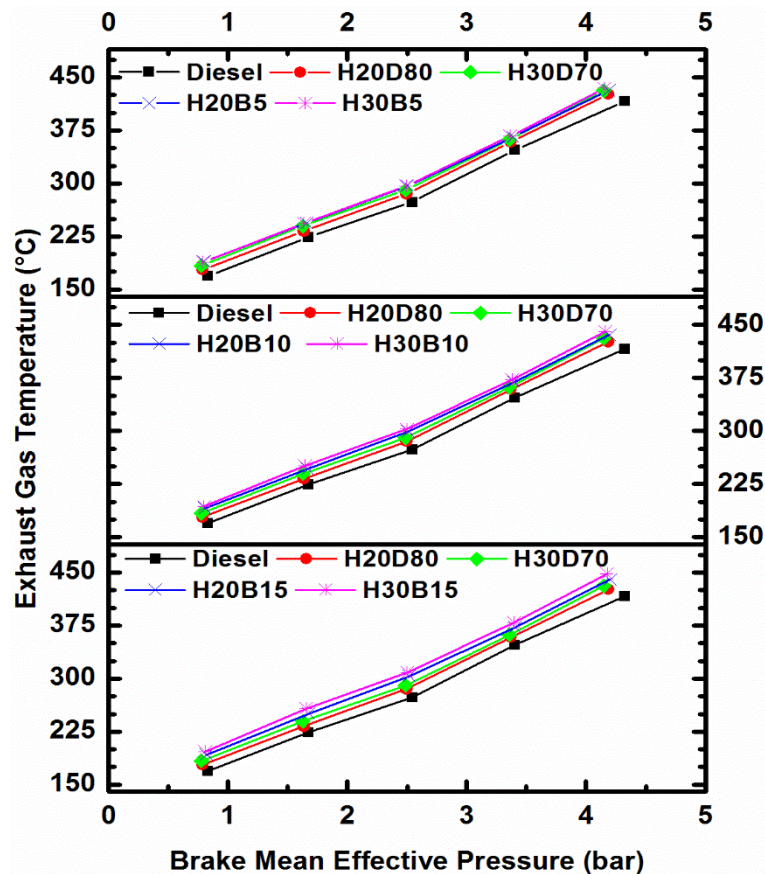
Fig. 5.28 Variation in exhaust gas temperature with biodiesel mixed in the blends

5.3.3. Emissions Characteristics

The variation in unburned hydrocarbon emissions with the load for the test fuels is shown in Fig. 5.29. The trends with all the fuel samples is same as diesel i.e. as the load on the engine increases the HC emission decreases. At full load, the HC emission is 2.5, 2.24, 2.13, 2.07, 1.99, 1.95, 1.82, 1.86, and 1.73g/kWh with diesel, H20D80, H30D70, H20B5, H30B5, H20B10, H30B10, H20B15 and H30B15, respectively. It is seen that in comparison to H20D80 and H30D70, the addition of biodiesel resulted in reduction in HC emissions. As the percentage of biodiesel increases in the blend, the emission further decreases. As the heat released with biodiesel addition is high, the

probability of combustion nearing completion is more that tends to decrease the unburned hydrocarbon emission. Another reason is the decrease in energy consumption with the biodiesel blended fuels due to the improvement in their thermal efficiency. This reduces the amount of fuel injected at a particular load thereby decreasing the hydrocarbon emission.
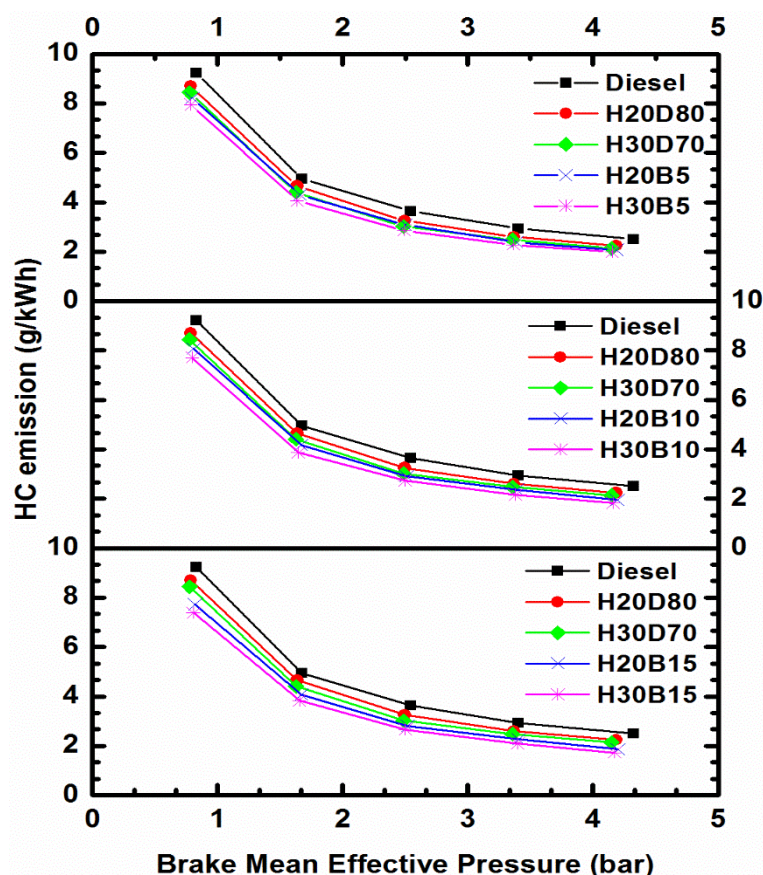
Fig. 5.29 Variation in unburned hydrocarbon emission with biodiesel mixed in the blends

The effect of the biodiesel blending on the CO emissions at different loads is shown in Fig. 5.30. The CO emission at full load with diesel, H20D80, H30D70, H20B5, H30B5, H20B10, H30B10, H20B15 and H30B15 is 31.42, 28.4, 27.07, 27.14, 26.73, 25.96, 24.97, 24.09, and 24.02g/kWh, respectively. It is seen that the CO emission also decreases for the test fuels and the lowest emission is observed with H30B15. As the amount of fuel injected with the biodiesel blends engine operation is less, the amount of carbon present in the cylinder during combustion is less, thereby reducing the CO

emission. As biodiesel replaces diesel in the sample, the amount of oxygen present in the blend increases, which further helps in the reduction of carbon monoxide. Also, due to higher paraffinic content of the hydrotreated oil, the combustion with the fuel is improved that further reduces the emission of carbon monoxide.
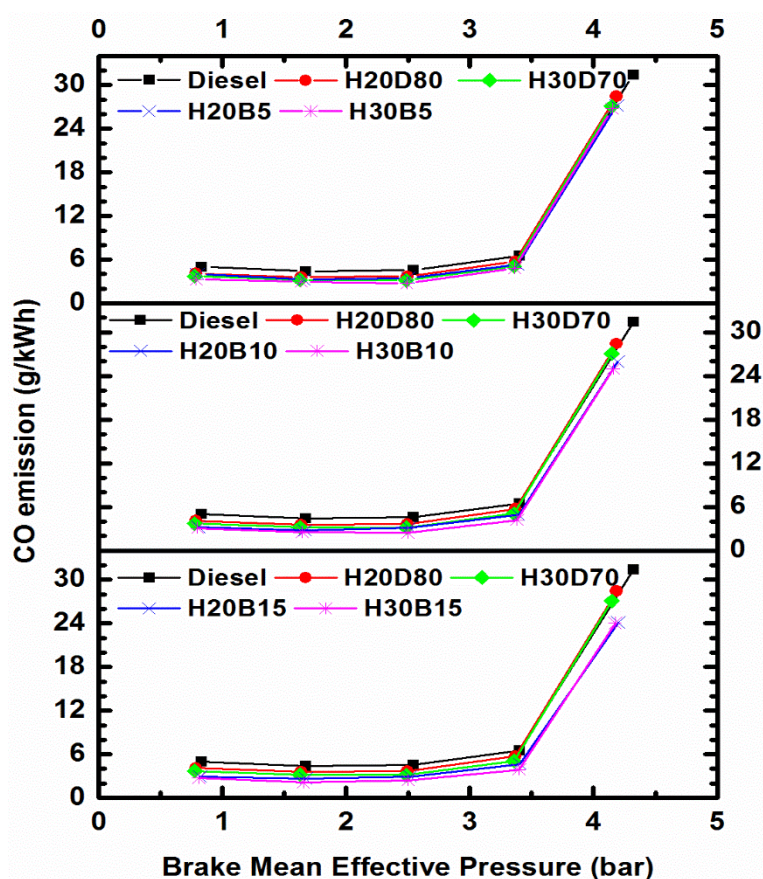
Fig. 5.30 Variation in carbon monoxide emission with biodiesel mixed in the blends

The variation in NO emission for the fuel samples at different loads is shown in Fig. 5.31. At full load, the NO emission is 4, 3.63, 3.52, 3.82, 3.61, 3.88, 3.66, 3.98 and 3.72g/kWh with diesel, H20D80, H30D70, H20B5, H30B5, H20B10, H30B10, H20B15 and H30B15, respectively. It is seen that the NO emission is lower with the blends of hydrotreated oil and diesel. As the biodiesel is added to these blends, the NO emission increases and as the percentage of biodiesel increases the NO emission increases. Further, the NO emission with biodiesel mixed in 20% of the hydrotreated oil is higher in comparison to 30% of the hydrotreated oil blend. The heat released in

the first phase of combustion with biodiesel addition is high than the fuel samples without biodiesel addition. The increase in heat release causes the combustion temperature to rise thereby increasing the thermal NO emissions. Also, the heat released with H20D80 is higher than H30D70, therefore, mixing biodiesel in 20% of the hydrotreated oil sample results in further increase in the heat release that tends to produce more NO than the biodiesel mixed in 30% of the hydrotreated oil samples. Moreover, addition of biodiesel increases the oxygen content of the charge, which further increases the probability of conversion of nitrogen into oxides of nitrogen and as the percentage of biodiesel increases, the oxygen content increases thereby increasing the emission.

The effect of the biodiesel blended samples on the smoke emissions is shown in Fig. 5.32. The smoke opacity with H20D80 and H30D70 engine operation was lower than diesel. As discussed earlier, due to low carbon atom chain and less aromatic content in the hydrotreated oil the particulate matter emission is less in the engine exhaust. Addition of biodiesel resulted in further decrease in the opacity. The smoke opacity at full load with diesel, H20D80, H30D70, H20B5, H30B5, H20B10, H30B10, H20B15 and H30B15 is 62.4, 55.9, 54.1, 54, 52, 52.8, 50.8, 51 and 49.2%, respectively. The soot particles are formed when the heavy fuel molecules are thermally cracked in the absence of oxygen. With the addition of biodiesel, the oxygen content increases and the ignition delay also increases. This gives more time for the fuel and air to mix resulting in higher heat release in the premixed combustion phase, thereby improving the utilization of air and hence reducing the smoke formation.
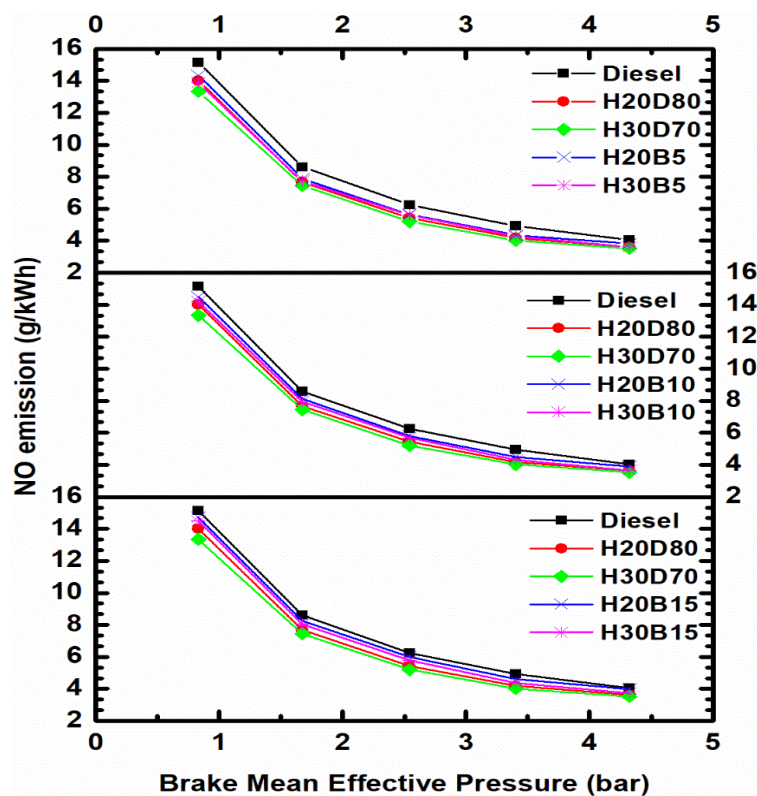
Fig. 5.31 Variation in oxides of nitrogen emission with biodiesel mixed in the blends
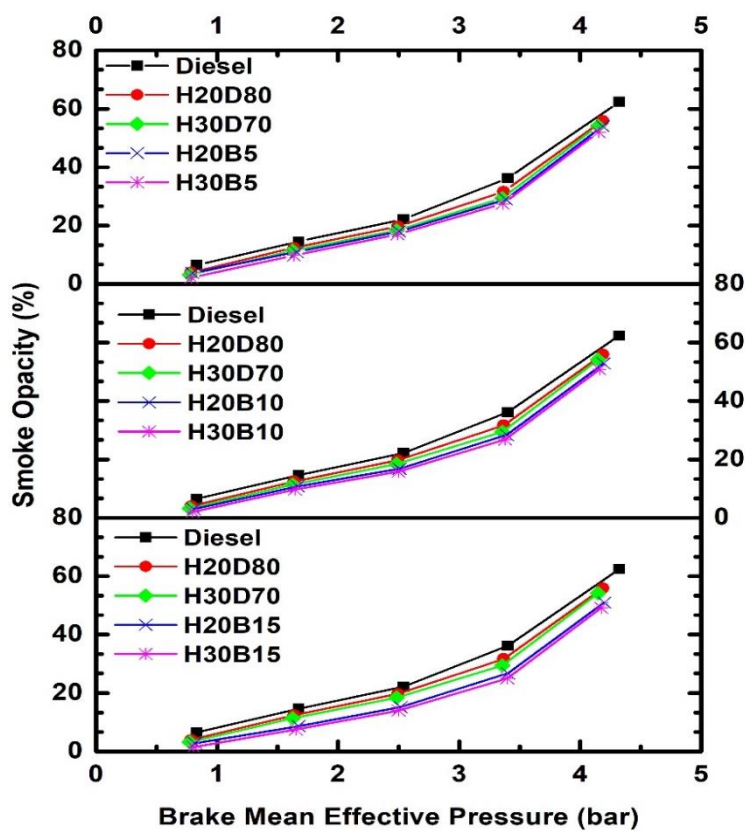
Fig. 5.32 Variation in smoke opacity with biodiesel mixed in the blends

CHAPTER 6

CONCLUSION AND FUTURE WORK

6.1. Conclusions

The present research aims to utilize the hydrotreating process as a method for producing diesel like fuel from the used cooking oil. It is found that this method is a vital approach in tackling the problem of ever changing crude oil prices, environmental pollution and the shelf life of biodiesel.

The following conclusions were drawn from the research study:

1. The parameters for the production of the hydrotreated oil were optimized using Taguchi method and fuzzy logic. The MPCI predicted by the method was 0.944 and the confirmation experiment with the best parameters gave an MPCI of 0.94 with 88.2% diesel selectivity and 89.7% conversion efficiency.

2. Almost all the physico-chemical properties of the blends are comparable to diesel and well within ASTM standards. Moreover, the cetane index of the neat hydrotreated oil was higher than diesel.

3. The neat hydrotreated oil resulted in the lowest evaporation time at all the loads and diesel had the highest evaporation time. The ignition probability of the neat oil was observed to be the highest at all the temperatures and diesel had the lowest ignition probability.

4. The SMD of the diesel was observed to be lowest and neat hydrotreated oil had highest SMD. The SMD of the blends is observed to be in between these two fuels.

5. Engine tests were carried out with the blends of the hydrotreated oil and diesel. The heat release rate with the blends of hydrotreated oil was lower than diesel

and the heat release started earlier than diesel due to its higher cetane index. This resulted in lower peak pressure.

6. The neat hydrotreated oil had lowest CoV among all the test fuel samples. A neural network was also trained for predicting the CoV. The neural network with 16 neurons in one hidden layer gave the best value of R^2, lowest value of MAPE and RMSE.

7. The thermal efficiency of the test fuel samples decreased in comparison to diesel. The lowest efficiency was observed with neat hydrotreated oil. At full load the thermal efficiency with diesel and H100 was 31.2% and 27%, respectively. The blends had efficiency in between the two fuels.

8. The brake specific energy consumption of the fuel samples was higher than diesel. At full load the energy consumption with H100 was 15.42% higher in comparison to diesel. The energy consumption of the blends was observed to be in-between the two samples.

9. The HC, CO and smoke emissions were found to decrease till H30D70 blend, further increase of the hydrotreated oil in the blend resulted in increase in smoke emission. The HC, CO and smoke emission at full load with H30D70 reduces by 14.4%, 16.93% and 11.7%, respectively in comparison to diesel.

10. The NO emissions on the other hand decreases as the percentage of the hydrotreated oil increases in the blend. The lowest NO emission was observed with H100 (3.1g/kWh), whereas engine operation with H30D70 resulted in 3.5g/kWh NO emission.

11. To further improve the efficiency of the engine and reduce the emissions, used cooking oil biodiesel (5%, 10% and 15% on volume basis) was also added to the blends of H20D80 and H30D70. The heat release rate of the engine increases

with the addition of biodiesel and as the percentage of biodiesel increases, the heat release rate increases. The peak in-cylinder pressure was also found to increase.

12. The ignition delay and combustion duration was higher with the biodiesel blends as compared to the blends without biodiesel.

13. The thermal efficiency of the biodiesel blends was found to be higher than H20D80 and H30D70. The higher the percentage of biodiesel in the blend, the higher is the thermal efficiency, but the efficiency is still lower than diesel. H20B15 resulted in the highest thermal efficiency.

14. The energy consumption was lower with the biodiesel in comparison to the hydrotreated oil blends without biodiesel but it was still higher than diesel. At full load, the lowest energy consumption was observed with H20B15.

15. The HC, CO and smoke emissions were observed to decrease with the increase in the biodiesel content in the blend. The lowest emissions were observed with H30B15. At full load, the reduction in HC, CO and smoke emissions with H30B15 is 30.8%, 23.5% and 21.15%, respectively.

16. The NO emissions were found to increase with increase in biodiesel content in the blend, but they were still lower than diesel.

6.2. Scope for future work

On the basis of the knowledge gained from this research work, the following future recommendations are underlined.

1. Future researchers can also focus on other non-edible feedstocks for diesel like fuel production using the hydroprocessing technique.

2. The spray analysis was carried out using the Spraytec instrument. Future researchers can also model the spray of the fuel sample using the computational fluid dynamics technique and compare with the experimental results.

3. The combustion characteristics can also be studied using multi-dimensional models provided in software's like ANSYS and validated with the experimental results.

4. Life cycle analysis can be carried out to study the environmental sustainability of the fuels.

5. Vibration and sound analysis can also be carried out to get a detailed effect of fuel on the engine's operation.

6. It is seen that NO increases with the biodiesel addition, in the future studies can be carried out to reduce the emissions with the help of techniques such as EGR and selective catalyst reduction.

REFERENCES

[1]   International Energy Agency. Key Energy World Statistics 2017. https://doi.org/10.1017/CBO9781107415324.004.

[2]   British Petroleum. British Petroleum Statistical Review of World Energy. 2019.

[3]   Ministry of Petroleum and Natural Gas Economic and Statistics. Indian Petroleum & Natural Gas Statistics. 2017.

[4]   Liguori R, Faraco V. Biological processes for advancing lignocellulosic waste biorefinery by advocating circular economy. Bioresour Technol 2016;215:13–20. https://doi.org/10.1016/j.biortech.2016.04.054.

[5]   Fells I. Clean and secure energy for the twenty-first century. Proc Inst Mech Eng Part A J Power Energy 2002;216:291–4. https://doi.org/10.1243/09576500260251138.

[6]   Crookes RJ, Kiannejad F, Nazha MAA. Systematic assessment of combustion characteristics of biofuels and emulsions with water for use as diesel engine fuels. Energy Convers Manag 1997;38:1785–95. https://doi.org/10.1016/S0196-8904(96)00202-6.

[7]   Faiz A, Sturm PJ. New directions: Air pollution and road traffic in developing countries. Dev Environ Sci 2002;1:241–3. https://doi.org/10.1016/S1474-8177(02)80010-9.

[8]   British Petroleum. BP Statistical Review of World Energy June 2017. 2017.

[9]   Xiao F, Liu S, Hwang JW, Son CU, Jeong JY, Han JH, et al. Plasma Treatment of Diesel Particulate for a Minibus. SAE Tech Pap Ser 2000:2000-01–3459. https://doi.org/10.4271/2000-01-3459.

[10]   Atabani AE, Silitonga AS, Ong HC, Mahlia TMI, Masjuki HH, Badruddin IA, et al. Non-edible vegetable oils: A critical evaluation of oil extraction, fatty acid compositions, biodiesel production, characteristics, engine performance and emissions production. Renew Sustain Energy Rev 2013;18:211–45. https://doi.org/10.1016/J.RSER.2012.10.013.

[11]   No S-Y. Inedible vegetable oils and their derivatives for alternative diesel fuels

in CI engines: A review. Renew Sustain Energy Rev 2011;15:131–49. https://doi.org/10.1016/J.RSER.2010.08.012.

[12] Sarin R, Sharma M, Khan AA. Studies on Guizotia abyssinica L. oil: Biodiesel synthesis and process optimization. Bioresour Technol 2009;100:4187–92. https://doi.org/10.1016/J.BIORTECH.2009.03.072.

[13] Ramadhas AS, Jayaraj S, Muraleedharan C. Biodiesel production from high FFA rubber seed oil. Fuel 2005;84:335–40. https://doi.org/10.1016/J.FUEL.2004.09.016.

[14] Mohibbe Azam M, Waris A, Nahar NM. Prospects and potential of fatty acid methyl esters of some non-traditional seed oils for use as biodiesel in India. Biomass and Bioenergy 2005;29:293–302. https://doi.org/10.1016/J.BIOMBIOE.2005.05.001.

[15] Singh SP, Singh D. Biodiesel production through the use of different sources and characterization of oils and their esters as the substitute of diesel: A review. Renew Sustain Energy Rev 2010;14:200–16. https://doi.org/10.1016/J.RSER.2009.07.017.

[16] Chhetri AB, Watts KC. Densities of canola, jatropha and soapnut biodiesel at elevated temperatures and pressures. Fuel 2012;99:210–6. https://doi.org/10.1016/J.FUEL.2012.04.030.

[17] Venkanna BK, Venkataramana Reddy C. Biodiesel production and optimization from Calophyllum inophyllum linn oil (honne oil) – A three stage method. Bioresour Technol 2009;100:5122–5. https://doi.org/10.1016/J.BIORTECH.2009.05.023.

[18] Ong HC, Mahlia TMI, Masjuki HH, Norhasyima RS. Comparison of palm oil, Jatropha curcas and Calophyllum inophyllum for biodiesel: A review. Renew Sustain Energy Rev 2011;15:3501–15. https://doi.org/10.1016/J.RSER.2011.05.005.

[19] Demirbas A. Production of biodiesel fuels from linseed oil using methanol and ethanol in non-catalytic SCF conditions. Biomass and Bioenergy 2009;33:113–8. https://doi.org/10.1016/J.BIOMBIOE.2008.04.018.

REFERENCES

[20] Subramanian KA, Singal SK, Saxena M, Singhal S. Utilization of liquid biofuels in automotive diesel engines: An Indian perspective. Biomass and Bioenergy 2005;29:65–72. https://doi.org/10.1016/J.BIOMBIOE.2005.02.001.

[21] Kibazohi O, Sangwan RS. Vegetable oil production potential from Jatropha curcas, Croton megalocarpus, Aleurites moluccana, Moringa oleifera and Pachira glabra: Assessment of renewable energy resources for bio-energy production in Africa. Biomass and Bioenergy 2011;35:1352–6. https://doi.org/10.1016/J.BIOMBIOE.2010.12.048.

[22] Kafuku G, Lam MK, Kansedo J, Lee KT, Mbarawa M. Heterogeneous catalyzed biodiesel production from Moringa oleifera oil. Fuel Process Technol 2010;91:1525–9. https://doi.org/10.1016/J.FUPROC.2010.05.032.

[23] Holser RA, Harry-O'Kuru R. Transesterified milkweed (Asclepias) seed oil as a biodiesel fuel. Fuel 2006;85:2106–10. https://doi.org/10.1016/J.FUEL.2006.04.001.

[24] Berman P, Nizri S, Wiesman Z. Castor oil biodiesel and its blends as alternative fuel. Biomass and Bioenergy 2011;35:2861–6. https://doi.org/10.1016/J.BIOMBIOE.2011.03.024.

[25] McCarthy P, Rasul MG, Moazzem S. Comparison of the performance and emissions of different biodiesel blends against petroleum diesel. Int J Low-Carbon Technol 2011;6:255–60. https://doi.org/10.1093/ijlct/ctr012.

[26] Rasul MG, Rudolph V, Carsky M. Physical properties of bagasse. Fuel 1999;78:905–10. https://doi.org/10.1016/S0016-2361(99)00011-3.

[27] Qureshi N, Saha BC, Hector RE, Hughes SR, Cotta MA. Butanol production from wheat straw by simultaneous saccharification and fermentation using Clostridium beijerinckii: Part I—Batch fermentation. Biomass and Bioenergy 2008;32:168–75. https://doi.org/10.1016/J.BIOMBIOE.2007.07.004.

[28] Amiri H, Karimi K, Zilouei H. Organosolv pretreatment of rice straw for efficient acetone, butanol, and ethanol production. Bioresour Technol 2014;152:450–6. https://doi.org/10.1016/J.BIORTECH.2013.11.038.

[29] Qureshi N, Saha BC, Dien B, Hector RE, Cotta MA. Production of butanol (a

biofuel) from agricultural residues: Part I – Use of barley straw hydrolysate. Biomass and Bioenergy 2010;34:559–65. https://doi.org/10.1016/J.BIOMBIOE.2009.12.024.

[30] McCarthy P, Rasul MG, Moazzem S. Analysis and comparison of performance and emissions of an internal combustion engine fuelled with petroleum diesel and different bio-diesels. Fuel 2011;90:2147–57. https://doi.org/10.1016/J.FUEL.2011.02.010.

[31] Agarwal AK. Biofuels (alcohols and biodiesel) applications as fuels for internal combustion engines. Prog Energy Combust Sci 2007;33:233–71. https://doi.org/10.1016/j.pecs.2006.08.003.

[32] Hribernik A, Kegl B. Performance and Exhaust Emissions of an Indirect-Injection (IDI) Diesel Engine When Using Waste Cooking Oil as Fuel. Energy & Fuels 2009;23:1754–8.

[33] FSSAI. Repurpose Used Cooking Oil. 2018.

[34] Kathirvel S, Layek A, Muthuraman S. Exploration of waste cooking oil methyl esters (WCOME) as fuel in compression ignition engines: A critical review. Eng Sci Technol an Int J 2016;19:1018–26. https://doi.org/10.1016/J.JESTCH.2016.01.007.

[35] Lapuerta M, Herreros JM, Lyons LL, García-Contreras R, Briceño Y. Effect of the alcohol type used in the production of waste cooking oil biodiesel on diesel performance and emissions. Fuel 2008;87:3161–9. https://doi.org/10.1016/J.FUEL.2008.05.013.

[36] Knothe G. Biodiesel and renewable diesel: A comparison. Prog Energy Combust Sci 2010;36:364–73. https://doi.org/10.1016/j.pecs.2009.11.004.

[37] Kuronen M, Mikkonen S, Aakko P, Murtonen T. Hydrotreated vegetable oil as fuel for heavy duty diesel engines. SAE Tech Pap Ser 2007. https://doi.org/10.4271/2007-01-4031.

[38] Patel M, Kumar A. Production of renewable diesel through the hydroprocessing of lignocellulosic biomass-derived bio-oil: A review. Renew Sustain Energy Rev

REFERENCES

2016;58:1293–307. https://doi.org/10.1016/j.rser.2015.12.146.

[39] Gary JH, Handwerk GE. Petroleum refining, technology and economics. 4th ed. New York: Marcel Dekker; 2001.

[40] Huber GW, Corma A. Synergies between bio- and oil refineries for the production of fuels from biomass. Angew Chemie Int Ed 2007;46:7184–220.

[41] Stumborg M, Wong A, Hogan E. Hydroprocessed Vegetable Oils for Diesel Fuel Improvement. Bioresour Technol 1996;56:13–8.

[42] Bezergianni S, Dimitriadis A, Sfetsas T, Kalogianni A. Hydrotreating of waste cooking oil for biodiesel production. Part II: Effect of temperature on hydrocarbon composition. Bioresour Technol 2010;101:7658–60. https://doi.org/10.1016/j.biortech.2010.04.043.

[43] Šimáček P, Kubička D, Kubičková I, Homola F, Pospíšil M, Chudoba J. Premium quality renewable diesel fuel by hydroprocessing of sunflower oil. Fuel 2011;90:2473–9. https://doi.org/10.1016/j.fuel.2011.03.013.

[44] Mikulec J, Cvengros J, Jorikova L, Kleinova A. Second generation diesel fuel from renewable sources. J Cleaner Prod 2010;18:917–26.

[45] Mäkinen R, Nylund N, Erkkilä K, Saikkonen P. Bus Fleet Operation on Renewable Paraffinic Diesel Fuel. SAE Tech Pap 2011. https://doi.org/10.4271/2011-01-1965.

[46] Murtonen T, Aakko-Saksa P, Koponen P, Lehto K, Sarjovaara T, Happonen M, et al. Emission reduction potential with paraffinic renewable diesel by optimizing engine settings or using oxygenate. SAE Int 2012. https://doi.org/10.4271/2012-01-1590.

[47] Caprotti R, Tang T, Ishibe N, R.In-ochanon, C.Tipdecho, S.Silapakampeerapap. Performance of Diesel containing Bio-Hydrogenated Component. SAE Pap 2011;2011-01–19. https://doi.org/10.4271/2011-01-1953.

[48] Bezergianni S. Catalytic Hydroprocessing of Liquid Biomass for Biofuels Production. Liq Gaseous Solid Biofuels - Convers Tech 2013:299–326. https://doi.org/10.5772/52649.

[49] B. Donnis, R.G. Egeberg, P. Blom KGK. Hydroprocessing of bio-oils and oxygenates to hydrocarbons. Understanding the reaction routes. Top Catal 2009;52:229–40.

[50] Gusmão J, Brodzki D, Djéga-Mariadassou G, Frety R. Utilization of vegetable oils as an alternative source for diesel-type fuel: hydrocracking on reduced Ni/SiO2 and sulphided Ni-Mo/γ-Al2O3. Catal Today 1989;5:533–44. https://doi.org/10.1016/0920-5861(89)80017-3.

[51] I. Kubickova, M. Snåre, K. Eranen, P. Maki-Arvela DM. Hydrocarbons for diesel fuel via decarboxylation of vegetable oils. Catal Today 2005;106:197–200.

[52] M. Snare, I. KubicKova, P. Maki-Arvela, D. Chichova, K. Eranen DM. Catalytic Deoxygenation of unsaturated renewable feedstocks for production of diesel fuel hydrocarbons. Fuel 2008;87:933–45.

[53] Veriansyah B, Han JY, Kim SK, Hong SA, Kim YJ, Lim JS, et al. Production of renewable diesel by hydroprocessing of soybean oil: Effect of catalysts. Fuel 2012;94:578–85. https://doi.org/10.1016/j.fuel.2011.10.057.

[54] S. Gong, A. Shinozaki, M. Shi EWQ. Hydrotreating of Jatropha oil over alumina based catalysts. Energy & Fuels 2012;26:2394–9.

[55] Liu J, Fan K, Tian W, Liu C, Rong L. Hydroprocessing of Jatropha oil over NiMoCe/Al2O3 catalyst. Int J Hydrogen Energy 2012;37:17731–7. https://doi.org/10.1016/j.ijhydene.2012.09.020.

[56] S.K. Kim, S. Brand, H.S. Lee, Y. Kim JK. Production of renewable diesel by hydrotreatment of soybean oil: effect of reaction parameters. Chem Eng J 2012;228:114–23.

[57] Chen S. Green Oil Production by Hydroprocessing. Int J Clean Coal Energy 2012;01:43–55. https://doi.org/10.4236/ijcce.2012.14005.

[58] P. Mäki-Arvela , I. Kubičková, M. Snåre, K. Eränen DYM. Catalytic deoxygenation of fatty acids and their derivatives. Energy & Fuels 2007;21:30–41.

REFERENCES

[59] Kochetkova D, Blažek J, Šimáček P, Staš M, Beňo Z. Influence of rapeseed oil hydrotreating on hydrogenation activity of CoMo catalyst. Fuel Process Technol 2016;142:319–25. https://doi.org/10.1016/j.fuproc.2015.10.034.

[60] A. Srifa, K. Faungnawakij, V. Itthibenchapong, N. Viriya-empikul, T. Charinpanitkul, S. Assabumrungrat. Production of bio-hydrogenated diesel by catalytic hydrotreating of palm oil over NiMoS2/c-Al2O3 catalyst. Bioresour Technol 2014;158:81–90.

[61] V.A. Yakovlev, S.A Khromova, O.V. Sherstyuk, V.O. Dundich, D.Y. Ermakov, V.M. Novopashina, M.Y. Lebedev, O. Bulavchenko VNP. Development of new catalytic systems for upgraded bio-fuels production from bio-crude-oil and biodiesel. Catal Today 2009;144:362–6.

[62] Guzman A, Torres JE, Prada LP, Nuñez ML. Hydroprocessing of crude palm oil at pilot plant scale. Catal Today 2010;156:38–43. https://doi.org/10.1016/j.cattod.2009.11.015.

[63] Q. Smejkal, L. Smejkalovaa, D. Kubicka. Thermodynamic balance in reaction system of total vegetable oil hydrogenation. Chem Eng J 2009;146:155–60.

[64] Kiatkittipong W, Phimsen S, Kiatkittipong K, Wongsakulphasatch S, W. Kiatkittipong, S. Phimsen, K. Kiatkittipong, S. Wongsakulphasatch, N. Wongsakulphasatch SA, Kiatkittipong W, et al. Diesel-like hydrocarbon production from hydroprocessing of relevant refining palm oil. Fuel Process Technol 2013;116:16–26. https://doi.org/10.1016/j.fuproc.2013.04.018.

[65] T. Morgan, D. Grubb, E. Santillan-Jimenez MC. Conversion of triglycerides to hydrocarbons over supported metal catalysts. Top Catal 2010;53:820–9.

[66] F. Shi, P. Wang, Y. Duan, D. Link BM. Recent developments in the production of liquid fuels via catalytic conversion of microalgae: experiments and simulations. RSC Adv 2012;2:9727–9747.

[67] Priecel P, Kubička D, Čapek L, Bastl Z, Ryšánek P. The role of Ni species in the deoxygenation of rapeseed oil over NiMo-alumina catalysts. Appl Catal A Gen 2011;397:127–37. https://doi.org/10.1016/j.apcata.2011.02.022.

[68] Kikhtyanin O V., Rubanov AE, Ayupov AB, Echevsky G V. Hydroconversion

Performance, Emission and Combustion Studies of a Modified Vegetable Oil in a Compression Ignition Engine

of sunflower oil on Pd/SAPO-31 catalyst. Fuel 2010;89:3085–92. https://doi.org/10.1016/j.fuel.2010.05.033.

[69] Krár M, Kovács S, Kalló D, Hancsók J. Fuel purpose hydrotreating of sunflower oil on CoMo/Al2O3 catalyst. Bioresour Technol 2010;101:9287–93. https://doi.org/10.1016/j.biortech.2010.06.107.

[70] Yang Y, Wang Q, Zhang X, Wang L, Li G. Hydrotreating of C18 fatty acids to hydrocarbons on sulphided NiW/SiO2–Al2O3. Fuel Process Technol 2013;116:165–74. https://doi.org/10.1016/j.fuproc.2013.05.008.

[71] Sankaranarayanan TM, Banu M, Pandurangan A, Sivasanker S. Hydroprocessing of sunflower oil-gas oil blends over sulfided Ni-Mo-Al-zeolite beta composites. Bioresour Technol 2011;102:10717–23. https://doi.org/10.1016/j.biortech.2011.08.127.

[72] J. Walendziewski, M. Stolarski, R. Luzny BK. Hydroprocessing of light gas oil – rape oil mixtures. Fuel Process Technol 2009;90:686–91.

[73] Al-Sabawi M, Chen J. Hydroprocessing of Biomass-Derived Oils and Their Blends with Petroleum Feedstocks A Review.pdf. Energy & Fuels 2012;26:5373–99. https://doi.org/10.1021/ef3006405.

[74] Lapuerta M, Villajos M, Agudelo JR, Boehman AL. Key properties and blending strategies of hydrotreated vegetable oil as biofuel for diesel engines. Fuel Process Technol 2011;92:2406–11. https://doi.org/10.1016/j.fuproc.2011.09.003.

[75] Bezergianni S, Dimitriadis A. Temperature effect on co-hydroprocessing of heavy gas oil-waste cooking oil mixtures for hybrid diesel production. Fuel 2013;103:579–84. https://doi.org/10.1016/j.fuel.2012.08.006.

[76] Hancsók J, Krár M, Magyar S, Boda L, Holló A, Kalló D. Investigation of the production of high cetane number bio gas oil from pre-hydrogenated vegetable oils over Pt/HZSM-22/Al2O3. Microporous Mesoporous Mater 2007;101:148–52. https://doi.org/10.1016/j.micromeso.2006.12.012.

[77] Chun-ya LIU, Hao Y, Zhong-yu J, Ke-zhong XI, Cong-zhen Q. Hydrodeoxygenation of fatty acid methyl esters and isomerization of products

REFERENCES

over NiP / SAPO-11 catalysts. J Fuel Chem Technol 2016;44:1211–6. https://doi.org/10.1016/S1872-5813(16)30052-4.

[78] Bezergianni S, Dimitriadis A, Chrysikou LP. Quality and sustainability comparison of one- vs. Two-step catalytic hydroprocessing of waste cooking oil. Fuel 2014;118:300–7. https://doi.org/10.1016/j.fuel.2013.10.078.

[79] Jha MK, Sinha AK, Agnihotri P. Hydroprocessing of jatropha oil to produce green fuels. Int J ChemTech Res 2013;5:765–70.

[80] Kov??cs S, Kasza T, Thernesz A, Horv??th IW, Hancs??k J. Fuel production by hydrotreating of triglycerides on NiMo/Al2O3/F catalyst. Chem Eng J 2011;176–177:237–43. https://doi.org/10.1016/j.cej.2011.05.110.

[81] Nimkarde MR, Vaidya PD. Toward Diesel Production from Karanja Oil Hydrotreating over CoMo and NiMo Catalysts. Energy and Fuels 2016;30:3107–12. https://doi.org/10.1021/acs.energyfuels.6b00138.

[82] Šimáček P, Kubička D, Šebor G, Pospíšil M. Hydroprocessed rapeseed oil as a source of hydrocarbon-based biodiesel. Fuel 2009;88:456–60. https://doi.org/10.1016/j.fuel.2008.10.022.

[83] Šimáček P, Kubička D, Šebor G, Pospíšil M. Fuel properties of hydroprocessed rapeseed oil. Fuel 2010;89:611–5. https://doi.org/10.1016/j.fuel.2009.09.017.

[84] Kubička D, Kaluža L. Deoxygenation of vegetable oils over sulfided Ni, Mo and NiMo catalysts. Appl Catal A Gen 2010;372:199–208. https://doi.org/10.1016/j.apcata.2009.10.034.

[85] Kubička D, Horáček J. Deactivation of HDS catalysts in deoxygenation of vegetable oils. Appl Catal A Gen 2011;394:9–17. https://doi.org/10.1016/j.apcata.2010.10.034.

[86] da Rocha Filho GN, Brodzki D, Djéga-Mariadassou G. Formation of alkanes, alkylcycloalkanes and alkylbenzenes during the catalytic hydrocracking of vegetable oils. Fuel 1993;72:543–9. https://doi.org/10.1016/0016-2361(93)90114-H.

[87] Bezergianni S, Dimitriadis A, Kalogianni A, Pilavachi PA. Hydrotreating of waste cooking oil for biodiesel production. Part I: Effect of temperature on

product yields and heteroatom removal. Bioresour Technol 2010;101:6651–6. https://doi.org/10.1016/j.biortech.2010.03.081.

[88] Toba M, Abe Y, Kuramochi H, Osako M, Mochizuki T, Yoshimura Y. Hydrodeoxygenation of waste vegetable oil over sulfide catalysts. Catal Today 2011;164:533–7. https://doi.org/10.1016/j.cattod.2010.11.049.

[89] Bezergianni S, Kalogianni A. Hydrocracking of used cooking oil for biofuels production. Bioresour Technol 2009;100:3927–32. https://doi.org/10.1016/j.biortech.2009.03.039.

[90] Bezergianni S, Dimitriadis A, Kalogianni A, Knudsen KG. Toward Hydrotreating of Waste Cooking Oil for Biodiesel Production, effect of pressure, H2/Oil Ratio, and Liquid Hourly Space Velocity. Ind Eng Chem Res 2011;50:3874–9. https://doi.org/10.1021/ie200251a.

[91] Sotelo-boy R, Liu Y, Minowa T, Sotelo-Boyás R, Liu Y, Minowa T. Renewable Diesel Production from the Hydrotreating of Rapeseed Oil with Pt/Zeolite and NiMo/Al2O3 Catalysts. Ind Eng Chem Res 2011;50:2791–9. https://doi.org/10.1021/ie100824d.

[92] Bezergianni S, Kalogianni A, Dimitriadis A. Catalyst evaluation for waste cooking oil hydroprocessing. Fuel 2012;93:638–41. https://doi.org/10.1016/j.fuel.2011.08.053.

[93] Zhao X, Wei L, Cheng S, Kadis E, Cao Y, Boakye E, et al. Hydroprocessing of carinata oil for hydrocarbon biofuel over Mo-Zn/Al2O3. Appl Catal B Environ 2016;196:41–9. https://doi.org/10.1016/j.apcatb.2016.05.020.

[94] Monnier J, Sulimma H, Dalai A, Caravaggio G. Hydrodeoxygenation of oleic acid and canola oil over alumina-supported metal nitrides. Appl Catal A Gen 2010;382:176–80. https://doi.org/10.1016/j.apcata.2010.04.035.

[95] Pinto F, Varela FT, Gonçalves M, Neto André R, Costa P, Mendes B. Production of bio-hydrocarbons by hydrotreating of pomace oil. Fuel 2014;116:84–93. https://doi.org/10.1016/j.fuel.2013.07.116.

[96] Bezergianni S, Kalogianni A, Vasalos IA. Hydrocracking of vacuum gas oil-

REFERENCES

vegetable oil mixtures for biofuels production. Bioresour Technol 2009;100:3036–42. https://doi.org/10.1016/j.biortech.2009.01.018.

[97] Bezergianni S, Dimitriadis A, Meletidis G. Effectiveness of CoMo and NiMo catalysts on co-hydroprocessing of heavy atmospheric gas oil-waste cooking oil mixtures. Fuel 2014;125:129–36. https://doi.org/10.1016/j.fuel.2014.02.010.

[98] Kumar R, Rana BS, Tiwari R, Verma D, Kumar R, Joshi RK, et al. Hydroprocessing of jatropha oil and its mixtures with gas oil. Green Chem 2010;12:2232. https://doi.org/10.1039/c0gc00204f.

[99] Breysse M, Afanasiev P, Geantet C, Vrinat M. Overview of support effects in hydrotreating catalysts. Catal Today 2003;86:5–16. https://doi.org/10.1016/S0920-5861(03)00400-0.

[100] Dhar GM, Srinivas B., Rana M., Kumar M, Maity S. Mixed oxide supported hydrodesulfurization catalysts—a review. Catal Today 2003;86:45–60. https://doi.org/10.1016/S0920-5861(03)00403-6.

[101] Barrera MC, Viniegra M, Escobar J, Vrinat M, de los Reyes JA, Murrieta F, et al. Highly active MoS2 on wide-pore ZrO2–TiO2 mixed oxides. Catal Today 2004;98:131–9. https://doi.org/10.1016/J.CATTOD.2004.07.027.

[102] Cedeño Caero L, Romero AR, Ramirez J. Niobium sulfide as a dopant for Mo/TiO2 catalysts. Catal Today 2003;78:513–8. https://doi.org/10.1016/S0920-5861(02)00342-5.

[103] Rana MS, Srinivas BN, Maity SK, Murali Dhar G, Prasada Rao TSR. Origin of Cracking Functionality of Sulfided (Ni) CoMo/SiO2–ZrO2 Catalysts. J Catal 2000;195:31–7. https://doi.org/10.1006/JCAT.2000.2968.

[104] Zhaobin W, Qin X, Xiexian G, Grange P, Delmon B. Titania-modified hydrodesulfurization catalysts: II. Dispersion state and catalytic activity of molybdena supported on titania-alumina carrier. Appl Catal 1991;75:179–91. https://doi.org/10.1016/S0166-9834(00)83131-0.

[105] Chiranjeevi T, Kumar P, Rana M., Murali Dhar G, Prasada Rao TS. Physico-chemical characterization and catalysis on mesoporous Al-HMS supported molybdenum hydrotreating catalysts. J Mol Catal A Chem 2002;181:109–17.

https://doi.org/10.1016/S1381-1169(01)00352-1.

[106] Welters WJJ, Vorbeck G, Zandbergen HW, van de Ven LJM, van Oers EM, de Haan JW, et al. NaY-Supported Molybdenum Sulfide Catalysts: I. Catalysts Prepared via Impregnation with Ammonium Heptamolybdate. J Catal 1996;161:819–28. https://doi.org/10.1006/JCAT.1996.0245.

[107] Dhar GM, Kumaran GM, Kumar M, Rawat KS, Sharma LD, Raju BD, et al. Physico-chemical characterization and catalysis on SBA-15 supported molybdenum hydrotreating catalysts. Catal Today 2005;99:309–14. https://doi.org/10.1016/J.CATTOD.2004.10.005.

[108] Rajesh M, Sau M, Malhotra RK, Sharma DK. Hydrotreating of Gas Oil, Jatropha Oil, and Their Blends Using a Carbon Supported Cobalt-Molybdenum Catalyst. Pet Sci Technol 2015;33:1653–9. https://doi.org/10.1080/10916466.2015.1036291.

[109] Sharma RKK, Anand M, Rana BSS, Kumar R, Farooqui SAA, Sibi MGG, et al. Jatropha-oil conversion to liquid hydrocarbon fuels using mesoporous titanosilicate supported sulfide catalysts. Catal Today 2012;198:314–20. https://doi.org/10.1016/j.cattod.2012.05.036.

[110] Yasir M, Azizan MT, Ramli A, Ameen M. Hydroprocessing of Crude Jatropha Oil Using Hierarchical Structured TiO2 Nanocatalysts. Procedia Eng 2016;148:275–81. https://doi.org/10.1016/j.proeng.2016.06.565.

[111] Anand M, Sinha AK. Temperature-dependent reaction pathways for the anomalous hydrocracking of triglycerides in the presence of sulfided Co-Mo-catalyst. Bioresour Technol 2012;126:148–55. https://doi.org/10.1016/j.biortech.2012.08.105.

[112] Chen L, Li H, Fu J, Miao C, Lv P, Yuan Z. Catalytic hydroprocessing of fatty acid methyl esters to renewable alkane fuels over Ni/HZSM-5 catalyst. Catal Today 2016;259:266–76. https://doi.org/10.1016/j.cattod.2015.08.023.

[113] Hartikka T, Kuronen M, Kiiski U. Technical Performance of HVO (Hydrotreated Vegetable Oil) in Diesel Engines. SAE Int 2012. https://doi.org/10.4271/2012-01-1585.

REFERENCES

[114] Agudelo JR, Prorok M, Boehman a. L. Bulk Modulus of Compressibility of Diesel / Biodiesel / HVO Blends. Energy & Fuels 2011;26:1336–43. https://doi.org/10.1021/ef201608g.

[115] Jaroonjitsathian S, Tipdecho C, Sukajit P, Namthirach N, Suppatvech S. Bio-Hydrogenated Diesel (BHD): Renewable Fuel for Advanced Diesel Technology. SAE Int 2013. https://doi.org/10.4271/2013-01-0070.

[116] Sugiyama K, Goto I, Kitano K, Mogi K, Honkanen M. Effects of Hydrotreated Vegetable Oil (HVO) as Renewable Diesel Fuel on Combustion and Exhaust Emissions in Diesel Engine. SAE Int J Fuels Lubr 2011;5:205–17. https://doi.org/10.4271/2011-01-1954.

[117] T. Hulkkonen, H. Hillamo, T. Sarjovaara ML, Hulkkonen T, Hillamo H, Sarjovaara T, Larmi M, T. Hulkkonen, H. Hillamo, T. Sarjovaara ML. Experimental Study of Spray Characteristics between Hydrotreated Vegetable Oil (HVO) and Crude Oil Based EN 590 Diesel Fuel. SAE Tech Pap 2011. https://doi.org/10.4271/2011-24-0042.

[118] G. Crepeau, P. Gaillard, D. van der Merwe PS. Engine Impacts and Opportunities of Various Fuels, Including GTL and FAME: Toward Specific Engine Calibration? SAE Tech Pap 2009.

[119] Kim D, Kim S, Oh S, No S-Y. Engine performance and emission characteristics of hydrotreated vegetable oil in light duty diesel engines. Fuel 2014;125:36–43. https://doi.org/10.1016/j.fuel.2014.01.089.

[120] Westphal GA, Krahl J, Munack A, Rosenkranz N, Schroder O, Schaak J, et al. Combustion of hydrotreated vegetable oil and jatropha methyl ester in a heavy duty engine: Emissions and bacterial mutagenicity. Environ Sci Technol 2013;47:6038–46. https://doi.org/10.1021/es400518d.

[121] Ogunkoya D, Roberts WL, Fang T, Thapaliya N. Investigation of the effects of renewable diesel fuels on engine performance, combustion, and emissions. Fuel 2015;140:541–54. https://doi.org/10.1016/j.fuel.2014.09.061.

[122] Imperato M, Tilli A, Sarjovaara T, Larmi M. Large-Bore Compression-Ignition Engines : High NOx Reduction Achieved at Low Load with Hydro-Treated

Vegetable Oil. SAE Int J Fuels Lubr 2011;5:225–32. https://doi.org/10.4271/2011-01-1956.

[123] Imperato M, Sarjovaara T, Larmi M. Hydrotreated Vegetable Oil and Miller Timing in a Medium-Speed CI Engine. SAE Int 2012. https://doi.org/10.4271/2012-01-0862.

[124] Singh D, Subramanian KA, Singal SK. Emissions and fuel consumption characteristics of a heavy duty diesel engine fueled with Hydroprocessed Renewable Diesel and Biodiesel. Appl Energy 2015;155:440–6. https://doi.org/10.1016/j.apenergy.2015.06.020.

[125] Rantanen L, Linnaila R, Aakko P, Harju T. NExBTL -Biodiesel Fuel of the Second Generation. SAE Tech Pap Ser 2005. https://doi.org/10.4271/2005-01-3771.

[126] Aatola H, Larmi M, Sarjovaara T, Mikkonen S. Hydrotreated Vegetable Oil (HVO) as a Renewable Diesel Fuel: Trade-off between NOx, Particulate Emission, and Fuel Consumption of a Heavy Duty Engine. SAE Int 2008. https://doi.org/10.4271/2008-01-2500.

[127] Pflaum H, Hofmann P, Geringer B, Weissel W. Potential of Hydrogenated Vegetable Oil (HVO) in a Modern Diesel Engine. SAE Int 2010;2010-32–00. https://doi.org/10.4271/2010-32-0081.

[128] Kopperoinen A, Kytö M, Mikkonen S. Effect of Hydrotreated Vegetable Oil (HVO) on Particulate Filters of Diesel Cars. SAE Int 2011;2011-01–20. https://doi.org/10.4271/2011-01-2096.

[129] Happonen M, Lähde T, Messing ME, Sarjovaara T, Larmi M, Wallenberg LR, et al. The comparison of particle oxidation and surface structure of diesel soot particles between fossil fuel and novel renewable diesel fuel. Fuel 2010;89:4008–13. https://doi.org/10.1016/j.fuel.2010.06.006.

[130] Murtonen T, Aakko-Saksa P, Kuronen M, Mikkonen S, Lehtoranta K. Emissions with heavy-duty diesel engines and vehicles using FAME, HVO and GTL fuels with and without DOC+POC aftertreatment. SAE Int J Fuels Lubr 2009;2:147–66. https://doi.org/10.4271/2009-01-2693.

REFERENCES

[131] Erkkilä K, Nylund N, Hulkkonen T, Tilli A, Mikkonen S, Saikkonen P, et al. Emission performance of paraffinic HVO diesel fuel in heavy duty vehicles. SAE Int 2011;2011-01–19. https://doi.org/10.4271/2011-01-1966.

[132] M. Hajbabaei, K.C. Johnson, R.A. Okamoto, A. Mitchell, A. Pullman, T.D. Durbin TD. Evaluation of the Impacts of Biodiesel and Second Generation Biofuels on NOx Emissions for CARB Diesel Fuels. Environ Sci Technol 2012;46:9163–73.

[133] Na K, Biswas S, Robertson W, Sahay K, Okamoto R, Mitchell A, et al. Impact of biodiesel and renewable diesel on emissions of regulated pollutants and greenhouse gases on a 2000 heavy duty diesel truck. Atmos Environ 2015;107:307–14. https://doi.org/10.1016/j.atmosenv.2015.02.054.

[134] Prokopowicz A, Zaciera M, Sobczak A, Bielaczyc P, Woodburn J. The Effects of Neat Biodiesel and Biodiesel and HVO Blends in Diesel Fuel on Exhaust Emissions from a Light Duty Vehicle with a Diesel Engine. Environ Sci Technol 2015;49:7473–82. https://doi.org/10.1021/acs.est.5b00648.

[135] Happonen M, Heikkilä J, Aakko-Saksa P, Murtonen T, Lehto K, Rostedt A, et al. Diesel exhaust emissions and particle hygroscopicity with HVO fuel-oxygenate blend. Fuel 2013;103:380–6. https://doi.org/10.1016/j.fuel.2012.09.006.

[136] Lehto K, Elonheimo A, Häkkinen K, Sarjovaara T, Larmi M. Emission Reduction Using Hydrotreated Vegetable Oil (HVO) With Miller Timing and EGR in Diesel Combustion. SAE Int J Fuels Lubr 2011;5:218–24. https://doi.org/10.4271/2011-01-1955.

[137] M. Happonen, J. Heikkila, T. Murtonen, K. Lehto, T. Sarjovaara, M. Larmi, J. Keskinen AV. Reductions in Particulate and NOx Emissions by Diesel Engine Parameter Adjustments with HVO Fuel. Environ Sci Technol 2012;46:6198–204.

[138] Lani NS, Ngadi N, Yahya NY, Rahman RA. Synthesis, characterization and performance of silica impregnated calcium oxide as heterogeneous catalyst in biodiesel production. J Clean Prod 2017;146:116–24. https://doi.org/https://doi.org/10.1016/j.jclepro.2016.06.058.

[139] Rabie AM, Shaban M, Abukhadra MR, Hosny R, Ahmed SA, Negm NA. Diatomite supported by CaO/MgO nanocomposite as heterogeneous catalyst for biodiesel production from waste cooking oil. J Mol Liq 2019;279:224–31. https://doi.org/https://doi.org/10.1016/j.molliq.2019.01.096.

[140] Abukhadra MR, Sayed MA. K+ trapped kaolinite (Kaol/K+) as low cost and eco-friendly basic heterogeneous catalyst in the transesterification of commercial waste cooking oil into biodiesel. Energy Convers Manag 2018;177:468–76. https://doi.org/https://doi.org/10.1016/j.enconman.2018.09.083.

[141] Du L, Ding S, Li Z, Lv E, Lu J, Ding J. Transesterification of castor oil to biodiesel using NaY zeolite-supported La2O3 catalysts. Energy Convers Manag 2018;173:728–34.
https://doi.org/https://doi.org/10.1016/j.enconman.2018.07.053.

[142] Manique MC, Lacerda LV, Alves AK, Bergmann CP. Biodiesel production using coal fly ash-derived sodalite as a heterogeneous catalyst. Fuel 2017;190:268–73. https://doi.org/https://doi.org/10.1016/j.fuel.2016.11.016.

[143] Chung ZL, Tan YH, Chan YS, Kansedo J, Mubarak NM, Ghasemi M, et al. Life cycle assessment of waste cooking oil for biodiesel production using waste chicken eggshell derived CaO as catalyst via transesterification. Biocatal Agric Biotechnol 2019;21:101317.
https://doi.org/https://doi.org/10.1016/j.bcab.2019.101317.

[144] Abed KA, El Morsi AK, Sayed MM, Shaib AA El, Gad MS. Effect of waste cooking-oil biodiesel on performance and exhaust emissions of a diesel engine. Egypt J Pet 2018;27:985–9. https://doi.org/https://doi.org/10.1016/j.ejpe.2018.02.008.

[145] Wei L, Cheung CS, Ning Z. Influence of waste cooking oil biodiesel on combustion, unregulated gaseous emissions and particulate emissions of a direct-injection diesel engine. Energy 2017;127:175–85. https://doi.org/https://doi.org/10.1016/j.energy.2017.03.117.

[146] Yesilyurt MK. The effects of the fuel injection pressure on the performance and emission characteristics of a diesel engine fuelled with waste cooking oil

REFERENCES

biodiesel-diesel blends. Renew Energy 2019;132:649–66. https://doi.org/https://doi.org/10.1016/j.renene.2018.08.024.

[147] Kuti OA, Sarathy SM, Nishida K. Spray combustion simulation study of waste cooking oil biodiesel and diesel under direct injection diesel engine conditions. Fuel 2020;267:117240. https://doi.org/https://doi.org/10.1016/j.fuel.2020.117240.

[148] Bencheikh K, Atabani AE, Shobana S, Mohammed MN, Uğuz G, Arpa O, et al. Fuels properties, characterizations and engine and emission performance analyses of ternary waste cooking oil biodiesel–diesel–propanol blends. Sustain Energy Technol Assessments 2019;35:321–34. https://doi.org/https://doi.org/10.1016/j.seta.2019.08.007.

[149] Guo JH, Xu GY, Shen F, Fu Y, Zhang Y, Guo QX. Catalytic conversion of Jatropha oil to alkanes under mild conditions with a Ru/La(OH)$_3$ catalyst. Green Chem 2015;17:2888–95. https://doi.org/10.1039/c4gc02406k.

[150] Mansur D, Ruliana, Rustana CE. Hydroprocessed Calophyllum inophyllum Oil for Linear Bio-alkane Fuel Production. Proc. Conf. Ind. Commer. Use Energy, ICUE, Asian Institute of Technology; 2018, p. 1–6. https://doi.org/10.23919/ICUE-GESD.2018.8635732.

[151] Fisher R. Statistical Methods for Research Worker. London: Oliver & Boyd; 1925.

[152] Montgomery D. Design and Analysis of Experiments. Singapore: Wiley; 1991.

[153] Sidharth, Kumar N. Performance and emission studies of ternary fuel blends of diesel, biodiesel and octanol. Energy Sources, Part A Recover Util Environ Eff 2020;42:2277–96. https://doi.org/10.1080/15567036.2019.1607940.

[154] Heywood JB. Internal Combustion Engine Fundamentals. Mc-Graw Hill; 1988.

[155] Assanis DN, Filipi Z, Fiveland SB, Syrimis M. A Methodology for Cycle-By-Cycle Transient Heat Release Analysis in a Turbocharged Direct Injection Diesel Engine 2000. https://doi.org/10.4271/2000-01-1185.

[156] Ma H, Kar K, Stone R, Raine R, Thorwarth H. Analysis of Combustion in a Small Homogeneous Charge Compression Assisted Ignition Engine. Int J Engine

Res 2006;7:237–53. https://doi.org/10.1243/146808705X60834.

[157] Hong S, Assanis DN, Wooldridge MS, Im HG, Kurtz E, Pitsch H. Modeling of Diesel Combustion and NO Emissions Based on a Modified Eddy Dissipation Concept. SAE Tech Pap 2004. https://doi.org/10.4271/2004-01-0107.

[158] Canakci M. Combustion characteristics of a turbocharged DI compression ignition engine fueled with petroleum diesel fuels and biodiesel. Bioresour Technol 2007;98:1167–75. https://doi.org/https://doi.org/10.1016/j.biortech.2006.05.024.

[159] Jang YJ, Ko YD, Jeong S. Optimal design of the wireless charging electric vehicle. IEEE Int. Electr. Veh. Conf., 2012, p. 1–5. https://doi.org/10.1109/IEVC.2012.6183294.

[160] Bittle J, Knight B, Jacobs T. Biodiesel Effects on Cycle-to-Cycle Variability of Combustion Characteristics in a Common-Rail Medium-Duty Diesel Engine. SAE Tech Pap 2010. https://doi.org/10.4271/2010-01-0867.

[161] Wirasingha SG, Schofield N, Emadi A. Plug-in hybrid electric vehicle developments in the US: Trends, barriers, and economic feasibility. IEEE Veh. Power Propuls. Conf., 2008, p. 1–8. https://doi.org/10.1109/VPPC.2008.4677702.

[162] Gürgen S, Ünver B, Altın İ. Prediction of cyclic variability in a diesel engine fueled with n-butanol and diesel fuel blends using artificial neural network. Renew Energy 2018;117:538–44. https://doi.org/10.1016/j.renene.2017.10.101.

[163] Bonges HA, Lusk AC. Addressing electric vehicle (EV) sales and range anxiety through parking layout, policy and regulation. Transp Res Part A Policy Pract 2016;83:63–73. https://doi.org/https://doi.org/10.1016/j.tra.2015.09.011.

[164] Lapuerta M, García-Contreras R, Campos-Fernández J, Dorado MP. Stability, Lubricity, Viscosity, and Cold-Flow Properties of Alcohol−Diesel Blends. Energy & Fuels 2010;24:4497–502. https://doi.org/10.1021/ef100498u.

[165] Selim MYE. Effect of engine parameters and gaseous fuel type on the cyclic variability of dual fuel engines. Fuel 2005;84:961–71.

REFERENCES

https://doi.org/https://doi.org/10.1016/j.fuel.2004.11.023.

[166] Ghobadian B, Rahimi H, Nikbakht AM, Najafi G, Yusaf TF. Diesel engine performance and exhaust emission analysis using waste cooking biodiesel fuel with an artificial neural network. Renew Energy 2009;34:976–82. https://doi.org/10.1016/j.renene.2008.08.008.

[167] Oğuz H, Sarıtas I, Baydan HE. Prediction of diesel engine performance using biofuels with artificial neural network. Expert Syst Appl 2010;37:6579–86. https://doi.org/10.1016/j.eswa.2010.02.128.

[168] Shojaeefard MH, Etghani MM, Akbari M, Khalkhali A, Ghobadian B. Artificial neural networks based prediction of performance and exhaust emissions in direct injection engine using castor oil biodiesel-diesel blends. J Renew Sustain Energy 2012;4. https://doi.org/10.1063/1.4769200.

[169] Roy S, Banerjee R, Bose PK. Performance and exhaust emissions prediction of a CRDI assisted single cylinder diesel engine coupled with EGR using artificial neural network. Appl Energy 2014;119:330–40. https://doi.org/10.1016/j.apenergy.2014.01.044.

[170] Çay Y, Çiçek A, Kara F, Sağiroğlu S. Prediction of engine performance for an alternative fuel using artificial neural network. Appl Therm Eng 2012;37:217–25. https://doi.org/10.1016/j.applthermaleng.2011.11.019.

[171] Davim JP, Gaitonde VN, Karnik SR. Investigations into the effect of cutting conditions on surface roughness in turning of free machining steel by ANN models. J Mater Process Technol 2008;205:16–23. https://doi.org/https://doi.org/10.1016/j.jmatprotec.2007.11.082.

[172] Javed S, Satyanarayana Murthy YVV, Baig RU, Prasada Rao D. Development of ANN model for prediction of performance and emission characteristics of hydrogen dual fueled diesel engine with Jatropha Methyl Ester biodiesel blends. J Nat Gas Sci Eng 2015;26:549–57. https://doi.org/10.1016/j.jngse.2015.06.041.

[173] Parlak A, Islamoglu Y, Yasar H, Egrisogut A. Application of artificial neural network to predict specific fuel consumption and exhaust temperature for a Diesel engine. Appl Therm Eng 2006;26:824–8.

https://doi.org/https://doi.org/10.1016/j.applthermaleng.2005.10.006.

[174] Yusaf TF, Buttsworth DR, Saleh KH, Yousif BF. CNG-diesel engine performance and exhaust emission analysis with the aid of artificial neural network. Appl Energy 2010;87:1661–9. https://doi.org/https://doi.org/10.1016/j.apenergy.2009.10.009.

[175] Kline SJ, McClintock FA. Describing uncertainties in single sample experiments. Mech Eng 1953:3–8. https://doi.org/10.1111/jcmm.13453.

[176] Kubička D, Bejblová M, Vlk J. Conversion of Vegetable Oils into Hydrocarbons over CoMo/MCM-41 Catalysts. Top Catal 2010;53:168–78. https://doi.org/10.1007/s11244-009-9421-z.

[177] Kubička D, Šimáček P, Žilková N. Transformation of Vegetable Oils into Hydrocarbons over Mesoporous-Alumina-Supported CoMo Catalysts. Top Catal 2009;52:161–8. https://doi.org/10.1007/s11244-008-9145-5.

[178] Tiwari R, Rana BS, Kumar R, Verma D, Kumar R, Joshi RK, et al. Hydrotreating and hydrocracking catalysts for processing of waste soya-oil and refinery-oil mixtures. Catal Commun 2011;12:559–62. https://doi.org/10.1016/j.catcom.2010.12.008.

[179] Murata K, Liu Y, Inaba M, Takahara I. Production of Synthetic Diesel by Hydrotreatment of Jatropha Oils Using Pt−Re/H-ZSM-5 Catalyst. Energy & Fuels 2010;24:2404–9. https://doi.org/10.1021/ef901607t.

[180] Liu Y, Sotelo-Boyás R, Murata K, Minowa T, Sakanishi K. Hydrotreatment of Jatropha Oil to Produce Green Diesel over Trifunctional Ni–Mo/SiO2 –Al2O3 Catalyst. Chem Lett 2009;38:552–3. https://doi.org/10.1246/cl.2009.552.

[181] Liu Y, Sotelo-Boyás R, Murata K, Minowa T, Sakanishi K. Production of Bio-Hydrogenated Diesel by Hydrotreatment of High-Acid-Value Waste Cooking Oil over Ruthenium Catalyst Supported on Al-Polyoxocation-Pillared Montmorillonite. Catalysts 2012;2:171–90. https://doi.org/10.3390/catal2010171.

[182] Liu Y, Sotelo-Boyás R, Murata K, Minowa T, Sakanishi K. Hydrotreatment of

REFERENCES

Vegetable Oils to Produce Bio-Hydrogenated Diesel and Liquefied Petroleum Gas Fuel over Catalysts Containing Sulfided Ni–Mo and Solid Acids. Energy & Fuels 2011;25:4675–85. https://doi.org/10.1021/ef200889e.

[183] Zhao C, Brück T, Lercher JA. Catalytic deoxygenation of microalgae oil to green hydrocarbons. Green Chem 2013;15:1720–39. https://doi.org/10.1039/C3GC40558C.

[184] Snåre M, Kubičková I, Mäki-Arvela P, Eränen K, Murzin DY. Heterogeneous Catalytic Deoxygenation of Stearic Acid for Production of Biodiesel. Ind Eng Chem Res 2006;45:5708–15. https://doi.org/10.1021/ie060334i.

[185] Osaka Y, Ikeda Y, Hashizume D, Iwamoto M. Direct hydrodeoxygenation of cellulose and xylan to lower alkanes on ruthenium catalysts in subcritical water. Biomass and Bioenergy 2013;56:1–7. https://doi.org/10.1016/J.BIOMBIOE.2013.04.012.

[186] He L, Wu C, Cheng H, Yu Y, Zhao F, Preparation C, et al. Supplementary Information Highly selective and efficient catalytic conversion of ethyl stearate into liquid hydrocarbons over Ru/TiO2 catalyst under mild conditions. Catal Sci Technol 2012;2:2–4. https://doi.org/10.1039/C2CY20157G.

[187] Patil SJ, Vaidya PD. Catalytic Hydrotreatment of Jatropha Oil over Lanthanum Hydroxide Supported Noble Metals: Effect of Promotion with Cerium. ChemistrySelect 2017;2:11918–25. https://doi.org/10.1002/slct.201702258.

[188] Patil SJ, Vaidya PD. On the production of bio-hydrogenated diesel over hydrotalcite-like supported palladium and ruthenium catalysts. Fuel Process Technol 2018;169:142–9. https://doi.org/10.1016/j.fuproc.2017.09.026.

[189] Mishra DK, Dabbawala AA, Hwang JS. Ruthenium nanoparticles supported on zeolite y as an efficient catalyst for selective hydrogenation of xylose to xylitol. J Mol Catal A Chem 2013;376:63–70. https://doi.org/10.1016/j.molcata.2013.04.011.

[190] Mishra DK, Dabbawala AA, Park JJ, Jhung SH, Hwang JS. Selective hydrogenation of d-glucose to d-sorbitol over HY zeolite supported ruthenium nanoparticles catalysts. Catal Today 2014;232:99–107.

https://doi.org/10.1016/j.cattod.2013.10.018.

[191] Ruinart de Brimont M, Dupont C, Daudin A, Geantet C, Raybaud P. Deoxygenation mechanisms on Ni-promoted MoS2 bulk catalysts: A combined experimental and theoretical study. J Catal 2012;286:153–64. https://doi.org/https://doi.org/10.1016/j.jcat.2011.10.022.

[192] Liu Q, Zuo H, Wang T, Ma L, Zhang Q. One-step hydrodeoxygenation of palm oil to isomerized hydrocarbon fuels over Ni supported on nano-sized SAPO-11 catalysts. Appl Catal A Gen 2013;468:68–74. https://doi.org/https://doi.org/10.1016/j.apcata.2013.08.009.

[193] Sonthalia A, Kumar N. Hydroprocessed vegetable oil as a fuel for transportation sector: A review. J Energy Inst 2019;92:1–17. https://doi.org/10.1016/j.joei.2017.10.008.

[194] Nakagawa Y, Liu S, Tamura M, Tomishige K. Catalytic Total Hydrodeoxygenation of Biomass-Derived Polyfunctionalized Substrates to Alkanes. ChemSusChem 2015;8:1114–32. https://doi.org/10.1002/cssc.201403330.

[195] Datta S, Bandyopadhyay A, Pal PK. Grey-based taguchi method for optimization of bead geometry in submerged arc bead-on-plate welding. Int J Adv Manuf Technol 2008;39:1136–43. https://doi.org/10.1007/s00170-007-1283-6.

[196] Yao AWL, Chi SC, Chen CK. Development of an integrated Grey–fuzzy-based electricity management system for enterprises. Energy 2005;30:2759–71. https://doi.org/10.1016/J.ENERGY.2005.02.001.

[197] Kumar P, Barua PB, Gaindhar JL. Quality optimization (multi-characteristics) through Taguchi's technique and utility concept. Qual Reliab Eng Int 2000;16:475–85. https://doi.org/10.1002/1099-1638(200011/12)16:6<475::AID-QRE342>3.0.CO;2-0.

[198] Datta S, Bandyopadhyay A, Pal PK. Desirability Function Approach for Solving Multi-Objective Optimization Problem in Submerged Arc Welding. J Manuf Sci Prod 2006;7:127. https://doi.org/10.1515/IJMSP.2006.7.2.127.

REFERENCES

[199] Sudhagar S, Sakthivel M, Mathew PJ, Daniel SAA. A multi criteria decision making approach for process improvement in friction stir welding of aluminium alloy. Measurement 2017;108:1–8. https://doi.org/https://doi.org/10.1016/j.measurement.2017.05.023.

[200] Paramasivam B, Kasimani R, Rajamohan S. Experimental assessment and multi-response optimization of diesel engine performance and emission characteristics fuelled with Aegle marmelos seed cake pyrolysis oil-diesel blends using Grey relational analysis coupled principal component analysis. Environ Sci Pollut Res 2019;26:6980–7004. https://doi.org/10.1007/s11356-019-04164-8.

[201] Radhakrishnan R, Raju R, Muthu krishnan N. Taguchi Multi-machining Characteristics Optimization in Turning of Al-15%SiC p Composites using Desirability Function Analysis. Int J Stud Manuf 2010;1:120–5.

[202] Lin J, Wang K, Yan B, Tarng Y. Optimization of the electrical discharge machining process based on the Taguchi method with fuzzy logics. J Mater Process Technol 2000;102:48–55. https://doi.org/10.1016/S0924-0136(00)00438-6.

[203] Satyarthi JK, Srinivas D. Fourier transform infrared spectroscopic method for monitoring hydroprocessing of vegetable oils to produce hydrocarbon-based biofuel. Energy and Fuels 2011;25:3318–22. https://doi.org/10.1021/ef200722q.

[204] Lam SS, Liew RK, Jusoh A, Chong CT, Ani FN, Chase HA. Progress in waste oil to sustainable energy, with emphasis on pyrolysis techniques. Renew Sustain Energy Rev 2016;53:741–53. https://doi.org/10.1016/J.RSER.2015.09.005.

[205] Fernando S, Karra P, Hernandez R, Jha SK. Effect of incompletely converted soybean oil on biodiesel quality. Energy 2007;32:844–51. https://doi.org/https://doi.org/10.1016/j.energy.2006.06.019.

[206] Manchanda T, Tyagi R, Sharma DK. Comparison of fuel characteristics of green (renewable) diesel with biodiesel obtainable from algal oil and vegetable oil. Energy Sources, Part A Recover Util Environ Eff 2018;40:54–9. https://doi.org/10.1080/15567036.2017.1405109.

[207] Dabelstein W, Reglitzky A, Schütze A, Reders K, Brunner A. Automotive Fuels.

Ullmann's Encycl Ind Chem 2016:1–41. https://doi.org/doi:10.1002/14356007.a16_719.pub3.

[208] Nolan DP. Chapter 4 - Physical Properties of Hydrocarbons and Petrochemicals. In: Nolan Gas, Chemical, and Related Facilities (Fourth Edition) DPBT-H of F and EPEP for O, editor. Handb. Fire Explos. Prot. Eng. Princ. Oil, Gas, Chem. Relat. Facil., Gulf Professional Publishing; 2019, p. 65–88. https://doi.org/https://doi.org/10.1016/B978-0-12-816002-2.00004-0.

[209] Bennett M. Ignition of combustible fluids by heated surfaces. Process Saf Prog 2001;10:29–36.

[210] Cengel Y, Turner R. Fundamentals of thermal fluid sciences. Fourth. New York: Mc-Graw Hill Education; 2017.

[211] Somandepalli V, Kelly S, Davis S. Hot Surface Ignition of Ethanol-blended Fuels and Biodiesel. SAE Tech Pap 2008;2008. https://doi.org/10.4271/2008-01-0402.

[212] Xiong TY, Yuen MC. Evaporation of a liquid droplet on a hot plate. Int J Heat Mass Transf 1991;34:1881–94. https://doi.org/https://doi.org/10.1016/0017-9310(91)90162-8.

[213] Arifin YM, Arai M. The effect of hot surface temperature on diesel fuel deposit formation. Fuel 2010;89:934–42. https://doi.org/https://doi.org/10.1016/j.fuel.2009.07.014.

[214] Arifin YM, Furuhata T, Saito M, Arai M. Diesel and bio-diesel fuel deposits on a hot surface. Fuel 2008;87:1601–9. https://doi.org/https://doi.org/10.1016/j.fuel.2007.07.030.

[215] No SY. Application of hydrotreated vegetable oil from triglyceride based biomass to CI engines - A review. Fuel 2014;115:88–96. https://doi.org/10.1016/j.fuel.2013.07.001.

[216] Bacha J, Freel J, et al. Diesel fuels technical review 2007:1–116. https://www.chevron.com/-/media/chevron/operations/documents/diesel-fuel-tech-review.pdf (accessed December 26, 2019).

REFERENCES

[217] Ejim CE, Fleck BA, Amirfazli A. Analytical study for atomization of biodiesels and their blends in a typical injector: Surface tension and viscosity effects. Fuel 2007;86:1534–44. https://doi.org/10.1016/J.FUEL.2006.11.006.

[218] Gao Y, Deng J, Li C, Dang F, Liao Z, Wu Z, et al. Experimental study of the spray characteristics of biodiesel based on inedible oil. Biotechnol Adv 2009;27:616–24. https://doi.org/10.1016/j.biotechadv.2009.04.022.

[219] Kumar N, Tomar M. Influence of nanoadditives on ignition characteristics of Kusum (Schleichera oleosa) biodiesel. Int J Energy Res 2019;43:3223–36. https://doi.org/10.1002/er.4446.

[220] Demirbas A. Biodiesel production via non-catalytic SCF method and biodiesel fuel characteristics. Energy Convers Manag 2006;47:2271–82. https://doi.org/10.1016/J.ENCONMAN.2005.11.019.

[221] Kousoulidou M, Dimaratos A, Karvountzis-Kontakiotis A, Samaras Z. Combustion and Emissions of a Common-Rail Diesel Engine Fueled with HWCO. J Energy Eng 2014;140:A4013001. https://doi.org/10.1061/(ASCE)EY.1943-7897.0000154.

[222] Singh D, Subramanian KA, Garg M. Comprehensive review of combustion, performance and emissions characteristics of a compression ignition engine fueled with hydroprocessed renewable diesel. Renew Sustain Energy Rev 2017;81:2947–54. https://doi.org/10.1016/j.rser.2017.06.104.

[223] McDaniel A, Dickerson T, Luning-Prak D, Hamilton L, Cowart J. A technical evaluation of New renewable jet and diesel fuels operated in neat form in multiple diesel engines. SAE Tech Pap 2016;2016-01–08.

[224] Mattson J, Depcik C. First and second law heat release analysis in a single cylinder engine. SAE Int J Engines 2016;9:536–45.

[225] Singh D, Subramanian KA, Bal R, Singh SP, Badola R. Combustion and emission characteristics of a light duty diesel engine fueled with hydro-processed renewable diesel. Energy 2018;154:498–507. https://doi.org/10.1016/j.energy.2018.04.139.

[226] Karthickeyan V, Thiyagarajan S, Ashok B, Edwin Geo V, Azad AK.

Experimental investigation of pomegranate oil methyl ester in ceramic coated engine at different operating condition in direct injection diesel engine with energy and exergy analysis. Energy Convers Manag 2020;205:112334. https://doi.org/https://doi.org/10.1016/j.enconman.2019.112334.

[227] Geo VE, Sonthalia A, Nagarajan G, Nagalingam B, Aloui F. Effect of Port Premixed Liquefied Petroleum Gas on the Engine Characteristics. J Energy Resour Technol Trans ASME 2019;141:1–8. https://doi.org/10.1115/1.4043698.

[228] Boopathi D, Thiyagarajan S, Edwin Geo V, Madhankumar S, Gheith R. Effect of geraniol on performance, emission and combustion characteristics of CI engine fuelled with gutter oil obtained from different sources. Energy 2018;157:391–401. https://doi.org/10.1016/J.ENERGY.2018.05.129.

[229] Subramanian T, Varuvel EG, Leenus JM, Beddhannan N. Effect of electrochemical conversion of biofuels using ionization system on CO2 emission mitigation in CI engine along with post-combustion system. Fuel Process Technol 2018;173:21–9. https://doi.org/https://doi.org/10.1016/j.fuproc.2018.01.004.

[230] Zhang Y, Li Z, Tamilselvan P, Jiang C, He Z, Zhong W, et al. Experimental study of combustion and emission characteristics of gasoline compression ignition (GCI) engines fueled by gasoline-hydrogenated catalytic biodiesel blends. Energy 2019;187:115931. https://doi.org/https://doi.org/10.1016/j.energy.2019.115931.

[231] Geo VE, Sonthalia A, Aloui F, Femilda Josephin JS. Study of engine performance, emission and combustion characteristics fueled with diesel-like fuel produced from waste engine oil and waste plastics. Front Environ Sci Eng 2018;12:8–17. https://doi.org/10.1007/s11783-018-1063-6.

[232] Varuvel EG, Sonthalia A, Subramanian T, Aloui F. NOx-smoke trade-off characteristics of minor vegetable oil blends synergy with oxygenate in a commercial CI engine. Environ Sci Pollut Res 2018;25:35715–24. https://doi.org/10.1007/s11356-018-3484-y.

[233] Godiganur S, Suryanarayana Murthy CH, Reddy RP. 6BTA 5.9 G2-1 Cummins

engine performance and emission tests using methyl ester mahua (Madhuca indica) oil/diesel blends. Renew Energy 2009;34:2172–7. https://doi.org/10.1016/J.RENENE.2008.12.035.

[234] Boopathi D, Thiyagarajan S, Edwin Geo V, Madhankumar S. Effect of the second generation and third generation biofuel blend on performance, emission and combustion characteristics of CI engine. Int J Ambient Energy 2018:1–8. https://doi.org/10.1080/01430750.2018.1492439.

[235] Subramanian T, Sonthalia A, Varuvel EG. Effect of calcite/activated carbon-based post-combustion CO_2 capture system in a biodiesel-fueled CI engine— An experimental study. Energy Sources, Part A Recover Util Environ Eff 2019;41:1972–82. https://doi.org/10.1080/15567036.2018.1548525.

[236] Ashok B, Nanthagopal K, Arumuga Perumal D, Babu JM, Tiwari A, Sharma A. An investigation on CRDi engine characteristic using renewable orange-peel oil. Energy Convers Manag 2019;180:1026–38. https://doi.org/10.1016/j.enconman.2018.11.047.

[237] Singh D, Sarma AK, Sandhu SS. A comprehensive experimental investigation of green diesel as a fuel for CI engines. Int J Green Energy 2019;16:1152–64. https://doi.org/10.1080/15435075.2019.1653882.

[238] Thiyagarajan S, Herfatmanesh MR, Geo VE, Peng Z. Experimental investigation into the effect of magnetic fuel reforming on diesel combustion and emissions running on wheat germ and pine oil. Fuel Process Technol 2019;186:116–24. https://doi.org/https://doi.org/10.1016/j.fuproc.2018.12.017.

[239] Karthickeyan V, Ashok B, Nanthagopal K, Thiyagarajan S, Geo VE. Investigation of novel Pistacia khinjuk biodiesel in DI diesel engine with post combustion capture system. Appl Therm Eng 2019;159:113969. https://doi.org/https://doi.org/10.1016/j.applthermaleng.2019.113969.

[240] Agarwal AK, Dhar A. Experimental investigations of performance, emission and combustion characteristics of Karanja oil blends fuelled DICI engine. Renew Energy 2013;52:283–91. https://doi.org/https://doi.org/10.1016/j.renene.2012.10.015.

Performance, Emission and Combustion Studies of a Modified Vegetable Oil in a Compression Ignition Engine

[241] Thiyagarajan S, Sonthalia A, Edwin Geo V, Ashok B, Nanthagopal K, Karthickeyan V, et al. Effect of electromagnet-based fuel-reforming system on high-viscous and low-viscous biofuel fueled in heavy-duty CI engine. J Therm Anal Calorim 2019;138:633–44. https://doi.org/10.1007/s10973-019-08123-w.

[242] Boopathi D, Thiyagarajan S, Sonthalia A, Parthiban P, Devanand S, Edwin Geo V. Effect of methanol fumigation on performance and emission characteristics in a waste cooking oil-fuelled single cylinder CI engine. Energy Sources, Part A Recover Util Environ Eff 2019;41:1088–96. https://doi.org/10.1080/15567036.2018.1539142.

[243] Chelladurai P, Geo VE. Experimental Investigation to Study the Effect of Properties of Coconut Oil Biodiesel and Castor Oil Biodiesel and its Blending with Diesel on the Performance in a CI Engine. SAE Int 2016;2016-28–01. https://doi.org/10.4271/2016-28-0145.

Appendix – I

Specification of Malvern Spraytec

Measurment Principle	Laser diffraction
Size range	0.1 – 2000μm
Optical Models	Mie theory and Fraunhofer Approximation including Patented Multiple Scattering correction
Lens ranges	750 mm lens: 2.0–2000μm (D_{v50}: 5–1600 μm)
Working range	100mm at 0.5μm, >1m at 10μm
Concentration range	Minimum acceptable transmission: 5% (dependent on particle size range)
Detection system	35 element log-spaced silicon diode detector array
Light source	632.8 nm, 5mW helium–neon laser
Maximum acquisition rate	Continuous mode: 1 Hz Rapid mode: 2.5 kHz as standard, 10 kHz with additional software feature key
Accuracy	Better than ±1% on the D_{v50}
Precisions/repeatability	Better than ±1% COV on the D_{v50}

Appendix – II

Specifications of the test engine

Make	Kirloskar
Brake power (kW)	3.5
Cylinders	One
Rated speed (rpm)	1500
Compression ratio	17.5:1 (VCR engine)
Stroke x Bore (mm)	110 x 87.5
Connecting rod length (mm)	234
Cooling type	Water Cooled
Variable compression ratio	12 to 18
Inlet valve closes at	35.5 degrees ATDC
Inlet valve opens at	4.5 degrees BTDC
The exhaust valve closes at	4.5 degrees ATDC
Exhaust valve opens at	35.5 degrees BBDC
Fuel injection timing	23 degrees BTDC
No. of injector holes	3
Nozzle diameter (mm)	0.148

Appendix – III

Technical Specifications of AVL Smoke Meter

Measurement principle	Extinction measurement	
Operating temperature	+5 - 45°C subject to measuring accuracy	
	+1 - 50°C measurement ready	
Humidity	Max. 90%, non-condensing	
Dimensions	395*285*136 (width*height(depth)	
Weight	3.5kg	
Opacity Chamber		
Measuring chamber heating	100°C	
Effective length	0.215m±0.0002m	
Maximum exhaust temperature	200°C	
Measurement parameters		
	Measurement Range	Resolution
Opacity	0 – 100%	0.1%
Absorption (k value)	0 – 99.99 1/m	0.01 1/m

Appendix – IV

Technical Specifications of AVL Di-Gas Analyzer 1000

Parameter	Measurement Range	Resolution	Precision
CO	0 – 15% vol.	0.01% vol.	<0.6% vol. ±0.03%vol. ≥0.6%vol. ±5% of reading
CO_2	0 – 20% vol.	0.01% vol.	<10% vol. ±0.5%vol. ≥10%vol. ±5% of reading
HC	0 – 30000ppm vol.	1ppm vol.	<200ppm vol. ±10ppm vol. ≥200ppm vol. ±5% of reading ≥10000ppm vol. ±10% of reading
NO	0 – 5000ppm vol.	1ppm vol.	<500ppm vol. ±50ppm vol. ≥500ppm vol. ±10% of reading
O_2	0 – 55% vol.	0.01% vol.	<2% vol. ±0.1%vol. ≥2%vol. ±5% of reading

Miscellaneous		
Measurement Principle	CO, CO_2, HC	Non-dispersive Infrared
	NO	Electrochemical
Power Drawn	Approximatelly 20W	
Operating Temperature	5 – 45°C	
Storage Temperature	0 – 50°C	
Relative Air Humidity	≤95%	Non – condensing
Dimensions (W*D*H)	270*320*85mm	
Weight	2.5kg	without accessories

Appendix – V

Sample calculation for finding the uncertainty

At 100% load condition

Speed $\qquad$ N = 1500rpm

Load $\qquad$ W = 12.5kg

Fuel Volume $\quad$ f = 10cc

Brake Power $\quad$ BP = 3.5kW

3. Brake Power

$$BP = \frac{2*\pi*N(rpm)*Load(kg)*9.81*Dynamometer\ arm\ length\ (m)}{60*1000}$$

$$BP = \frac{2*\pi*1500*12.5*9.81*0.185}{60*1000} = 3.5kW$$

$$BP = f(W)$$

$$\frac{\partial BP}{\partial W} = \frac{2*\pi*1500*9.81*0.185}{60*1000} = 0.285$$

$$\Delta BP = \left[\sqrt{\left(\frac{\partial BP}{\partial W}*\Delta W\right)^2}\right]$$

$$\Delta BP = \left[\sqrt{(0.285*0.2)^2}\right]$$

$$\Delta BP = 0.057kW$$

Therefore, the uncertainty in brake power is ±0.057kW and the uncertainty limits in the calculation of BP are 3.5±0.057kW.

4. Total fuel consumption

$$TFC = \frac{10*3600*0.835}{t*100}$$

$$TFC = \frac{10*3600*0.835}{29.5*100} = 1.02kg/h$$

$$TFC = f(t)$$

$$\frac{\partial \text{TFC}}{\partial t} = -\frac{10 * 3600 * 0.835}{t^2 * 100}$$

$$\frac{\partial \text{TFC}}{\partial t} = -\frac{10 * 3600 * 0.835}{29.5^2 * 100} = -0.0345$$

$$\Delta \text{TFC} = \left[\sqrt{\left(\frac{\partial \text{TFC}}{\partial T} * \Delta T \right)^2} \right]$$

$$\Delta \text{TFC} = \left[\sqrt{(-0.0345 * 0.18)^2} \right]$$

$$\Delta \text{TFC} = 0.00621 \text{kg/h}$$

The uncertainty in TFC is ±0.00621kg/h and the limits of uncertainty are 0.93±0.00517kg/h.

5. Brake thermal efficiency

$$\eta = \frac{\text{BP} * 3600 * 100}{\text{mass flow rate} * \text{Calorific value}}$$

$$\eta = \frac{3.5 * 3600 * 100}{1.02 * 42570} = 29.01\%$$

$$\eta = f(\text{BP, MFR})$$

$$\frac{\partial \eta}{\partial \text{BP}} = \frac{3600 * 100}{\text{MFR} * 42570}$$

$$\frac{\partial \eta}{\partial \text{BP}} = \frac{3600 * 100}{1.02 * 42570} = 8.29$$

$$\frac{\partial \eta}{\partial \text{MFR}} = -\frac{\text{BP} * 3600 * 100}{\text{MFR}^2 * 42570}$$

$$\frac{\partial \eta}{\partial \text{MFR}} = -\frac{3.5 * 3600 * 100}{1.02^2 * 42570} = -28.45$$

$$\Delta \eta = \left[\sqrt{\left(\frac{\partial n}{\partial \text{BP}} * \Delta \text{BP} \right)^2 + \left(\frac{\partial n}{\partial \text{MFR}} * \Delta \text{MFR} \right)^2} \right]$$

$$\Delta \eta = \left[\sqrt{(8.29 * 0.057)^2 + (-28.45 * 0.00621)^2} \right]$$

$\Delta\eta = 0.5044\%$

The uncertainty in brake thermal efficiency is $\pm0.5044\%$ and the limits of uncertainty are $29.01\pm0.5044\%$.

6. Brake specific energy consumption

$$BSEC = \frac{\text{mass flow rate} * \text{Calorific value}}{BP * 1000}$$

$$BSEC = \frac{1.02 * 42570}{3.5 * 1000} = 12.406 \text{MJ/kWh}$$

BSEC = f(MFR, BP)

$$\frac{\partial BSEC}{\partial MFR} = \frac{42570}{BP * 1000}$$

$$\frac{\partial BSEC}{\partial MFR} = \frac{42570}{3.5 * 1000} = 12.16$$

$$\frac{\partial BSEC}{\partial BP} = -\frac{MFR * 42570}{BP^2 * 1000}$$

$$\frac{\partial BSEC}{\partial BP} = -\frac{1.02 * 42570}{3.5^2 * 1000} = 3.544$$

$$\Delta BSEC = \left[\sqrt{\left(\frac{\partial BSEC}{\partial BP} * \Delta BP\right)^2 + \left(\frac{\partial BSEC}{\partial MFR} * \Delta MFR\right)^2}\right]$$

$$\Delta BSEC = \left[\sqrt{(3.544 * 0.057)^2 + (12.16 * 0.00621)^2}\right]$$

$$\Delta BSEC = 0.2156 \text{MJ/kWh}$$

The uncertainty in brake specific energy consumption is ±0.2156MJ/kWh and the limits of uncertainty are 12.406 ± 0.2156MJ/kWh.

7. Temperature measurement

Uncertainty in temperature is: $\pm 1\%$ (T > 150 °C)

         $\pm 2\%$ (150 °C < T < 250 °C)

         $\pm 3\%$ (T < 250 °C)

8. Percentage of uncertainty for NO, HC, CO, smoke and pressure is given below.

         NO   :1.2

HC   : 0.1

CO   : 0.76

Smoke   : 2.1

Pressure   : 1.3

Appendix – VI

Equation for predicting the CoV

Table A6.1: Weights between input layer and hidden layer

i	$F_i = \dfrac{1}{1 + e^{-(w_1*load + w_2*blend\ ratio + \theta_i)}}$		
	w_1	w_2	θ_i
1	0.960	2.092	0.927
2	-3.272	-1.424	2.099
3	1.121	1.993	1.068
4	0.954	2.095	0.919
5	1.763	0.994	0.378
6	5.244	4.653	-4.278
7	6.482	14.598	-0.628
8	1.723	1.062	0.534
9	0.980	2.081	0.954
10	6.849	-0.648	-2.687
11	3.382	5.856	2.937
12	13.582	1.058	-14.214
13	9.232	5.473	-3.075
14	5.836	-2.647	-1.045
15	0.735	2.220	0.533
16	5.157	-4.706	3.280

$$X = -0.141 * F_1 - 6.585 * F_2 - 0.022 * F_3 - 0.144 * F_4 + 1.332 * F_5 -$$
$$3.27 * F_6 - 6.175 * F_7 + 1.156 * F_8 - 0.128 * F_9 - 3.388 * F_{10} - 2.561 *$$
$$F_{11} - 5.921 * F_{12} - 2.799 * F_{13} + 2.52 * F_{14} - 0.231 * F_{15} - 2.747 * F_{16}$$
$$\text{(A6.1)}$$

$$COV = \frac{1}{1 + e^{-(X+16.799)}} \qquad\qquad \text{(A6.2)}$$

LIST OF PUBLICATIONS

International Journals

1. **Ankit Sonthalia,** Naveen Kumar, 2019, *Hydroprocessed vegetable oil as a fuel for transportation sector: A review*. Journal of the Energy Institute; 92: 1-17. DOI: 10.1016/j.joei.2017.10.008. (Publisher: Elsevier)

2. **Ankit Sonthalia,** Naveen Kumar, 2019, *Comparison of fuel characteristics of hydrotreated waste cooking oil with its biodiesel and fossil diesel.* Environmental Science and Pollution Research, In Press. DOI: 10.1007/s11356-019-07110-w. (Publisher: Springer)

3. Naveen Kumar, **Ankit Sonthalia,** Mukul Tomar, Rashi Koul, 2020, *An Experimental Investigation on Spray, Performance and Emission of Hydrotreated Waste Cooking Oil Blends in an Agricultural Engine.* International Journal of Engine Research. In Press. DOI: 10.1177/1468087420928734. (Publisher: Institution of Mechanical Engineers, SAGE)

4. Naveen Kumar, **Ankit Sonthalia,** Rashi Koul, 2020, *Optimization of the process parameters for hydrotreating used cooking oil by the Taguchi method and Fuzzy logic*. Journal of Energy Resources Technology; 142(12): 123006. (Publisher: American Society of Mechanical Engineers)

International Conferences

1. Naveen Kumar, **Ankit Sonthalia,** 2020, Performance and emission characteristics of a single cylinder diesel engine fuelled with hydrotreated waste cooking oil. Proceedings of 8th International Symposium on Fusion of Science and Technology (ISFT – 2020).

2. Naveen Kumar, **Ankit Sonthalia,** 2020, Effect of blends of hydrotreated used cooking oil, biodiesel and diesel on the performance and emission characteristics of a single cylinder diesel engine. Proceedings of 8th International Symposium on Fusion of Science and Technology (ISFT – 2020).

Curriculum Vitae

Personal Details:

Name: Ankit Sonthalia
Father's Name: Gopal Krishna Sonthalia
Mother's Name: Late Vibha Sonthalia
Date of Birth: 11th February 1987
Linguistic Abilities: Speak, Read & Write: English & Hindi
Permanent Address: 59/26, Birhana Road, Kanpur, Uttar Pradesh, 208 001, India
Mobile No: 9962466825/8175956848
Email Id: ankit.sont@gmail.com / ankit_sont@yahoo.co.in

Educational Qualification:

Education	Degree	Institute	Board/ University	Year	Marks Percentage/ CGPA
Ph. D	Ph. D	Delhi Technological University, Delhi	DTU	Pursuing	NA
M. Tech.	Automotive Engineering	VIT, Vellore/ARAI Pune	VIT, Vellore	2014	8.66
B. Tech.	Mechanical Engineering	VIT, Vellore	VIT, Vellore	2010	8.88

Academic Projects:

M. Tech Projects

- Simulation of Piston Ring Friction in an IC engine using MATLAB.
- Simulation of an IC engine using MATLAB – Simulink and Waste Heat Recovery from the engine using Vapor Absorption Refrigeration System and Thermoelectric Converter.
- Testing of Hydrogen and CNG mixtures on a single cylinder Spark Ignition Engine.
- Final Semester Project: Selection and Matching of a Turbocharger for a Naturally Aspirated CNG engine using GT – Power at ARAI Pune.

B. Tech Projects

- "Performance Optimization of a Single Cylinder Diesel Engine using Biodiesel as fuel" received Rs. 50,000 as financial assistance for this project from L-RAMP (Lemelson Recognition and Mentoring Programme, an initiative of IIT Madras) nodal centre VIT- TBI.
- Performance and emission test of a single cylinder diesel engine using ISO 8178 standards for BS III norms.

- Final Semester Project: Development of new approaches to study wear and energy saving of engine oils.

Papers Published:

- Naveen Kumar, Ankit Sonthalia, Mukul Tomar, Rashi Koul, 2020, An Experimental Investigation on Spray, Performance and Emission of Hydrotreated Waste Cooking Oil Blends in an Agricultural Engine. International Journal of Engine Research. In Press. DOI: 10.1177/1468087420928734. (**SCI Indexed, Impact Factor: 2.382**)

- Naveen Kumar, Ankit Sonthalia, Rashi Koul, 2020, Optimization of the process parameters for hydrotreating used cooking oil by the Taguchi method and Fuzzy logic. Journal of Energy Resources Technology; 142(12): 123006. (**SCI Indexed, Impact Factor: 2.759**)

- S. Thiyagarajan, **Ankit Sonthalia**, V. Edwin Geo, T. Prakash, V. Karthickeyan, B. Ashok, K. Nanthagopal, B. Dhinesh, Effect of manifold injection of methanol/n-pentanol in safflower biodiesel fuelled CI engine. Fuel, 261, 116378 (**SCI Indexed, Impact Factor: 5.128**).

- **Ankit Sonthalia,** Naveen Kumar, Comparison of fuel characteristics of hydrotreated waste cooking oil with its biodiesel and fossil diesel, Environmental Science and Pollution Research, 2019, In Press. (**SCI Indexed, Impact Factor: 2.8**)

- **Ankit Sonthalia**, Shivam Garg, Rishav Sharma, S. Thiyagarajan, Naveen Kumar, Effect of electrostatic precipitator on exhaust emissions in biodiesel fuelled CI engine. Environmental Science and Pollution Research, 2019, In Press. (**SCI Indexed, Impact Factor:** 2.8)

- S. Thiyagarajan, **Ankit Sonthalia**, V. Edwin Geo, B. Chokkalingam, Effect of Waste Exhaust Heat on Hydrogen Production and its Utilization in CI Engine, International Journal of Hydrogen Energy, 2019 (In Press) (**SCI Indexed, Impact Factor: 4.229**).

- V. Edwin Geo, **Ankit Sonthalia**, G. Nagarajan, B. Nagalingam, Fethi Aloui, Effect of Port Premixed LPG on the Engine Characteristics, Journal of Energy Resources technology, 2019, 141(11), (**SCI Indexed, Impact Factor: 2.759**).

- **Ankit Sonthalia**, Naveen Kumar, Hydroprocessed vegetable oil as a fuel for transportation sector: a review, Journal of Energy Institute, 2019, 92(1), 1-17. (**SCI Indexed, Impact Factor: 4.2**).

- S. Thiyagarajan, **Ankit Sonthalia**, V. Edwin Geo, B. Ashok, K. Nanthagopal, V. Karthickeyan, B. Dhinesh, Effect of electromagnet-based fuel-reforming system on high-viscous and low-viscous biofuel fueled in heavy-duty CI engine, Journal of Thermal Analysis and Calorimetry, 2019, (**SCI Indexed, Impact Factor:** 2.2)

- S. Thiyagarajan, **Ankit Sonthalia**, V. Edwin Geo, Effect of calcite/activated carbon-based post-combustion CO_2 capture system in a biodiesel-fueled CI engine—An experimental study, Energy Sources, Part A: Recovery, Utilization, and Environmental Effects, 2019, 41(16), 1972-1987, (**SCI Indexed, Impact Factor:** 0.894)

- D. Boopathi, S. Thiyagarajan, **Ankit Sonthalia**, P. Parthiban, S. Devanand & V. Edwin Geo, Effect of methanol fumigation on performance and emission characteristics in a waste cooking oil-fuelled single cylinder CI engine. Energy Sources, Part A: Recovery, Utilization, and Environmental Effects, 2019, 41 (9), 1088-1096, DOI: 10.1080/15567036.2018.1539142. (**SCI Indexed, Impact Factor:** 0.894)

- V. Edwin Geo, **Ankit Sonthalia**, S. Thiyagarajan, Fethi Aloui, NOx-smoke trade off characteristics of minor vegetable oil blends synergy with oxygenate in a commercial CI engine. Environmental Science and Pollution Research, 2108, 25(35), 35715-35725. (**SCI Indexed, Impact Factor:** 2.8)

- Femilda Josephin J,S., V. Edwin Geo, **Ankit Sonthalia**, C. Bharatiraja, Fethi Aloui, Predicting the different engine parameters of a rubber seed oil-ethanol dual fuel engine using artificial neural networks. International Journal for Global Warming, 2018, 16(4), 485-506. (**SCI Indexed, Impact Factor:** 0.66)

- V. Edwin Geo, **Ankit Sonthalia**, Fethi Aloui, Femilda Josephin J,S., Study of engine performance, emission and combustion characteristics fueled with diesel-like fuel produced from waste engine oil and waste plastics. Frontiers of Environmental Science and Engineering, 2018, 12(4), 8. (**SCI Indexed, Impact Factor:** 1.961)

- V. Edwin Geo, **Ankit Sonthalia**, G. Nagarajan, B. Nagalingam, Studies on performance, combustion and emission of a single cylinder diesel engine fuelled with rubber seed oil and its biodiesel along with ethanol as injected fuel. Fuel, 2017. (**SCI Indexed, Impact Factor: 5.128**).

- Boopathy D, **Ankit Sonthalia**, Devanand S, Experimental investigations on the effect of hydrogen induction on performance and emission behaviour of a single cylinder diesel engine fuelled with palm oil methyl ester and its blend with diesel, Journal of Engineering Science and Technology, 12(7), 2017, 1972-1987. (**Scopus Indexed**)

- **Ankit Sonthalia,** Somesh Reddy, C. Ramesh Kumar, and Keval Kamani, Theoretical Investigation of Waste Heat Recovery from an IC Engine Using Vapor Absorption Refrigeration System and Thermoelectric Converter, Heat Transfer—Asian Research, 44(6), 2015 pp. 499-514 (**Scopus Indexed**).

- **A. Sonthalia**, C. Rameshkumar, U. Sharma, A. Punganur, S. Abbas, Combustion and Performance Characteristics of a Small Spark Ignition Engine fuelled with HCNG, Journal of Engineering Science and Technology, 2015,Volume (10) Issue (4) 404- 419. (**Scopus Indexed**).

- Somesh T Reddy, **Ankit Sonthalia,** C. Rameshkumar, Performance Analysis of Single Module Thermoelectric Generator, Advanced Materials Research, 2014, Vols. 875-877 pp. 1625-1629 (**Scopus Indexed**).

- **Ankit Sonthalia,** C. Rameshkumar, The effect of compression ring profile on the friction force in an Internal Combustion Engine, Tribology in Industry, 2013, Volume 35, No.1 74-83 (**Scopus Indexed**).

- C. Rameshkumar, **Ankit Sonthalia,** Rahul Goel, Experimental Study on Waste Heat Recovery from IC engine using Thermoelectric Technology, Journal of Thermal Science, 2011, Volume 15, No. 4, pp. 1011-1022. (**SCI Indexed, Impact Factor: 1.228**)

- C. Rameshkumar, **Ankit Sonthalia,** Rahul Goel, A new approach to study wear and energy saving engine oils using nano lubricants in IC engine, International Journal of Nanotechnology and Application, 2010, Volume 4, No.3 pp. 169-183.

Conferences Attended:

- Naveen Kumar & **Ankit Sonthalia**, Performance and emission characteristics of a single cylinder diesel engine fuelled with hydrotreated waste cooking oil, 8th International Symposium on Fusion of Science and Technology (ISFT – 2020)
- Naveen Kumar & **Ankit Sonthalia**, Effect of blends of hydrotreated used cooking oil, biodiesel and diesel on the performance and emission characteristics of a single cylinder diesel engine, 8th International Symposium on Fusion of Science and Technology (ISFT – 2020)
- Design and Analysis of a Submarine Hull and its Varied Features, (2009), RAIME 09 at National Engineering College Kovilpatti.
- Performance and Emission Characteristics of a Hydrogen fuelled SI engine, ICAMB 09 at VIT University

Book Chapters Published:

- Naveen Kumar, **Ankit Sonthalia**, Harveer S. Pali, Sidharth Bansal, Next Generation Biofuels – Opportunities and Challenges, In: Gupta A., De A., Aggarwal S., Kushari A., Runchal A. (eds) Innovations in Sustainable Energy and Cleaner Environment. Green Energy and Technology. Springer, Singapore, 2019, 171-191. DOI: https://doi.org/10.1007/978-981-13-9012-8_8
- Naveen Kumar, **Ankit Sonthalia**, Harveer S. Pali and Sidharth Bansal. Alternative Fuels for Diesel Engines: New Frontiers, In: Richard Viskup (eds) Diesel and Gasoline Engines, IntechOpen, 2018, DOI: https://doi.org/10.5772/intechopen.80614.

Work Experience:

- SRM University, NCR Campus, Ghaziabad: **Assistant Professor** in the Department of Mechanical and Automobile Engineering, (Dec 2015 – Present)
- SRM University, Kattankulathur/Chennai Campus: **Assistant Professor** in the Department of Automobile Engineering, (Feb 2015 – Dec 2015)
  Course Taught: Thermodynamics, Applied Thermal for Automotive Engineers, Automotive Engine, Engine Systems, Alternate Fuels and Pollution Control, Vehicle Performance and Testing, Gas Dynamics and Space Propulsion, Engineering Mechanics, Machine Drawing, and Engineering Graphics.
  Responsibilities at SRM University, NCR Campus:
  Time Table Coordinator of the department
  UGC and NAAC Coordinator of the department
  Part of the internal assessment test conducting team

- Tech Mahindra (formerly Mahindra Satyam), Hyderabad, India (August 2010 – July 2012)
  Job Profile: Software Developer
  Responsibilities:
  Develop software using C# .Net 3.0 technology and test planning
  Communicated continuously with clients for brain storming sessions.
  Learned to solve problems in quick time, with innovative solutions.
  Acquired sound business knowledge and ability to adapt to responsibilities.
  Received Pat on Back award for successful completion of project.

Other Activities

1. Received Research Excellence Award at Delhi Technological University for publishing paper
2. Reviewed paper for International Journal of Hydrogen Energy (Elsevier)
3. Reviewed papers for Energy (Elsevier)
4. Reviewed papers for SAE International Journal of Fuels and Lubricants.
5. Reviewed paper for Fuel journal (Elsevier)
6. Member of Society of Automotive Engineers (SAE, India)
7. Member of Institution of Engineers, India
8. Member of Centre for Advanced Studies & Research in Automotive Engineering
9. Attended workshop on Research Methodology through ICT organized by NITTR Chandigarh
10. Attended workshop on Recent Trends in Automobile Engineering through ICT organized by NITTR Chandigarh
11. Completed NPTEL Online Course: IC Engines and Gas Turbines
12. Qualified Gate in 2010.

Place: Delhi   (Ankit Sonthalia)